STUDIES OF FACTORS INFLUENCING THE PHOTOCHEMICAL CLEAVAGE OF WATER

BY

MICHAEL CHARLES PERRY

A THESIS PRESENTED FOR THE DEGREE OF DOCTOR OF PHILOSOPHY IN THE UNIVERSITY OF ASTON IN BIRMINGHAM

MAY 1986

THE UNIVERSITY OF ASTON IN BIRMINGHAM

STUDIES OF FACTORS INFLUENCING THE PHOTOCHEMICAL CLEAVAGE OF WATER

Michael Charles Perry Ph.D. 1986

SUMMARY

It has been known for some time that the excited state of the tris (2,2'-bipyridine) ruthenium (II) dication, $Ru(bipy)_3^{2+}$, is thermodynamically capable of facilitating the photochemical cleavage of water into dihydrogen and dioxygen. Surfactant derivatives of $Ru(bipy)_3^{2+}$ as monolayers [16] and contained on dispersed particles [36] have enabled the cleavage reaction, but irreproducibly. Solution studies have tended to use the surfactant as an intermediary or relay in the cleavage reaction.

The investigations described in this thesis examine factors which may affect the photochemical behaviour of the surfactant derivative in all three physical states.

Studies of the thickness of various monolayers reveal that film: support slide deposition ratios cannot always be taken at 'face value' and heterogeneous layering of monomolecular layers is inferred. A monomolecular layer of the dioctadecyl ester of (4,4'-dicarboxy-2,2'-bipyridine)bis(2,2'-bipyridine)ruthenium (II)$^{2+}$ (first used by Whitten [16] to cleave water) is found to be 35Å thick.

Particle size distribution studies of dispersions of the surfactant support medium seem to indicate that the particle shape need not always be of a pre-assumed spherical form. In general, dispersions are found to be unaffected by the preparative technique, dilution, long term standing, and their properties are fairly reproducible. Inclusion of the surfactant with the dispersion does not affect the dispersion initially. In general the size of dispersed particles is distributed about 2μ.

N.M.R. studies of water in solutions containing surfactant derivatives of $Ru(bipy)_3^{2+}$ suggest the formation of several transient collision complexes of differing stoicheiometries (an overall equilibrium constant 1.71×10^4, based on mole fractions, was deduced). As a consequence of this discovery, a unique N.M.R. analogue of the Job-method [119] for determining complex stoicheiometries is developed. However, time did not permit this method to be implemented for further studies in solution of the interaction between water and surfactant derivatives of $Ru(bipy)_3^{2+}$.

Ruthenium Water Photocleavage Stoicheiometry N.M.R.

ACKNOWLEDGMENTS

I would like to express my sincere thanks to my supervisor, Dr. J. Homer, for his invaluable assistance throughout the course of this work, and in particular for the many helpful discussions and suggestions on the interpretation of the results.

I am also grateful to my late close friend and colleague, Dr. M. C. Cooke, for his continual encouragement and helpful discussions, to Mr. M. S. Mohammadi for his advice and assistance on some of the computer programming; to Mr. E. J. Hartland, Mr. S. Ludlow and the technical staff of the Analytical Services section of the Department of Molecular Sciences for their support.

My thanks are due to Professor W. R. McWhinnie, Head of the Department of Molecular Sciences for allowing me part-time release from my full-time employment and for the provision of laboratory facilities. I am also grateful to the authorities of the University of Aston in Birmingham, for the waiver of tuition fees.

Finally, I would like to thank my wife for typing a lengthy and difficult manuscript, and both my wife and mother for their unceasing encouragement throughout my studies.

CONTENTS

CHAPTER 2

Monolayer assemblies and determination of molecular thickness

CHAPTER 4

A N.M.R. study of the molecular interaction in a solution between a diester surfactant derivative of $Ru(bipy)_3^{2+}$,$((bipy)_2Ru(II)(2,2'\text{-bipy-}4,4'(COOC_{18}H_{37})_2))^{2+}(PF_6)_2^{2-}$, and water.

CHAPTER 6

The development of a N.M.R. method to establish the stoicheiometry of the molecular complex/es formed between a surfactant derivative of $Ru(bipy)_3^{2+}$ and water.

FIGURES

CHAPTER 3

Phase distribution studies.

CHAPTER 4

A N.M.R. study of the molecular interaction in solution between a diester derivative of $Ru(bipy)_3^{2+}$ and water.

CHAPTER 6

The development of a N.M.R. method to establish the stoicheiometry of the molecular complex/es formed between a surfactant derivative of $Ru(bipy)_3^{2+}$ and water.

TABLES

CHAPTER 5

CHAPTER 6

CHAPTER 1

CONSIDERATION OF FACTORS RELATED TO THE PHOTOCHEMICAL CLEAVAGE OF WATER USING SOLAR ENERGY

1.1. USING SOLAR ENERGY TO PRODUCE A FUEL

The ever diminishing natural fuel resources such as fossilised coal, oil, gas and wood that currently meet most of the worlds energy needs (see fig. 1.1) together with continued public distrust about the use of nuclear fuels as an alternative, has stimulated scientific research in its attempt to harness other energy forms. Of the other alternatives, only sunlight is sufficiently widespread over the Earth's surface to benefit the majority of the populace and to all 'intents and purposes' it is continuously renewable and transmitted.

Sunlight as a source of energy, is often misrepresented, in that attention has been more frequently drawn to its heating effects rather than its photonic properties: A photonic process in this instance describes a chemical reaction (somewhat incorrectly) which is induced by a specific wavelength of light (its so-called threshold wavelength; designated as λ_g). From this it follows that different frequencies (presenting changing wavelengths) of solar radiation may or may not fulfil the thermodynamic requirement for a particular chemical process to occur and in consequence λ_g is a major controlling factor in the preparation of a fuel as a means of solar energy storage.

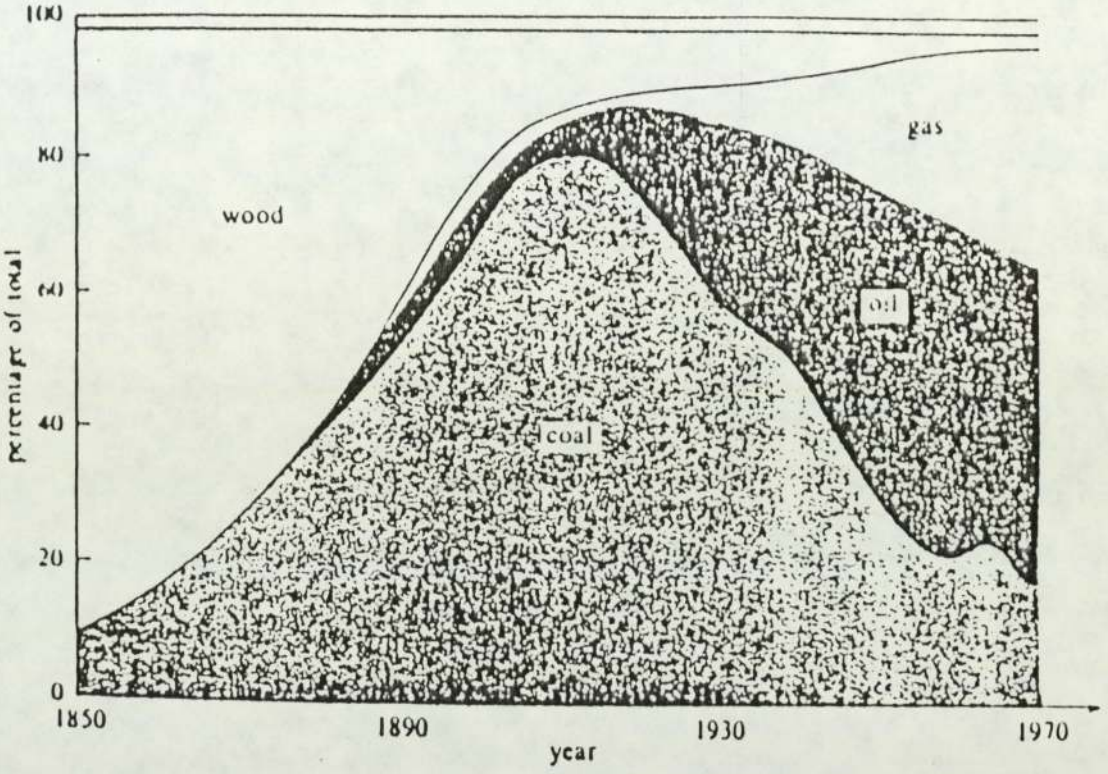

Fig 1.1 - Proportional use of principle fuels since 1850, in which the top narrow section represents other energy sources, such as hydroelectric and nuclear. [1]

How this energy transference may possibly be accomplished has typically, of late, fallen into three broad topics of research, photochemical, photoelectrochemical and photobiological. For the purposes of this project, investigations are restricted to a photochemical approach, although it is realised that evidence from all three sciences may be fundamental to each other.

1.2 CONSIDERATIONS ON THE USE OF WATER AS A RAW MATERIAL FOR DIHYDROGEN FUEL PRODUCTION

Unfortunately for the chemistry purist the controlling impetus for the preparation of a fuel which can gain both commercial and ecological acceptance, is more often than not restrained by its economical viability. Idealistically, the raw photoreactant must therefore be plentiful, widely distributed, non-polluting and capable of meeting the thermodynamic criteria for the fuel producing reaction to proceed.

Quite clearly, water certainly meets some of the pre-requisites that have just been put forward. From a thermodynamic standpoint the successful photochemical cleavage of water to form dihydrogen (a combustable fuel) and dioxygen (a by-product) would appear to depend solely on meeting the energetics of an accepted route to redox (reduction-oxidation) reaction.

However, before looking further into the energetics of photocleavage of water, it is appropriate at this stage of the

discussion to examine briefly some features of redox reactions. Any redox reaction may be given in terms of two half reactions or couples, which are convenient for describing the oxidation or reduction steps. However, as a means of quantifying oxidizing or reducing power it is not possible to determine the absolute potential of a single couple only the difference in potential (E^{o}) between two couples. After general agreement, the problem was overcome by fixing the potential of the hydrogen ion - hydrogen gas couple, H^{+}/H_{2}, at zero (standard conditions), that is

$$H^{+}(1.18M) + e^{-} \rightarrow 1/_{2}H_{2}\ (101325Nm^{-2})\ E^{o} = 0(25^{o}C) \qquad (1.1)$$
activity = 1

and deriving the potentials of any other couples by reference to this.

Therefore, of considerable value to the chemist are the tables which have been compiled that give the standard redox potentials (sometimes called standard electrode potentials) of a large number of half reactions. Each redox potential is given a + or - sign which can alternate according to the convention by which all the half-reactions are written (e.g. as a reduction step as in equation (1.1) or vice versa).

In the context of this work for instance, the most thermodynamically favoured redox reactions for water at pH7, involve dielectronic reduction (1.2) and tetraelectronic oxidation (1.3), which given in strict accordance to current convention on redox potentials are read as,

$$2H^+(10^{-7}M)+2e^- \rightarrow H_2\ (101325Nm^{-2})\quad E^o = -0.41V \quad (1.2)$$

$$O_2\ (101325Nm^{-2})+ 4H^+(10^{-7}M)+ 4e^- \rightarrow 2H_2O \qquad E^o = +0.82V \quad (1.3)$$

As E^o for the $2H^+/H_2$ couple (equation 1.2) at pH7 is -0.41V this would mean that hydrogen (going to H^+) is a better reducing agent (electron donor) at pH7 than under standard conditions (see equation 1.1). Similarly for equation (1.3), where E^o is +0.82V, water at pH7 (going to hydrogen ions and oxygen) provides a much poorer reducing agent than hydrogen of the standard hydrogen couple or electrode (S.H.E.). However, an alternative interpretation of equation (1.3) is that at pH 7 the hydrogen ions with associated oxygen (in going to water) constitute a better oxidizing agent (electron acceptor) than that presented by H^+ of the standard hydrogen couple. For this reason equation (1.3) can in respect of equation (1.2) in the situation given, be written as an oxidation process (equation 1.4), such that

$$2H_2O \rightarrow O_2 + 4H^+ + 4e^- \qquad E^o = +0.82V \qquad (1.4)$$

and by appropriate use of equations 1.2 and 1.3 a complete $4e^-$ reaction is obtained, whereby,

$$H_2O \rightarrow H_2 + 1/_2O_2 \qquad \Delta G = +1.23eV \qquad (1.5)$$

where ΔG is the free energy voltage equivalent for the transfer of one electron. On the basis of thermodynamics it can be shown that λ_g of around 1000nm should satisfy the free energy requirement of reaction (1.5) and in so doing, photoinduce reaction. In an equivalent sense a couple having a redox potential more positive than + 0.82V should oxidize water. Conversely a couple having a redox potential more negative than - 0.41V should reduce water.

Alternatively, the redox reactions for monoelectronic reduction (1.6) and oxidation (1.7) at pH7 produces hydrogen atoms and hydroxyl radicals,

$$H^+ + e^- \longrightarrow H^\bullet \qquad E^0 = -2.5V \qquad (1.6)$$

$$H_2O \longrightarrow {}^\bullet OH + H^+ + e^- \qquad E^0 = +2.5V \qquad (1.7)$$

and an overall dissociation reaction (1.8).

$$H_2O \longrightarrow H^\bullet + {}^\bullet OH \qquad \Delta G = +5eV \qquad (1.8)$$

for which λ_g is less than 250nm. Thus, it becomes evident, that to initiate redox reactions of the type shown in the latter scheme,

requires a much greater input of energy. Balzani et al [2] have taken issue over the formation of intermediate radicals, which are described as energy wasters, because they are not storable.

Although, thermodynamics gives the energetics to photocleavage of water, other factors determine whether or not there is a net chemistry to the redox reactions. Significantly, Balzani [2] points out that the emission spectrum of the sun at the surface of the Earth (see fig. 1.2) does not overlap the electronic absorption spectrum of water and it would appear that neither reaction 1.5 or 1.8 are photoinducible by solar radiation alone.

In referring to fig. 1.2, it is important to note, that as the sun's rays traverse the Earth's atmosphere in passing to its surface, ultraviolet radiation of wavelengths shorter than 300nm is totally removed by an ozone layer. Furthermore, other major atmospheric constituents such as water, carbon dioxide and oxygen, also partially absorb solar radiation. It is clear that the λ_g to initiate reaction 1.8 is not defined in the solar spectrum at the surface of the Earth, whilst the intensity of λ_g of reaction 1.5 is weak. However, it would seem reasonable on energetic grounds to expect reaction 1.5 to be induced by radiation of a wavelength less than that pertaining to its threshold (since a smaller wavelength of energy can also fulfil the free energy requirement for initiation of reaction). Such a reaction would be extremely inefficient, in that most of the excess energy would be dissipated as heat. In practice, reaction 1.5 does not happen and thus it becomes apparent that kinetic and mechanistic

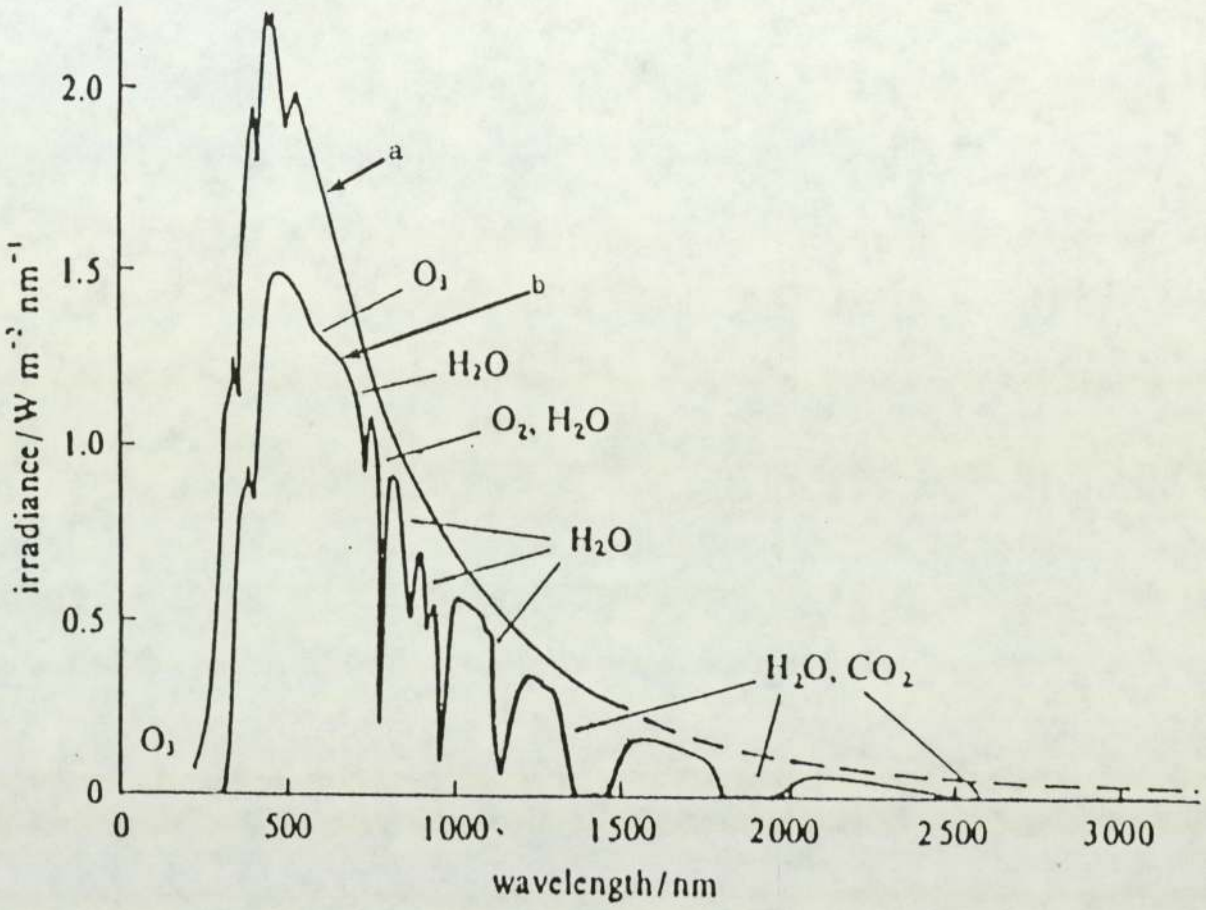

Fig. 1.2 The variation of the intensity of solar radiation with wavelength, (a) outside the Earth's atmosphere and (b) on the surface of the Earth, for which the atmospheric absorption bands of water are identified.

features also play a major role in photoinduced cleavage reactions; as for instance, rapid counterproductive back reactions preventing the isolation of any products. Obviously, any side reactions will also oppose the effectiveness of solar radiation to start photoreaction (photolysis).

The possibility of using a catalytic sensitizer (see section 1.3.2) to overcome the energy void in the absorption spectrum of water at sea level and outside the Earth's atmosphere is also developed by Balzani [2] using various chemical cycles. The investigations place particular significance on the efficiency of the reaction in terms of the quantum yield, its threshold wavelength and the exclusion of radicals within the proposed reaction mechanism. The merits of using different transition metal complexes in cyclic schemes are shown and it is proposed that the distinctive photoexcited states of such types of species may provide an eventual route to efficient solar energy transfer.

1.3 PHOTOCATALYTIC SENSITIZERS AS A MEANS OF CLEAVING WATER

1.3.1 INTRODUCTION

By achieving the threshold wavelengths that initiate a photochemical reaction, it is implied that a characteristic band of energy has also been absorbed in that same instance by the system. Indeed, in terms of conventional photochemical experiments for a molecule to be defined as photochemically active or excited, the

Grotthus-Draper principle simply states that radiation must be absorbed. The energetics of a newly formed photochemical system may now be described mathematically as

$$\Delta E = E_2 - E_1 \tag{1.9}$$

where E_1 is characteristic of ground state molecules, E_2 excited state molecules (normally prefixed with * to signify its state) and ΔE the energy difference.

Moreover, the expression may be related to the threshold wavelength (λ_g) such that

$$\lambda_g = \frac{hc}{E_2 - E_1} \tag{1.10}$$

where c is the velocity of light and h is Planck's constant.

The Stark-Einstein principle refined the photochemical description further by stating that a molecule can absorb only one quantum of radiation (in the strictest sense). This leads to the quantum yield expression

$$\text{Quantum Yield} = \frac{\text{Number of molecules undergoing the photochemical process}}{\text{Number of quanta absorbed}} \tag{1.11}$$

For the purposes of photochemical cleavage of water it is apparent that either a water molecule cannot, on the surface of the Earth, absorb sufficiently high energy solar radiation for the desired photoreaction to take place or counteracting properties prevent its forward progression. In essence, it becomes the objective of the photochemist to initiate absorption of radiation via a suitable system and control the photoprocess in terms of achieving the best quantum yield.

1.3.2 ABSORPTION OF LIGHT

Fortunately in the context of cleaving water by solar energy the photoexcited state of a molecule can have properties that differ from its ground state, namely, lifetime, new acid base properties, luminescence, energy transference and electron transfer. It is such properties that photochemists have for years utilized to prepare new materials and which could possibly lead to efficient photochemical preparation of dihydrogen fuel from water. Importantly for this 'goal', some molecules are able to absorb radiation and then transfer it in some physical form to different ground state molecules that it is required to react at a particular threshold wavelength; such types of molecules are by definition called photosensitizers (PS).

Interestingly, a further examination of the redox reactions 1.2 (reduction) and 1.4 (oxidation) given earlier in section 1.2, shows that it might be possible to mediate the reactions by

deactivation (quenching) of a suitably excited photosensitizer, *PS, in which the reduction step becomes,

$$*PS + H^+ \rightarrow PS^+ + 1/_2 H_2 \qquad (1.12)$$

and the oxidation step

$$*PS + 1/_2\ H_2O \rightarrow PS^- + H^+ + 1/_4\ O_2 \qquad (1.13)$$

provided the couple $PS^+/*PS < -0.41V$ and the couple $*PS/PS^- > +0.82V$.

Thus, it was with considerable interest that many photochemists viewed the work of Demas and Adamson [3] who introduced tris (2,2'bipyridine) ruthenium (II) chloride as a new sensitizer, the discovery of which was to prove to have far reaching consequences for those researchers interested in the photochemical cleavage of water. It was in properties intrinsic to the dication $Ru(bipy)_3^{2+}$ (see below) that the sensitizer held photochemical uniqueness and although the report sets out to demonstrate some novel substitution reactions of co-ordination compounds, it also proposes that $Ru(bipy)_3^{2+}$ and its derivatives could find wide use as low energy sensitizers in both organic and inorganic photochemical studies. The overall appeal for $Ru(bipy)_3^{2+}$ sensitization arises mainly because

1. It was found to be photochemically and thermally inert (see 1.3.3)

2. It has a strong absorption covering a sizable region of the short wavelength end of the visible spectrum (λ_{max} = 452nm)

3. Spectrophotometric studies using absorption and emission methods provide determinations on sensitizer deactivation (or quenching) and donor-acceptor reactions (see section 1.3.3a).

4. It is water soluble unlike many organic sensitizers.

5. Derivatives behave similarly (except that changes of ligand offers systematic variation of redox potentials)

6. It has a relatively long excited state lifetime (680ns).

1.3.3. CONSIDERATIONS OF $Ru(bipy)_3^{2+}$

a) The excited state of $Ru(bipy)_3^{2+}$ and some of its derivatives is a first triplet charge transfer state ^{3} or $^{(3)}$CT in a shorthand version. The initial part of the description (first triplet or T_1) gives information on the electronic spin multiplicity of the molecule, which

for $Ru(bipy)_3^{2+}$ is derived in stages, after direct irradiation of the ground state molecule (S_0), as shown in fig. 1.3. The difference between the S_1 and T_1 states (fig. 1.3a) originates from the spin alignment of two unpaired electrons, which have spins arranged antiparallel and parallel respectively (see fig.1.3b). However, it should be appreciated that quite often, irradiation alone will not always lead to the triplet state (as strictly speaking the transition in going from S_1 to T_1 is breaking a spin selection rule) and consequently the only route to attain T_1 is by sensitization shown in fig. 1.4

It is known that the induced triplet state of molecules have extended lifetimes over the parent singlet state and one can reason that in certain instances of photochemical reaction that a more favourable reaction pathway may be achieved by using a different energy state. For example, adding specificity to a molecule by triplet state induction, has given chemists a sole route to the preparation of certain cis-trans isomers and by implication an energy state might be found, to investigate the sensitized cleavage of water (see section 1.3.5).

It is equally important to appreciate that an extension to the lifetime of an excited state molecule (characteristic of triplet states over singlet states) allows for it to incur a greater number of diffusional encounters with an acceptor molecule (at a given concentration), which is a considerable advantage for the overall reactivity of the photosystem.

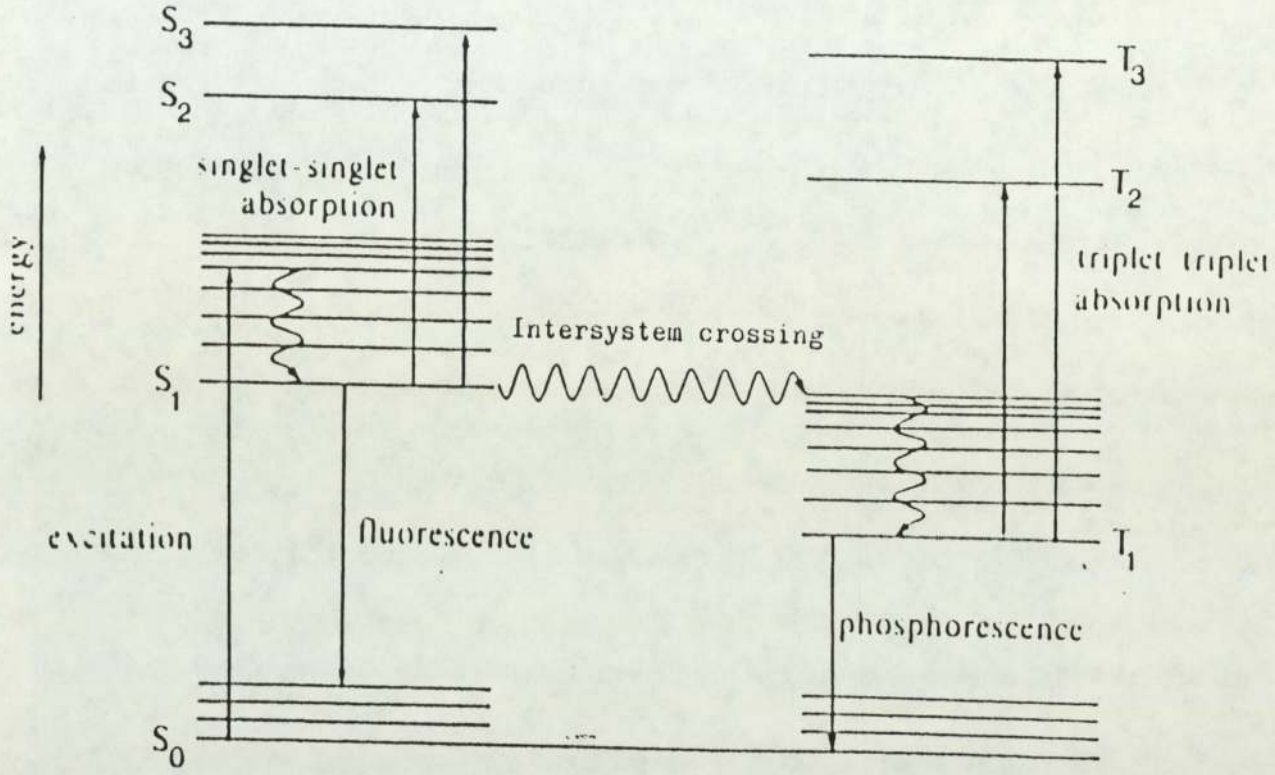

Fig. 1.3a - Intramolecular decay processes originating from S_1 and T_1 excited states

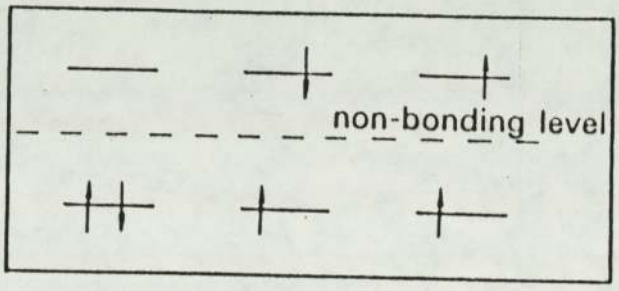

Fig. 1.3b - Distribution of electrons in ground, excited singlet and triplet states (from left to right respectively)

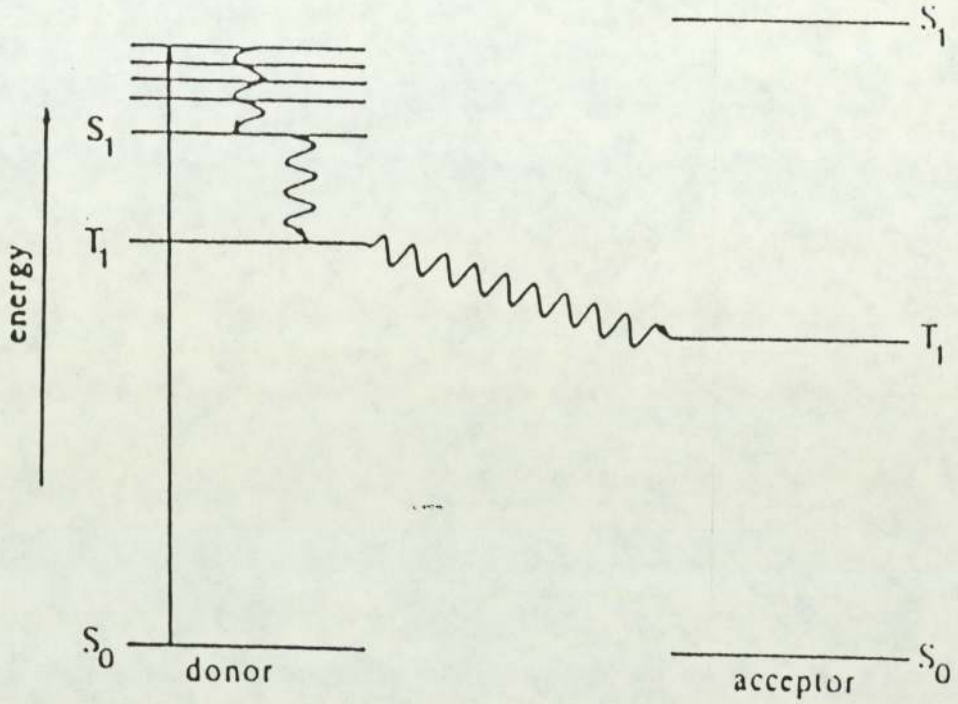

Fig. 1.4 - Favourable arrangement of donor-acceptor energy levels for triplet-triplet energy transfer (sensitization).

The excited state lifetime of a molecule is normally very short (typically picoseconds - milliseconds) due to the destabilizing effect of absorbed energy and consequently it is highly reactive. Thus, if one is considering a sensitizer of the triplet type it is important that its lifetime is long and that a high triplet yield is produced from the absorption of light. Moreover, it is important that intersystem crossing must be fast compared with other processes depleting the first singlet state; the work of Demas and Adamson [3] indicates that $Ru(bipy)_3^{2+}$ starts to comply with these prerequisites.

Further study of fig. 1.3a also reveals that the reaction system can also lose energy by emitting light at wavelengths specific to fluorescence or phosphorescence (the latter being spin forbidden) in respect of singlet or triplet excited states respectively; the description of energy loss by a radiative process is more often covered by the general expression of luminescence. Demas and Adamson [3] point out that luminescence would appear natural to all $Ru(bipy)_3^{2+}$ type charge transfer systems and utilize the phenomenon to monitor sensitizer quenching by studying emission characteristics spectrofluorimetrically.

b) In partly classifying the sensitizer as a charge transfer molecular type, indicates that the chelate structure of the $Ru(bipy)_3^{2+}$ complex is formulated by movement of electron density between donor ligands (e.g. bipyridine) and the metallic acceptor centre (ruthenium II).

It is fortunate for the photochemist that charge transfer type complexes are usually intensely coloured, thereby having large extinction coefficients (for $Ru(bipy)_3^{2+}$, ϵ = 14,600 in aqueous solutions [3, 7, 8]) which readily facilitate spectrophotometric absorption studies. Indeed, Demas and Adamson [3] state that low sensitizer concentrations should enable the detection of sensitized reaction.

Moreover, the colour of the complex takes on another significance in that it indicates that a specific bandwidth of light is being efficiently absorbed.

1.3.4 THE DEVELOPMENT OF THE UNDERSTANDING OF $Ru(bipy)_3^{2+}$ BASED SENSITIZERS

One aspect of post photoexcitation of the molecule not yet mentioned concerns the redress of ionization potentials and electron affinity, which must follow the redistribution of electrons within the molecule, as fig 1.5 demonstrates. The new electronic configuration of the molecule imparts properties to its excited state which differ widely from its ground state, as for instance, the excited molecule is a much stronger reductant.

The first publication offering practical evidence on the redox properties of $Ru(bipy)_3^{2+}$ was given by Adamson and Gafney [4], who describe the reduction of a series of cobalt (III) compounds, and

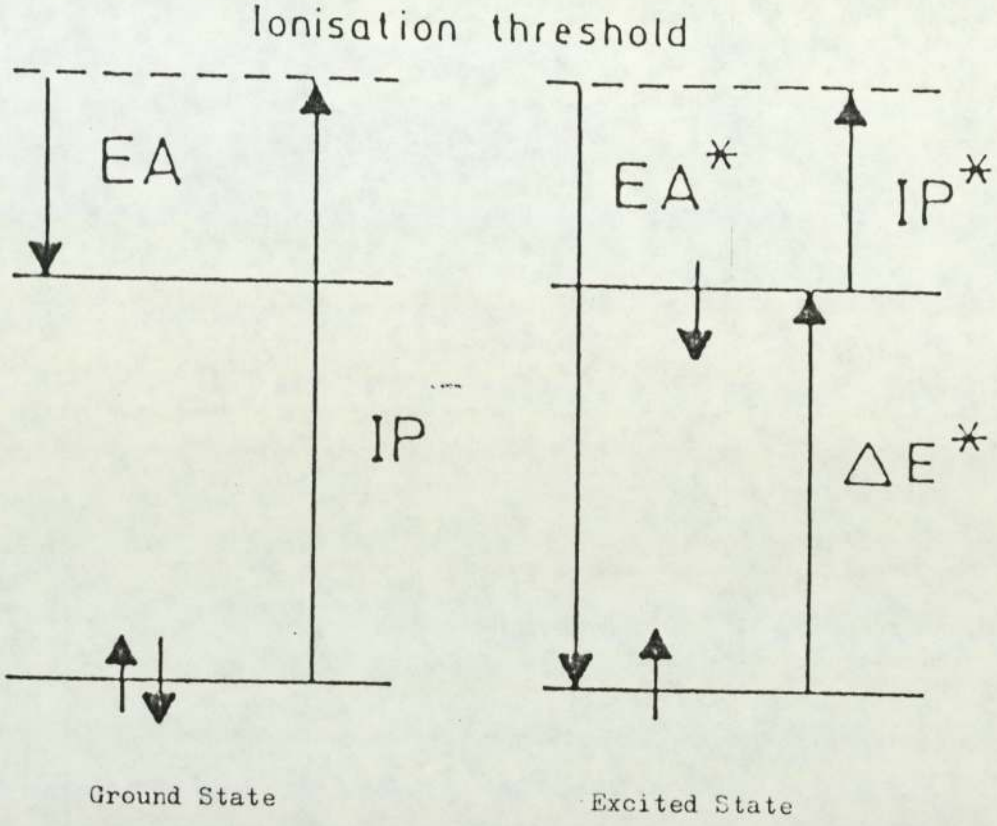

Fig. 1.5 - An illustration of the modification of the ionization energy (I.P.) and electron affinity (E.A.) of a ground state molecule after excitation (E).

propose that $Ru(bipy)_3^{2+}$ behaves as an electron transfer reductant. It is significant to note that although $Ru(bipy)_3^{2+}$ (see section 1.2 for a definition of redox terms) is reported as a good reductant, the quenching process results in the strong oxidant $Ru(bipy)_3^{3+}$, the implications of the disclosure seemingly passing by those interested in the photochemical cleavage of water. The suggestion that the luminescent excited state of $Ru(bipy)_3^{2+}$ is quenched by electron transfer reactions is followed up by Demas and Adamson [5] who conclude that its use in sensitized redox decomposition of $Co(C_2O_4)$ proceeds via one electron transfer. However, work by Natarajan and Endicott [6] tends to refute the idea of quenching by electron transfer and suggest that the effect occurs largely as a result of triplet-triplet energy transfer. This energy transfer notion was soon opposed by Whitten et al [7] on the grounds of evidence from flash photolysis studies of $Ru(bipy)_3^{2+}$ quenching, using an organic cation and some transition metal ion complexes, the results of which showed that the electron transfer phenomenon is energetically correct. Subsequent publications [8,9] serve to substantiate the electron donor/acceptor appeal of excited state $Ru(bipy)_3^{2+}$.

The first workers to draw attention to the potential of excited state $Ru(bipy)_3^{2+}$ designated $^* Ru(bipy)_3^{2+}$, to promote the photochemical cleavage of water were Creutz and Sutin [10], whose proposals were essentially empirically based on studies of $Ru(bipy)_3^{2+}$ -hydroxide reactions (the thermodynamic feasibility of the reaction from redox potentials is made apparent by other workers [11-14] (see fig. 1.6)). The proposed reaction scheme may be represented as a two fold process, where the initiation step is the reduction of water to dihydrogen

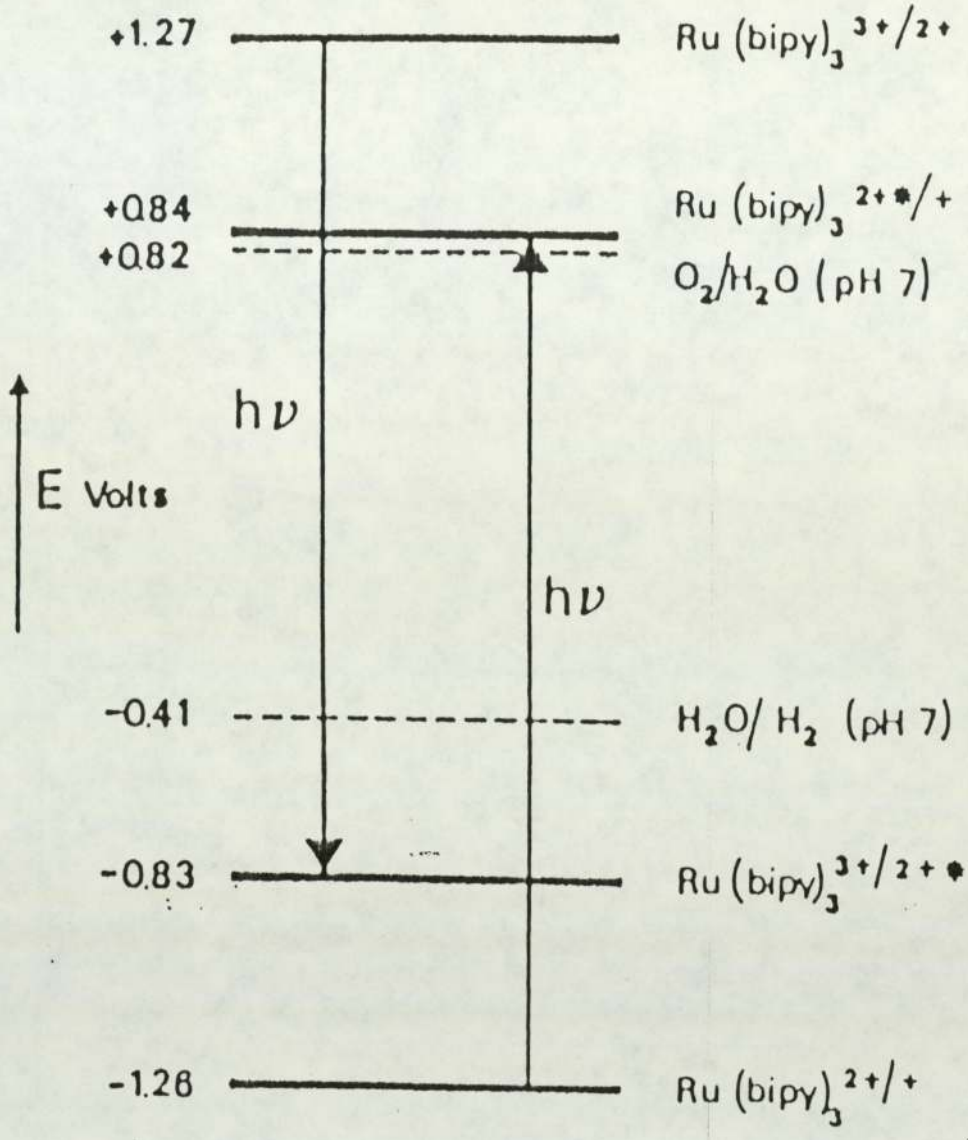

Fig. 1.6 - Redox potentials of various couples of ruthenium tris (bipy) cationic species, which demonstrate the thermodynamic feasibility of the cleavage reaction (also see section 1.2). The potentials are referred to the standard hydrogen electrode.

$$*Ru(bipy)_3^{2+} + H_2O \rightarrow Ru(bipy)_3^{3+} + 1/_2\ H_2 + OH^- \qquad (1.14)$$

terminated by concomitant production of base $Ru(bipy)_3^{2+}$ and dioxygen, through oxidation of the hydroxide.

$$Ru(bipy)_3^{3+} + OH^- \rightarrow Ru(bipy)_3^{2+} + 1/_4\ O_2 + 1/_2\ H_2O \qquad (1.15)$$

From the above scheme it is evident that if $Ru(bipy)_3^{2+}$ is to function in a catalytic role then the $Ru(bipy)_3^{3+}$ must be used rapidly to regenerate the photoactive dicationic species. It is the efficiency of this final conversion which is the crux of a reaction scheme that uses $Ru(bipy)_3^{2+}$ type compounds to photocatalytically cleave water and continues to provoke interest for researchers with its numerous aspects.

Another encouraging feature in the redox chemistry of $Ru(bipy)_3^{2+}$ was revealed by Whitten et al [15] who demonstrated that virtually all the excitation energy of $*Ru(bipy)_3^{2+}$ can be applied to drive a selected photoreduction process. Such conclusions were founded on the study of $Ru(bipy)_3^{2+}$ and its reaction with several nitrobenzene derived quenching agents.

1.3.5. PHOTOCHEMICAL CLEAVAGE OF WATER USING SURFACTANT DERIVATIVES OF $Ru(bipy)_3^{2+}$

The work of Demas and Adamson [3] has shown that the excited state of $Ru(bipy)_3^{2+}$ in water is relatively long lived (680ns at 25°C),

but generally unquenched. Consideration of redox potentials in respect of $Ru(bipy)_3^{2+}$ can also reveal that the cleavage reaction is thermodynamically favoured. However, solar energy conversion through photochemical cleavage of water, by a $Ru(bipy)_3^{2+}$ type sensitizer, was not realized until the publication of the findings of Whitten et al [16]. In Whitten's investigation it is proposed that the photolysed $Ru(bipy)_3^{2+}$ water system undergoes competing reactions, in which, the electron transfer process is prevented from predominating over counteractive excited state decay, by kinetic barriers (unspecified), the effect of which is to slow any reduction step. In addition, it is also suggested that the products of photolysis will rapidly recombine before the next electron transfer event.

Whitten introduces a novel scheme to surmount the apparent kinetic deficiency of the electron transfer process by using surfactant derivatives of $Ru(bipy)_3^{2+}$ deposited as monolayer assemblies on glass supports before immersion in water. The $Ru(bipy)_3^{2+}$ had been modified by replacing a single unit of 2,2' bipyridine with either the dioctadecyl ester, or (bis dihydrocholesteryl) ester, of 4,4' - dicarboxy - 2,2' - bipyridine, which in contrast, renders the respective derivatives 1 and 2 (see fig. 1.7), insoluble in water.

Whitten focuses the discussion of the experimental results on the role of 1, which seemingly photocatalytically sensitizes the cleavage of water into dihydrogen and dioxygen. The conclusion is drawn from several factors some of which are very worthy of note.

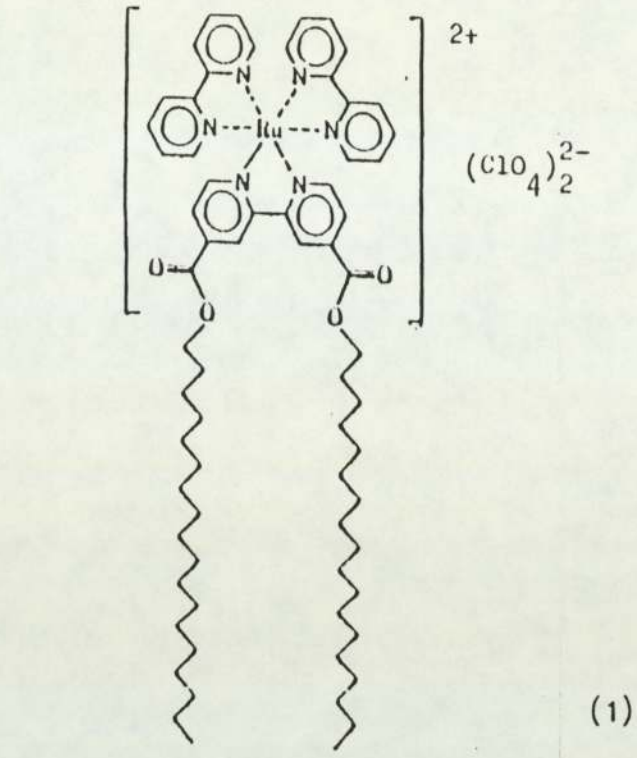

(1)

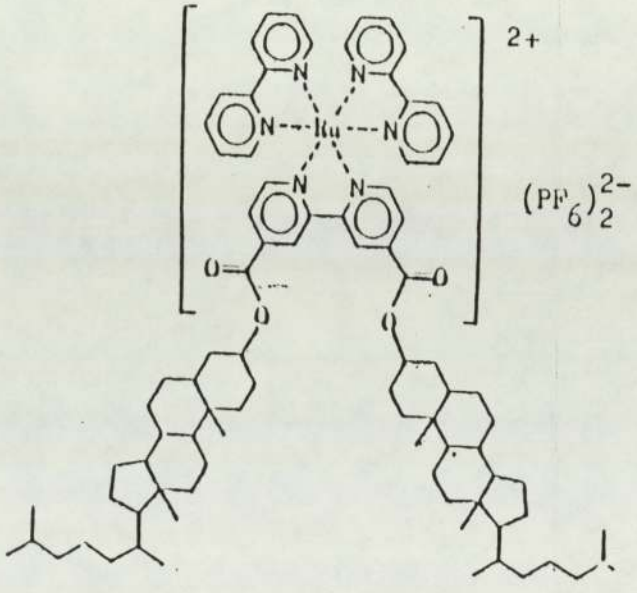

(2)

Fig. 1.7 Whitten-type surfactants 1 and 2

1. Mass spectrometric determination of the gaseous products yielded by photolysis of 1 and 2 showed that dihydrogen and dioxygen had been produced.

2. The characteristic luminescence of 1 was found to be almost entirely quenched by water, but recoverable (sensitization).

3. A turnover rate of several molecules of gas were produced per single molecule of 1 (catalysis).

4. Absorption spectra of 1 remained unchanged through all experimental conditions.

From a thermodynamic standpoint the cleavage reaction is just as feasible with $Ru(bipy)_3^{2+}$ as 1, however, Whitten suggests that by using monolayer assemblies of 1, the kinetic barrier to the electron transfer process is lowered. Alternatively, it is advanced that the phase boundary which arises from the condensed environment of the hydrophobic monolayer assembly of 1 could influence the kinetics of electron transfer by impeding the recombination of highly energetic initial photo products; an idea which gets acceptance from subsequent workers (see later). Although the cleavage reaction gives a measured quantum efficiency of 0.3 for surfactant 1 (which is far from ideal) and despite Whitten's initial mechanistic theory being somewhat imprecise, the experiment did provide a substantial stimulus for other workers in the field.

1.4 FURTHER INVESTIGATIONS ON WHITTEN-TYPE SURFACTANTS

Whitten's preliminary communication on sensitized cleavage of water using surfactants [16] was soon followed by a comprehensive report [17]. However, the outcome of these further investigations with purified forms of surfactant 1, chiefly served to demonstrate the irreproducibility of the first experiment [16], which Whitten reasons, could possibly be explained by the synergistic effect of impurities in the original surfactant preparations.

Predictably, the immediate response of other research groups with similar interest, centre on repeating or questioning Whitten's initial findings, whilst the solution chemistry of $Ru(bipy)_3^{2+}$ and its derivatives in solution, became briefly less topical.

The first workers to query the validity of Whitten's evidence for photocleaving water were Gaines and Valenty [18], whose unsuccessful reproduction attempt was hampered by difficulties when preparing the surfactant complexes. Other workers incurred problems [19 - 22], one of whom [22] is categoric in stating that Whitten-type surfactants do not sensitize the cleavage of water. All workers fail to reproduce Whitten's original surface area for a monolayer of 1 and it is noticeable that there is a lack of consistency for this parameter throughout their studies.

Much of the early physical chemistry of $Ru(bipy)_3^{2+}$ derived surfactants, emanated from those same workers [18 - 22], who had tried in part to reproduce Whitten's findings [16]. From such studies it is evident that the classical Langmuir film balance used to deposit the monolayered surfactant onto glass supports, enables the determination of some extremely useful monolayer parameters (monolayer surface area for instance). Not surprisingly, spectrofluorimetry and spectrophotometry feature frequently, as these analytical methods are invaluable for investigations on sensitization and quenching properties.

Prior to Whitten's publication on the successful cleavage of water [16], Henry and Hoffmann [23] had used spectrofluorimetry to establish the existence of covalent hydrates of bipyridyl free base and monocation to gain some insight into the ground state chemistry of $Ru(bipy)_3^{2+}$ in solution. The worth of nuclear magnetic resonance methods for studying $Ru(bipy)_3^{2+}$ in solution was later demonstrated by Gillard and Hughes [24] who show that the behaviour of it or its derivatives in aqueous media (in which the cation is unchanged) is far from simplistic. Novel equilibria effects for various ruthenium (II) bipyridyl systems are elucidated through the addition of nucleophiles and protonates and an association with the photochemical reactivity of $Ru(bipy)_3^{2+}$ is inferred [24].

Of the other complementary physical chemistry studies made of Whitten-type photocatalyzed reactions [16], the quantification of any evolved gaseous products is seen as important by all workers; as its

measurement relates to the quantum efficiency and catalytic property of the photosystem. Valenty [25] takes account of the initial probability that such products will constitute poor quantum yields and describes a procedure for the determination of dissolved trace gases in water using gas chromatography. Whitten [16, 17], like many other investigators, relies on interfaced gas chromatography and mass spectrometry. Some workers choose to use the instrumental methods uncombined and in particular, Yellowlees [19] has demonstrated a mass spectrometric gas determination using a vacuum technique.

Following on from Whitten's widely publicised communication on the photoreactivity of monolayer assemblies of surfactant derivatives of $Ru(bipy)_3^{2+}$ [16], the literature sees a first report from Whitten et al [26] concerning the redox chemistry of some structurally related compounds in solution. In this latter report Whitten still adheres to the empirical view that hydrophobic ligands of the type seen in the preparation of surfactant 1 (see section 1.3.5) impart selectivity to electron transfer reactions by restricting energy wasting back-electron transfer processes. Indeed, it was demonstrated that the incorporation of bulky hydrophobic groups around the periphery of the $Ru(bipy)_3^{2+}$ core retard both quenching and the reverse electron step. The proposed redox schemes are given as,

SCHEME 1 OXIDATIVE QUENCHING

$$*Ru\,L_3^{2+} + Ox^n \xrightarrow{a} (RuL_3^{3+}, Ox^{n-1}) \xrightarrow{b} RuL_3^{3+} + Ox^{n-1} \qquad (1.16a,b,c,d)$$

solvent cage

c ↓ d ↙

$$RuL_3^{2+} + Ox^n$$

SCHEME 2 REDUCTIVE QUENCHING

$$*RuL_3^{2+} + Red^n \xrightarrow{a} (RuL_3^{+}, Red^{n-1}) \xrightarrow{b} RuL_3^{+} + Red^{n-1} \qquad (1.17a,b,c)$$

$$\downarrow c$$

$$RuL_3^{2+} + Red^n$$

where L is the ligand, Ox^n an oxidant and Red^n a reductant. Moreover, it was shown that attention to the choice of ligand can make available a second redox site, besides that usually associated with the metallic centre.

The changes of ligand in the derivatives produced different redox potentials and reductive quenching is demonstrated [26]. It was envisaged that a wide range of redox processes could be achieved provided that the oxidation states of the derivatives were closely spaced, as this is essential if the derivatives are to serve as an electron donor or electron acceptor: Organic molecules or single ions can in general serve as either but not as both, as there is a much greater separation of the oxidation states. A subsequent report [27] served to consolidate Whitten's viewpoint that excited state

hydrophobic derivatives of $Ru(bipy)_3^{2+}$ can act as electron donor or electron acceptor in solution and underline the potential of photoinduced electron transfer reactions.

Of other variations on the use of $Ru(bipy)_3^{2+}$ in solution, the inclusion of an electron relay material to promote the reduction of water is interesting, as the effective role of $Ru(bipy)_3^{2+}$ is that of a catalytic photosensitizer principally facilitating the absorption of light [28, 29]. Unfortunately, a sacrificial donor material is required to prevent thermal back electron transfer between the relay and sensitizer, whilst expensive colloidal platinum is used as a microheterogeneous catalyst to ensure the formation of dihydrogen. Moreover, the electron relay reactions appear dependent on the order of priority of participating redox couples and some side reactions can impede useful propagation steps.

The wealth of research which now exists on the use of electron relays as intermediaries in the photocleavage of water, was pioneered by Shilov et al [30], who in their original work used acridine yellow, methyl viologen and cysteine or ethylenediamine tetraacetic acid as sensitizer, electron relay and electron donor respectively. Of more recent publications on the subject, a review article on microheterogeneous systems [31] is particularly interesting since it shows that separation of photoredox products is more efficient for a triplet process than for the analogous singlet process.

The schemes given for the electron transfer processes are detailed in fig. 1.8 where S and A represent sensitizer and acceptor respectively. The first stage for either process is electron oxidative quenching of the excited photosensitizer (*PS) and concomitant formation of a solvent cage (the latter is bracketed in fig. 1.7). For the singlet process, reverse electron transfer (kR) and subsequent formation of ground state products happens quite rapidly, as the transition is spin allowed. In contrast, before reverse electron transfer (kR) is possible in the triplet process, there is a time delay for spin rephasing within the solvent cage, as the transition T_1 to S_1 is spin forbidden. Consequently, in this instance, more ions escape the solvent cage (kE) and the reverse electron transfer (kR) for those ions become diffusion controlled.

However, the impact of Whitten's initially successful monolayer experiments remained and continues to influence the direction of solar energy research for other workers.

1.5 THE DETERMINATION OF RESEARCH DIRECTIONS THROUGHOUT THIS PROJECT

1.5.1 GENERAL INTRODUCTION

The discovery of anomalies in the chemistry of the Whitten-type surfactants, in monolayer experiments concerned with photoinduced cleavage of water [17], represented the starting point for this project. Whitten and other workers [12, 17, 21], in order to qualify the sole success of his first experiment [16] favoured an impurity theory, in

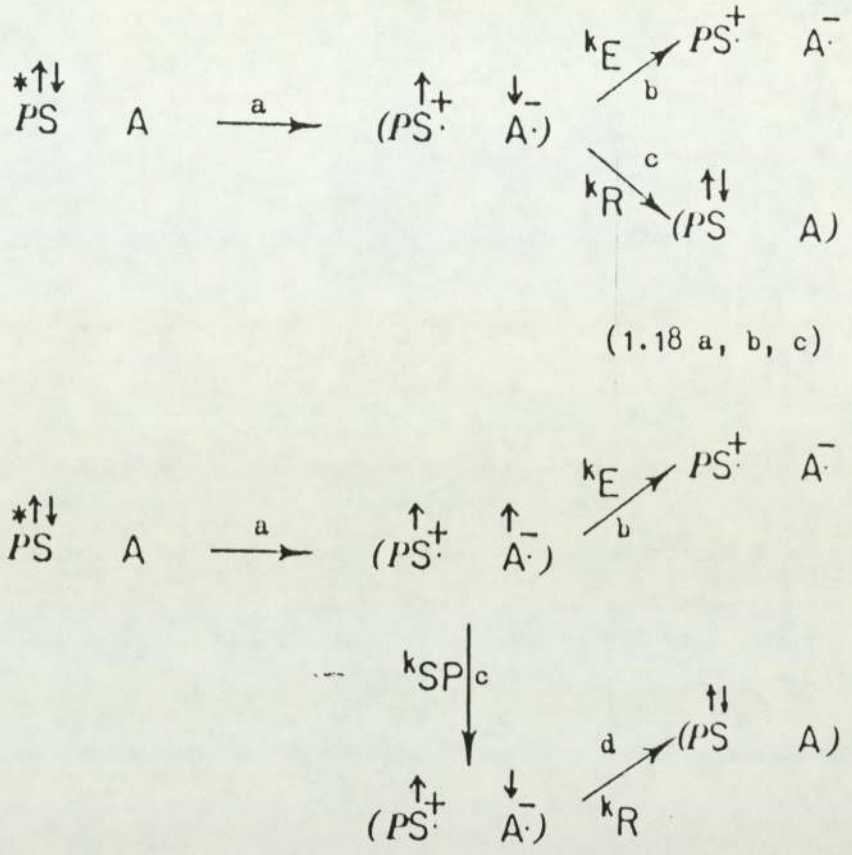

Fig. 1.8 - Electron transfer processes for excited singlet (1.18a, b, c) and triplet (1.19a, b, c, d) states.

which an inactive substance is activated by another (the synergist). This view was shared by some members of the research group which initiated this project.

Others considered that the interactive nature of the surfactants at molecular level could be important, although this contention in relation to both deposited monolayer [16-22] and solution [26, 27] was essentially based on hypothesis. Interestingly, the molecular environment presented by the two physical states to the excited molecule, provides two distinct aspects of its intermediary redox chemistry for which a knowledge of either may be complementary to the other.

In solution the electron transfer process takes place when the electron donor molecule and electron acceptor molecule have come close to each other by diffusion [32]. In contrast, an appropriate matrix structure for monolayer organizates may be visualized as inhibiting molecular diffusion. Consequently, a variation in the interface between donor and acceptor reaction sites determines to some extent the efficiency of the photoinduced electron transfer process [33].

Thus, it became a primary purpose for this project to investigate factors which might affect molecular donor/acceptor interrelationships, both for solution and monolayer, while developing new techniques and/or methods as was considered appropriate.

1.5.2 MONOLAYERS

a) INTRODUCTION

From the beginning of this project, it was evident that very little information had been forthcoming on the precise thicknesses of monolayer assemblies, which incorporated Whitten-type surfactants. Yet the accurate measurement of this parameter, coupled with a knowledge of molecular area, affords detail about the orientation of a single molecule within the monolayer. Furthermore, combined information on the proximity and spatial arrangement of neighbouring monolayers is important as they could influence electron transfer processes (requiring near contact of donor and acceptor molecules [33]) by retarding back reactions, through the shielding effect of hydrophobic ligands [16, 26, 27, 34].

Although it is reasonable and common to approximate molecular thicknesses by utilising the calculated areas of deposited monolayer and glass support, it is in many ways an assumptive method, in which it is accepted that the spread monolayer is uniformly transferred in the most rational orientation to the support.

b) STUDY PROPOSAL

The initial objective for this project was to devise and use a suitable method for the measurement of the thickness of monolayer assemblies, the structure of which could include surfactant derivatives of $Ru(bipy)_3^{2+}$.

1.5.3 DISPERSIONS

a) INTRODUCTION

At the outset of the monolayer study, a fellow researcher, Cooke [35], was directing intensive investigations towards devising various monolayer assemblies that contained Ru $(bipy)_3^{2+}$ surfactant derivatives This was in an effort to realize photocatalytic cleavage of water and so emulate to some extent Whitten's [16] original findings. Thus, a further objective for undertaking monolayer thickness measurements was to partially complement the photolysis work of Cooke by examining similar systems. In collating the results from both types of study it was felt that a better understanding of the monolayer reactivity of the $Ru(bipy)_3^{2+}$ surfactant derivatives in respect of their orientation within the monolayer, could be gained.

Although the photolysis experimentation proved partly successful in that some gaseous products were produced, they represented low quantum yields, which caused various analytical problems for reasons such as:-

1. The analytical options were limited, because the required detection levels could not be met as a result of incurring significant losses of product material in its transference from one sampling vessel to another.

2. The analytical instrumentation had to be continually operated near to the extreme of its sensitivity range in order to register a detector response. Unfortunately, this requirement meant an inevitable increase in the electronic noise of the measuring instrument (background), which resulted in a weak detector signal being difficult to observe.

3. It was possible that the detection level of the analytical instrument was insufficient to reveal trace levels of product gases.

Eventually, it became apparent that, to ensure evidence for photochemical cleavage of water, it was essential to increase the amount of gaseous products regardless of quantum efficiency. An obvious route to satisfy this requirement necessitated an increase in the number of supported monolayer assemblies undergoing reaction. However, because of the numerous practicalities involved in producing and irradiating multiple monolayer assemblies, this solution was considered impracticable.

An alternative method for increasing the reaction sites of the surfactant derivatives of $Ru(bipy)_3^{2+}$ used in the photosensitized breakdown of water was put forward by Cooke [36]. In attempting to maximize the sensitizer surface area he produced dispersions of a potentially inert hydrocarbon and the surfactant (i.e. pre-mixed before dispersion) in water, using an *ultrasonic dispersing technique (the two materials being insoluble in water). Such experiments are particularly apt because, as Shaw [37] points out, dispersion science is closely linked with surface chemistry since, at the interface between the dispersed phase (the phase forming the particles) and the dispersion medium (the medium in which the particles are distributed), characteristic surface properties such as adsorption and electric double layer effects are evident (see section 2.11.3b). These types of phenomena serve a very important function in determining the overall physical properties of the particulate system.

* Ultrasonics represent sound waves of a higher frequency than 20,000Hz and, as such are just outside the accepted audible range of human beings. If ultrasonics are applied to liquids, they create minute vacuum retaining spaces (the process being referred to as 'cavitation') which exert telling pulls on extraneous matter and thereby enable its breakdown and dispersion into finer particulate species to occur. More typical applications of ultrasonics are to facilitate rapid dissolution of substances or to augment the solvent action in cleaning processes.

It was postulated by Cooke that, provided the hydrocarbon was initially dispersed in a liquid state for a finite time, then its condensed form could be visualized as that of a sphere (see section 3.2.5). In terms of a photochemical role it was envisaged that the initially dispersed hydrocarbon would subsequently be encompassed by added sensitizer material (as both materials possess hydrophobic character), thus increasing its availability for photochemical reaction. Additionally, in using a multi-directional 'spherical' hydrocarbon base supporting medium, it was hoped that the reaction area would be increased (an attribute of all dispersions is the large area to volume ratio of the particles involved) and any yields of gaseous product correspondingly affected.

The results obtained from irradiation of dispersions with ultraviolet/visible light were very encouraging in that, in different instances, the yields of gaseous product had increased several fold compared with amounts produced in corresponding monolayer experiments [36]. Moreover, the use of deuterium oxide (D_2O) proved, through the detection of D_2 and HD in the gaseous products, that water had been photochemically cleaved. However, the attempts at reproducing the high yielding dihydrogen dispersion systems were unsuccessful, which effectively highlighted the need for a greater insight into the molecular dimensions of dispersions.

The solid state of the particulate material within Cooke - type dispersions can be visualized as being unique in that it exhibits properties related to shape and size of subdivision, as well as to extent and composition, all of which could affect the overall

photoreactivity of that dispersion. In terms of hypothesis, it is likely that such properties largely result from the ultrasonification procedure (often abbreviated to sonification), as it is probable that a variable dispersion effect could be experienced by the particulate matter (or particles). This is because:-

1. The environment of a particle undergoing sonification will be governed to some extent by the shielding effect of its neighbouring particles.

2. The starting size for particles will vary according to their manufacturing processes (which are often random).

3. Other physical or chemical effects may be operating, which might be dependent on 1) and 2) above.

All aspects of sonification mentioned so far should result in a distribution of 'sphere' sizes of the particulate solid phase material (often referred to as a one-dimensional distribution), although the shape of a particle remains accountable (its inclusion would make the distribution multi-dimensional). It was hypothesized that the form of the particle size distribution appertaining to Cooke's photosensitizer dispersions could dictate their overall effectiveness in producing the gaseous photolysis products.

b) STUDY PROPOSALS

Several different experimental parameters were seen to affect the particle size distribution and photoreactivity of Cooke-type dispersions, the possibilities being numerous. However, it was concluded that some fundmental ones might be:-

1. Sonification time
2. Sonification method
3. Sonification temperature
4. Hydrocarbon chain length

It followed that a considerable research effort was needed to understand the influence of the aforementioned parameters on the photoreactivity of Cooke-type dispersions and to identify the role of any others. With the advent of the availability of a particle size analyzer, it became a further aspect of this project to examine particle size distributions associated with dispersions of Whitten-type surfactants and hydrocarbon support in water.

1.5.4 SOLUTION

a) INTRODUCTION

The investigations on monolayers and dispersions were restricted, owing to unforseen external demands placed on the measuring instruments by their administrators, but it is believed that the scientific knowledge gained, made the experimentation worthwhile and demonstrated the potential of the instrumental methods used.

However, the termination point to the aforementioned studies proved timely in many ways, as it allowed for the undertaking of a more extensive study of the properties and effects of molecular interaction in solution, relevant to the mechanistic behaviour of $Ru(bipy)_3^{2+}$ derivatives of the Whitten-type. Moreover, as previously mentioned, such studies had always been a planned part of this project, because the research team who initiated this project, was able to offer considerable expertise and experience on aspects of molecular interaction in solution.

In solution the initial association of $Ru(bipy)_3^{2+}$ (or its derivatives) and water, behaving as acceptor (A) and donor (D) respectively, poses some extremely important, but hitherto unanswered questions about the disposition of water molecules about the chelate centre. All workers seem content to talk about or accept the association of acceptor and donor in terms of a solvent cage or shell [26, 31] (whereby donor molecules surround the interactive molecules to buffer the effect of bulk solvent [38]), apparently without any proper

understanding of its true dimensions; That this is important would appear obvious, because the extent of molecular association could govern electron transfer, reverse electron transfer, spin rephasing and other properties. Furthermore, it seems reasonable to assume that the disposition of donors about the acceptor could be influenced by their rates of diffusion; as other workers found when observing some kinetic aspects of an electron quenching reaction [32].

From the considerable documentary evidence on molecular interaction in solution, it is clear that some type of weakly bound transiently formed complex ensues after the initial meeting of donor and acceptor, all of which equilibriate to give

$$A + nD \quad \longrightarrow \quad AD_n \ , \qquad (1.20)$$

where n equals an integer, that leads to the overall stoicheiometry of the complex. The idea that a molecular complex is encompassed by a solvent cage has found wide acceptance for different reasons, which Foster [39] conveniently reviews while examining some aspects of solvation of the complex.

The dynamic state of equilibrium for reaction (1.20) will be disrupted if electron transfer between acceptor and donor occurs. An influx of the donor should rapidly replace those that react, because its molecular encounter with the acceptor only happens transiently and the most energetically favoured stoicheiometry of the complex will be retained.

b) STUDY PROPOSALS

Quite clearly there are many aspects to the formation of a transiently formed complex, but for the purposes of this project, it was decided to develop a method to ascertain the stoicheiometry of the complex and examine any interesting features that could influence its existence.

CHAPTER 2

MONOLAYER ASSEMBLIES AND DETERMINATION OF MOLECULAR THICKNESS

2.1 MONOLAYERS

Although later reports on the use of Whitten-type surfactants [18-22] as monolayers would appear to contradict Whitten's initial findings [16], it is well acknowledged amongst researchers that relatively very little is known about the micro-environment of a molecule after its incorporation into a monomolecular film (or monolayer). It is, therefore, possible that factors influencing this could have facilitated Whitten's success [16]. Thus, an alternate explanation to the synergist theory, that has so far qualified Whitten's sole success to cleaving water, is the fortuitous formation of a monolayer with a unique structure. Indeed, it is held by Whitten [34] and others [40,41] that notable differences in the reactivity of monolayers relative to a macro-molecular state can be attributed to certain specific factors, namely concentration, hydrophilic-hydrophobic interrelationships, diffusion restrictions, packing arrangements and orientation.

Often the assumption is, as made by Whitten [16,17], that a monomolecular layer is deposited. The intention of this aspect of the work is to investigate this by measuring the thickness of the films.

Much of the present knowledge of monolayers stems from the development of the so-called film balance, devised by Langmuir in 1917 [42] and later refined by Adam [43], which remains the principal instrument of study (see fig 2.1). Primarily it facilitates the

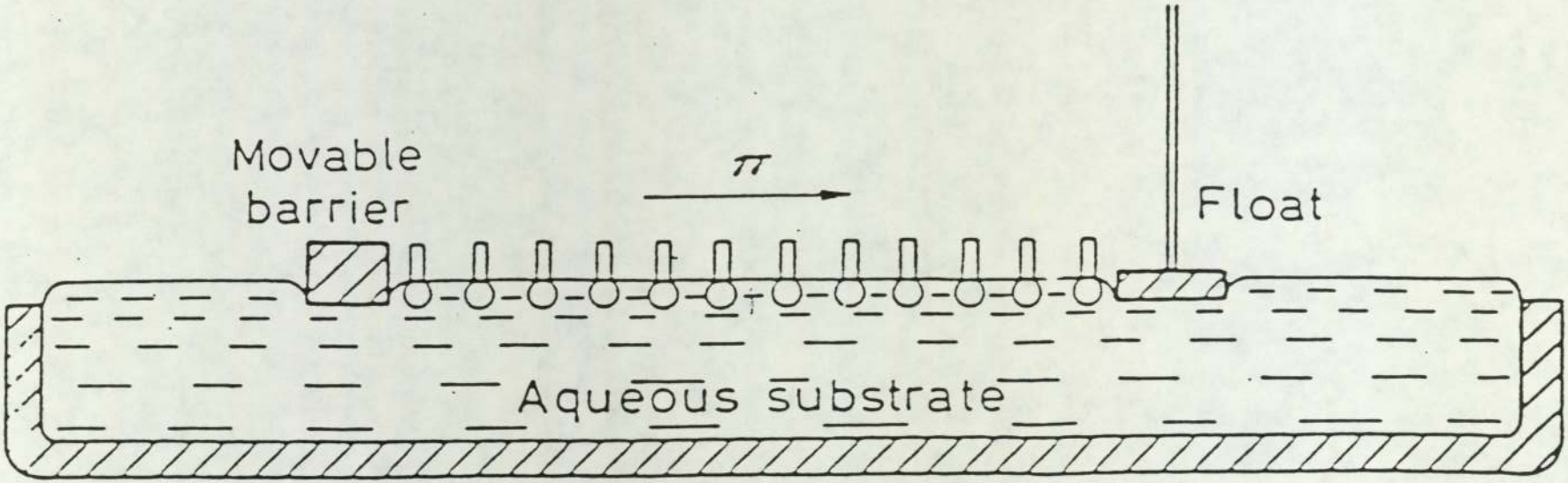

Fig. 2.1 The principle of Langmuir - Adam surface balance.

spreading of molecules on a liquid, as films of a mono-molecular thickness. Langmuir [42] rightly concluded that the ability of such materials to form films of this type was a direct consequence of the structure of the molecules. These must possess both polar groups and extensive non-polar hydrocarbon groups and are thereby defined as amphiphilic molecules. From fig 2.1, it can be seen that the hydrophilic polar heads of the molecule (represented by circles) are immersed in the aqueous subphase, whilst the hydrophobic nature of the non-polar groups (represented by rectangular blocks) ensure that they are orientated away from the water.

As the surface-active material (or surfactant) is strongly adsorbed at the surface, it is essentially in a state of dynamic equilibrium. This arises because of the thermal motion of the molecules in the surface film, which exists due to its balanced tendencies to adsorb or completely mix with the subphase. This phenomenon is equally applicable to other interfaces (e.g. liquid-solid).

In routine practice, use of the Langmuir apparatus (see fig. 2.1) is commenced by preparing a solution of known concentration of surfactant in a volatile solvent and spreading a measured volume of this solution onto an aqueous subphase. The solvent is then allowed to evaporate to leave a surface film of the surfactant.

If the film is compressed, intermolecular repulsions resist the compression and consequently generate a surface pressure (Π). This pressure initially moves the float (see fig. 2.1) and can be measured

directly if an equivalent counteracting force is exerted on the float to maintain its original position.

The film is compressed by the movable barrier to form a 'monolayer', the existence of which can be detected by the initial rapid increase in pressure detected at the float. The total area of the 'monolayer' film can be measured using the accurate scale on the perimeter of the Langmuir trough retaining the spread film. When a portion of the film is taken from the trough and deposited onto a support slide of known area, the resulting change in the total area of the film can be readily measured. The film: support slide area deposition ratio can then be determined.

The film's surface pressure may also be viewed as the lowering of surface tension of the subphase due to presence of the monolayer. Thus,

$$\Pi = \gamma_0 - \gamma \qquad (2.1)$$

where γ_0 and γ are the surface tensions on the clean interface and interface plus monolayer respectively.

Film balances with appropriate modifications can facilitate the measurement of the surface pressure and other related film properties such as surface viscosity and potential [46].

Although Langmuir [44] pioneered the process of transferring a floating insoluble monolayer onto a solid support (or substrate), it was Blodgett [45] who extended the applications of the technique and as

such, it is often prefixed with her name. These achievements in deposition of the monolayer were the forerunners to the present activity in the pursuance of monolayer studies.

2.2 MOLECULAR FILM THICKNESS MEASUREMENTS

Work by Pitt and Walpitta [47] has demonstrated the value of investigating the propagation of optical waves along a Langmuir-type thin film (the monolayer assembly). They show that any modification to propagation properties can be related to molecular length, refractive index and film thickness. Hence they derive an expression to calculate the film thicknesses of various substances using certain approximations. The apparent downfall of the method in its application to monolayers of surfactant derivatives of $Ru(bipy)_3^{2+}$, is that it is extremely difficult to assign refractive indices when light is strongly absorbed by the specimen of interest. However, their method [47] provides useful references for thicknesses of fatty acids and their derivatives, together with corresponding refractive indices.

The use of multiple beam interferometry, described by Tolanski [48] and developed by Scott [49] enables very accurate film thicknesses to be determined. Unfortunately, the degree of accuracy is also strongly related to the film thickness and consequently, errors in the measurement increase as the film thickness decreases.

Fortunately, a more sensitive method for film thickness measurement derives from the reflection of polarised light by surface metals and films. In order to briefly illustrate this phenomenon (a more in depth description is given later) it is necessary to represent

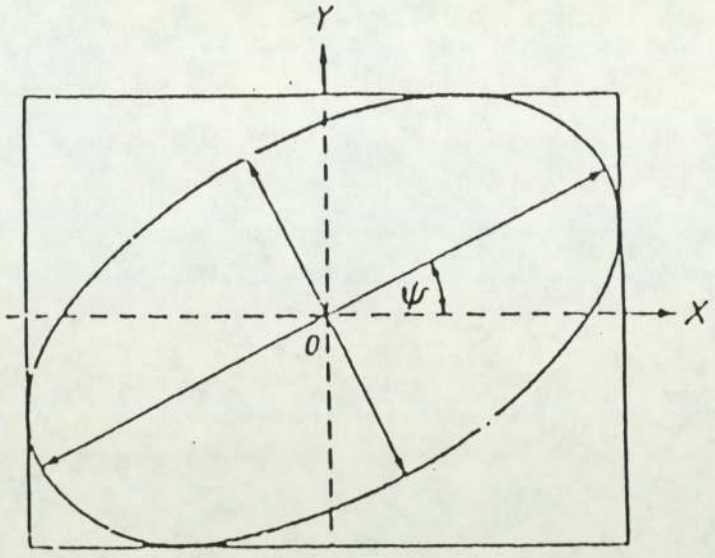

Fig. 2.2 The Polarisation ellipse for the electric vector (E); the ratio of the lengths of minor to major axes of the ellipse determines its ellipticity (γ).

the linearly polarised light, which impinges on the surface initially, as an electric vector which has two equivalent vector components that vibrate perpendicularly to each other and to the propagation direction, but outside the plane of incidence (this statement will be qualified later). As a consequence of interaction at a surface layer one component will be reflected, while relatively more of the other component is transmitted and as a result, the tip of the vibrating vector (emerging after reflection) traces an ellipse (see fig. 2.2). The ellipticity, γ, which essentially describes the ellipse in terms of the ratio of the lengths of its minor to major axes (the axes being at 90^{o} to each other) is dependent on film thickness. Consequently,

the elliptically polarised light contains information about refractive index and of the surface or film. The study and measurement of modified polarised light has been called ellipsometry by Rothen [50].

The recent revival of the ellipsometry technique is due mainly to the availability of modern-day computers, which are essential for the numerous analytical calculations involved. Its application is further augmented by claims of versatility by Oshea [51] and accuracy of thickness measurement by Rothen [52]. McCrackin et al [53] also claim that the lower limit of film thicknesses that can be studied by ellipsometry is at least an order of magnitude smaller than can be studied by other means such as interferometry. Therefore, the ellipsometric method possibly offers the best route for the measurement of thicknesses of monolayers of surfactant derivatives of $Ru(bipy)_3^{2+}$.

2.3 ELLIPSOMETRY

2.3.1 GENERAL DESCRIPTION OF THE ELLIPSOMETRIC EXPERIMENT

Fig. 2.3 represents the typical ellipsometric experiment. The monochromatic light is first linearly polarised and then impinges on the surface to be studied. The reflected beam, which is elliptically polarised, is returned to linear polarisation by the compensator; the angle of this polarisation is determined principally by the setting of the analyser so that the detector sees zero light. Thus, the experimentally measured quantities are the polariser angle and the analyser angle x. These angles give the fundamentally desired quantities, viz, the phase difference, Δ, between the parallel and

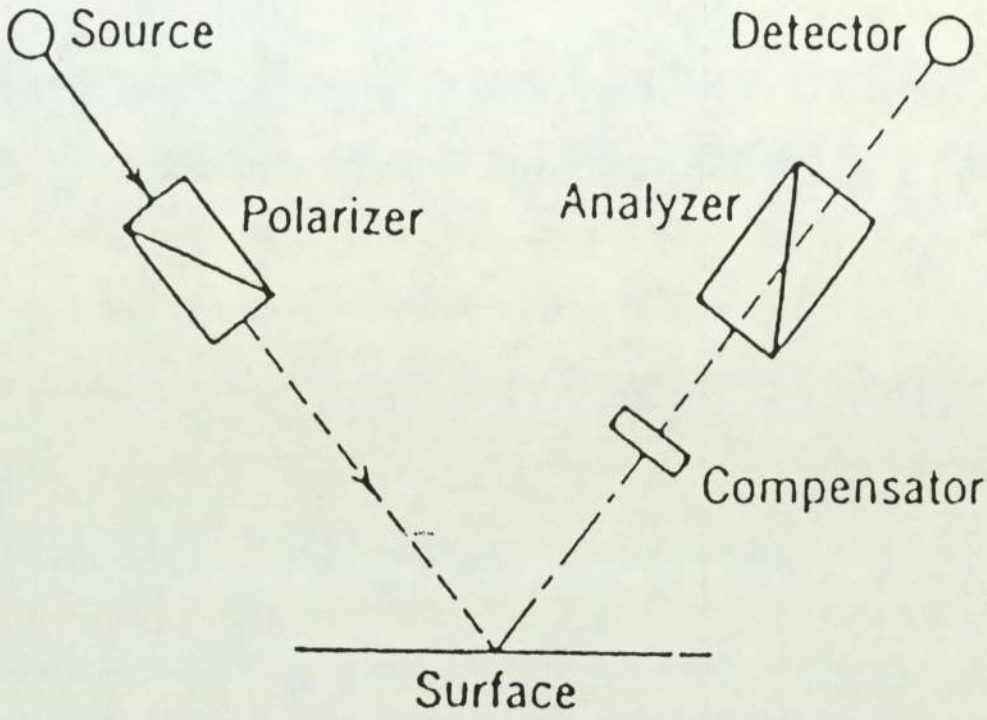

Fig. 2.3 Schematic representation of the ellipsometric experiment; ---- unpolarised light; - - - linearly polarised light; --- - --- elliptically polarised light.

perpendicular components of the electric vector and the change in amplitudes of these components, tan ψ. It can be shown that $\Delta = 2x + 90^{0}$.

2.3.2 THE ACHIEVEMENT OF LINEARLY POLARISED LIGHT

Clerc Maxwell, in about 1865, was the first to give a foundation to the composite nature of the continuum of wavelengths that comprise the electromagnetic spectrum. In so doing, he demonstrated that light could be described in terms of the interdependence of related phenomena, namely electric charge, electrostatic field and magnetic field. Thus, visible light may be resolved into electric and magnetic vector components that vary sinusoidally (see fig 2.4), the frequency of which is dependent on the electronic transition within an atom or molecule (a movement of charge) that caused the emission of light.

The vectors oscillate at right angles to each other and to the direction of propagation (see fig. 2.4), cannot be separated and are functions of space and time. A changing electric vector produces a corresponding change in the magnetic vector and vice versa. However, it is conventional practice in optical descriptions to only specify the electric vector in preference to the magnetic vector. Clark and Grainger [54] give comprehensive details to the reasons for its use.

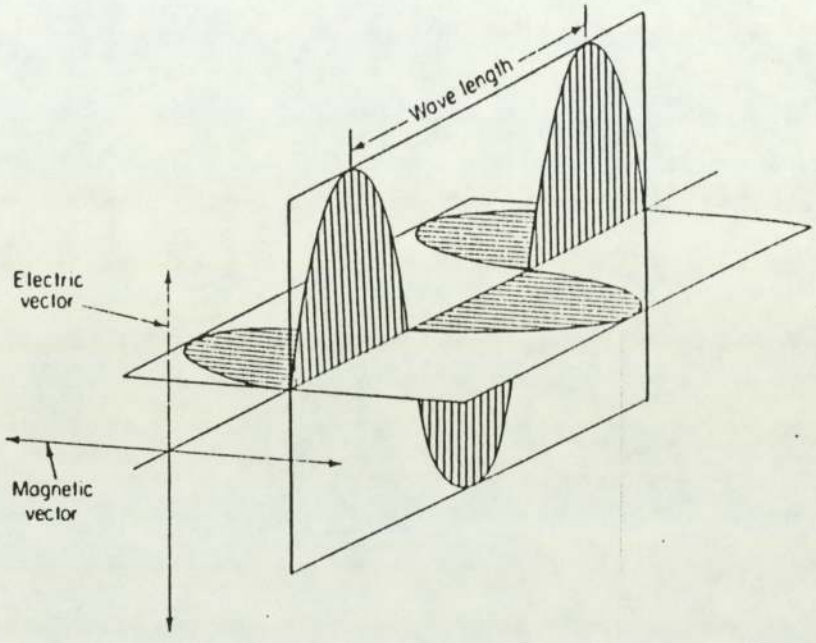

Fig. 2.4 Electromagnetic wave represented by electric and magnetic vector components.

Normally the electric vector will vary in direction from one instant to the next to occupy all positions around the direction of propagation. Conversely, if the electric vector is restricted to one perpendicular direction about the propagation direction, the light is then termed as linearly polarised in a given plane (see fig. 2.5a). This latter state is often achieved by the selective absorption of light by crystalline substances that are anisotropic: Quinine iodosulphate and calcite are typical examples (see fig. 2.5b).

2.3.3 THE USE OF LINEARLY POLARISED LIGHT IN ELLIPSOMETRY

If the electric vector (E) is resolved into its two components, these are considered to be vibrating perpendicularly to each other and in phase (see fig. 2.6). In further reference to fig. 2.6, where linearly polarised light is travelling in the x direction, E makes an angle α with the y direction and $90^{o} - \alpha$ in the z direction, such that

$$E_y = E\cos\alpha = E_p \qquad (2.2)$$

$$E_z = E\sin\alpha = E_s \qquad (2.3)$$

where E_p and E_s are resolved components parallel and perpendicular to the plane of incidence. If linearly polarised light is now arranged such that it is incident on a homogeneous isotropic surface film which has parallel boundaries, then only when E_p and E_s are vibrating parallel and perpendicular to the plane of incidence will conditions (2.2) and (2.3) stand true after reflection: These unique propagation directions are called azimuths and are used as reference positions.

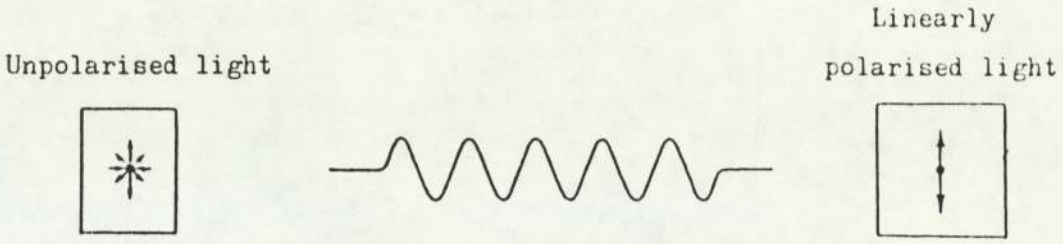

Fig. 2.5a Linearly polarised light represented as a projection of a light wave on a plane intercepting the axis of propagation.

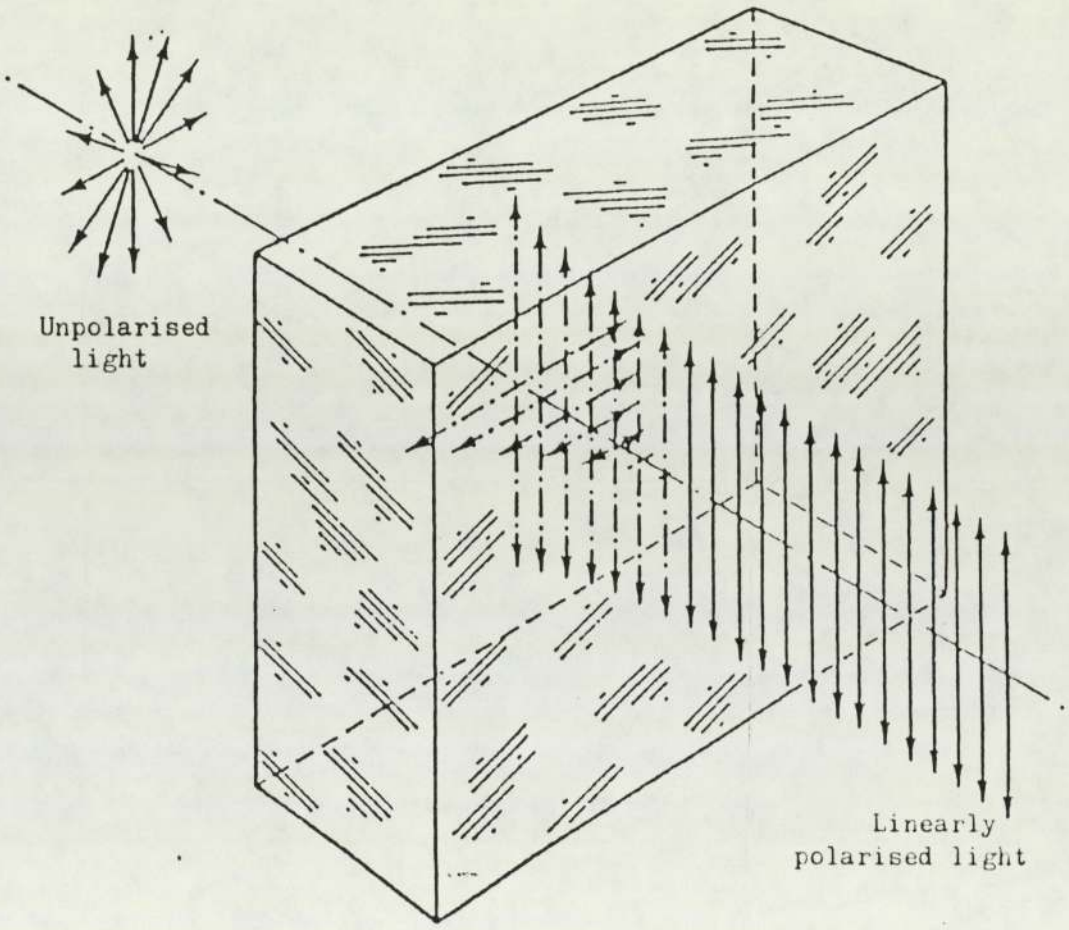

Fig. 2.5b Linear polarisation by selective absorption.

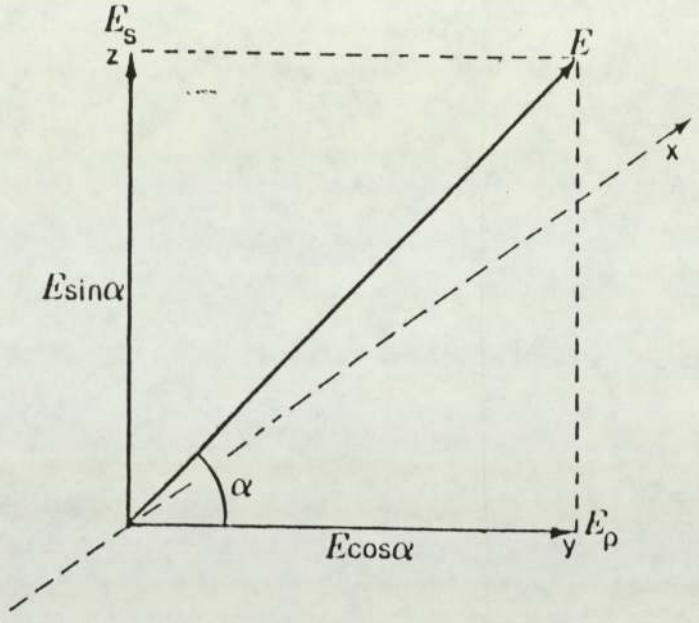

Fig. 2.6 The electric vector (E) resolved into parallel (E_p) and perpendicular (E_s) components, acting at right angles to each other and to the propagation direction.

Otherwise reflection at the surface can in general change the relative amplitude and/or phases of E_p and E_s, which emerge with the same frequency, but have different amplitudes and are out of phase.

It can be shown that after reflection the nature of the curve which the terminus of the electric vector describes at a typical point in space, is the locus of the points, the co-ordinates of which (E_y, E_z) are given by

$$E_y = E_p \cos(wt + \theta_y) \tag{2.4}$$

$$E_z = E_s \cos(wt + \theta_z) \tag{2.5}$$

If both components are in phase $\theta_y = \theta_z$ or if in opposite phase $\theta_y - \theta_z = \pm\pi$ rad (180^o) and therefore

$$E_y/E_z = \pm E_p/Es \tag{2.6}$$

However, if E_p and E_s have arbitrary phase, as in equations (2.4) and (2.5), the resultant vector can be considered to be compounded of two simple harmonic motions (S.H.M.'s) of the vector components which are out of phase and represented by the general equation of an ellipse:

$$(E_y/E_p)^2 + (E_z/E_s)^2 - 2(E_yE_z/E_pE_s)\cos\Delta = \sin^2\Delta \tag{2.7}$$

where $$\Delta = \theta_y - \theta_z \tag{2.8}$$

and for which Δ is a non integral value of π rad: Fig. 2.7a shows the light path for right-elliptically polarised light, for which the tip of the electric vector (E) proceeds in the form of a 'flattened

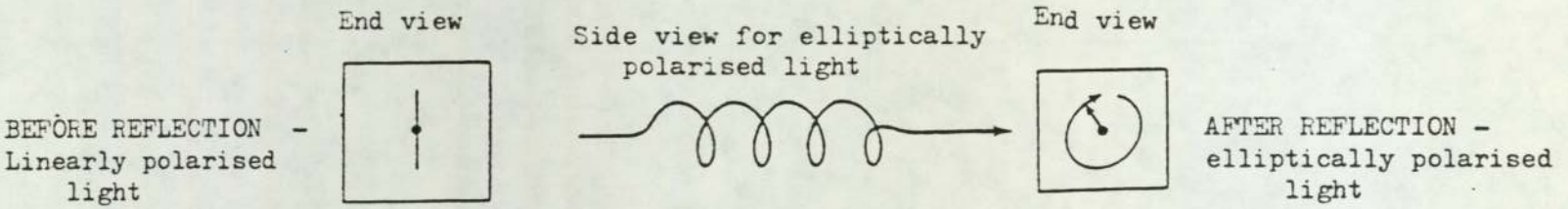

Fig. 2.7a The change in the electric vector (E) for different states of polarisation.

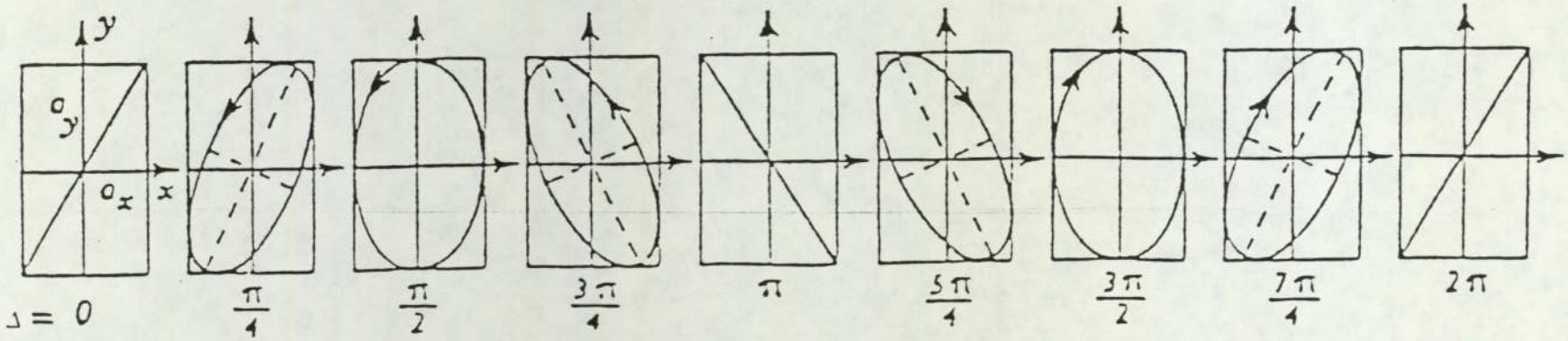

Fig. 2.7b The combination of the S.H.M.'s of E_p and E_s after reflection from a surface: a_x and a_y represent the amplitudes of E_p and E_s respectively.

helix'. A summary of the effects of some principal phase changes (Δ) to E_p and E_s, because of reflection from a surface, is given in fig. 2.7b (the light path is towards the observer) in terms of π rad.

In further reference to fig. 2.7b, when $\Delta = 0, \pi, 2\pi$ ---, linearly polarised light results, because E_p and E_s, which are in phase (coherent) or opposite phase, are aligned with the reference azimuths. Alternatively, when $\Delta = \pi/4, 3\pi/4, 7\pi/4$ ---, this will give rise to an ellipse with axes across the reference azimuths: E_p and E_s being out of phase by a non-integral value of π. By similar arguments when $\Delta = \pi/2$ and $3\pi/2$ an ellipse results, but the axes of the ellipse fall in-line with the azimuths. Interestingly, in this later case, circularly polarized light will be produced if the amplitudes of E_p and E_s are equal. From this, it is important to note that differences in the value of E_p and E_s before and after reflection provides a measure of corresponding amplitude change to the electric vector, E. Thus, for circularly polarised light $E_p/E_s = 1$, but becomes less than 1 for elliptically polarised light. It will be shown that

$$E_p/E_s = \tan\psi \qquad (2.9)$$

where ψ is a measurable angle that represents the amplitude change for E.

The objective of ellipsometric measurement is to determine values for the phase (Δ) and amplitude (ψ) changes of the electric

vector (E). To do this requires some knowledge of the interaction of linearly polarised light at an optical boundary (defined at the beginning of this section). If the incident light is vibrating in a plane outside the azimuthal directions, then reflection from a surface film can produce a phase difference (Δ) for E_p and E_s, because light is coming from upper and lower levels of the optical boundary (see fig 2.8): There is also a change to the amplitude ratio of E_p and E_s (ψ).

2.4 CHARACTERIZING A SURFACE

The whole process of reflection of linearly polarised light from a surface (an optical boundary) is described in terms of Fresnel reflection coefficients. In its basic form the Fresnel coefficient r at the boundary between two media is given by

$$r = \frac{\text{amplitude of the reflected vector}}{\text{amplitude of the incident vector}} \qquad (2.10)$$

The application of equation (2.10) to resolved components of the electric vector, produces r_p and r_s, which correspond to vector vibrations parallel and perpendicular to the plane of polarisation respectively, (but outside the azimuthal directions).

2.4.1 NON-ABSORBING MEDIA

In dealing with two non-absorbing media (see fig 2.8) the basic Fresnel expression may be put in an alternative form that incorporates

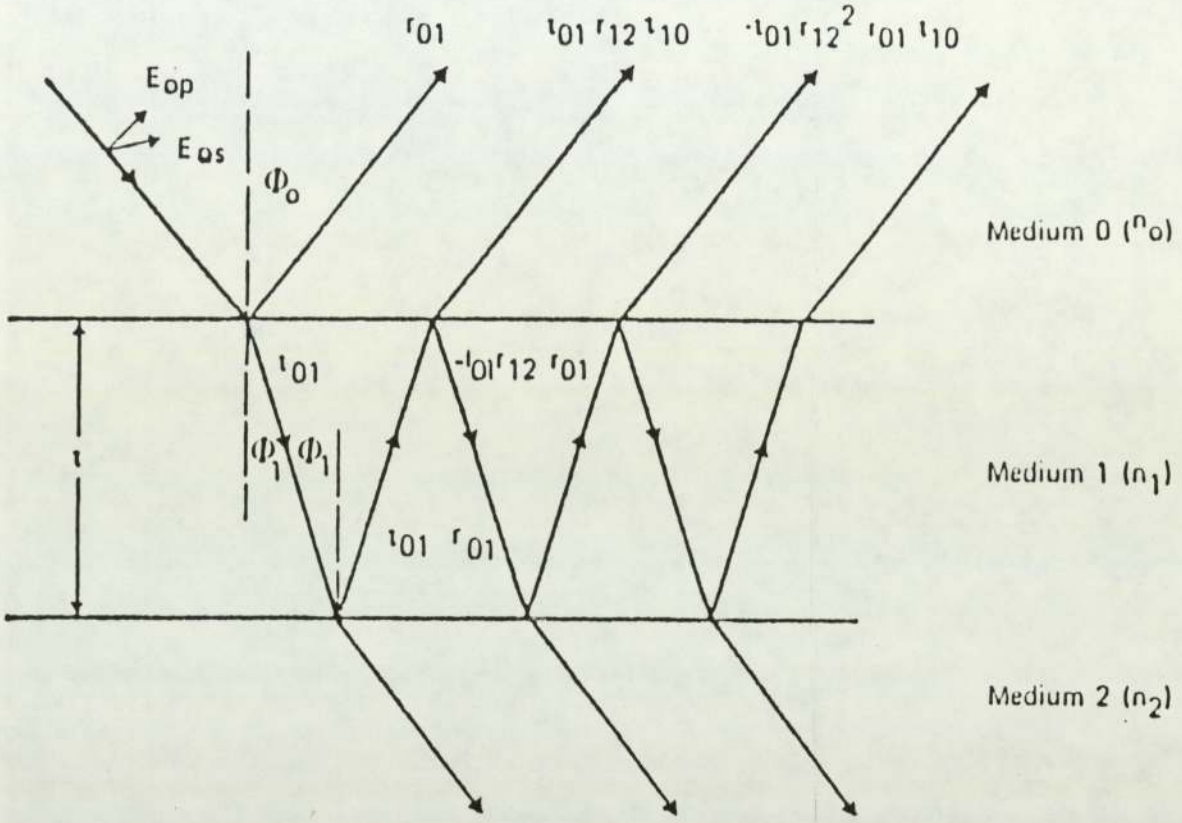

Fig. 2.8 Multiple reflections in a film or surface layer.

the angle of incidence $\emptyset_0$ in medium 0, the angle of refraction $\emptyset_1$ in medium 1 and the respective refractive indices; (n_0 and n_1) such that,

$$(r_{01})_p = \frac{n_0\cos\emptyset_1 - n_1\cos\emptyset_0}{n_0\cos\emptyset_1 - n_1\cos\emptyset_0} \qquad (2.11)$$

Equation (2.11) represents the reflection coefficient at the boundary of medium 0 and medium 1 for the electric vector resolved parallel to the plane of incidence. A similar expression may be produced for the electric vector resolved perpendicular to the plane of incidence, $(r_{01})_s$.

Ultimately it is possible, through mathematical derivation (illustrated by Oshea [51]), to arrive at an equation that summarises the whole physical perturbation as follows:-

$$(r_{01})_p/(r_{01})_s = \tan\psi\, e^{i\Delta} \qquad (2.12)$$

where $\tan\psi$ represents the relative amplitude reduction and Δ the phase difference for the (p) and (s) components of the electric vector (see section 2.7, fig 2.14 for a more precise description of $\tan\psi$). Although equation (2.12) is shown in its simplest form, it describes the outline of an ellipse and is the fundamental equation of ellipsometry. The parameters ψ and Δ are related through the Fresnel reflection coefficients to the refractive index and thickness of the

specimen film, (see fig. 2.8) together with the angle of incidence of the selected light beam. ψ and Δ are determinable by instrumentation (see later).

2.4.2 ABSORBING SURFACE MEDIA

For absorbing layers the Fresnel reflection coefficients are complex, because the classical refractive index has to be replaced by a complex refractive index (see below). The terms in the complex refractive index are referred to as optical constants, which will now be discussed.

Optical constants were invoked initially to explain the optical properties of metals and it was Drude [57] in 1902 who first suggested the concept of penetrative interaction when light impinged on a metal with a resulting change in electrical conductivity. Cauchy [58] introduced the idea of a complex refractive index to explain the coupling of light and metals. In his treatment the electrical field inside the metal is represented by:-

$$E = E_0 e^{-kwx} \cos w\left(\frac{nx}{c} - t\right) \quad (2.13)$$

where n, the refractive index, and k, the extinction coefficient, are optical constants. In order to incorporate a factor for absorbing media, equation (2.13) now becomes more complex, viz

$$E = E_0 e^{-iw\left(\frac{Nx}{c} - t\right)} \quad (2.14)$$

where

$$N = n - (ik) \quad (2.15)$$

and is called the complex refractive index: For non-absorbing media the k value is equated to zero and the refractive index assumes the classical form. In equation (2.15) the bracketed term, which is derived to explain absorption, takes on particular significance in the application of ellipsometry to vividly coloured charge transfer derivatives of $Ru(bipy)_3^{2+}$.

Provided that the angle of incidence (denoted $\emptyset_0$) is known, it is possible to calculate the optical constants for a particular surface type at a given wavelength by using Ditchburn's [59] equations for absorbing surface media. In his equations $n^2 - k^2$ and nk are expressed as functions of ψ , Δ, and the angle of incidence, $\emptyset_0$, as follows:-

$$n^2-k^2 = \frac{\sin^2\emptyset_0\tan^2\emptyset_0(\cos^2 2\psi - \sin^2 2\psi\sin^2\Delta) + \sin^2\emptyset_0}{(1 + \sin^2\psi\cos\Delta)^2} \qquad (2.16)$$

$$2nk = \frac{\sin^2\emptyset_0\tan^2\emptyset_0\sin 4\psi\sin\Delta}{(1 + \sin 2\psi\cos\Delta)^2} \qquad (2.17)$$

The addition of any thicknesses of film to the starting substrate (the films support medium) will give a unique set of optical constants while incorporating changes for the parameters ψ and Δ.

2.5 THE RELATIONSHIP OF THE PARAMETERS n, k, ψ, Δ AND $\emptyset_1$ TO FILM THICKNESS (t)

2.5.1. NON-ABSORBING LAYERS

In the case of a non-absorbing surface Neal [60] has written the Fresnel reflection coefficients for media 0, 1 and 2 as:-

$$(r)_{p,s} = [(r_{01})_{p,s} + (r_{12})_{p,s} \exp(D)] \; [1 + (r_{01})_{p,s}(r_{12})_{p,s} \exp(D)] \qquad (2.18)$$

where $$D = 4\pi(\cos\emptyset_1)n_1 t/\lambda \qquad (2.19)$$

n_1 is the refractive index of the surface film, t the layer thickness, $\emptyset_1$ the angle of refraction and λ the wavelength of light.

2.5.2 ABSORBING LAYERS

Previously, it has been demonstrated that, if a surface layer is absorbing, then the value n_1, and correspondingly r_s and r_p, are given more complex roles and $(n_1 - ik_1)$ is used as a direct replacement for n_1. In this instance equation (2.19) becomes:-

$$D = 4\pi i(\cos\emptyset_1)n_1 t/\lambda \qquad (2.20)$$

Whereas the previous equation (2.19) shows that there are two unknown quantities n_1 and t, there are three values to be found in the latter equation (2.20), namely n_1, k and t. In order to alleviate the

tedium involved with their derivation it is essential to have access to computer facilities. In this present work a computer program, written in Algol language by Oshea [51], is utilised to calculate ψ and Δ for assumed values of n and k. In practice n and k are varied iteratively until consistency between the deduced and experimental values of ψ and Δ is achieved. The iteratively selected values of n and k are then used with ψ and Δ to yield the film thickness, t.

2.6 A BRIEF INTRODUCTION TO THE ELLIPSOMETER

2.6.1. COMPENSATOR METHOD

An ellipsometer (see fig. 2.9 for construction details) can facilitate the determination of the angles ψ and Δ, representing amplitude and phase changes to the electric vector (E) respectively, by

1) Applying a reciprocal phase difference through a compensator (see fig. 2.10) to the electric vector of the elliptically polarised light to re-establish linearly polarised light (called compensation).

2) Measuring the respective angles of ψ and Δ from a polariser (this unit gives linearly polarised light that is incident on the surface layer) and an analyser (this unit examines the state of polarisation of the light after reflection from a surface): ψ being the angle between polarisation setting and the horizontal azimuth at extinction (that is when no light is transmitted), while Δ is derived from the angle x, which lies between the analyser and the horizontal axis at extinction.

$\Delta = 2x - 90$ (see section 2.8 for derivation of Δ) (2.21)

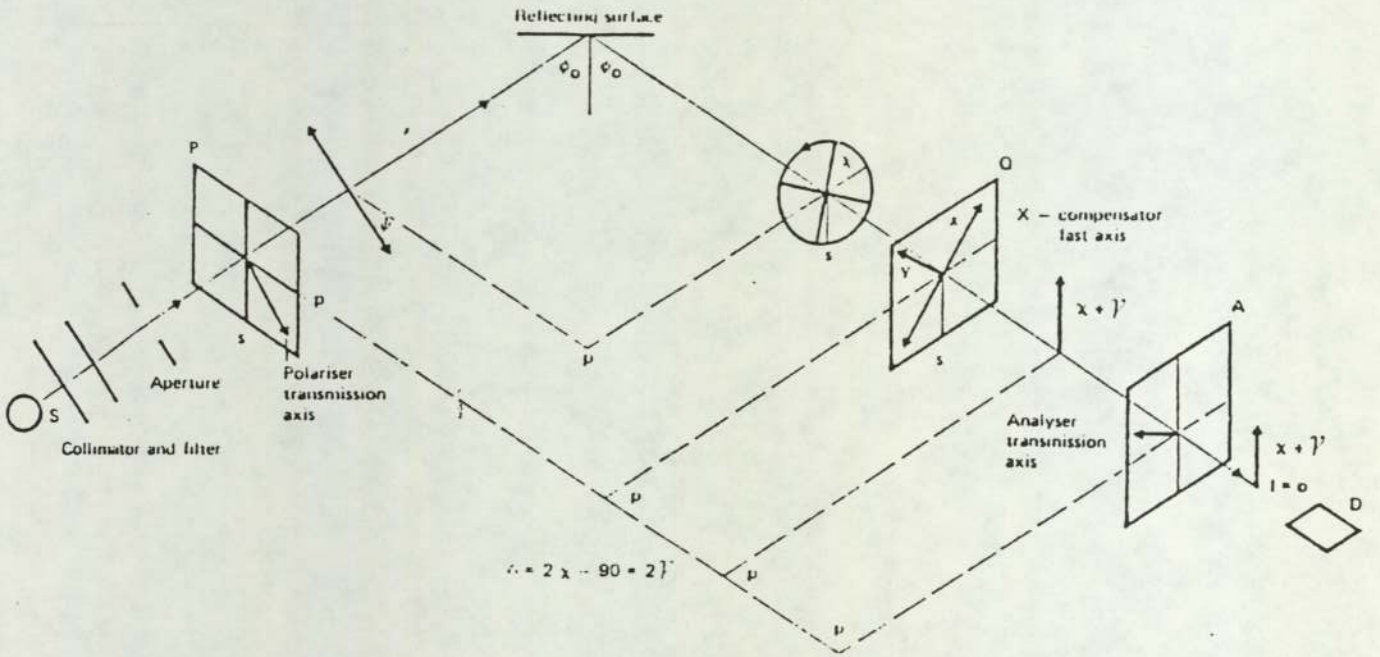

Fig. 2.9 The arrangement for the basic components of an ellipsometer (compensator method).

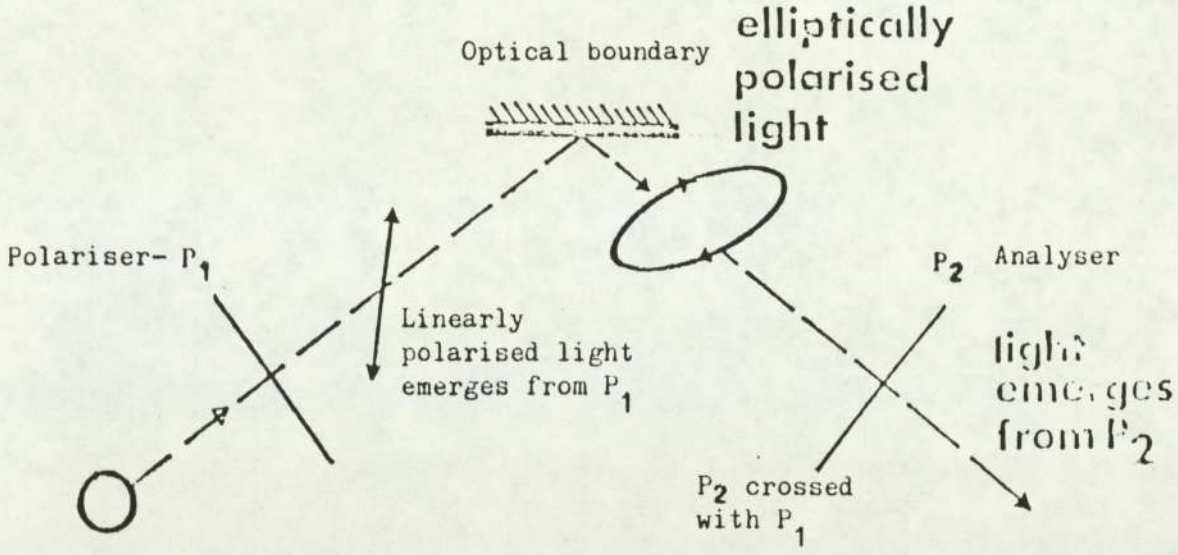

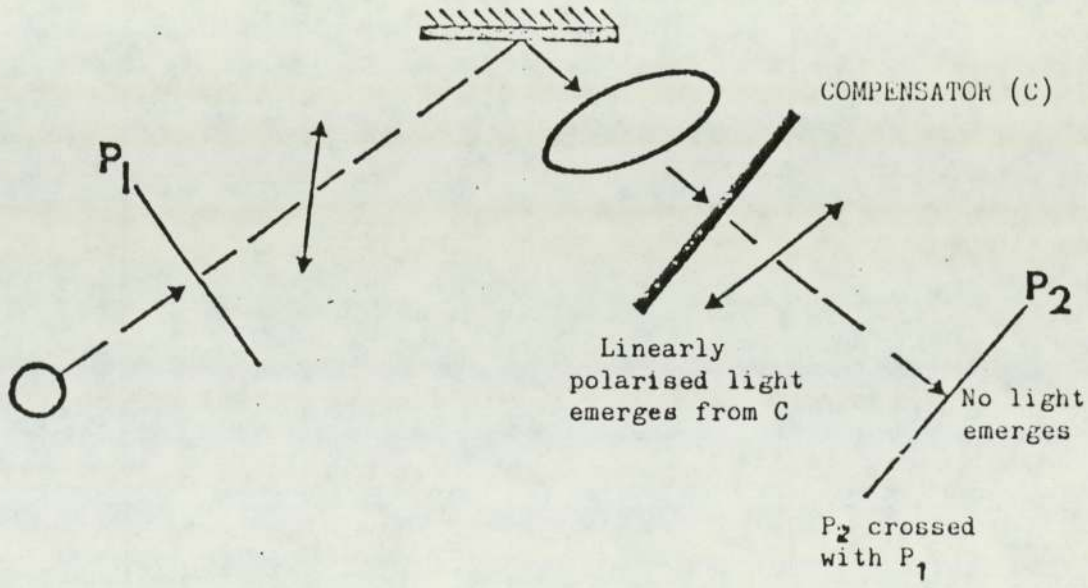

Fig. 2.10 The effect of a compensator

It is important to note, that by solely applying phase compensation to the electric vector (E) does not guarantee extinction if E has also changed in amplitude and consequently the polariser has to be rotated to achieve full extinction.

2.6.2 AN ALTERNATIVE TO THE COMPENSATOR METHOD

The research work of Beattie and Conn [55] showed that reflectivity measurements in the infra-red region were relatively insensitive and they devised an alternative method of measuring the polarisation ellipse. This was based on the theoretical work of Conn and Eaton [56], and dispensed with the compensator. Although the latter method is applicable to the visible region it is dependent upon obtaining absolute intensity measurements, whereas the compensator method only requires the determination of certain instrumental positions from the polariser, analyser and compensator at extinction to obtain ψ and Δ.

The compensator method is preferred when a sample is a strong absorber of light, as the intensity of the reflected light will normally show marked attenuation over the incident light. Consequently, the compensator method was chosen for the ellipsometric study of surface films of Whitten-type surfactants, as their 'vivid colours' effectively categorised the compounds as 'strongly absorbing' from an optics viewpoint.

2.7 BASIC THEORY OF COMPENSATOR ELLIPSOMETRY

Certain crystalline anisotropic substances, such as calcite, mica and quartz, can transform a beam of monochromatic visible light into two distinct refracted beams (or rays) of linearly polarised light. The two rays of light travel through the crystal at velocities determined by their alignment with axes of the crystal structure. Such axes are sometimes referred to as privileged directions of the crystal, but more often the privileged direction corresponding to the faster ray is called the fast axis and that for the slow ray, the slow axis.

The terms ordinary and extraordinary are the terms used to describe the rays depending on whether their respective vibrational directions are in or out of the plane of incidence of the light beam (see fig 2.11). The phenomenon is known as double refraction, or birefringency, and is the foundation of the development of compensator devices in ellipsometry.

The passage of linearly polarised light through a birefringent crystal generally produces elliptically polarised light (circularly and linearly polarised light results under certain circumstances - see below) because one resolved component of the electric vector is moving through the crystal with a greater velocity than the other (see fig.2.12). The extent to which E_p and E_s vary in velocity, will depend on the orientation of E in relation to the optical axes of the crystal. Consequently, the electric vector varies in phase about the direction of propagation, such that its terminus is moving in an ellipse. Therefore, it follows that the form of the ellipse is

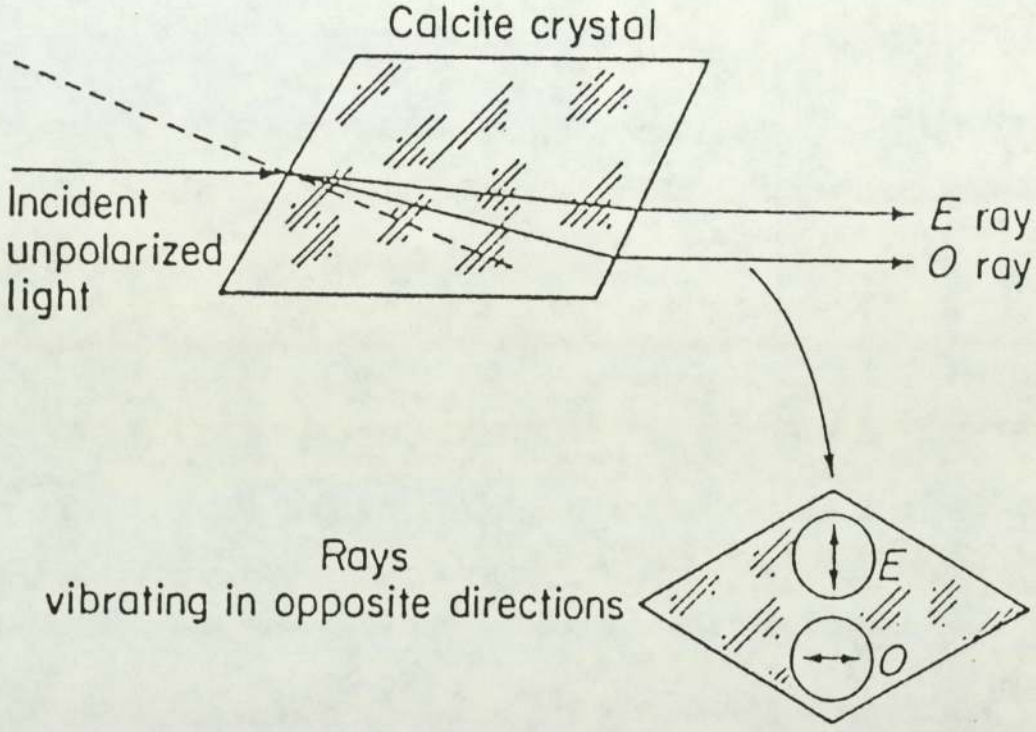

Fig. 2.11 Double refraction in the calcite crystal.

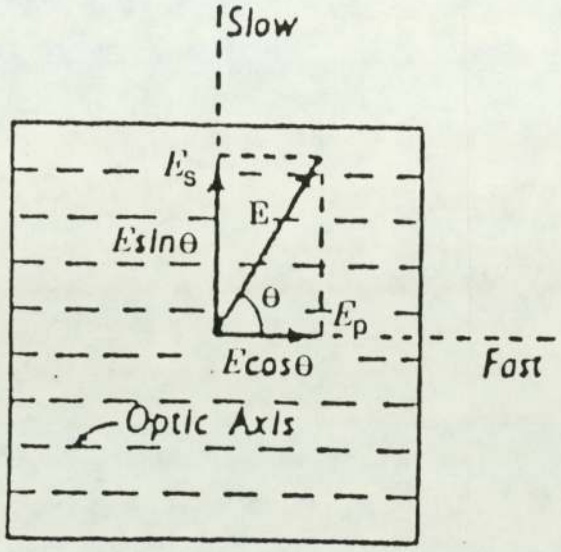

Fig. 2.12 Resolution of E_s and E_p along the fast and slow axes of an anisotropic crystal.

dependent on differences in phase and magnitude for emerging E_p and E_s components of the electric vector. It is important to note that E_p and E_s are superimposed upon emerging from the crystal.

It is also possible to change elliptically polarised light into linearly polarised light. However, for this transformation to occur, the birefringent material must be of a thickness such that it imparts a phase difference of 90^o between the ordinary and extraordinary rays of the electric vector. As there is already a phase difference of $>$or$<90^o$ for vibrations of E_p and E_s along the major and minor axes of the ellipse, these are again brought into phase on emerging from the crystal. Consequently, the superimposition of the emerging E_p and E_s rays (which differ in phase by 90^o at the point of emergence from the crystal) results in linearly polarised light (see fig. 2.13).

Quite clearly the acquired phase change of 90^o arises because the faster component of the electric vector leads the slower component by a path difference of a quarter of a wavelength of the incident radiation ($\lambda/4$) for any orientation of the ellipse. Appropriately, the birefringent compensator is now called a quarter wave plate.

Essentially, the ellipsometry experiment is striving to achieve equality for E_p and E_s components of the electric vector in order that the reflected amplitude ratio $E_s/E_p = 1.0$. If this condition is satisfied, the electric vector will be positioned at an angle

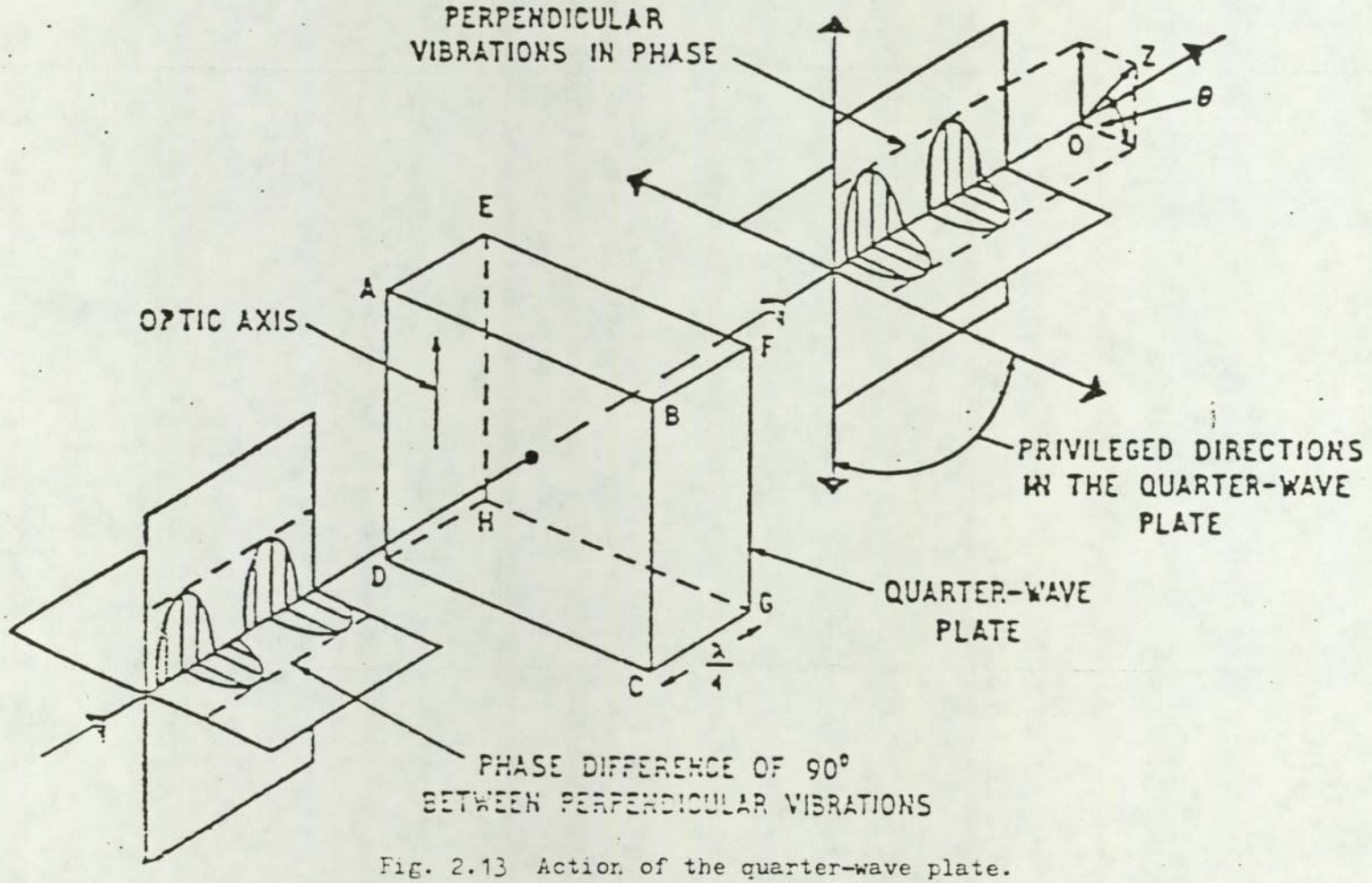

Fig. 2.13 Action of the quarter-wave plate.

(designated ψ) of 45^0 to the horizontal azimuth of the polariser (see fig 2.14), because $\tan \psi = 1.0$, it follows that $\tan^{-1} 1 = 45^0 = \psi$. Additionally, an angle of 45^0 for ψ , will only result via compensation of circularly polarised light, since its E_p and E_s components have equal amplitude but differ in phase.

For elliptically polarised light, differences in phase and amplitude can co-exist for the E_p and E_s components of the electric vector. Although the relative phase change of E_p and E_s components remains determinable, after compensation, from analyser measurements, the direct measurement of ψ off the polariser (see fig 2.14) will now reflect the difference in amplitude of E_p and E_s. Consequently, ψ cannot correspond to an angle of 45^0, as in previously mentioned circumstances, because this would require no movement of the polariser to achieve extinction. However, the major axis of the ellipse will be inclined at 45^0 to the plane of incidence (see fig 2.14) and it is, therefore, convenient, but a matter of choice, to set the compensator at 45^0 to its fast axis (see fig 2.12), in order that light of any ellipticity is converted to linearly polarised light. The analyser and polariser may then be set to their light extinction positions, since linearly polarised light is now prevailing. Accordingly a sum of 8 readings (separated by 90^0) is now made available from the analyser and polariser for one distinct setting of the compensator.

There are three other similar compensator positions separated by 90^0, which may also be utilised in measurement, this would give a total of 32 polariser and analyser positions per sample. In practice the analyser and polariser are moved by equivalent amounts either side

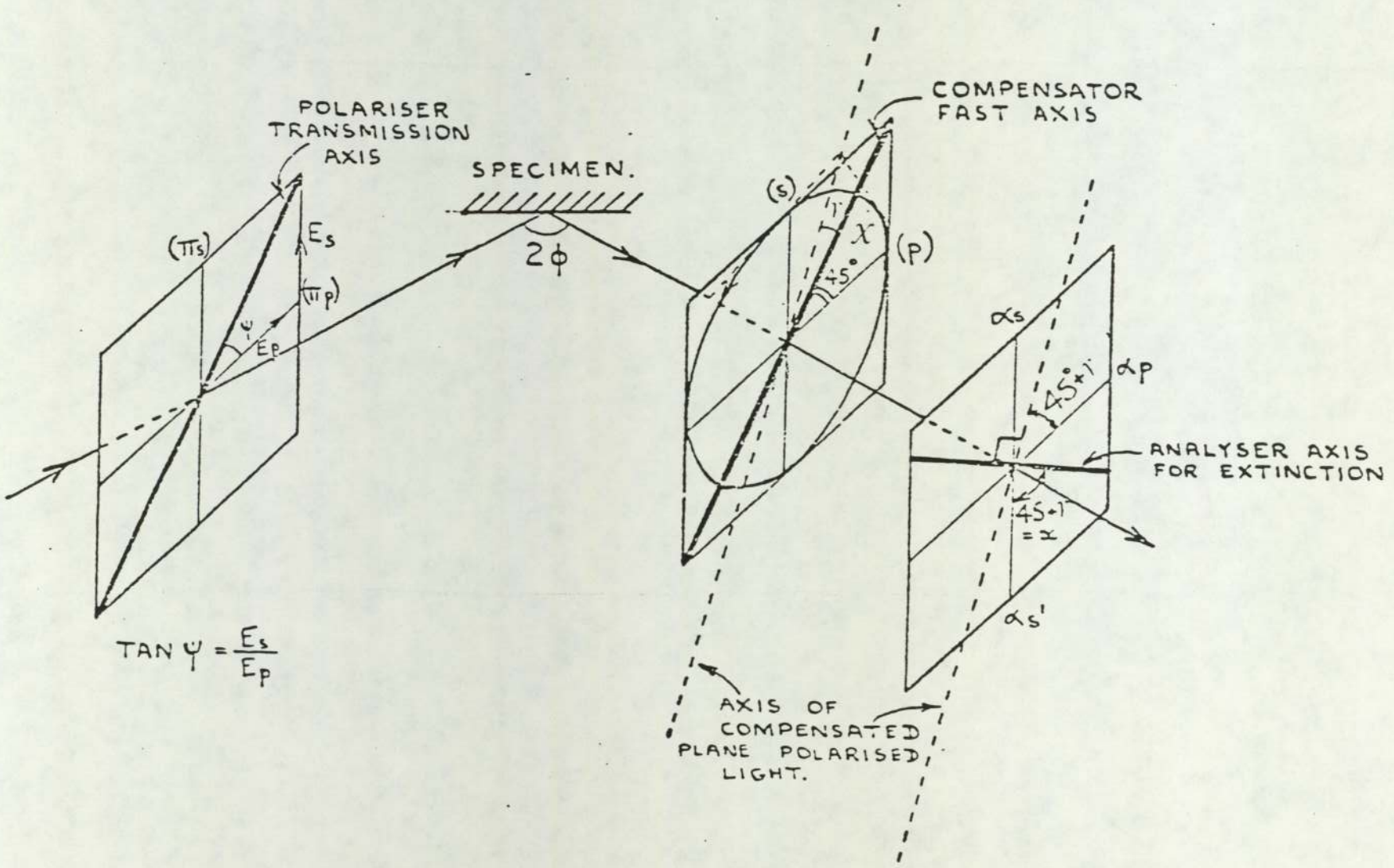

Fig. 2.14 A diagram to show the various ellipsometric parameters.

of their extinctions, so that an average value may be derived (see section 2.9.7c). As this would double the number of measurements per sample to 64, it is customary, in order to quicken the analysis time to choose only two positions of the compensator.

2.8 DETERMINATION OF THE RELATIVE PHASE DIFFERENCE (Δ) FOR P AND S COMPONENTS OF THE ELECTRIC VECTOR, FROM ANALYSER MEASUREMENTS

It is now established that elliptically polarised light results partly because there is a phase difference (Δ) for p and s components of the electric vector. In deriving Δ from analyser measurements, it may be shown that

$$\tan\Delta = \frac{\tan 2\psi}{\sin 2\chi} \qquad (2.22)$$

where ψ is the ellipticity of the polarisation ellipse and represents the angle between the major axis of the ellipse and the horizontal azimuth (see fig 2.9).

$$\text{Since } \chi = 45^{\circ}, \quad \text{(see fig. 2.14)} \qquad (2.23)$$

$$\sin 2\chi = 1 \qquad (2.24)$$

$$\text{therefore } \tan\Delta = \tan 2\psi \qquad (2.25)$$

Referring to figs. 2.9 and 2.14, the ellipticity is represented as a measurable term by the angle ψ, which also embodies the accompanying phase difference Δ. Effectively, the compensator azimuth has now been modified by an amount $45^{\circ}+\psi$ and likewise, the analyser will have its extinction position at $45^{\circ}+\psi$ (now termed x) with respect to the 'real' horizontal azimuth. From manipulation of

the experimentally measured quantity x, Δ may be derived from:-

$$x = 45 + \psi = 45 + \Delta/2 \qquad (2.26)$$

$$\text{therefore,} \quad \Delta = 2x - 90 \qquad (2.27)$$

2.9 EXPERIMENTAL DETAILS OF ELLIPSOMETRY STUDIES

2.9.1 INSTRUMENTATION - GENERAL DESCRIPTION OF THE ELLIPSOMETER

The basic instrument used for this work is shown in fig. 2.15. The components illustrated are bolted on to two optical benches, for which the relative displacement angle is set accurately at approximately 64^{o}. The light source generally used for ellipsometric surface studies in the visible region is a 24 volt, 150 watt tungsten filament* projector lamp operated from a suitable variac.

The collimator section consists of a condenser lens, the focal point of which is perfectly incident on the centre of a pin hole system. Consequently, the rays of light are now constrained, such that a parallel beam of light is produced, which may be readily monochromated by an appropriate Balzer interference filter.

* The tungsten light source is being rapidly replaced by the laser: Laser light offers the considerable advantage of being more intense, directional, monochromatic and coherent than the ordinary light produced by the tungsten source.

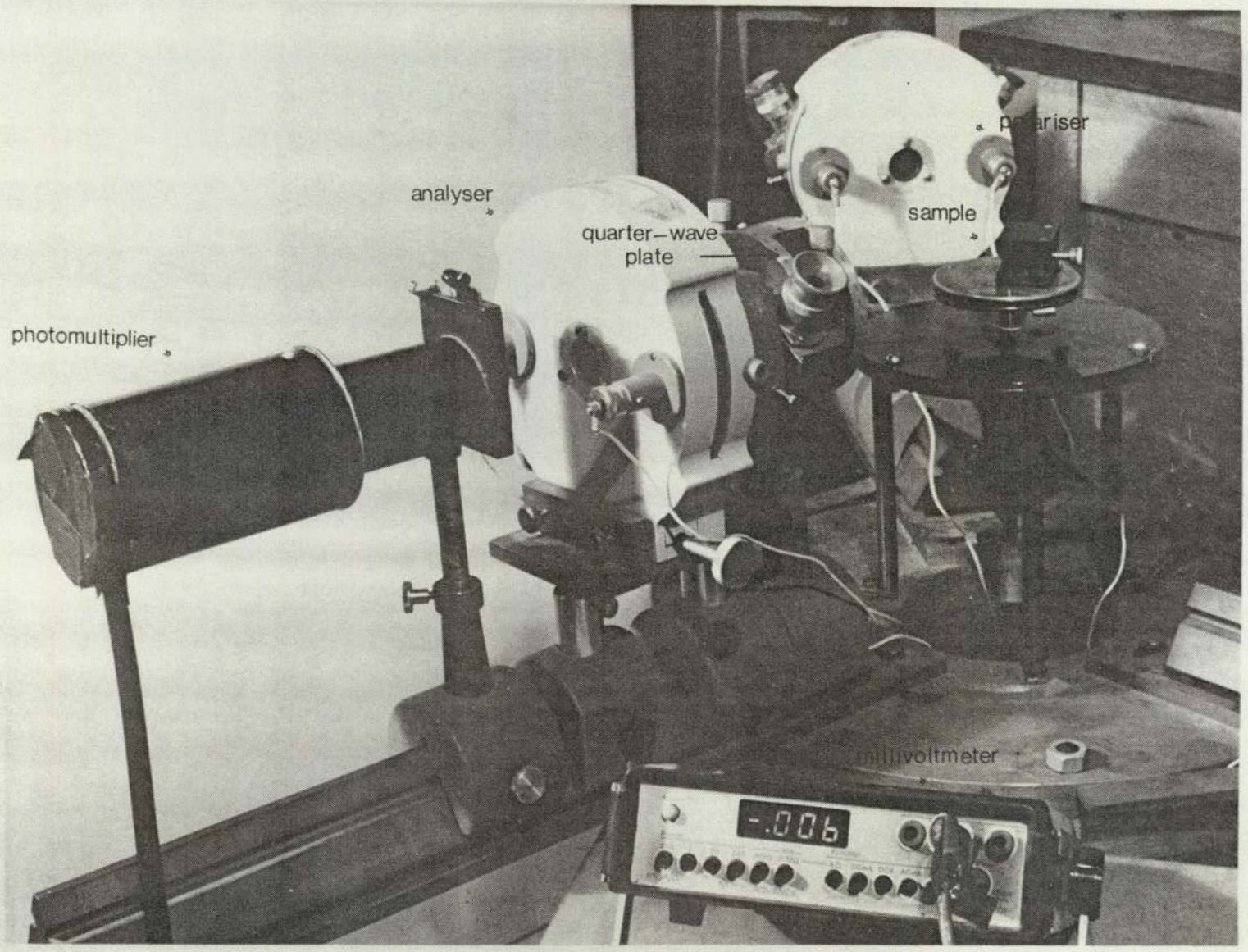

Fig. 2.15 The ellipsometer used in this study

The passage of selected light is then directed through a suitable polariser to achieve the required degree of polarisation. Its construction material, like that of the analyser, can be of three types, namely polaroid, nicol prism or Glan Thomson prism. The choice of material is governed by the needs for accuracy of polarisation, for this particular experiment polaroid was used.

Following the interaction of the beam on the analyte surface, the resulting reflection radiation (tracing an ellipse) is passed through a compensator (or, more strictly, quarter wave plate) corresponding to the chosen wavelength of incident light. An analyser system then meets any emergent beam in order to detect linearly polarised light. Finally, detection is achieved using a photo-multiplier coupled to a digital voltmeter.

2.9.2 SUBSTRATE PREPARATION

In order to meet the requirements of ellipsometry and equate to the conditions of slides in a photoreactor, a batch of glass slides was prepared for which one face of each slide had been carefully ground with ultra-fine aggregate carburundum, in order to improve reflection. Although attempts were made to measure the thickness of 'monolayer assemblies' deposited on the ground slides, it was found necessary to run the ellipsometer's detection system near to the limits of its sensitivity, to overcome the high attenuation of the intensity of reflected light: This proved experimentally intolerable.

In essence, while it is customary to deposit monolayers on to highly polished glass slides prior to photolysis, this practical arrangement is totally unsuitable for the purposes of ellipsometry, because the reflectivity for glass (in terms of the Fresnel reflection coefficients) is very small. As indicated above, grinding one surface of the slides does not help matters. However, the reflectivity of metals * is generally high, the effect being proportional to electrical conductivity, which is enhanced by the presence of free electrons within the metallic matrix.

Attention was therefore, turned to gold coated slides. Gold offers adequate reflective capabilities for ellipsometry (by giving highly reflective, smooth and flat surfaces [53]) and, moreover, is esteemed to be virtually chemically inert. The achievement of an acceptable state of preparation for the 'gold' slides required several attempts.

* Under the influence of an electric field (e.g. light) the free electrons move through the metal and give rise to rapid damping of light entering the metal. These conduction currents, which dissipate some of the incident energy in the form of heat, at the same time reradiate energy in the form of intense reflected waves. Hence, the intensity of reflected light is easy to handle from the point of view of detection sensitivity.

The initial process of thoroughly cleaning glass slides (pre-cut to fit the ellipsometers sample holder) was accomplished by boiling them as follows:-

1) In "Decon" detergent followed by sonification (see section 1.5.3)
2) In distilled water followed by further sonification.
3) Finally, in several batches of iso-amyl alcohol followed by sonification.

The gold coating process consisted of subjecting the clean slides to low atmospheric pressures (approaching 10^{-6} torr), before subjecting one side of the slides to a spread band of gold vapour and producing the required coverage by allowing condensation of the gold at a measured rate. The gold was vaporised from molybdenum boats heated by the resistive passage of high electrical current.

A visual examination of the gold coated slides from the initial preparation revealed some surface imperfections. If the slides were held at various angles in bright light, it was possible to identify surface 'pinholes' measuring fractions of a millimeter (microscopic examination was considered impractical because of the possibility of introducing contaminants to the gold surface during any manipulative process). This surface condition was suspected to be due to contaminants in the gold bulk and it was remedied by positioning a metallic shield above the gold during the first moments of its evaporation, thereby retaining any volatile impurities.

A later refinement to the vaporisation technique was achieved by bombardment of the glass surface with high velocity electrons (prior to gold coating). This was done by applying a large negative potential between the slide holder and cathodic electrode. However, this operation did not appear to improve the final appearance of the slides and so the process was abandoned because it also proved more time consuming than the previous method.

2.9.3 STORAGE OF THE GOLD COATED SLIDES

Storage of the gold coated slides proved to be a further problem because of the many contaminant particles present in the air and as a result, two ideas were explored.

Firstly, the slides were kept submerged in purified iso-amyl alcohol but, for inexplicable reasons, the gold layers subsequently tended to lose adhesion during the Langmuir film deposition process. Secondly, the slides were kept in vacuum desiccators containing 'self indicating' silica gel desiccant. The slides were rested with their 'non-active' glass back supported by a teflon stop. This latter method of storage proved better and was also used for gold coated slides subsequently prepared.

2.9.4 FILM DEPOSITION

All films were spread using a classical Langmuir film balance which had been extensively modified and improved by a fellow worker [61]. Appropriately, this operator controlled the instrument during the deposition processes (see fig. 2.16 for constructional

details and section 2.1 for a general description of the principles of operation of the Langmuir trough) which generally produced a slide with a monolayer coating on both sides of the slide (see later for details).

Careful inspection of the film on the gold coated slides revealed a distinct boundary between deposited film and clean gold. This occurred because the teflon coated trough utilised in the Langmuir experiment was of a narrow depth, which did not allow for complete dipping of the slide during the deposition processes.

2.9.5 CHOICE OF THE MOST SUITABLE WAVELENGTH OF LIGHT FOR ELLIPSOMETRIC MEASUREMENT OF FILMS OF TRIS (2,2' BIPYRIDYL) RUTHENIUM (II) DERIVATIVES

There were two important considerations in selecting the monochromator (usually an interference filter) for the ellipsometry experiment, namely:-

1) The sample surface must not absorb significantly at the transmission wavelength of the monochromator otherwise the intensity of reflected light (which is measured) would be drastically reduced.

2) A compensator (or quarter wave plate) of matching wavelength is required to achieve the 90^{o} phase difference necessary for the formulation of linearly polarised light from that of elliptically polarised light. Alteration of the wavelength and not the compensator or vice versa would not fulfil this requirement.

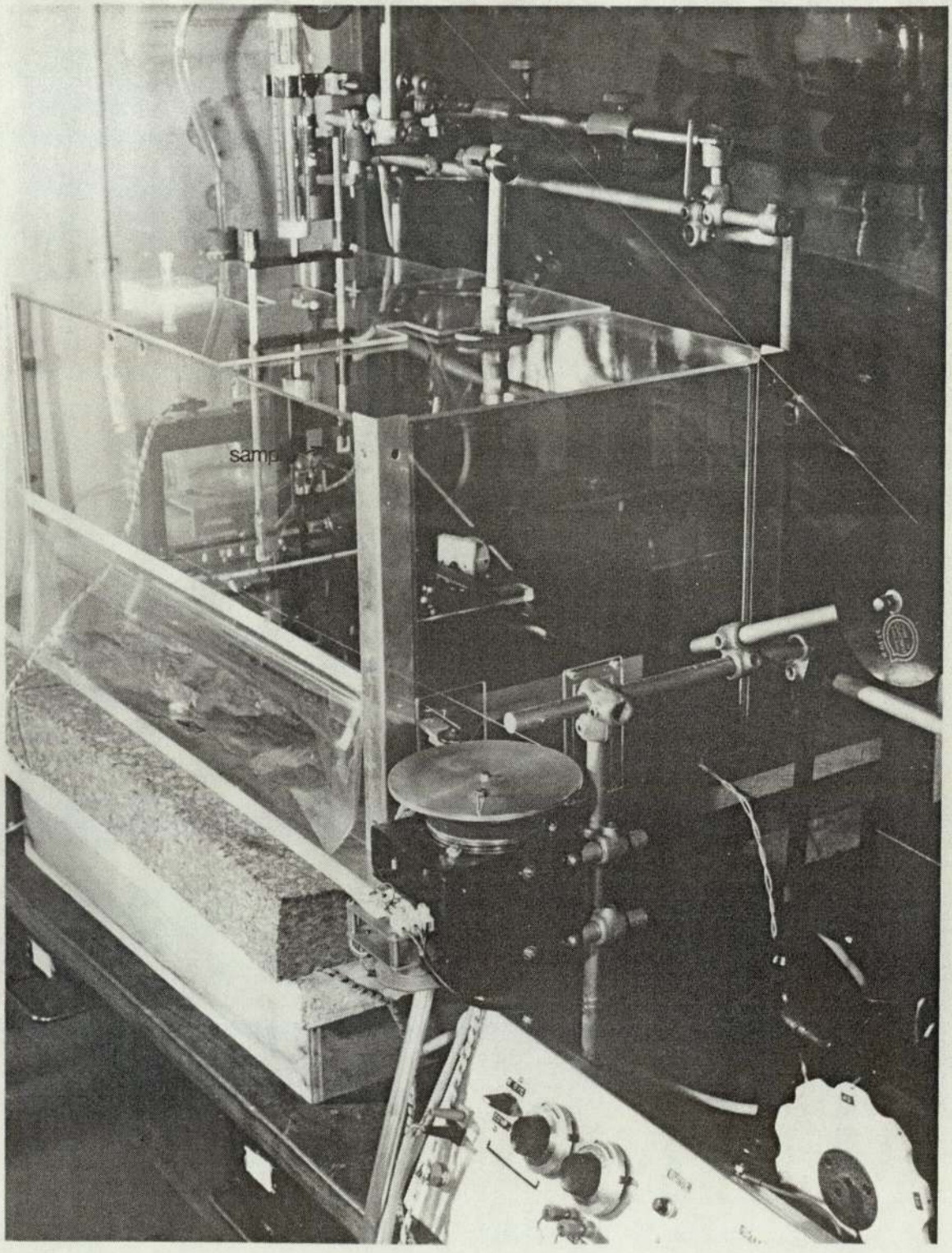

Fig. 2.16 The Langmuir film balance used in this study.

In order to satisfy these objectives an ultra-violet/visible spectrum (see fig. 2.17) of a Whitten-type surfactant was obtained and the positions of the resulting absorption bands noted (λ_{max} is normally used to describe the points of maximum absorption of light). Fortunately, the typical spectral minimum at 546.1 nm is of convenient wavelength for ellipsometric applications and effectively determines the choice of wavelength for the compensator and complementary filter. Consequently, 546.1nm was chosen for the wavelength of the compensator and filter.

2.9.6 SETTING THE ELLIPSOMETER FOR MEASUREMENT

In order to start to locate the light beam, the sample was set approximately in its holder and both compensator and photomultiplier removed. The back of the sample holder was now slowly rotated, while looking down the analyser tube, until the light beam was centred within the tube. The sample could now be carefully moved across its holder to the position where light was impinging on the centre of the film area (see section 2.9.4). Finally, the photomultiplier was re-attached and remaining adjustments were made by optimising the output to a millivoltmeter by delicate movements of the sample holder.

2.9.7 OPERATION OF THE ELLIPSOMETER

2.9.7a GENERAL DESCRIPTION OF THE PROCEDURE FOR DETERMINING REFERENCE AZIMUTHS

Although the azimuths for the particular ellipsometer operated had been pre-determined, it was deemed 'good technique' to re-examine the noted values and elucidate any possible errors. Fortunately, the

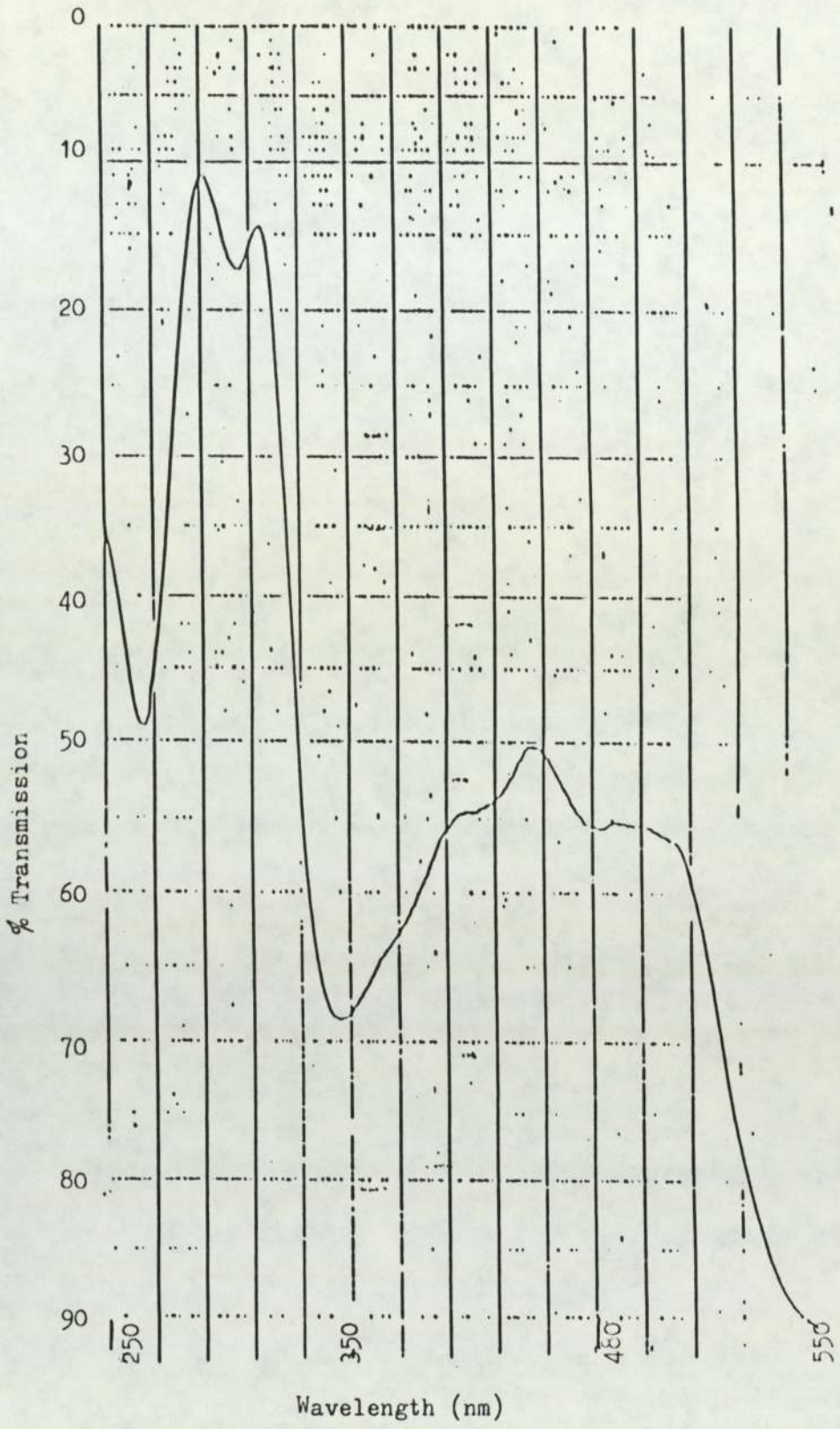

Fig. 2.17 An ultra-violet/visible spectrum of a Whitten-type surfactant, $((bipy)_2RuII(2,2'\text{-}bipy\text{-}4,4'(COOC_{18}H_{37})_2))^{2+}(PF_6)_2^{2-}$

previous determinations could be used to set approximate positions for horizontal and vertical polarisation directions for both polaroids (polariser and analyser), relative to the plane of incidence (the required reference directions).

The compensator was removed prior to the commencement of the azimuth determinations and the estimated transmission axes of the polaroids were aligned perpendicular to the plane of incidence. The polariser was then rotated through approximately 90^{o} to bring its transmission axis parallel to the plane of incidence and thus horizontal. The resulting extinction of polarised light was then optimised by arranging a minimum value for the millivoltmeter by slight adjustments of polariser and analyser (by convention the relative positions of the polaroid transmission axes at extinction are termed crossed - see fig. 2.10).

It has been mentioned previously that the material from which a polariser is constructed generally determines its polarisation efficiency and, consequently, extreme care is required in the measurement of the extinction position in order to achieve acceptable experimental accuracy. This task was accomplished by, alternately off-setting the polariser and analyser to record equivalent millivoltmeter readings either side of the apparent minimum and then averaging the values of the slightly erroneous azimuth positions (this technique is often called 'bracketing'). Similar positions were then found for respective rotations of the analyser and polariser by 180^{o}, 90^{o} and finally 180^{o} again. All azimuth positions were labelled according to Osheas [51] nomenclature (see fig. 2.18 overleaf).

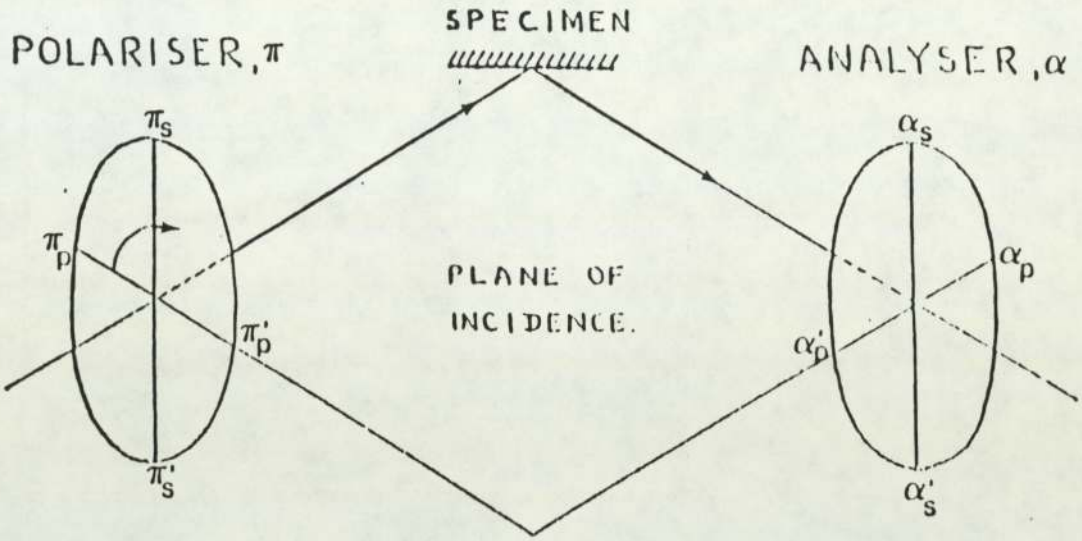

Definitions:-

π_p Polarizer reference position that transmits parallel to the plane of incidence

π'_p Position at 180° to the above

π_s Polarizer reference position that transmits perpendicular to the plane of incidence

π'_s Position at 180° to the above

α_p Analyser reference position that transmits parallel to the plane of incidence

α'_p Position at 180° to the above

α_s Analyser reference position that transmits perpendicular to the plane of incidence

α'_s Position at 180° to the above

Fig. 2.18 Oshea's nomenclature for reference azimuths.

2.9.7b COMPENSATOR SETTINGS

It was the initial aim of the experiment to find the respective transmission axes * of the compensator (now termed reference positions) to allow the selective passage of linearly polarised light parallel and perpendicular to the plane of incidence (azimuth directions). The initial reference position was found by setting the polariser and analyser to 'uncrossed' reference positions and then searching for minimum light transmission by gradual rotation of the compensator. The exact extinction position was attained by the 'bracketing technique' mentioned previously.

The procedure was repeated to find a similar position at 90^{o} from the former position. Two more positions at 180^{o} were also available, but were disregarded to shorten the overall analysis time. The compensator position was now offset by 45^{o} from one of the newly found reference positions and the procedure detailed below initiated.

* As mentioned previously these are traditionally termed fast and slow axes.

2.9.7c DETERMINATION OF REVISED EXTINCTION POSITIONS FOR POLARISER AND ANALYSER

The now familiar procedure of 'bracketing' was once again adopted. Overall, eight extinction positions were found and each labelled using the nomenclature devised by Oshea [51]. Of the four polariser positions, two of these, P_1 and P_2 were found symmetrically placed about the plane of incidence, which also corresponds to the π_p azimuth (see fig. 18). Similarly, positions P_3 and P_4 were also found at, nominally, 180^o to P_1 and P_2 respectively and either side of the π_p' azimuth, which was 180^o from the π_p azimuth.

The analyser readings A_1 and A_2 were separated by 90^o and situated at 180^o from A_3 and A_4 respectively.

The whole procedure was then repeated after the compensator had been set at 90^o from its former value (whereby the transmission axes of the compensator were again fixed at 45^o to the azimuth directions).

The polariser readings were used to derive an average value for the parameter ψ, while the quantity x and, subsequently, the required Δ (see section 2.8.4) were obtained from the analyser readings.

In practice a series of initial measurements was made for the uncoated gold substrates, so that an eventual statistical average value (from closely matched results for ψ and Δ) could be produced. These ellipsometric values then served as background values for subsequent measurements of deposited films. This method was chosen because the condition of the gold substrates prior to film deposition

had to be assumed, in that it was considered that any previous manipulation of the gold covered slides (for measurement before deposition) would undoubtedly lead to an unacceptable level of slide contamination. Subsequently, the various deposited films were also examined in an identical manner.

2.10 SURFACE FILMS EXAMINED BY ELLIPSOMETRY

The compounds examined as surface films by ellipsometry are shown in table 2.1 together with all ellipsometric parameters. Such compounds were chosen because they either related to a Whitten-type surfactant and their molecular lengths were well documented or they were the 'same' as the Whitten-type surfactants.

Although the surface films were prepared by a fellow worker, [61] it is worthwhile at this stage of the discussion to briefly examine the deposition processes (details on film: slide deposition ratios, spread film surface pressure and area are given at more convenient places in the text).

SAMPLES A, B, AND C

When referring to table 2.1 it should be noted that samples A, B and C were prepared by the Langmuir-Blodgett (coating) technique in which the slide is immersed in the subphase, the monolayer then formed over the subphase and the deposition process completed by drawing the slide up through the monolayer. It is important to note, that the subphase was re-used after the first deposition process in order to complete a duplicate pair. Each sample film was examined only once.

Table 2.1 Ellipsometric parameters for various films of surfactant derivatives of $Ru(bipy)_3^{2+}$ and some related compounds. n_3, k_3 and n_2, k_2 represent the optical constants of the gold substrate and the deposited film respectively.

	Compound	n_2	k_2	n_3	k_3	Theoretical Δ	Theoretical Ψ	Experimental Δ	Experimental Ψ	Film thickness Å
(A)	Arachidic acid	1.4550	0.7000	0.5754	2.4561	109.281	37.381	109.159	37.222	95
	" "	1.5000	0.0000	0.5754	2.4561	115.619	39.920	115.619	39.920	29
(B)	Octadecanoic acid	1.4500	0.6150	0.5754	2.4561	104.155	36.404	104.152	36.34	160
	" "	1.4600	0.0820	0.5050	2.5200	115.696 115.514	40.494 40.494	115.639	40.49	39 - 40
(C)	$((bipy)_2$ Ru (II) (bipy $(COOC_{18}H_{37})_2))^{2+}$ $(ClO_4^-)_2$	1.4600	0.8000	0.5754	2.4561	102.781	35.441	102.797	35.462	175
		1.4550	0.9000	0.5754	2.4561	114.679 114.582	38.698 38.668	114.568	38.664	35
	Background	-	-	-	-	-	-	110.538	39.801	0
(D)	$((bipy)_2$ Ru (II) (bipy (2,2' - bipy - 4, 4' - $(COO C_{18}H_{37})_2))^{2+}$ $(PF_6)^{2-}$	1.5000	0.0000	1.6880	3.1945	136.027 135.501	36.240 36.207	135.78	34.23	17 - 18
		1.4600	2.1600	0.5399	2.2964	114.305 114.296	37.147 37.070	114.29*	37.15*	59 - 61
		1.50	0.0000	1.6880	3.1945	136.50	36.21	136.50	36.23	10 - 11
	" " (Background)	-	-	-	-	-	-	137.52 115.04*	36.10 39.72*	0
(E)	" "	1.4600	1.3000	0.2836	2.1444	109.145 108.995	40.941 40.854	109.10	40.90	23 - 25
	Background	-	-	-	-	110.946	41.974	110.92	41.98	0
(F)	Ru/B_2A	1.4900	0.2500	0.511	2.184	113.532 113.356	39.536 39.517	113.438	39.527	22 - 24
(G)		1.5100	0.1100	0.5411	2.1184	113.184 113.097	39.705 39.704	113.113	39.705	26 - 27
	Background	-	-	-	-	-	-	115.50	39.75	0

Measurement tolerance = ± 0.2%

This was partly because the deposition ratios were approximately the same and it was thought that the reproducibility of film thickness could be tested by measuring deposited films which were nominally equivalent: Also the time allocation of the instrument was limited.

SAMPLE D

Sample D was deposited by the dipping method in which the slide is dipped through the monolayer film and withdrawn through the monolayer surface. The duplicate of sample D was prepared on a separate occasion.

Ellipsometric measurements were made on sample D on two separate occasions,

SAMPLE E, F, G.

Samples E, F and G were prepared by either the Langmuir-Blodgett technique or dipping technique or a combination of both for multilayer preparations.

2.11 DISCUSSION OF DERIVED FILM THICKNESSES FOR SURFACTANT DERIVATIVES OF $Ru(BIPY)_3^{2+}$ AND SOME RELATED COMPOUNDS

Considerable time was spent in acquiring expertise in the handling the various computational manipulations necessary to achieve sensible theoretical counterparts to experimentally obtained ellipsometric parameters. This did not emerge to reasonable satisfaction until the later stages of this work. Much of the difficulty lay in the fact that, for a surfactant derivative of $Ru(bipy)_3^{2+}$, three unknowns (the film optical constants, n and k, and the film thickness (t)) had to be determined. Of these, n and k, had to be varied iteratively until the calculated Δ and ψ parameters matched those measured by ellipsometry, whereupon t was finally calculated from n, k, ψ and Δ. The following results hopefully result from a satisfactory manipulative technique.

2.11.1 ARACHIDIC ACID (EICOSANOIC ACID) - $CH_3(CH_2)_{18}CO_2H$

	Surface pressure	Deposition ratio	Molecular thickness (Å)
1st subphase	30 mNm^{-1}	0.87	95
2nd subphase	30 mNm^{-1}	0.96	29

In the original communication of Whitten et al [16], in which they outline the discoveries concerning the photochemistry of surfactant derivatives of $Ru(bipy)_3^{2+}$, it is noted that arachidic acid is used as an initial surfactant. Although ultra-clean glass is accepted by Gaines [62] to be wettable, surface hydrophilicity is commonly assured by using a fatty acid type coating before depositing the active layer. It seemed fitting therefore, to initially examine some fatty acid compounds relevant to photo-induced cleavage of water. As there are numerous documentations pertinent to fatty acid compounds, these serve

as initial reference points and checks for the ellipsometric measurement of molecular thicknesses.

The so called 'Langmuir-Blodgett' technique [44] of film deposition was operated in which immersion of the solid support into a subphase (see fig. 2.1) was followed by spreading of the arachidic acid film and then raising the slide.

The thickness measurements reported by Pitt and Walpitta [47], using a wave guiding technique, indicate that arachidic acid has a molecular length of 26.4 - 28.0Å. In contrast to their findings, this work shows the molecular length to be virtually 29Å if the same subphase is used in a repeat deposition procedure. However, the initially used subphase of freshly deionised water (pH5.5 - 6.0) gave a molecular thickness of 95Å, which is consistent with trilayer formation. On each occasion the deposition ratio (area of compressed film deposited relative to the area of the glass support) can be approximated to unity.

The difference between the thicknesses of arachidic acid obtained from this work (29Å after the second use of the subphase) and that given by Pitt and Walpitta [47] (26.4 - 28.0Å) seems tolerable if the bounds of experimental error outlined by Rothen [52] of ±3Å are employed i.e. Rothens experimental error is quoted for data obtained from relatively crude apparatus. Furthermore, it is well documented that several factors may operate during the film deposition process and Pitt and Walpitta [47] draw specific attention to the following factors which they consider have an important bearing on the deposition of Langmuir films:-

1. A contamination free sub-phase (water) and purified film material

2. The pressure - relative molecular area relationship

3. The pH of the subphase

4. The temperature of the subphase

5. The deposition rate and pressure variation occurring in the suspended monolayer during deposition.

Another relevant investigation, by Bikerman, [63] has demonstrated that films will bridge surface imperfections of the solid support (see fig. 2.19). This would suggest that, in ellipsometry applications, the analysing light beam may be penetrating down to a gold surface that, in microscopic terms, may be 'grooved'. These surface variations may give experimental inconsistencies that may appear to be errors because of the following:-

2.11.1a MODIFIED REFLECTIONS

In referring to fig. 2.19 it is observable that the light beam can travel various distances to reach the solid substrate. Therefore, it follows that the form of the polarisation ellipse pertaining to the area of a particular monolayer will be averaged since reflections from

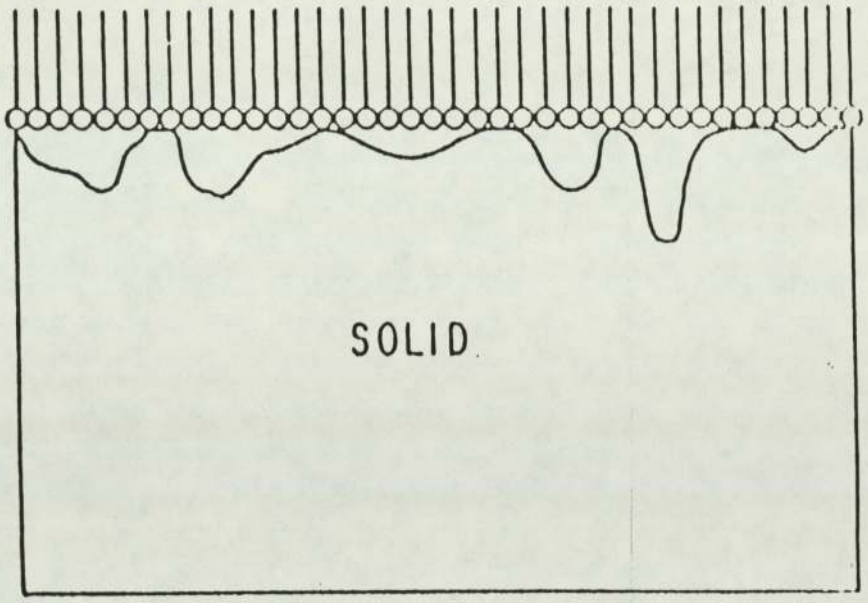

Fig. 2.19 Schematic diagram to demonstrate the manner in which a close packed monolayer may bridge over surface roughness as it is deposited on a solid (substrate).

angled surface contours are diffuse. Consequently, variation of the path of reflected light will cause a corresponding change in the polarisation ellipse, which in turn will lead to the film thickness calculation giving a value which is not truly representative of that film.

2.11.1b CHEMICAL TRAPPING

It is stated, by Bikerman [63] that macroscopic voids between monolayer and the substrate are considered to retain subphase material. The constituents and homogeneity of this void filling material could again alter the shape of the reflected polarisation ellipse.

2.11.1c FILM COLLAPSE

Bikerman [63] also notes that the monolayer structure is destroyed in the event that the void material is dried out or drained. The polarisation ellipse would then change accordingly.

Although considerable efforts were made to minimise mechanical vibration during the deposition process, spread film surface movement was still evident. Therefore, concurrent movement of the subphase could induce stresses during the Langmuir deposition process, possibly giving rise to reorientation of parts of the monolayer. In this context an analogy is drawn with the concept of the Maragoni effect [64], which is an induced subphase flow, resulting from a surface tension gradient. This phenomenon is commonly met when film deposition is accomplished by the 'touching method', introduced by Schulman et al [65], in which the slide is first wetted and one of its

edges is brought into inclined surface contact, to allow the monolayer to spread. Unfortunately, the monolayer disturbance inherent in the touching procedure seems to be a contributing factor in the production of imperfect surface films.

2.11.1d SUBPHASE DEPENDENCE

The discovery of a marked difference in molecular thicknesses for two separate, but nominally equivalent (see section 2.11.1), monolayers of arachidic acid of 95Å and 29Å was unexpected, since the deposition parameters were assumed to be virtually identical. In retrospect, the most noteworthy experimental issue would appear to be the re-use of the subphase originally used when depositing the second monolayer (29Å thickness) of arachidic acid onto a second gold substrate. This procedure is commonly implemented when several slides have to be coated, because of time saving and only entails the removal of the previously spread film prior to the next deposition. A new film is then organised over a freshly submerged slide, which in turn is then raised through the film to complete the process.

The fundamental role of the subphase during monolayer deposition, which has been previously mentioned in connection with film thickness measurements carried out by Pitt and Walpitta [47], is now reintroduced in an attempt to explain the above experimental inconsistencies. Such is the profoundness of subphase involvement during film deposition that the subphase must be suspected as having a distinct influence on the overall 'monolayer' structure during the processing of sequentially prepared slides viz., those of thicknesses

of 29Å and 95Å of arachidic acid, mentioned above. Interestingly, Gaines et al [22] show that the mechanical and luminescence properties of Whitten-type monolayers can strongly depend on anions contained in the subphase. Furthermore, the interaction of divalent cationic impurities and fatty acids, illustrated by Myers et al [66], may have played an important role during arachidic acid depositions of this work. For instance, cationic impurities in the deionised water that constitutes the subphase may have been drawn into the monolayer or, conversely, impurities in the monolayer constituent released into the subphase after the spreading of the first film. It is reported by Gaines [67] that subphase impurities present in p.p.m. can cause defects in the monolayer assembly. However, Gaines adds caution in remarking that the same impurities may have an innocuous effect on other types of monolayer. The importance of selecting suitable purification techniques is so justified, for all monolayer investigations.

It may be concluded, that after spreading the first film the subphase was contaminated and the second film (29Å) deposited in a different way from the first (95Å).

2.11.1e HYDROPHILIC BEHAVIOUR OF GOLD AND GLASS SURFACES

Although the gold substrates on glass slides appeared to behave similarly to their pure glass counterparts (wettability appearing the same) certain small areas of opacity of the gold coated slides (without a sample film present) were highlighted during their visual examination under sunlight. The possibility that the observed areas had a degree of hydrophobic character relative to the deposited

film was not accounted for by the usual method of carefully viewing a wetted surfactant layer 'by eye'. If hydrophobic character was introduced to any extent at a microscopic level, it is possible to envisage constricted film disorder and a subsequent build up of monolayer assemblies in well confined areas. Since ellipsometry is specific to a minute analytical area, the possibility exists of focussing the analysing beam on to zones of different thicknesses and even gradient layers. This postulate implies that a 1:1 slide film area deposition ratio need not mean that a monolayer is formed. Thus, in hindsight it would have been prudent to do ellipsometric measurement on two different areas of all the prepared surface films. Such action was not implemented, because of the mistaken belief that 1:1 deposition (accepted by Whitten [16] and others) corresponds to a monolayer covering of the slide.

2.11.2 STEARIC ACID (OCTADECANOIC ACID) - $CH_3(CH_2)_{16}CO_2H$

	Surface pressure	Deposition ratio	Molecular thickness (Angstroms)
1st subphase	$30mNm^{-1}$	1.03	160Å
2nd subphase	$30mNm^{-1}$	0.99	39 - 40Å

An identical deposition procedure as that described in section 2.11.1 (arachidic acid) was followed and again, a second use of the subphase resulted in the deposition of a film which had a smaller thickness. The molecular thickness of 40Å from this work bears only rough comparison with that of 24.2 - 25.8Å for stearic acid, reported by Pitt and Walpitta [47] but the 160Å thickness of stearic acid obtained using the fresh subphase initially is divisable by four and it follows that a four layer deposition might be tentatively proposed.

The arguments in section 2.11.1d, relating to subphases, would appear to apply to stearic acid systems and, likewise, the idea of gradient layering (section 2.11.1e) is also another possibility.

2.11.3 SURFACTANT DERIVATIVES OF THE DICATIONIC SPECIES (TRIS (2,2' - BIPYRIDYL) RUTHENIUM (II)) $^{2+}$

Surfactant derivatives of tris (2,2' - bipyridyl)-ruthenium (II)) $^{2+}$ had been synthesised [61] in accordance with the original specifications of Whitten [16]. Effectively, the overall reaction replaces a single 2,2' bipyridine unit with a potentially surface active unit of the dioctadecyl ester of 4,4' - dicarboxy - 2,2' - bipyridine. The usual counterion is either hexafluorophosphate ion or pechlorate ion. The basic structure illustrated below in fig. 2.20 shows the hydrophobic tail, consisting of non-polar hydrocarbon units, and the polar carboxyl head.

Molecular length can be estimated by adding the lengths of molecular units: the molecular length of the stearic acid units, which basically comprise the tail structure, has been given by Pitt and Walpitta [47] as 24.2 - 25.8Å and the head dimension as approximated from tabulated bond length data is about 10Å. However, the approximate molecular length so obtained does not account for orientation of the molecule while residing in a monolayer assembly on a gold substrate, but does serve as a guide as to the credibility of any measured monolayer thicknesses of the Whitten-type surfactant.

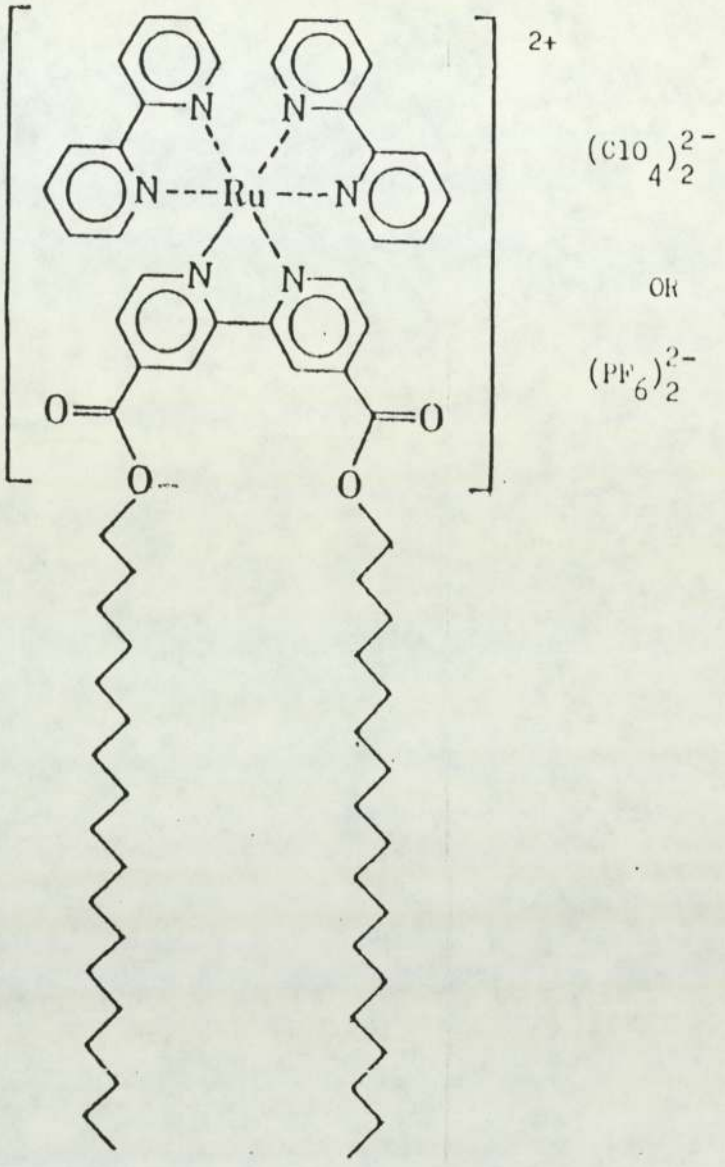

Fig. 2.20 The structure of the dioctadecyl ester of (4,4'-dicarboxy-2,2'-bipyridine)bis(2,2'-bipyridine)ruthenium(11)$^{2+}$

2.11.3a $\underline{((bipy)_2Ru(II)(2,2'\text{ - bipy - }4,4'(COOC_{18}H_{37})_2))^{2+}(PF_6)_2^{2-}}$

For similar surface pressure-area (π -A) isotherms of surfactant $((bipy)_2Ru(II)(2,2'\text{-bipy-}4,4'\text{-}(COOC_{18}H_{37})_2))^{2+}(ClO_4)_2^{2-}$, Whitten [16] details the existence of two molecular areas, namely 40Å^2/molecule and 85Å^2/molecule, at a surface pressure of 30 mNm^{-1}, depending on which purification routes were used to obtain the surfactant. The 40Å^2/molecule area, which, according to Whitten, applied during the photo-induced cleavage of water, was unique: Similar attempts [17] to obtain the 40Å^2/molecule dimension, using the hexafluorophosphate salt, resulted in a value of 85Å^2/molecule at a surface pressure of $30mNm^{-1}$ but the corresponding isotherm was much steeper. The idea of having a different packing arrangement in the film is then put forward as a plausible explanation for having two molecular areas, although the possibility of having interaction from impurities in both surfactant and subphase are not discounted by Whitten [17].

Therefore, the work of Cooke [61] appeared extremely promising, in view of the findings of other workers [18 - 22], when his attempts to re-establish Whitten's surfactant molecular areas using the available hexafluorophosphate salt, $((bipy)_2RuII(2,2'\text{-bipy-}4,4'\text{-}(COOC_{18}H_{37})_2))^{2+}(PF_6)_2^{2-}$, proved reasonably successful. Using this surfactant Cooke was able to prepare molecular areas of 90Å^2/molecule and 43Å^2/molecule. Consequently, it was of considerable interest to measure thicknesses of the films prepared by the Cooke method, in which film depositions were made at a surface pressure of 30 mNm^{-1}, using conductivity water as a subphase (pH 7.2). In contrast to the coating method used for fatty acids (see section 2.11.1), in which the monolayer is spread over a slide already immersed in the subphase,

Cooke had implemented the so called dipping method. In this case the deposition operation is accomplished in two controlled stages, in that the substrate slide is initially dipped below the spread surfactant layer, followed by slowly withdrawing the slide upwards through the assembled monolayer.

As previously mentioned two attempts were made at measuring the surface film, such that

Molecular area from Whitten's work [16]	Molecular area from this work [61]	Film thickness first attempt	Film thickness second attempt
85Å^2/molecule	90Å^2/molecule	17 - 18Å	59 - 61Å
40Å^2/molecule	43Å^2	10 - 11Å	(unattainable since ellipsometry parameters drastically changed)

In the case of the molecular area of 90Å^2/molecule this was only deposited as a consequence of upwards motion of the slide, which suggests that some type of hydrophilic-hydrophobic repulsion happened during the dipping sequence. From the film thicknesses measured at the first attempt (17 - 18Å and 10 - 11Å) it might be construed that a surfactant had not been deposited, because the thickness of the surfactant has been approximated to be 35Å (see above). However, it should be pointed out that the monolayer deposition process is often laden with elements of unpredictability because of the risk of unknown

surface film-subphase interaction. If such a mechanism is to be believed, the film thickness values for the surfactant of (17 - 18Å and 10 - 11Å) seem rather spurious and much less than expected if for instance stearic acid (24.2 - 25.8Å) or a derivative is a decomposition product as a monolayer. A possibility is that the thickness of 17 - 18Å and 10 - 11Å for the surfactant, represent the results of monolayer collapse.

In the second attempt at measuring thicknesses of the 'same films', it is noticed that sensible ellipsometric parameters could not be obtained for the surfactant when it had a molecular area of 43Å^2/molecule. This would seem to indicate that the deposited monolayer film has fragmented. As a consequence of this finding, the measured thickness value of 59 - 61Å (at the second attempt) for the surfactant having a molecular area of 90Å^2/molecule cannot be accepted as a true evaluation of the initial film immediately after deposition. Thus, the long term stability of monolayers would seem to be questionable. There are two experimental aspects which may account for film thickness discrepancies, as follows:-

1) The gold substrates had been prepared by the electron bombardment method (see section 2.9.2) which requires less evacuation time for the removal of atmospheric gases from on and around the substrates glass support. It is feasible that incomplete degassing of the glass slide, prior to gold coating, could confer an undesirable surface activity.

2) An intrinsic property of the ester linkage is its susceptibility to chemical attack. In view of this reaction characteristic, G.L. Gaines Jnr. et al [22] have probed the extent to which monolayers of surfactant derivatives of $Ru(bipy)_3^{2+}$ are hydrolysed, by varying the pH level of the subphase supporting the monolayer. Thus, the phenomenon of ester breakdown might be offered as a part explanation for the varied film thicknesses of the complex.

2.11.3b $\underline{((bipy)_2RuII(2,2'\text{ - }bipy\text{ - }4,4'(COOC_{18}H_{37})_2))}^{2+}\underline{(PF_6)_2}^{2-}$

In order to substantiate the postulate submitted above (section 2.11.3a - No.2), it was considered a necessary experimental step to examine a film of the same surfactant derivative of $Ru(bipy)_3^{2+}$ deposited on a gold substrate, which had been prepared by an alternative procedure (see section 2.9.2). In this instance a molecular area approximating to Whitten's 40Å^2/molecule was obtained.

Molecular area	Film thickness
42.4Å^2/molecule	23 - 25Å

All experimental parameters were kept as described immediately above. Once again the observed film thickness of 23-25Å is less than can be expected for spatial arrangements of the surfactant (35Å), but of the same order of film thickness connected with stearic acid. As suggested in section 2.11.3a the notion of hydrolytic attack on the sufactant monolayer must be contemplated as the cause of the unexpected film thicknesses.

As mentioned previously, the rate of hydrolysis of the surfactant has been studied by Gaines et al [22], whose limited investigation shows that, with increasing pH, there is a corresponding decrease in the measured molecular area of the surfactant. Ultimately, upon conclusion of the rate-terminating step, a film area ratio is attained of two molecules of octadecanol for each initial surfactant molecule. Adam's [68] work on characterising surface films by Π-A diagrams has shown that the molecular area of fatty acids and alcohols is near 20Å^2/molecule at high surface pressure (see fig 2.21); it is evident that the overall molecular area of two molecules of octadecanol approximate to the experimentally obtained value of 42.4Å^2/molecule for the diester surfactant derivative of $Ru(bipy)_3^{2+}$. Its hydrolysis reaction is given by

$$((bipy)_2RuII(bipy(COOC_{18}H_{37})_2))^{2+} + OH^- \text{-----}>$$

$$((bipy)_2RuII(bipy(COOC_{18}H_{37}))^+(COO^-) + \underset{\text{(Octadecanol)}}{C_{18}H_{37}OH} \qquad (2.28)$$

$$((bipy)_2RuII(bipy(COOC_{18}H_{37}))^+(COO^-)) + OH^- \text{---}>$$

$$(bipy)_2RuII(bipy(COO^-)_2) + C_{18}H_{37}OH \qquad (2.29)$$

(soluble in water).

It is proposed by Gaines [22] that the soluble ruthenium carboxylate may diffuse away from the surface film positioned above a subphase. Moreover, since the primary surface layer is credited with a localised positive charge (normally neutralised by counterions from the surfactant (PF_6^-), that complete the so called electric double layer - see fig 2.22) it is reasoned by Gaines [22] that this will initially give rise to an induced OH^- concentration near the surface due to

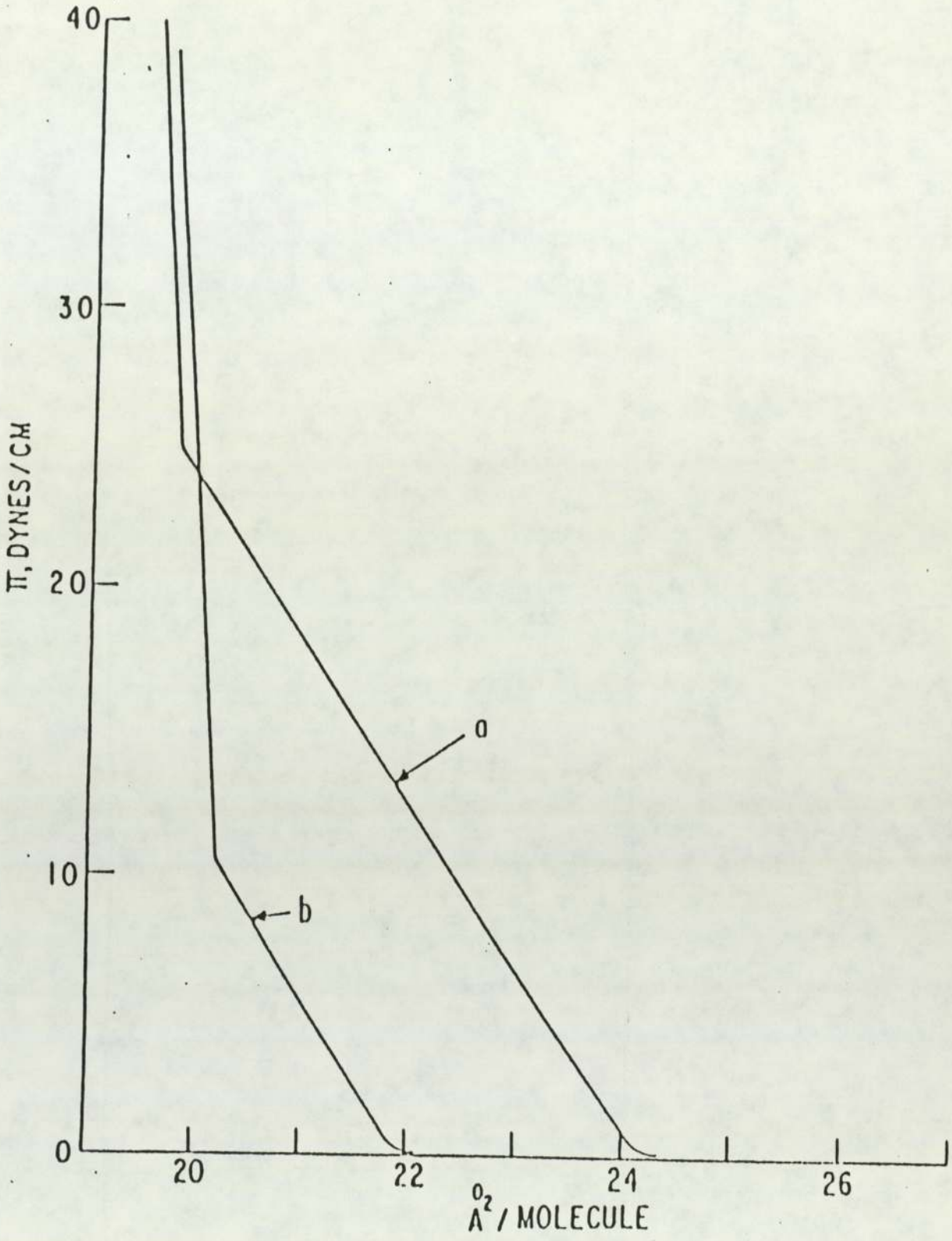

Fig. 2.21 Typical Π – A diagrams of condensed monolayers of long chain compounds: Un-ionised fatty acids (a) and fatty alcohols (b) both have molecular areas near 20 A^2 at high surface pressures.

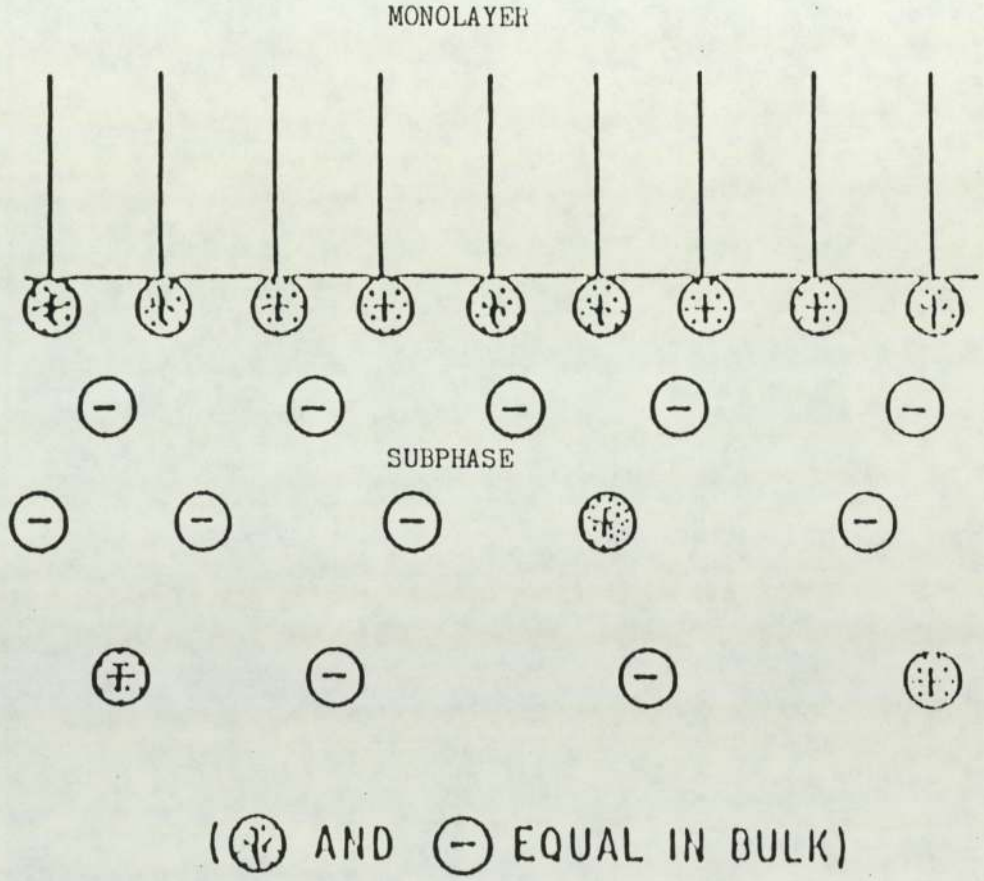

Fig. 2.22 An electrical double layer at the monolayer - subphase interface.

attractive forces. Accordingly, it is contended by Gaine's [22] that an increased pH at the surface layer (described in equation 2.30) affords an enhanced hydrolysis rate

$$\text{pH surface} = \text{pH bulk} + \frac{e\psi}{2.3kT} \qquad (2.30)$$

where ψ is the surface potential approximated from Davies's [69] equation, k= Boltzmann constant and T = temperature in Kelvins.

The film thickness of octadecanol can be estimated by referring to the known film thickness of its oxidised form, (stearic acid (24.2 - 25.8Å)[47]). It follows, from bond length data, that a chemically reduced form of the latter should have a molecular length reduced by 1-2Å, although it is conceivable, in an experimental context, that residual contaminants will be additive to any film thickness. Hence the film thickness of 23-25Å serves a two fold purpose, in that it supports the idea of octadecanol production and gives further ratification to Gaines's work [22] on aspects of the hydrolysis of Whitten-type surfactant. However, the chemical pathway to Whitten's original molecular area of 40Å^2/molecule for a surfactant which is nominally identical, remains undefined.

2.11.4 MULTILAYER PRODUCTION USING A WHITTEN-TYPE SURFACTANT DERIVATIVE

2.11.4a INTRODUCTION

In an attempt to improve the quantum efficiency for sensitized cleavage of water by a surfactant derivative of $Ru(bipy)_3^{2+}$, Whitten [17] built multilayers (monolayer assemblies) containing mixed layers of the surfactant and arachidic acid. The reason for the

presence of arachidic acid in the multilayer was as an aid to the assembly of the monolayer, by providing a wettable hydrophilic base material at different stages in the deposition process (which Whitten [17] found a necessary experimental step in multi-layer production). However, Whitten [17] expresses difficulty in constructing pre-conceived multilayer assemblies of a $Ru(bipy)_3^{2+}$ derivative and arachidic acid. The use of other surfactant molecules was also proven detrimental to devising an outer layer of the $Ru(bipy)_3^{2+}$ derivative. Although Whitten achieved the deposition of three layers of the derivative onto glass slides satisfactorily, it is reported that the best solution to its deposition was arrived at when the derivative was the ultimate layer on a hydrophilic base assembly.

Accordingly, the task of measuring the film thickness of multi-layers which had been prepared using the hexafluorophosphate salt [70] was undertaken as part of this project.

2.11.4b CONTROL EXPERIMENT

As a controlling step, a single layer of the complex $((bipy)_2RuII(2,2'\text{-bipy-}4,4'(COOC_{18}H_{37})_2))^{2+}(PF_6)_2^{2-}$) was initially examined. This was coated by a single uplift of the slide (deposition ratio 1:1) at a surface pressure of $30mNm^{-1}$ using conductivity water as a subphase (pH7.2).

Film thickness 22-24Å

In agreement with previous descriptions, the film thickness appears to confirm octadecanol formation.

2.11.4c MULTILAYER EXPERIMENT

A second experiment attempted to construct a 'pure' multi-layer of the complex $((bipy)_2RuII(2,2'\text{-bipy-}4,4'(COOC_{18}H_{37})_2))^{2+}(PF_6)_2^{2-}$, but that apart, all initial experimental parameters were set as above (section 2.11.4b). The stepwise slide deposition process revealed 1:1 depositions for the first uplift and dipping motions. A second uplift of the slide indicated no film uptake, which tended to bear out the deposition difficulties encountered by Whitten.

Film thickness 26-27Å

Interestingly, the measured deposition ratios would seem to indicate bilayer deposition, but it is apparent from the determined film thickness that a monolayer with a film thickness near to that of stearic acid has been formed. The formation of octadecanol (from hydrolytic attack on the surfactant) again seems to be evident, although the film thickness is slightly larger than that typified in previous experiments. However, in regarding the different layering processes, the acceptance of residual contamination seems reasonable and could account for the relatively small discrepancy.

2.11.4d OTHER MULTILAYERS

Without the prior knowledge of hydrolysis effects on surfactant derivatives of $Ru(bipy)_3^{2+}$ other multi-layers were assembled using

alkaline subphases (pH11). The ellipsometry results subsequently revealed an unacceptable spread for Δ and ψ , which is considered consistent with rapid hydrolytic attack on the surfactant.

2.11.5 FILM THICKNESS MEASUREMENTS ON A SAMPLE OF 'WHITTEN'S' DIESTER DERIVATIVE OF $Ru(bipy)_3^{2+}$, $((bipy)_2\ Ru(II)\ (2,2'\text{-bipy-}4,4'\text{-}(COOC_{18}H_{37})_2))^{2+}(ClO_4^-)_2$

It is apparent from the recent wealth of literature on surfactant derivatives of $Ru(bipy)_3^{2+}$ that the associated counterions undoubtedly have an extensive role to play in shaping the final form of the monolayer. The idea that the surfactant's counterion affects the parent monolayer is illustrated by the work of Goddard et al [71], whose investigation of the singly charged cationic surfactant, docosyltrimethyl ammonium bromide (having a similar surface pressure - molecular area isotherm to the ruthenium (II) surfactant), demonstrates the need for better theoretical approaches to account for specific ion effects. It is Gaines [22] who reaffirms this viewpoint, after studying the effects of polyvalent anions on surfactant derivatives of $Ru(bipy)_3^{2+}$ and infers that the application of electrostatic theory for charged species gives inconclusive results.

Consequently, it was deemed a fitting conclusion to the film measurements to re-examine 'Whitten's original system', in which the perchlorate salt was used, to prepare the monolayer. The now typical surface pressure of $30mNm^{-1}$ was retained whilst the films were assembled on a subphase of specially prepared water with a guaranteed low level of impurity [72]. The films were deposited using the Langmuir - Blodgett technique.

	Deposition ratio	Film thickness
First attempt	1.16	175Å
Second "	0.91	35Å

The effects of re-using the subphase emerge once again and the discussion of subphases and localized layering of the film (see section 2.11.1) are again offered in part explanation of the difference between the two results.

The film thickness of 35Å would appear to be direct evidence that a monolayer of the Whitten-type surfactant has been contrived, if account is taken of the molecular dimensions of the stearic acid type tail structure and the hydrophilic head spatial arrangement. Furthermore, it follows that the other film thickness of 175Å supports a pentalayer structure.

2.12 CONCLUSION

The success of Whitten's pioneering photochemical experiment, using a perchlorate salt of the diester derivative of $Ru(bipy)_3^{2+}$ as a surfactant still remains unique. This may be due to the effects of contaminants in the surfactant or aqueous subphase and also due to interaction at the deposition stage between the counterion and the charged monolayer film. Such factors start to explain the inconsistent behaviour of Whitten-type surfactants in nominally equivalent monolayer experiments. The present work on film thickness suggests that the significant knowledge gained from film to substrate deposition ratios are misleading, and cannot be taken at 'face value'

and interpretated in such a way that the deposited monolayer is considered to evenly cover the substrate. The most topical idea of having a chemical synergist involved with the surfactant, during the deposition and photochemical reaction stages remains.

As a final consideration the possibility of having non-uniformity in the monolayer or its assemblies could produce a unique conformation of monolayers that enables photochemical cleavage of water by the surfactant.

CHAPTER 3

PHASE DISTRIBUTIONS STUDIES

3.1 GENERAL INTRODUCTION

In the introduction to this thesis it has been mentioned that a fellow researcher, Cooke [36], was investigating the photolytic properties of a surfactant derivative of $Ru(bipy)_3^{2+}$ (acting as photosensitizer in the cleavage of water) supported by particulately dispersed hydrocarbon material in water: The system was produced by the injection of a molten pre-mix of the surfactant and hydrocarbon into sonificated water: i.e. to achieve homogeneous distribution of the surfactant throughout the liquid hydrocarbon (prior to injection) required the addition of a polar solvent. It was suggested by Cooke [36] that the interfacial regions of the dispersion so formed would mimic similar regions of the surfactant deposited on glass slides. However, a major advantage of the dispersion is that it could offer much larger (typically one hundred times [36]) interfacial areas compared with areas of the monolayer assemblies.

Photolysis of the Cooke-type dispersions produced dihydrogen gas, which, based on evidence of similar experiments using deuterium oxide as the dispersive medium, was proved to originate from water. The yield of dihydrogen from photolysis of the Cooke-type dispersions was considerably higher than the yield of dihydrogen from analogous monolayer experiments [35]. However, Cooke's dispersion experiments were irreproducible. This unpredictable behaviour of the Cooke-type dispersions prompted this present study into the distribution of particle sizes in dispersed phase systems of the aforementioned type.

3.2 CHARACTERIZING THE DISPERSION

3.2.1 INTRODUCTION

Systems of one or more bulk phases are often described in terms of temperature and composition, together with rate or equilibrium relationships. It is inherently more difficult to describe particulate dispersed-phase systems, because one or more independent properties arise for each individual particle (whether solid, liquid or gas) in the dispersed system. For example the particle can alter in size by molecular additions or degradations that are imposed by changes in the equilibrium state of the dispersion, or it may cease to exist as an entity by coalescence or dispersion through dissolution. For each particle in its newly equilibrated environment, we can assign values for its size and sometimes its internal concentration if this is known to be variant.

Before proceeding it becomes necessary to give a meaning to the terms concentration and size in the context of their application to particulate dispersed distribution studies.

3.2.2 PARTICLE CONCENTRATION

As an example, concentration could characterize droplets of one phase, dispersed in a second phase, with transfer of a third dilute component across the droplet interface (solvent extraction) as an inherent characteristic. For a more apt example it may be visualized that the concentration of individual particles in Cooke-type dispersions may differ by the amount of surfactant

supported by the hydrocarbon. However, for the purposes of this study particles of equivalent size are considered to have identical films of adhering surfactant, since there seems no justification for supposing that some hydrocarbon particles (originating from the same source) get a preferential coating of surfactant.

3.2.3 PARTICLE SIZE

If all particles of the dispersion are spherical, then it might seem a straightforward task to describe a particle's size by its diameter. However, diameter is a term which has also been used for the description of sizes of irregular particles (see below) and consequently it is necessary to define the term diameter in its application to particle size.

For instance Martin [73] has proposed that for an irregular particle its diameter is the distance between opposite sides of the particle, measured crosswise on a line bisecting its projected area (see fig. 3.1). As an alternative Feret [74] has suggested that the diameter of an irregular particle is the length of the distance between two tangents on opposite sides of the particle (see fig. 3.1). However, Patterson and Cawood [75] have defined particle diameter as that of a circle the area of which is equal to the projected area of the particle. It is this last definition which has been extensively used and one which seems suited to the particles in question, since the shape of particles in Cooke-type dispersions is a speculative consideration.

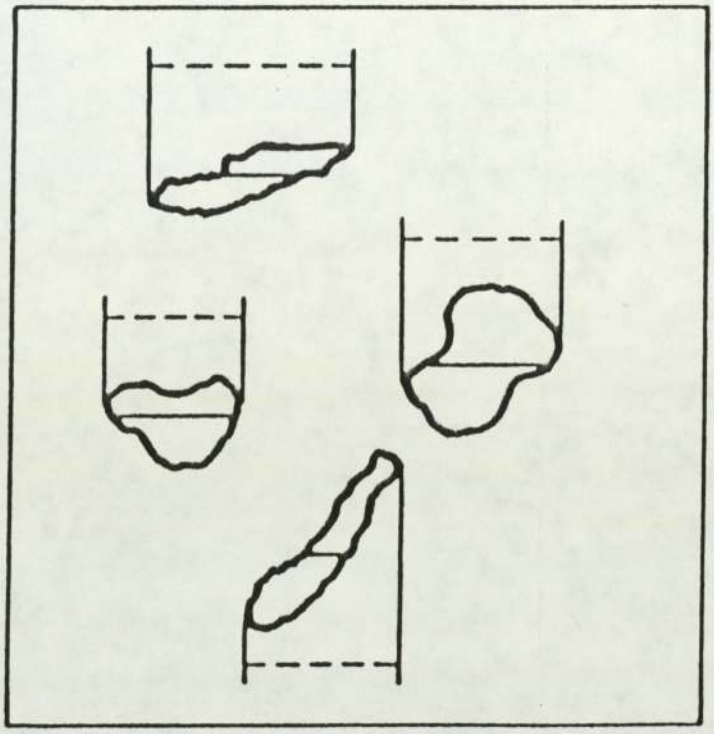

Fig. 3.1 Martin's [73] diameter (solid lines bisecting particles) and Feret's [74] diameter (dashed lines).

3.2.4 CONSIDERATIONS ON THE REPRESENTATION OF DISTRIBUTIONS OF PARTICLE SIZES

Particle size and concentration are independent property co-ordinates which can have values allotted at any time for each member in the system. In general, not all particles are of the same size or concentration and consequently, a distribution of particle sizes and concentrations evolves.

In order to uniquely describe a particulate system, it is necessary to formulate a dimensional distribution from two types of co-ordinate, which Randolph and Larson [76] define as the,

a) Internal co-ordinates; which are properties associated with the internal state of a single particle e.g. size, shape, concentration, chemical activity, temperature etc.

b) External co-ordinates; which give the spatial location of a particle in terms of the magnitude of x, y, and z axes that define any point in the system in three dimensional space. For instance, such co-ordinates become applicable if it is required to describe a particle as a member of a phase gradient e.g. restricted mixing.

The combination of the internal and external co-ordinate region of the particulate system is referred to as particle phase space, which for m independent internal co-ordinates is said to result [76] in (m + 3) dimensional space and a m + 3 dimensional distribution is required to completely characterize the system. Provided the

particulate system is "homogeneously mixed", then the spatial location of the particles has no meaning and the dimension of the distribution solely depends on the value of m. It would appear from the literature that particle size is the most frequently encountered internal co-ordinate property of naturally occurring particulates, whilst that of concentration is often limited to the description of liquid solvent droplets found in extraction processes. The use of other internal co-ordinate properties in the dimensional distribution is normally met in specialist applications. Thus, m equals 1 quite often and the one dimensional distribution of particle sizes which results, may be represented analytically or empirically by a variety of graphical plots.

3.2.5 ONE-DIMENSIONAL DISTRIBUTION FUNCTIONS APPLIED TO COOKE-TYPE DISPERSIONS

A further postulate from Cooke suggests that the hydrocarbon particle is shaped in a spherical form, because of considerations of surface tension. Surface tension forces for any molecular system arise from intermolecular attractions, whereby molecules in the bulk of the liquid assume a lower potential energy than those in the surface and these experience an inward force. As the attainment of a stable equilibrium for any given system corresponds to its lowest potential energy, there will be a minimum number of molecules occupying the liquid surface and consequently, the surface area of a given volume of the liquid will also be a minimum. Mathematically, it can be shown that the shape of a given volume of liquid with a minimum surface area is a sphere. Experimentally, this phenomenon is proven, as for example:-

1. At room temperature the density of aniline is slightly greater than water, but at higher temperatures their densities are approximately the same. At this latter stage the aniline forms liquid spheres which rise and fall in the water, because the gravitational effect on the aniline is opposed by the upthrust of the surrounding liquid.

2. If molten lead is sprayed from the top of a high tower shot is produced, because the falling globules of liquid lead, form spheres through the action of surface tension forces.

Based on arguments of this type, it is initially assumed that the particles have a spherical form and consequently, a one-dimensional distribution function should adequately describe the distribution of particle sizes of hydrocarbon and the instances when it has an adhering catalyst. Essentially therefore, only the size internal co-ordinate (axis) is considered.

A variety of empirical forms or models are used for expressing a one-dimensional distribution about a co-ordinate axis (see fig 3.2). Quite often the functions may be interpretated in alternative ways depending on the geometric similarity of particles (e.g. all spherical) and the needs, but generally they may be transformed from one to the other. For example the distribution may be described in terms of:-

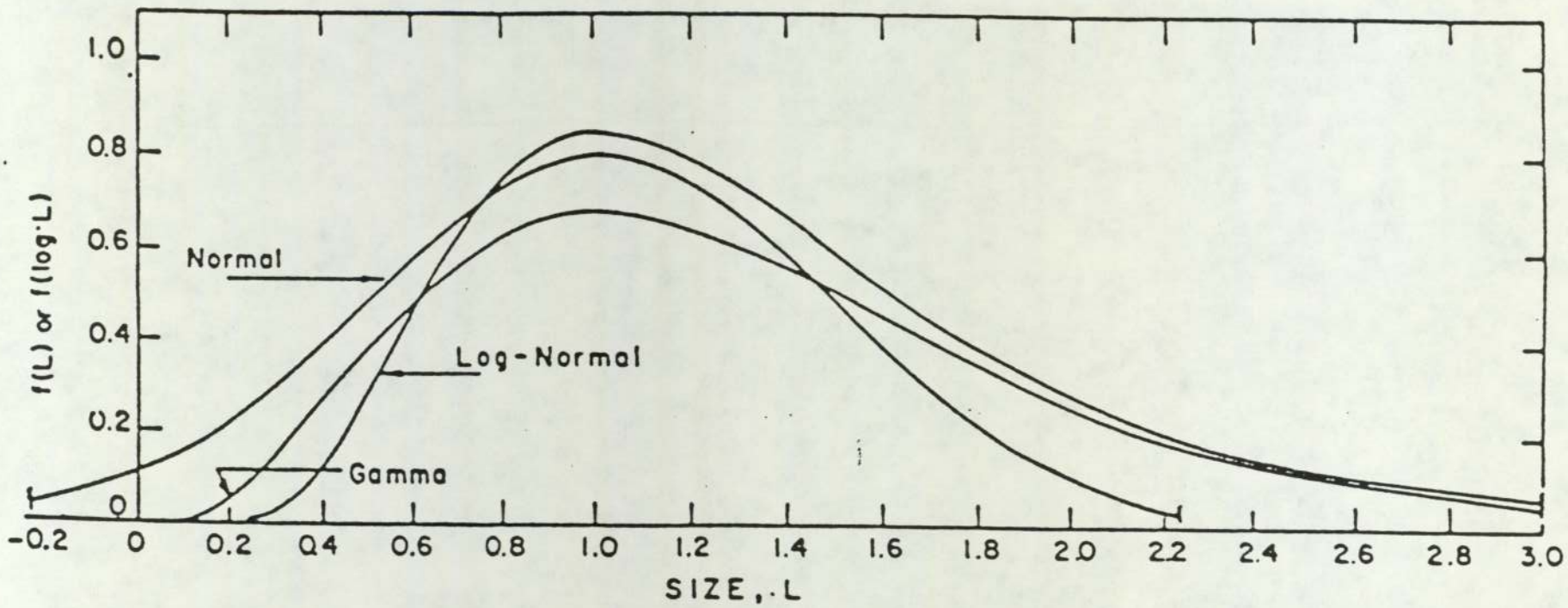

Fig. 3.2 Plots of three commonly used distribution functions

1. Members of a population (a size range) having respective values of the independent property co-ordinate e.g. population versus size.

   or

2. A dependent property of the population as it is distributed about the independent property axis, e.g. weight versus size.

In the case of 2 above, particle weight is proportional to particle size cubed, (provided the size of the particle is given in terms of radius) and this is used as a multiplication factor to obtain the weight distribution from the population distribution.

3.2.6 THE NORMAL DISTRIBUTION

The most well known one dimensional distribution function is the normal distribution, which is expressed as,

$$f(L) = [1/\sigma(2\pi)^{1/2}]\exp[-(L-\bar{L})^2/2\sigma^2] \qquad (3.1)$$

where f(L) indicates the relative frequency of particle size L, σ the standard deviation of particle sizes and $\bar{L}$ is the sample mean of particle sizes. Referring to fig. 3.2 the function is defined as finite over the interval $-\infty$ to $+\infty$, which can impose difficulties to the interpretation of some wide distributions, since weight in

negative particle sizes is implied. Furthermore, particle size distributions based on population or weight are typically assymetrically shaped and, hence, poorly represented by the symmetric bell-shaped gaussian curve of a normal distribution.

3.2.7 THE LOG-NORMAL DISTRIBUTION

An empirical representation of particle size distributions is often facilitated using the log-normal distribution function, such that

$$f(\log L) = [(2\pi)^{1/2}(\log \sigma')]^{-1} \exp[- (\log^2(L/\bar{L}'))/(2\log^2 \sigma')] \quad (3.2)$$

where f(log L) is the weight frequency at particle size L, whilst $\bar{L}'$ and σ' are the geometric mean and geometric standard deviation of particle sizes respectively (as the particles are considered to have similar geometries). The log-normal law has found particular prominence in its application to comminution processes such as grinding, milling etc. Such particle size distributions are typically assymetric and skewed towards the larger sizes (see fig 3.2), this takes account of weight over a size range corresponding to 100:1 in the sample. Additionally, the distribution does not exist below zero size, thus overcoming the problem of predicting finite population for negative values of L (compare with the normal distribution in fig. 3.2).

3.2.8. OTHER TYPES OF DISTRIBUTION FUNCTION

The Rossin Rammler distribution function has found acceptability in modelling size distributions of broken coal, sands, ores, clays, aerosol droplets etc., whereas the gamma distribution function (see fig. 3.2) is chiefly applicable to particle size distributions from crystallisation processes.

3.3. INSTRUMENTATION - GENERAL DESCRIPTION OF THE PARTICLE SIZE ANALYSER USED IN THIS STUDY

All particle size distribution measurements were carried out on a 'Malvern' 2200/3300 particle sizer (shown schematically in fig. 3.3a). This permits measurement of size distributions by weight (over a range 1 - 1800 microns (μ)) of

1. Solids in gas or liquid suspensions

2. Liquid droplets in gas or other immiscible liquids

3. Gas bubbles in liquids

Referring to fig. 3.3.b which is a schematic representation of the sizer instrument, a noticeable feature of the particle field is that it is able to behave very much like a diffraction grating, because the various interparticulate distances resemble a series of light apertures. Any points of interception along the plane wavefront of monochromatic light (from a laser source) and the particle field

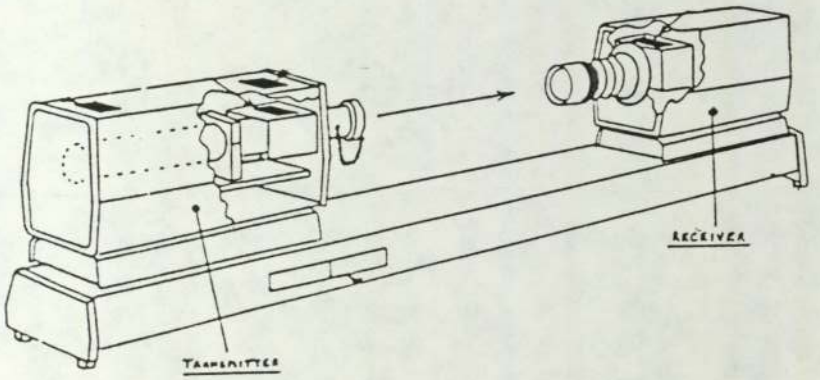

Fig. 3.3a The Malvern 2200/3300 particle sizer

Fig. 3.3b Schematic representation of the particle sizer

can be considered as secondary coherent sources of radiation from which light emanates forward in all directions (Huygens principle); coherent sources have identical frequencies and are in phase with each other. From the secondary sources it is observable that some light is bent outwards from the extreme confines of the parallel beam, but its coherency is subseqently affected (and some light is lost) through interference phenomena. This, results in a pattern of light bands, of an intensity depending on the population of particles. The optics of the instrument are so arranged as to only measure a Fraunhofer diffraction pattern (see fig. 3.4a), which may be distinguished from the more well known Fresnel type (see fig. 3.4b) by the fact that in the absence of a focussing lens its diffraction field is infinitely distant from its wavefront and the detector; thus parallel diffraction is possible over relatively long distances. To have a Fresnel diffraction pattern it is usual to have no lens system involved, because the source and detector are at finite distances from the diffraction field. Conveniently for particle sizer instrumentation design the Fraunhofer diffraction pattern is obtainable regardless of particle movement and, as such will always reflect the instantaneous size distribution in the sampling area.

Provided a continuous flux of particles is maintained in the sampling area over an appropriate integration period (integration of the diffraction pattern followed by iterative comparison with a chosen model), which is determined by the integration method chosen, the final measured diffraction pattern will be representative of the bulk of the sample. At the final stage of the optical system the diffraction pattern is focused by means of a fourier transform lens

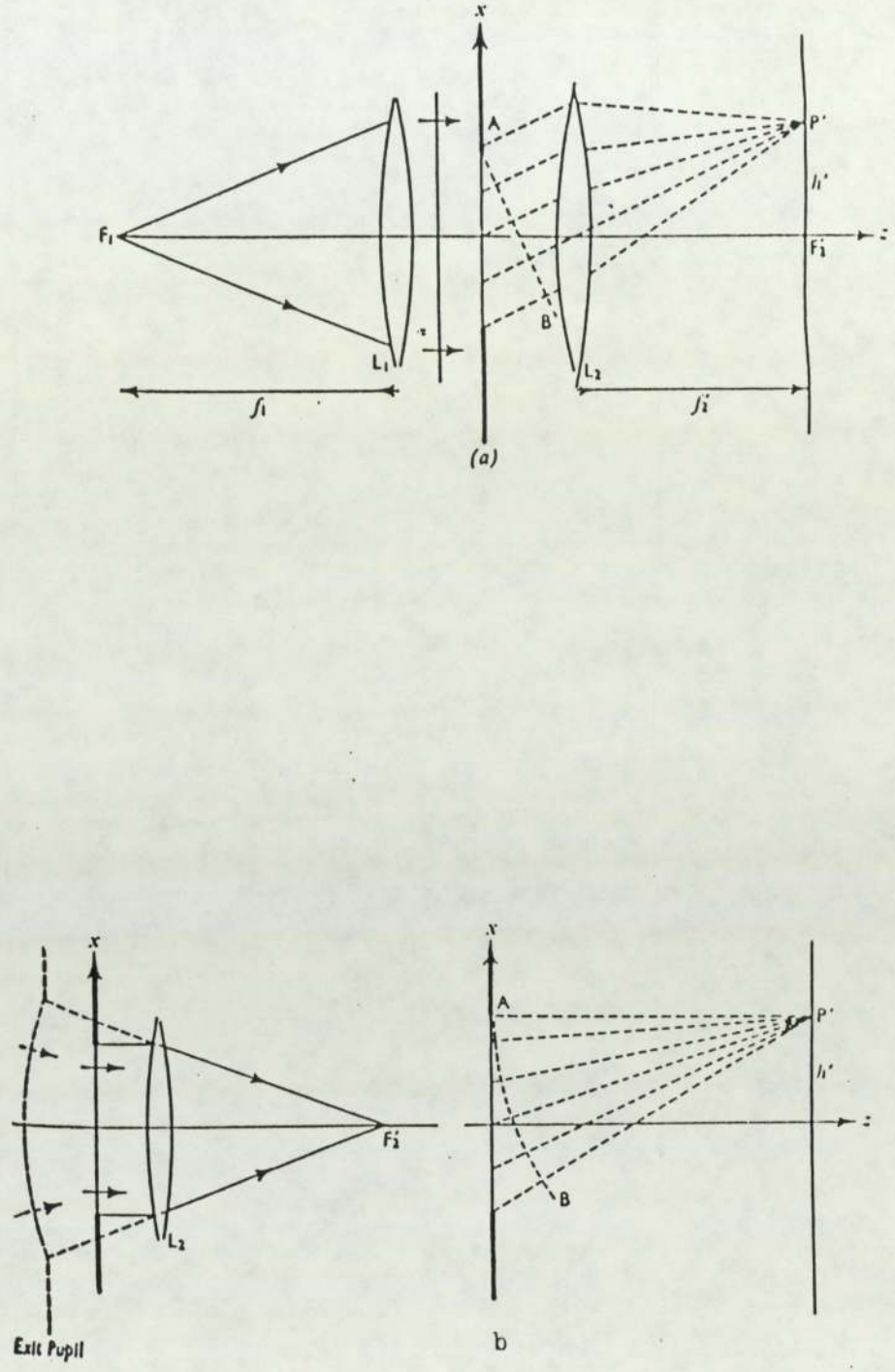

Fig. 3.4 The difference between Fraunhofer (a) and Fresnel (b) diffraction for a single aperture

on to a multi-element photo-electrical detector, which produces an analogue signal proportional to the intensity of light it receives. The integration of the diffraction pattern is facilitated by an analogue to digital converter interfaced to a computer.

Provided that the particulate system can adequately be described as a one-dimensional model, then its respective size distribution can be analytically generated from any of the previously mentioned two parameter models (see sections 3.2). In these, the mathematical method of non-linear least squares is utilised by the computer to find the closest fitting diffraction pattern. The computer is then able to display a size distribution by weight (over a suitable range) on a visual display unit (V.D.U.) or give a printed 'hard copy' of the results. Other presentations of the results are also available.

3.3.1 THE MODEL INDEPENDENT DISTRIBUTION

Because it has been established that computer programs using the normal and log-normal distribution models etc., are limited in their application to one-dimensional distributions, an alternative program for analysing multi-dimensional distributions has been devised for use on the Malvern 2200/3300 particle sizer. This program is called 'model independent' because no analytical model is assumed and it is thereby capable of accommodating all dimensions of the size distribution. Consequently, particle co-ordinates such as shape and concentration can be tolerated in the calculation of the distribution of particle sizes.

As its initial objective the model independent program formulates 15 weight bands, the quality of which is dependent upon the receiver lens used in the measurement. To obtain the proportion of weight in each of the bands involves a heuristic technique, which allows an initial distribution to be produced by taking a sensible guess. This distribution then enables a representative diffraction pattern to be generated and compared with that measured (also a principal step in the two parameter program for one-dimensional distribution functions). The fitting process is then repeated applying iterative adjustments, until an optimised distribution is obtained. Throughout this procedure it is possible to observe the development of broad distribution characteristics on a V.D.U. and at the same time observe the incremental improvements in terms of a log error. Although the log error for the model independent algorithm is comparable with that of the two parameter case, it is normal to obtain a better data-fit with the 'model independent' algorithm, because it is better able to compensate for sample abnormalities. However, this flexibility in data handling means that the finalised distribution may incorporate errors evolved by a bad measurement technique. Additional errors may also result from the experimental assumption that the whole of the sample is represented in 15 fixed weight bands and makes no predictions about weight outside these enforced weight limits, to do so, would violate the principle of model independence. A further drawback in using the model independent algorithm is that its execution period is 2 - 3 times more than that of the two parameter case (which covers the modelled distributions), because increased sensitivity is achieved by iterative refinement of 15 parameters.

3.4. EXPERIMENTAL DETAILS OF PARTICLE SIZE MEASUREMENTS

3.4.1 STANDARD CONDITIONS

In all dispersion experiments the following details were common (unless specified).

1. The dispersed phase was octadecane (m.p. 28^{o}C) as used by Cooke [36], whilst the dispersion medium was a proprietary grade of conductivity water [72].

2. Ultrasonics at a set frequency (~20 KHz) were used under controlled conditions to effect the dispersion of the insoluble particulate hydrocarbon in water.

3. In order to resolve the distribution of particle sizes of the dispersion, it was found necessary to apply the model independent algorithm. Prototype distribution experiments using various solid dispersions (see below) and some common one-dimensional algorithms (discussed in section 3.2) had surprisingly shown that they were mismatched, as no sensible distribution could be attained (in many cases the experimental plot was devoid of any distribution and yet fine particulate matter was 'visible by eye').

4. Most dispersions were of the solid type (see section 3.4.2a below) which were favoured by Cooke, apart from the liquid dispersion the preparation of which is detailed in section 3.4.2.b.

3.4.2. CONTROLLED CONDITIONS

3.4.2.a SOLID DISPERSIONS

A small quantity of octadecane (in the range 0.1 -0.2g) was slowly melted in a beaker and transferred to a microsyringe (see section 3.4.2c for other techniques). This aliquot was injected into $650 \times 10^{-3} dm^3$ of sonificated water, which was initially at room temperature and a dispersion of fine solid particles resulted. Ultrasonics were applied throughout the preparative experiments which lasted for 5, 10, 30 and 50 minutes.

The initial volume of water was also varied before making the dispersion up to $650 \times 10^{-3} dm^3$.

3.4.2b LIQUID DISPERSIONS

These experiments parallelled those pertaining to solid dispersions in most respects, except that temperature of the water was arranged to be slightly above the melting point of octadecane. Therefore, the dispersion produced initially, was of the liquid-liquid type.

3.4.2c TECHNIQUES

Alternative methods for introducing the dispersed phase into the dispersion medium were investigated for solid dispersions only, since they were pertinent to Cooke's original photolysis work.

An optional injection method used 2 x $10^{-3}dm^3$ hypodermic syringe (Cooke's primary method), but unlike the microsyringe it tended to offer less control over the delivery of the octadecane.

In an attempt to increase the interaction area for the sonification effect, the molten octadecane was spread over the large area of a water heated glass block to form a thin liquid film (T.L.F.), which was then immersed in the water. This method had been developed by Cooke on the basis of observations made during some preliminary syringe experiments, whereby octadecane, thinly coated on the melting vessel, was found to be readily dispersed. Overall, the T.L.F. method did not provide dispersions of a visibly superior quality over those obtained by hypodermic or micro syringe techniques and in addition tended to be more time consuming. Consequently, all further experiments for the production of solid dispersions were conducted using either of the syringe techniques.

3.4.2d OTHER TYPES OF DISPERSIONS

On each preparative occasion a fresh dispersion was made up under standard conditions, in order to check dispersion reproducibility. The initial dispersion from that series was then repeatedly measured over an extended analytical period (1 - 15 days) to enable time dependent phenomena to be monitored. Other experiments concentrated on determining the effects of diluting the finalised dispersion and changing the initial dispersion volume of water. The concluding experiment was a comparative examination of two standard dispersions, one of which, incorporated a Whitten type surfactant.

3.5 RESULTS AND DISCUSSION

Diagrammatical representations of the distribution of particle sizes for the various dispersions are given in histogram form, in the discussion section, where for the purposes of description and convenience, the top left-hand diagram of each figure shows a relative size range of 1.2 - 118.4 microns (μ): This scale is applicable to all distributions presented. It should also be noted that unavoidably the computer print out of the histograms gives their horizontal axes slightly misplaced from the vertical axes, but no ambiguities to the interpretation of particle sizes has resulted. The % WT/SIZE scale is assigned by the computer on the assumption that the total distribution of particle sizes observed relate to 100% of the material dispersed. For example in fig. 3.5a (solid dispersions) the band of particle sizes at 54.9μ represents approximately 20% of the total material dispersed. It has to be emphasised, therefore, that the amount of dispersed material that is analysed need not necessarily be constant in different experiments, although the sum of the heights of all of the bands observed in the histograms is taken to represent the total amount of material dispersed (variable) and assigned to 100% on the vertical scale.

3.5.1 SOLID AND LIQUID DISPERSIONS

In view of the fact that only the model independent algorithm fitted the particle size distributions of selected octadecane dispersions (solid) in water and those same distributions did not conform with the one-dimensional functions in common use, suggests that other internal co-ordinates (apart from size) might be used to describe the particle. However, the need to include extra internal

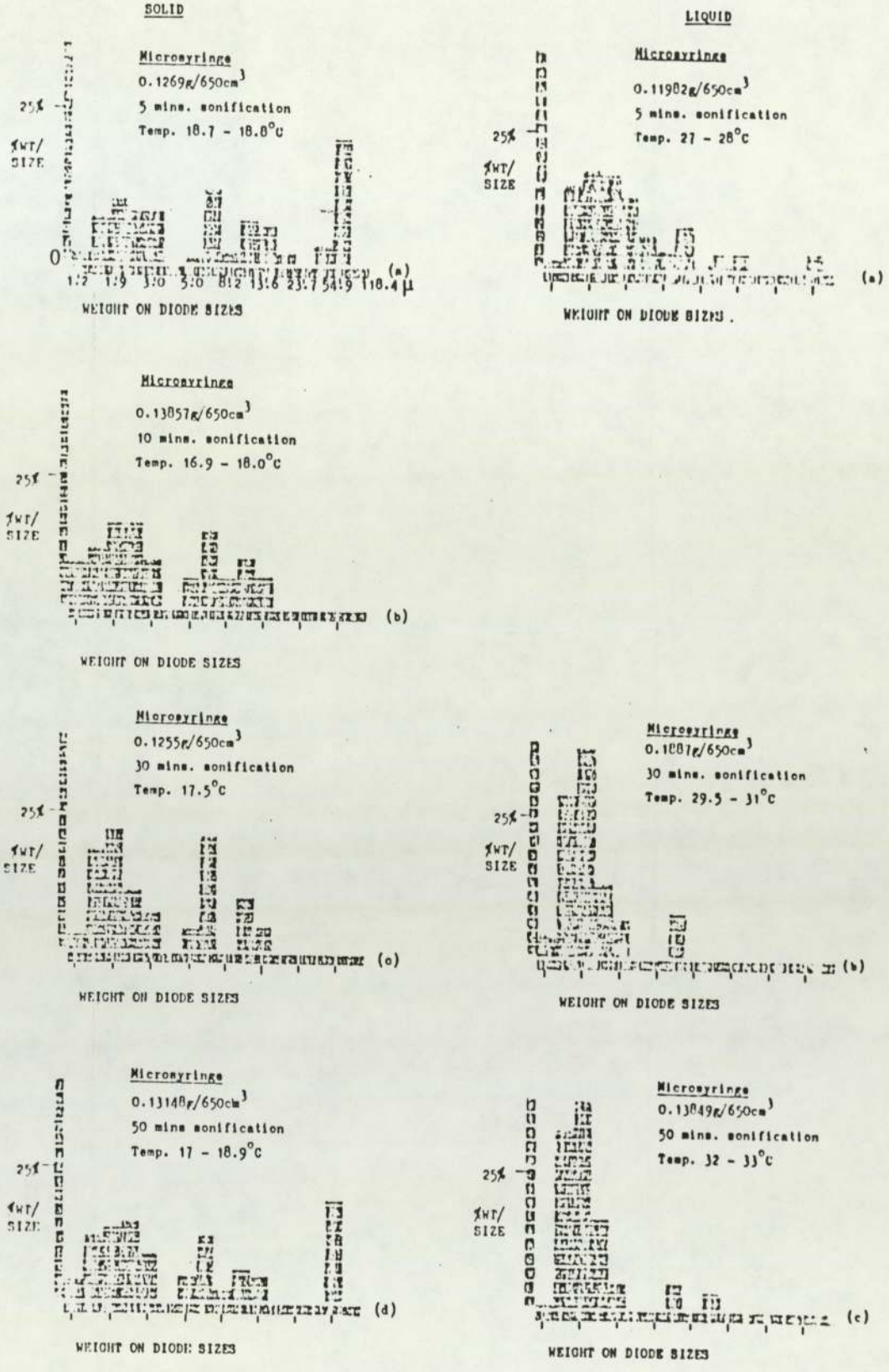

Fig. 3.5. Comparison of Solid and Liquid Dispersions

co-ordinates (such as particle shape or concentration) to complete the description of the particulate system, can at this stage, only be tentatively hypothesized from the limited amount of data available. Nevertheless, the influence of particle shape (a co-ordinate axis) might be deduced from comparison of the distributions of solid and liquid dispersions (shown in fig. 3.5) as follows:-

Cooke has postulated a spherical shape for the particles solely on surface tension considerations (see section 3.2). However, fig. 3.5 shows that the distribution of particle sizes for the solid and liquid dispersions are markedly different. Perhaps the most evident dissimilarity between the two types of dispersion is found at their preparative stages. In liquid dispersions the hydrocarbon remains liquid after its addition to the water, whereas the converse is true for solid dispersions. In the case of liquid dispersions, it is likely that surface tension forces prevail to an extent such that sphericity is more easily maintained (i.e. Homer [77] has recently shown by N.M.R. that liquids in dispersions are spherical) and sonification quickly has a limited disruptive effect on the particles: Indeed only small changes are noticeable in the particle size distributions of dispersions that have undergone 30 and 50 minutes of sonification (fig. 3.5). Moreover, the restricted effect of sonification places the majority of particle sizes in the 1.2 - 3.0 micron range.

Identical experiments on solid dispersions indicate that sonification continues affecting the size of particles, up to 50 minutes duration, although the limiting range of particle sizes of 1.2 - 3.0 microns, still clearly predominates. There is also an increased number of aggregates at larger particle sizes. In order to try to explain these observations for dispersed solids it is possible that

as the particles exist as rigid condensed forms (spherical or otherwise) they may be randomly cleaved into smaller irregular fragments by sonification. Such particles can then coalesce (through hydrophobic attractive forces) or remain as single entities and thereby constitute a distribution, to which a one-dimensional algorithm would remain inapplicable.

3.5.2 A COMPARISON OF THE TECHNIQUES USED FOR PREPARING DISPERSIONS

A comparative study of the distribution of particles of solid dispersions generated by syringe, microsyringe and T.L.F. techniques (see fig 3.6) appear to confirm the evidence from crude visual examinations, which generally revealed few differences. A predominance of particles in the lower range of sizes is noted. The data in fig. 3.6 indicate the reproducibility of the preparative techniques.

3.5.3 THE EXAMINATION OF DISPERSIONS OVER VARIOUS TIME PERIODS

The measurement of particle size distributions for a given solid octadecane dispersion over prolonged durations, are illustrated in fig. 3.7 and they provide some insight into the long term stability of the original dispersion. As might now be expected, the dispersion on day 1 has most of its particle size distribution centred at the lower end of the size scale with minor particle entities at higher values. This distribution trend is followed up to and including day 9, although the relative band intensity of the larger particles has increased.

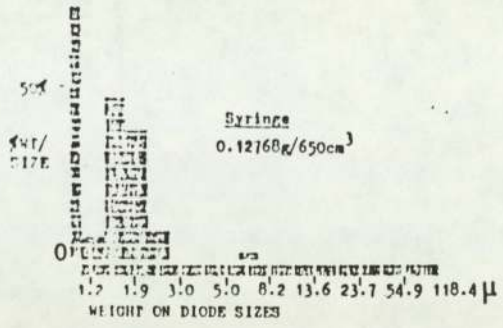

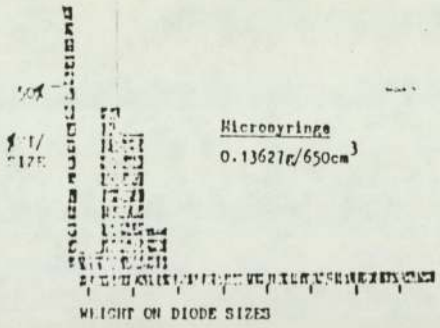

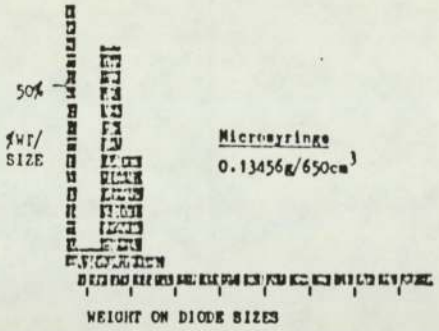

Fig. 3.6. A comparison of the technique used for preparing dispersions

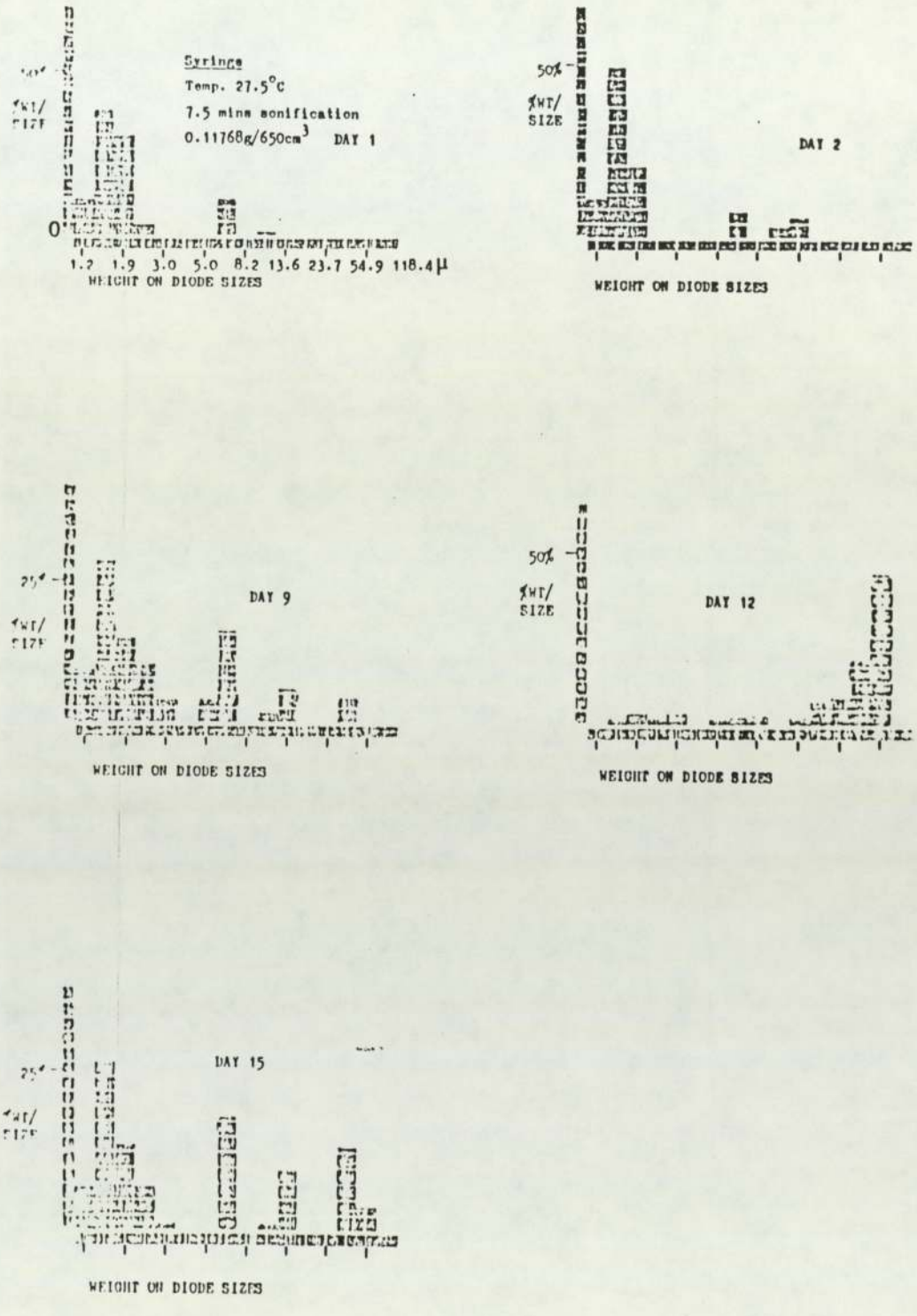

Fig. 3.7. An examination of the same dispersion over an extended time period

On day 12 there is virtually a complete reversal of the distribution with the majority of particles near the higher extremity of the size range. This increase in the amount of larger particles could subsequently result in aggregation to give a precipitated solid, which became visually evident after day 9.

The distribution assumes a more typical form on day 15, in that it resembles the distribution of days 9, 2 and 1. This observation may be misleading for the following reasons: As has been stated before in section 3.5, 100% on the vertical axis of the histogram relates to the total amount of material dispersed, which need not be the same from sample to sample. Consequently, if dispersed octadecane has been removed by precipitation after day 12 (perhaps through coalescence of the larger aggregates) the effect of assigning 100% to the octadecane remaining dispersed, is to essentially amplify the lower size bands of day 12 to yield an histogram on day 15 similar in appearance to that of days 9, 2 and 1.

It is also noticeable that the pattern of gaps which appears in the particle size range is repeated throughout the overall set of analyses and they obviously represent unfavoured particle sizes.

As the experimental period for this dispersion study covered several days, this enabled the particle size distribution of a new dispersion (produced by a standard method) to be determined on each analytical occasion (see fig 3.8). Thus, the resulting distribution series tests the reproducibility of standard dispersions and indicates once more, that most particles (see figs. 3.8a, c, d, and e) are confined to a lower range of sizes (1.2 - 3.0μ). The distribution of particle sizes shown in fig. 3.8b is more spread than the other

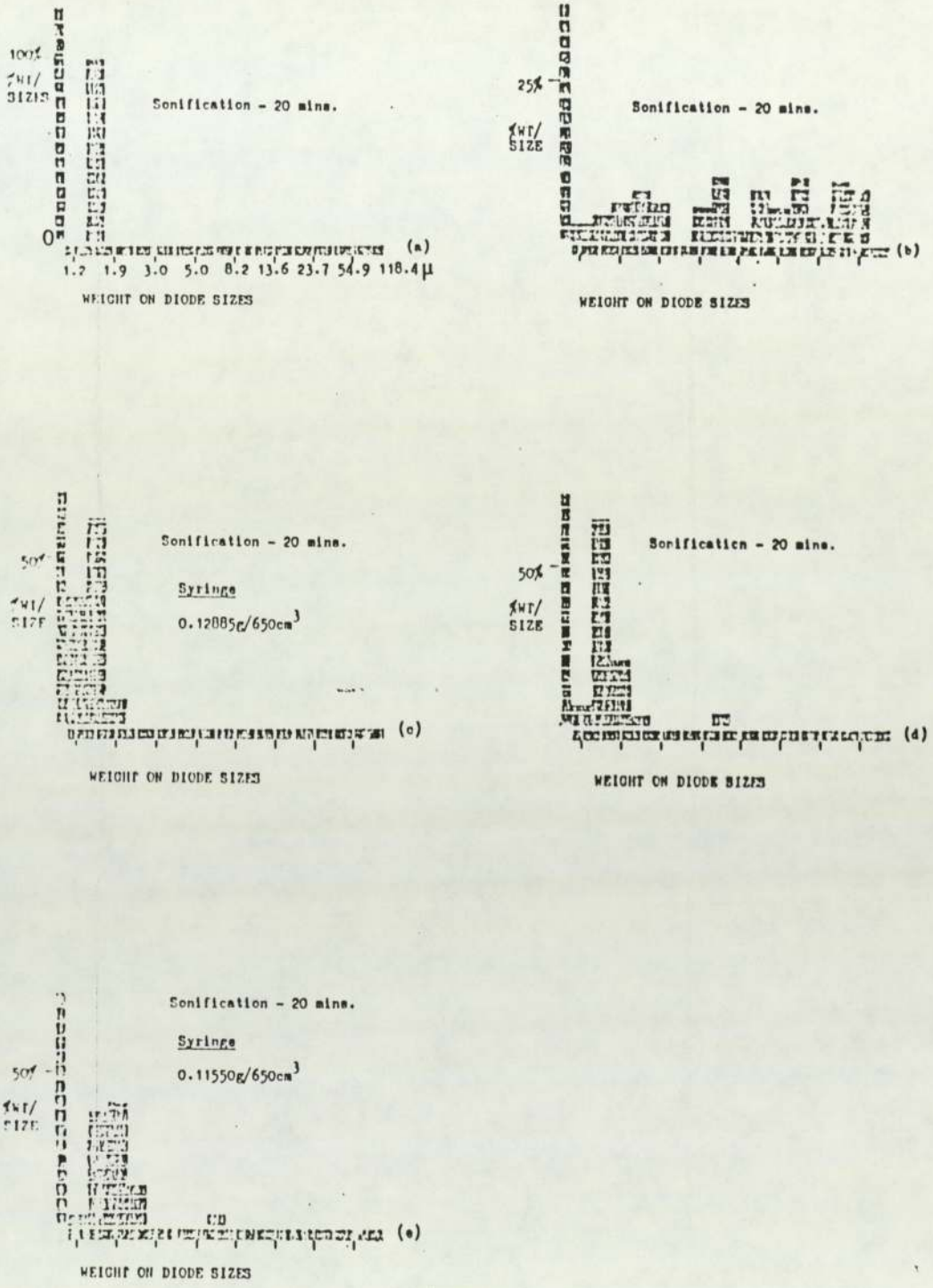

Fig. 3.8. An examination of the reproducibility of standard dispersions

distributions shown in fig. 3.8, but no explanation can be offered as to the reasons for this effect.

3.5.4. THE EFFECTS OF DILUTION ON THE DISPERSION

3.5.4A DIRECT DILUTION

In referring to fig 3.9.1 it is evident that straight dilution of the standard octadecane dispersion with water has no notable effect on its particle size distribution (e.g. compare 3.9.1a with 3.9.1b). Provided that there is no introduction of phase gradients (e.g. from lack of stirring) such a short term outcome is to be expected, because to impose changes on the particle size requires their chemical composition or physical forces to be changed.

3.5.4B VARIATION OF THE INITIAL VOLUME OF THE DISPERSION MEDIUM

As previously mentioned in section 3.3.5A a slightly different aspect of dilution for solid type dispersions was also investigated. For this, the initial volume of the dispersion medium (water) was varied, a constant weight of the hydrocarbon dispersed phase added and the resulting dispersion removed from sonification before being finally made up to its normal level of $650 \times 10^{-3} dm^3$ with water. The particle size distributions from these dispersions are shown in fig. 3.9.2 and represent a sample of the different preparations initially and 24 hours later. Their particulate features are generally similar.

From an overall standpoint, it is concluded that the controlled dilution of a standard octadecane dispersion has no significant effect on the outcome of its particle size distribution, which is mainly located in the lower size range (1.2 - 3.0μ).

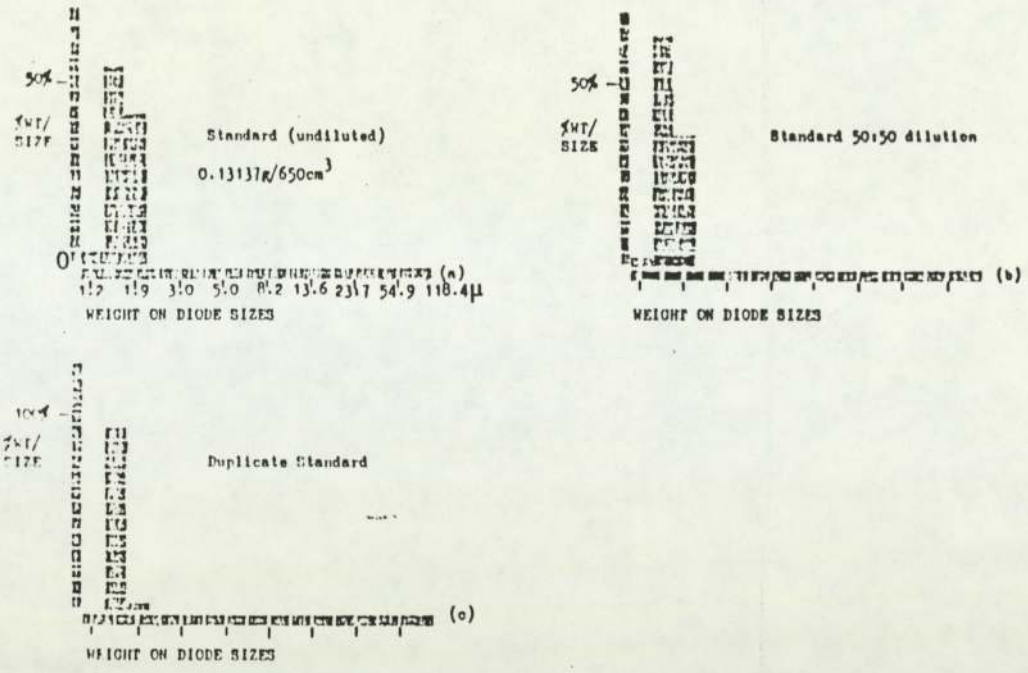

Fig. 3.9.1. The effects of direct dilution on the dispersion

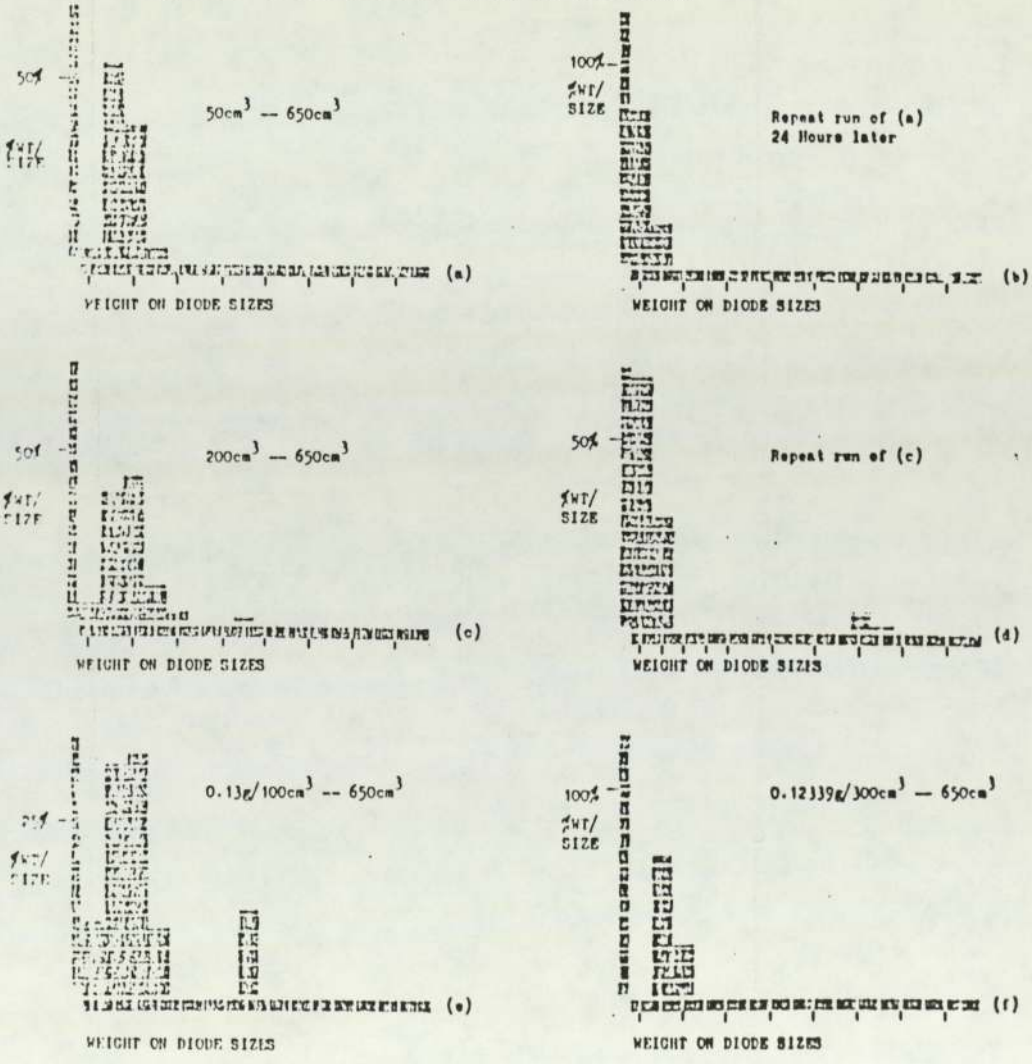

Fig. 3.9.2. The effects of varying the initial volume of the dispersion medium

3.5.5 DISPERSIONS OF OCTADECANE WITH A SURFACTANT DERIVATIVE OF $Ru(bipy)_3^{2+}$ (WHITTEN-TYPE) Ru/G.M.C./2 [78]

$((bipy)_2RuII(2,2'\text{-bipy-}4,4'(COOC_{18}H_{37})_2))^{2+}(PF_6)_2^{2-}$

The effects on the particle size distribution of an octadecane dispersion due to the addition of Whitten-type surfactant, $((bipy)_2RuII(2,2'\text{-bipy-}4,4'(COOC_{18}H_{37})_2))^{2+}(PF_6)_2^{2-}$, are displayed in fig. 3.10 which outlines the respective distributions just after preparation and 24 hours later. The distributions of new octadecane dispersions with and without surfactant are very similar (with the preferred low particle sizes again evident) but there are striking contrasts between the two distributions after a lapse of 72 hours, in that the bulk of the particles of the catalytic dispersion have aggregated to form particles of a much larger size. This distribution resembles that of an octadecane dispersion measured on day 12 in the long term experiment, (see fig. 3.7). Furthermore, the distribution covers the entire particle size range, allowed by the model independent program, which is markedly different from most previous distributions of octadecane dispersions.

An explanation for the time dependent aggregation may be found by examining the initial behaviour of the charged surfactant and its octadecane support. It is reasonable to believe that the cation of the surfactant 'adheres' to octadecane by forces which might be attributed to their hydrophobic character, such that the extensive hydrophobic tail of the cation is directed towards its octadecane particulate base. When there are sufficient cations surrounding an octadecane particle (the number of cations being possibly determined by the particles surface area) the 'coated' particle's ability to aggregate with other similar particles becomes prohibited by

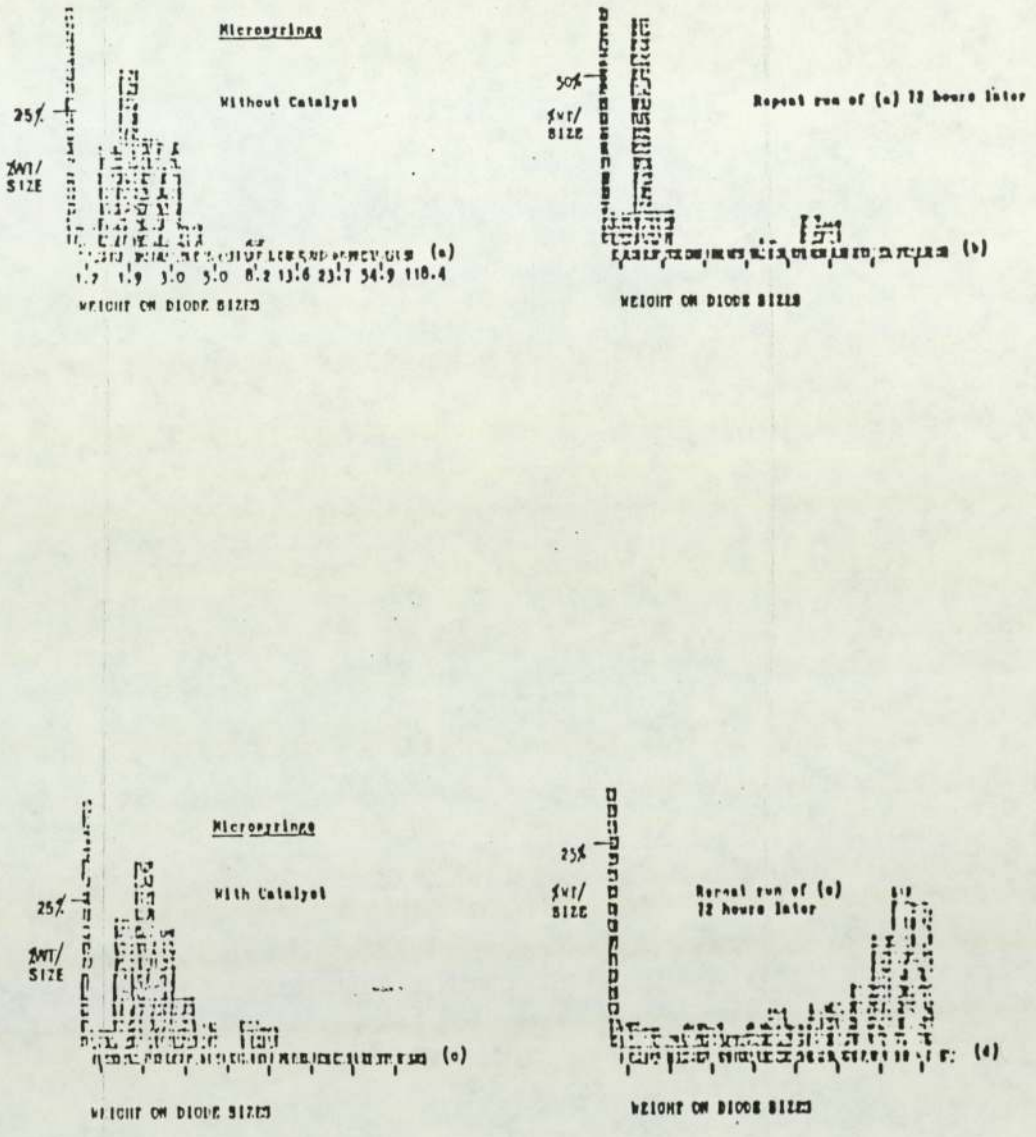

Fig. 3.10 Dispersions of Octadecane with and without a surfactant derivative of $Ru(bipy)_3^{2+}$ (Whitten-type) Ru/G.M.C./2[74]

interparticulate electrostatic repulsions and as a consequence the parent dispersion is stabilized. Thus, it is possible that the particle aggregation that results after a lapse of time is a consequence of hydrolysis of the surfactant (see section 2.11.3b) to give (with octadecanol and ruthenium carboxylate) 'octadecane particles' with reduced surface charges which may aggregate.

3.6. CONCLUSION

To summarise: From differences found between solid and liquid dispersions it might be construed that particle shape is in the case of solid dispersions a factor that must be included in the description of its particles, but particles in liquid dispersions are adequately described as spheres. Prolonged sonification has a limited effect on both types of dispersion. In general the preparative techniques all produce similar dispersions with the majority of particles in the 1.2 - 3.0μ range. While direct dilution of the initial dispersion and varying the volume of water in which the octadecane is initially dispersed had no significant effect on the distribution of particle sizes. The dispersions seem to be fairly reproducible if standard conditions are used, however, long term studies of a selected standard dispersion have shown that the particles undergo a varied amount of aggregation over a 15 day period. Finally, the incorporation of a surfactant into the hydrocarbon particle made little difference to the distribution of particle sizes initially produced. However, that dispersion underwent several changes to its particle size distribution after a time lapse of 72 hours: Hydrolysis of the surfactant being the most likely explanation for this occurrence.

Although this investigation into the distribution of particle sizes of octadecane (and added Whittten-type surfactant) is in its infancy, it has revealed several features (some now published [36]) that seem worthy of further examination. The effect of particle shape is particularly interesting, because irregularly sized solid octadecane particles would provide different surface areas on which to support the surfactant. Consequently, this could mean that particles (with

adhering surfactant) of a nominally equivalent size (as defined by diameter [75]) might have concentrations of surfactant determined by heterogeneous intermolecular forces, rather than homogeneous intermolecular forces which are presumed to prevail for spherical particles. Such speculations, might explain the inconsistency of Cooke's photolysis experiments [36] using dispersions.

CHAPTER 4

A N.M.R. STUDY OF THE MOLECULAR INTERACTION IN SOLUTION BETWEEN A DIESTER SURFACTANT DERIVATIVE OF $Ru(bipy)_3^{2+}$, $((bipy)_2Ru(II)(2,2'\text{-bipy-}4,4'(COOC_{18}H_{37})_2))^{2+}(PF_6)_2^{2-}$, AND WATER

4.1 INTRODUCTION

The nature of molecular interactions in solution has frequently confounded, yet challenged numerous researchers, and unsurprisingly, it is their ingenuity that has given the many analytical techniques which have been successfully used to resolve some unique properties of the interacting species. Of all the techniques used for studies of this kind, those provided by nuclear magnetic resonance (N.M.R.) spectroscopy have been found particularly informative.

N.M.R. is particularly useful for the study of the formation of molecular complexes in reactions of the type represented by equation (4.1).

$$A + nD \; \langle\text{-}\text{-}\text{-}\rangle \; AD_n \qquad (4.1)$$

Here A and D often represent the respective acceptor and donor components of a complex, as for instance, that which has been formerly proposed (Chapter 1) for the equilibrium reaction between a surfactant derivative of $Ru(bipy)_3^{2+}$ and H_2O. Because the N.M.R. investigations reported in this thesis are based on the determination of chemical shifts, a brief resume of the most pertinent aspects of chemical shift theory is now outlined.

4.2 CHEMICAL SHIFTS

The fundamental description of the nuclear magnetic resonance condition for any nucleus with spin or angular momentum (I), is

$$\nu = \frac{\gamma B_0}{2\pi} \qquad (4.2)$$

for which ν is the frequency of an oscillating magnetic field (that is derived from a radio frequency signal) necessary to induce nuclear magnetic resonance and γ is the nuclear gyromagnetic constant: The latter term defines a ratio between the magnetic moment, (which can simply be considered to arise from the spinning nuclear charge) and the angular momentum. The value of γ is characteristic of any resonant nucleus.

When an atom or molecule is subjected to a magnetic field (B_0) the applied magnetic field will only be felt by a nucleus after traversing an electronic screen that is dependent on specific molecular surroundings. Consequently, a secondary magnetic field is induced that depends on the magnitude of B_0 and the nature of the electrons in the vicinity of a nucleus.

In order to accommodate electronic phenomena in the classical description of the N.M.R. experiment, it is necessary to modify equation (4.2) to account for the shielding described above. Therefore, a screening constant,σ, which can show the extent to which the resonant nucleus is screened (or shielded) from the effects of B_0, is included as follows:-

$$\nu = \frac{\gamma B_0}{2\pi}(1 - \sigma) \qquad (4.3)$$

If nuclei reside in different electronic environments the screening constants for each resonant nucleus (say A and B) will be different. The respective resonance frequencies will therefore, be different and given by 4.4 and 4.5.

$$\text{As} \quad \nu_A = \frac{\gamma B_0}{2\pi}(1 - \sigma_A) \qquad (4.4)$$

$$\text{and} \quad \nu_B = \frac{\gamma B_0}{2\pi}(1 - \sigma_B) \qquad (4.5)$$

$$\text{It follows that} \quad \nu_A - \nu_B = \frac{\gamma B_0}{2\pi}(\sigma_B - \sigma_A) \qquad (4.6)$$

From a practical standpoint the measurement of resonance frequencies for the two nuclear resonance conditions is readily achieved. Because the frequencies depend on B_0, it proves convenient to eliminate B_0 from the equation 4.6 by dividing by for example ν_A, which gives

$$\frac{\nu_A - \nu_B}{\nu_A} = \frac{\sigma_B - \sigma_A}{(1 - \sigma_A)} \qquad (4.7)$$

If it is assumed that $\sigma_A < 1$, the equation takes the form

$$\frac{\nu_A - \nu_B}{\nu_A} = \sigma_B - \sigma_A = \delta_{B-A} \qquad (4.8)$$

where δ_{B-A} is called the chemical shift between B and A. Equation (4.8) provides a workable relationship for studying screening effects by measuring the fractional frequency change measured in hertz (Hz). This may be expressed in parts per million (p.p.m.) and is independent of the oscillating radio frequency used.

4.3 ORIGINS OF THE CHEMICAL SHIFT

For any resonant nucleus, A, its total screening, σ^A, can be expressed in an expanded form [79] that is made up of contributions from intramolecular and intermolecular screenings, σ^A_{intra} and σ^A_{inter} respectively, such that

$$\sigma^A = \sigma^{AA}_{intra} + \sigma^{AA}_{inter} \qquad (4.9)$$

A change in the chemical shift of A with respect to a given reference, will happen if a difference occurs in the magnitude of any of the contributing terms.

4.3.1 INTRAMOLECULAR EFFECTS σ^A_{intra}

It was Saika and Slichter [80] who originally accounted for σ^{AA}_{intra} by considering it in terms of three atomic contributions. (They, however, apparently overlooked the effects of interatomic currents, in which electrons move from one atom to another). A more complete description of σ^A_{intra} was to follow [79], that is represented by

$$\sigma^{A}_{intra} = \sigma^{AA}_{dia} + \sigma^{AA}_{para} + \sum_{B \neq A} \sigma^{AB}_{mag} + \sigma_{deloc} \qquad (4.10)$$

Each contributing term in equation (4.10) will now be discussed.

4.3.1a THE DIAMAGNETIC TERM σ^{AA}_{dia}

For an atom having a spherically symmetric electronic distribution, the application of a magnetic field B_0, will induce the free rotation of electrons about their nucleus. The screening effect that results from this induced current is diamagnetic, opposes the primary field and is represented by the magnitude of the term σ^{AA}_{dia}. As the value of σ^{AA}_{dia} is governed by electron density, the electronegativity of groups around the nucleus will also have an effect on chemical shifts. Reference is made to fig. 4.1 for an example.

4.3.1b THE PARAMAGNETIC TERM σ^{AA}_{para}

The induced mixing of ground and low lying excited electronic states of an atom by an applied magnetic field is covered in the term σ^{AA}_{para} [81, 82]; this also arises from localised fields at the resonant nucleus. Provided electrons are confined to a pure s orbital, then it can be reasoned that σ^{AA}_{para} has no value [83], but outside this set limit, the evaluation of σ^{AA}_{para} is difficult to calculate, since the energies and wave functions of the ground and excited states of the parent molecule are not normally known. Reference is made to fig. 4.2 for an example.

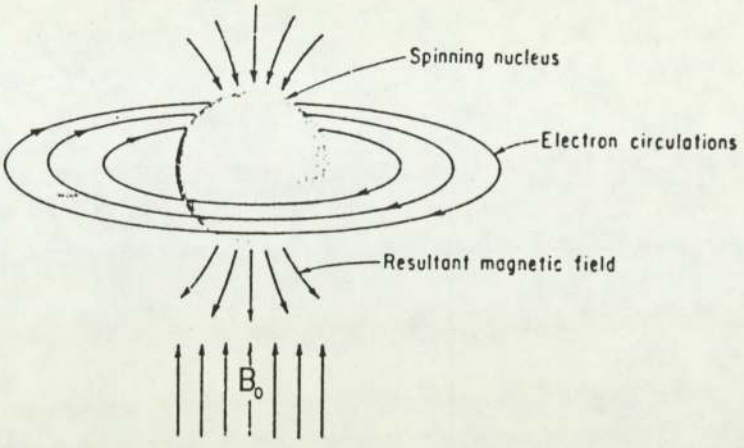

Fig. 4.1 The effect of diamagnetic electronic circulations about a nucleus and the induced secondary magnetic fields that oppose B_0.

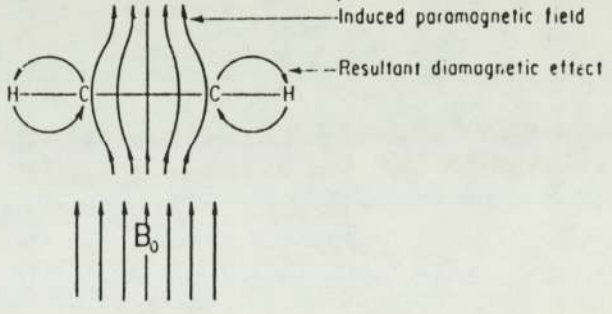

Fig. 4.2 Shielding of the protons of acetylene when it is alligned perpendicularly to B_0. The electrons which are confined to the s orbitals of hydrogen do not contribute to the paramagnetic effect.

4.3.1.c INTERATOMIC SCREENING σ^{AB}_{mag}

If a molecule has two adjacent atoms that constitute an anisotropic electron group and this is placed in an applied magnetic field, different magnetic moments are induced along the principal axes of the bonds. These constitute induced magnetic dipoles that give rise to secondary fields at neighbouring nuclei (the so called neighbour anisotropy effect [84]). This is characterized by the interatomic shielding term σ^{AB}_{mag}. The magnitude of σ^{AB}_{mag} depends on the nature and spatial arrangement of the atom or group causing the secondary field. Reference is made to fig. 4.3 for an example.

4.3.1d DELOCALISED ELECTRON SCREENING σ_{deloc}

For conjugated molecules, the induced electronic currents that result from the applied magnetic field, set up secondary fields which have screening effects (represented by σ_{deloc}) depending on the position of nuclei within the moleucle. For instance, in the case of aromatic molecules, the secondary fields induced by the circulation of π electrons can either add or substract from the applied magnetic field which is effective at a nucleus, such that nuclei lying in the plane of the ring experience the greater deshielding. Reference is made to fig. 4.4 for an example.

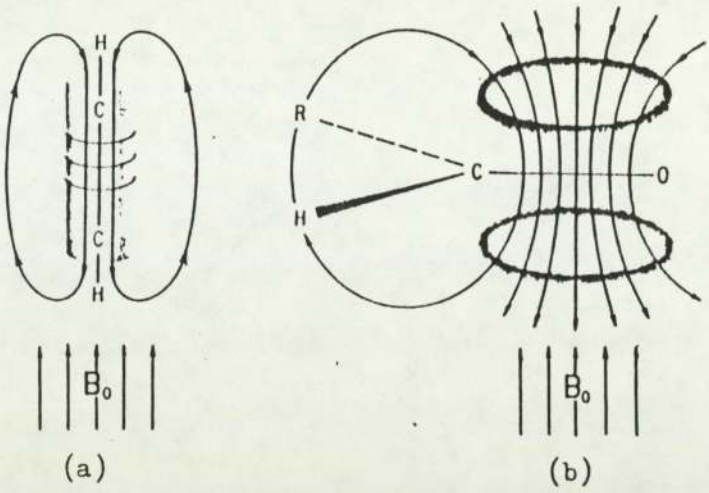

Fig. 4.3 The screening arising from diamagnetic anisotropic effects is dependent on the orientations of protons of the molecule relative to B_0. For instance in (a) the acetylenic proton is shielded, whereas in (b) the aldehydic proton is deshielded.

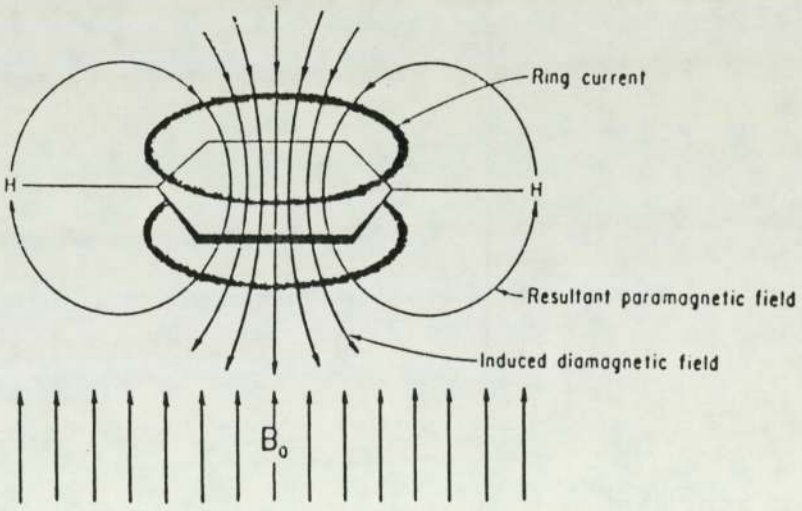

Fig. 4.4 The ring of delocalized π electrons of a aromatic molecule induces screening effects which are opposed to B_0 along the six-fold axis but reinforce it at the aryl protons.

4.3.2 INTERMOLECULAR SCREENING EFFECT σ_{sol}

The screening of a solute nucleus in the liquid phase has a screening contribution σ^{A}_{inter} or σ_{sol}, the magnitude of which is a measure of the total effect (from direct or indirect mechanisms) felt by that nucleus from surrounding solvent molecules.

In the context of the present studies it is expedient to consider those intermolecular screening effects that contribute to σ_{sol} [85]. It is now accepted that σ_{sol} can be represented by

$$\sigma_{sol} = \sigma_b + \sigma_a + \sigma_w + \sigma_E + \sigma_c \qquad (4.11)$$

for which the respective terms on the right hand of the equation are now discussed.

4.3.2a SCREENING DUE TO BULK MAGNETIC SUSCEPTIBILITY, σ_b

At a later stage in this thesis the importance of σ_b corrections will be introduced in a practical context and therefore, σ_b is examined more fully than the other screening terms that contribute to σ_{sol}.

A chosen nucleus in its molecular environment experiences some screening due to the magnetic properties of its bulk environment that are induced in the presence of B_0. The magnitude of this screening depends on the geometry of the N.M.R. sample. This effect is treated by considering that each of the solute molecules occupies a spherical cavity in a diamagnetic medium [86] that is regarded as a continuum of solvent molecules. In the presence of an applied magnetic field, (B_0), the medium, of volume magnetic susceptibility, χ_v, becomes polarised, such that the effective magnetic field, B_{eff}, at the solute nucleus becomes a modification of B_0, the extent of which is given by

$$B_{eff} = B_0 \left(1 + \left(\frac{4\pi}{3} - \alpha\right) \chi_v\right) \qquad (4.12)$$

where α is a shape factor, and is $4\pi/3$ for a sphere and 2π for a cylinder, for which the radius is considerably smaller than its length.

Most modern high resolution N.M.R. spectrometers use cylindrical vessels to contain the sample and as such the contribution to the observed intermolecular screening arising from the susceptibility of the medium is given by $\frac{2\pi}{3}\chi_v$, so that

$$\sigma_{obs} = \sigma_0 + \sigma_{mol} + \frac{2\pi}{3}\chi_v \qquad (4.13)$$

where σ_0 is the intra-molecular term, and σ_{mol} represents the other screening effects contributing to σ_{sol}.

If a reference material (R) is to be used to measure the shift of the sample or solute (S), then there are different ways to make the measurements and, therefore, interpret the effect that susceptibilities will have on the screening of the sample, in terms of the relative chemical shifts δ_{S-R}.

If mixing of the reference and solute is chemically undesirable, an external reference contained within a vessel inside the sample can be used; the enclosed reference material may additionally provide an external resonance for a field/frequency locking feature on the N.M.R. spectrometer. In both instances a susceptibility correction is required, unless as can be seen by putting $\alpha = 4\pi/3$ in equation (4.12) the reference vessel is perfectly spherical [84]. In practice, vessels of this latter type are extremely difficult to fabricate and it becomes necessary to determine their shape factors; such procedures are often laden with problems [87, 88].

If on the other hand a perfectly cylindrical reference vessel can be employed for the N.M.R. measurement, then the true or corrected shift, δ_{corr}, is related to the observed shift [87] by

$$\delta^{S-R}_{corr} = \delta^{S-R}_{obs} + \frac{2\pi}{3}(\chi_R - \chi_S) \qquad (4.14)$$

where χ_R and χ_S are the volume magnetic susceptibilities of the reference material and the analytical sample respectively.

If the sample is internally referenced (by homogeneously mixing the sample and reference) the bracketed susceptibility term in equation 4.14 is set at zero and screening arising from volume magnetic susceptibilities in the sample may, therefore, be neglected.

In general, internal referencing is considered satisfactory for the measurement of N.M.R. chemical shifts, but it has been demonstrated that such shifts might provide an unreliable base for the study of weak molecular complexes [89]. To overcome this problem, dispersed liquid phase references would appear to provide a unique answer [77].

4.3.2b SOLVENT ANISOTROPY σ_a

A quite significant contribution will be made to σ_{sol}, if the solvent molecules exhibit anisotropy in their magnetic susceptibility, the consequence of which, is that the local field experienced by other molecules within the sample will be affected. The extent to which this screening effect, σ_a, is important, is governed by, amongst other things, the orientation that the solute molecule adopts in relation to the solvent molecule, e.g. by reason of steric or other specific interactions. Several workers [90 - 95] have had varying success in determining σ_a and providing an explanation of the large differences in chemical shifts observed for solutes in aromatic and in non aromatic molecules.

4.3.2c VAN DER VAALS OR DISPERSION SCREENING σ_W

If intermolecular distances are short, there is a synchronous oscillation of the electrons in adjacent molecules. These give rise to time varying electric dipoles which generate electric fields that can polarise the electron clouds of the interacting molecules. This gives rise to the van de Waals screening, σ_W, which contributes to σ_{sol} [96, 97]. Such mutual distortions to the electronic configuration of the molecules give rise to an effect which is paramagnetic in nature.

4.3.2d REACTION FIELD OR ELECTRIC FIELD SCREENING σ_E

When a polar molecule containing a solute nucleus polarises a given volume of neighbouring solvent, an electric field, E, is set up (the reaction field), which will act on electrons in the solute molecule in a direction along the axis of the dipole that caused the effect. Again this contributes to σ_{sol}. Screening due to a reaction field is covered by the term σ_E, the magnitude of which is given by [79].

$$\sigma_E = (2 \times 10^{-5}) - (2 \times 10^{-2})\, E_z - (10^{-18})\, E^2 \qquad (4.15)$$

For cases in which E arises from an external field, its effective average value at any nucleus in the liquid or gas phase is zero. The same will not be true if E is the result of an internal

effect caused by the polar molecule. Procedures have been proposed for calculating σ_E for spherical molecules [98, 99] and non spherical molecules [100].

4.3.2e THE EFFECT OF SPECIFIC ASSOCIATION σ_c

Specific types of molecular interaction do occur between solute and solvent or different solute molecules in the same solution. Often these interactions do not lead to permanent bond formation. Examples of this type of interaction are seen in H-bonding, charge transfer, dipole-dipole and dipole-induced dipole phenomena, all of which can contribute to σ_{sol} and are represented by the term σ_c. While effects due to molecular anisotropy and all bonding interactions may sometimes form part of σ_c, it is more generally applied in the description of intermolecular screening arising from the formation of a transiently formed collision complex. As previously mentioned the formation of a complex of this type should result from the equilibrium reaction of a surfactant derivative of $Ru(bipy)_3^{2+}$ and water. However, it remains a matter of conjecture at this stage as to the origins of the interaction that would most likely give the complex.

4.4 AN EXAMPLE OF THE EXPERIMENTAL USE OF CHEMICAL SHIFTS

A particularly interesting experimental use of chemical shifts has been demonstrated by Cresswell and Allred [101] amongst others, in studying intermolecular complex formation between chloroform and benzene in the inert solvent cyclohexane. This reaction can be represented by

$$A + D \underset{\text{cyclohexane}}{\overset{\longrightarrow}{\longleftarrow}} A\text{------}D \qquad (4.16)$$

(chloroform) (benzene) complex

As it will be shown, appropriate experiments can afford information on the stoicheiometry of the complex, the ease of reaction and the spatial arrangement of components of the complex.

In the experimental procedure the change in chemical shift of chloroform relative to the spectral position of cyclohexane, acting as internal reference, is followed for various concentrations of benzene and cyclohexane. These chemical shifts provide data for a N.M.R. adaptation of the Benesi-Hildebrand's [102] spectrophotometric procedure for studying complex formation. The Benesi-Hildebrand method (N.M.R. equivalents shown in parentheses) depends on a measurable property, P, of A that is subsequently modified through complex formation from P_{free} (δ_{free} - representing the relative chemical shift of chloroform

in cyclohexane only) to $P_{complex}$ ($\delta_{complex}$). Any observable intermediate stages along the reaction route are represented by P_{obs} (δ_{obs}).

In the N.M.R. variant of the Benesi-Hildebrand method a chemical shift Δ_{obs} is obtained from ($\delta_{obs} - \delta_{free}$) which represents, at any one instance, a weighted average of the chemical shifts for free chloroform and that for the complex. The limiting shift of the complex (which is represented by Δ_c or $\delta_c - \delta_{free}$) cannot be measured directly because the complex is formed transiently. However, Δ_c can be derived from an appropriate mathematical treatment of the data. The overall experimental approach is depicted in fig. 4.5 and summarised in equation (4.17) given below.

$$\delta_{obs} = \frac{n_{AD}}{n_A}\,\delta_{complex} + \frac{n_A - n_{AD}}{n_A}\,\delta_{free} \qquad (4.17)$$

where n_A is the total number of moles of A present initially and n_{AD} is the number of moles of complex at equilibrium.

In keeping with the original Benesi-Hildebrand concepts, the N.M.R. method also involves an equilibrium constant which may be represented by

$$K = \frac{[AD]}{[A][D]} \qquad (4.18)$$

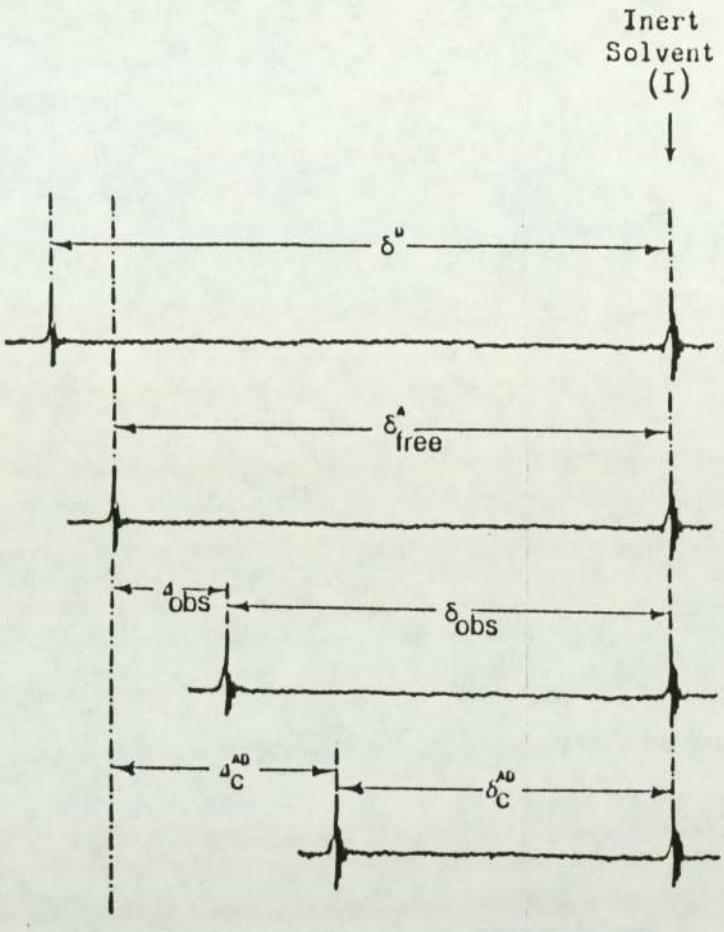

Fig. 4.5 The relationship between Δ_{obs}, Δ^{AD}_{c}, δ_{obs}, δ^{A}_{free} and δ^{AD}_{c}.

A value for K and the full chemical shift induced in the complex (Δ_c) can be obtained generally when [D] >> [A] [102] from the well known Benesi-Hildebrand equation

$$\frac{1}{\Delta_{obs}} = \frac{1}{x_D K_x \Delta_c} + \frac{1}{\Delta_c} \qquad (4.19)$$

or

$$\frac{1}{\Delta_{obs}} = \frac{1}{c_D K_c \Delta_c} + \frac{1}{\Delta_c} \qquad (4.20)$$

depending on whether a mole fraction (x_D) or molar concentration (c_D) scale is used.

Both equations (4.19) and (4.20) are analogues to the original Benesi-Hildebrand equation and plots of Δ_{obs}^{-1} against x_D^{-1} or c_D^{-1} can give straight line graphs (which some workers [103, 104] take as indicating the complex has a 1:1 stoicheiometry) from which values of K_c and Δ_c are obtainable. The equilibrium constants K_c and K_x are known to be interrelated through the mean molar volume of the mixture (V_{mol}), such that

$$K_c = K_x V_{mol} \qquad (4.21)$$

Studies at various temperatures can yield ΔH, ΔG and ΔS for complex formation.

In the instance shown, the value of Δ_c represents the excess screening of chloroform by benzene. This value of Δ_c has been used by Johnson and Bovey [105] to ascertain the precise reaction site on benzene where it interacts with chloroform. Other benzene complexes may be similarly studied.

4.5 THE USE OF CHEMICAL SHIFT MEASUREMENTS TO STUDY WATER SOLVATED TO A SURFACTANT DERIVATIVE OF $Ru(bipy)_3^{2+}$

The original Benesi-Hildebrand method, depends on the assumption that it deals only with 1:1 complexes. For a system containing a surfactant derivative of $Ru(bipy)_3^{2+}$ and water in an inert solvent, the assumption of 1:1 stoicheiometry cannot be justified and superficially the use of the Benesi-Hildebrand approach to the proposed study appears to be limited. Nevertheless, an investigation using the Benesi-Hildebrand principles could be useful if for no other reason that it would establish if some specific interaction between water and the surfactant occurred.

Therefore, the aim of the initial experiment was to conduct a chemical shift study of systems containing varying concentrations of water together with virtually identical concentrations of Whitten-type surfactant in a suitable solvent. The effect of the surfactant could be established by comparing these results with those from a study of systems which were essentially the same, but minus the content of the surfactant.

4.6 GENERAL DESCRIPTION OF THE N.M.R. SPECTROMETER USED IN AN INITIAL STUDY

The measurement of appropriate chemical shifts to the required accuracy was facilitated by the use of a 'Perkin Elmer' R12B nuclear magnetic resonance spectrometer with a supplementary field-locking attachment (see fig. 4.6). The sample is subject to a polarising magnetic field of 1.4092T, which in order to achieve the N.M.R. response, requires the application of a radio frequency field oscillating at approximately 60MHz from an orthogonal direction to B_0. Because a permanent magnet is used the instrument is essentially operating at one field strength and one radio frequency, oscillating at 60MHz, the function of allowing each differently screened nuclear type to be observed is achieved by tuning over a fixed sweep range. In order to improve signal/noise a sideband mode of detection is used at 60.006 MHz.

The field-locking device of the spectrometer relies upon the detection of the dispersion signal from a reference material (e.g. T.M.S.). From this, correction signals are derived. At the exact resonance position the correction voltage is zero. Any drift in positive or negative directions due to changes in either the radio frequency or the magnetic field is immediately counteracted by providing a correction voltage that is used to alter the magnetic field until the exact resonance position is regained.

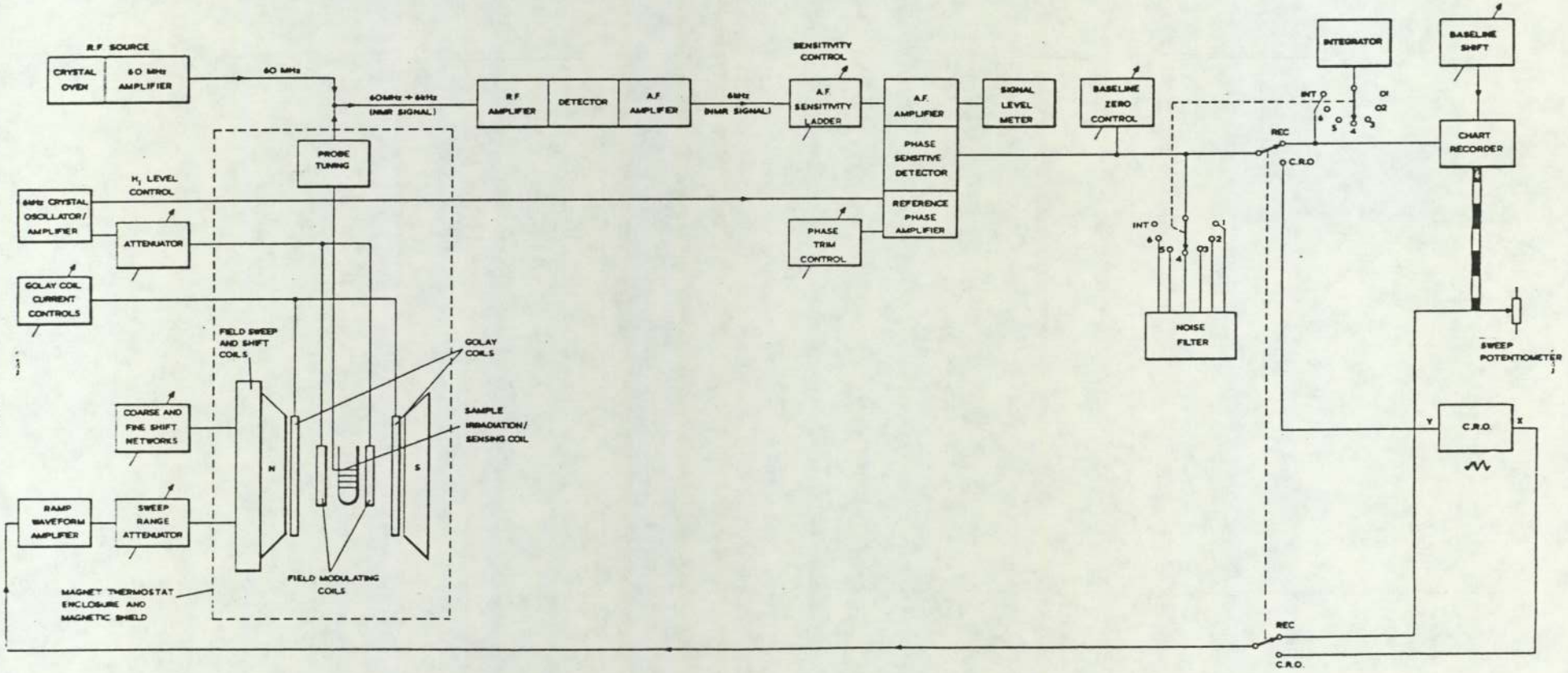

Fig. 4.6 A schematic representation of a "Perkin-Elmer" R12B N.M.R. spectrometer.

4.7 EXPERIMENTAL DETAILS

4.7.1 CHOICE OF SOLVENT AND ITS PURIFICATION

In order to implement the Benesi-Hildebrand method a suitable solvent is needed. The criteria surrounding its choice are:

1) Ideally the solvent should behave inertly to the interacting species at all stages of experimentation.

2) A solvent which enables a fairly rapid "rate of dissolution" is desirable.

3) The N.M.R. resonance position of the solvent needs to be well apart from that of the surfactant and water.

4) The solvent spectrum is required to be simple (e.g. lack multiplicity) to alleviate spectral overlap and to aid peak searching of field locking devices.

The search for the most suitable solvent for the surfactant derivative of $Ru(bipy)_3^{2+}$ and water had been previously undertaken by Luton [106]. Several typical N.M.R. solvents and mixtures, derived from them, were tried in order to satisfy the above criteria [106]; these included benzene, chloroform, cyclohexane, carbon tetrachloride and acetone. Only the last named of the solvent series could comply to a reasonable extent with all of the above criteria, but there must be

some doubt as to whether condition 1 is met. Being the only available solvent it was nevertheless used.

4.7.2 PURIFICATION OF ACETONE

Analytical reagent grade acetone is stated by Vogel [107] to contain about 1% of water. This can be conveniently removed by forming an addition compound, using sodium iodide.

$$NaI + 3C_3H_6O \text{ -----> } NaI,3C_3H_6O \qquad (4.22)$$

The adduct decomposes on heating to give highly pure acetone, which is effectively free of water and hence, particularly suitable for the proposed study.

The preparative procedure required virtually stoicheiometric amounts of both acteone and sodium iodide to be mixed by slowly dissolving the sodium iodide in boiling acetone under reflux. The resulting solution was rapidly cooled in a mixture of ice and salt (-8^oC) and the ensuing crystals were filtered off and transferred to a dry distillation flask. Finally, the crystalline adduct was decomposed by gently heating; the purified acetone was distilled off, (b.p.56.2^oC at $101325Nm^{-2}$ atmospheric pressure) and retained in a well sealed vessel.

4.7.3 PREPARATION OF SAMPLES

The water used was partially purified using commercial deionisation equipment. The chosen Whitten-type surfactant, $((bipy)_2$ Ru(II) (2,2' - bipy -4,4'$(COOC_{18}H_{37})_2))^{2+}$ $(PF_6)_2^{2-}$, was that donated by an outside chemical company* which specializes in the production of compounds derived from rare metals.

Because of the limited amount and cost of the surfactant available, only small quantities of it were used. The ratio of water to surfactant covered a range that extended from 15:1 to 900:1. In each sample the amount of acetone used was such as to fill the N.M.R. tube to a workable level. Similarly, reference samples were made containing the same concentration of water in acetone, but without the inclusion of surfactant.

In order to measure the quantities of materials used to the required accuracy, a balance with a weighing capability of 0.00001g was used. However, the volatility of the liquid constituents of the samples posed problems and weighings had to be carried out in encapsulated bottles. The preparative procedure consisted of initially weighing the dried surfactant into a open weighing vessel, before forming an 'enclosed system' by applying a self sealing cap ('Subaseal'variety). Subaseals allowed acetone or water to be accurately injected into the weighing vessel by syringe without losing significant amounts of material by evaporation.

* Thanks are due to the Johnson Matthey Organisation for the provision of this substance.

In the final experimental step, the mixture was carefully shaken to achieve an homogeneous solution and withdrawn via a syringe through the subaseal. Care was taken to ensure the solution was released at the base of a clean N.M.R. tube, to allow its open top to be sealed in a bunsen flame without igniting any residual material: Burnt material prevents a proper glass seal being formed.

Tables 4.1 and 4.2 gives sample weights in grams and moles respectively. It should be noted that the last three samples were prepared significantly later than the others. For reasons outlined later, various factors could apply that throw doubt on the value of the quoted compositions of these three samples.

4.7.4 CHEMICAL SHIFT DETERMINATIONS

In order to utilise the optimum sweep range for each series of chemical shift measurement it was necessary to pre-examine N.M.R. spectra of samples at extremes of the analytical range. For most measurements a 100Hz sweep range was found to be sufficiently accurate.

The field-locking device (described previously in section 4.6 was employed to attain the desired precision (±0.5 Hz) in the measurement of each chemical shift. In practice measurements were made from the centre of the lock signal beat pattern (which corresponded to the acetone resonance signal) to the centre of the sole N.M.R. resonance signal of water (thus producing negative shifts).

SYSTEMS + (S)				SYSTEM - (S)	
H_2O:(S)	$H_2O(g)\times10^2$	S $(g)\times10^2$	$(CH_3)_2CO(g)\times10^2$	$H_2O(g)\times10^2$	$(CH_3)_2CO(g)\times10^2$
15.1	0.168	1.014	4.5283	0.176	4.5363
25.1	0.354	1.020	4.5192	0.354	4.5189
40.1	0.485	1.146	4.5641	0.478	4.5667
60.1	0.774	1.105	4.5330	0.732	4.5399
75.1	0.975	1.058	4.5520	0.971	4.5454
85.1	1.033	1.091	4.4932	1.029	4.5444
100.1	1.348	0.986	4.6023	1.332	4.5123
150.1	1.863	0.988	4.5212	1.868	4.5265
200.1	2.476	1.003	4.5550	2.473	4.5538
250.1	3.192	1.057	4.5942	3.137	4.6040
300.1	3.622	1.000	4.5054	3.564	4.5138
350.1	4.492	0.992	4.5293	5.161	4.5265
400.1	5.079	1.045	4.5370	5.142	4.5578
500.1	7.523	0.979	4.5074	7.373	4.5169
700.1	8.513	1.071	4.5146	8.593	4.4922
900.1	6.480	0.604	2.6370	6.728	2.6370

Table 4.1 Sample weights (g) for all systems: S represents the diester derivative of $Ru(bipy)_3^{2+}$, $((bipy)_2Ru(II)(2,2'\text{-bipy-}4,4'\text{-}(COOC_{18}H_{37})_2))^{2+}$ $(PF_6)_2^{2-}$

SYSTEMS + (S)			SYSTEM - (S)	
$n_{H_2O} \times 10^3$	$n_{(CH_3)_2CO} \times 10^3$	$n_S \times 10^6$	$n_{H_2O} \times 10^3$	$n_{(CH_3)_2CO} \times 10^3$
0.0930	7.807	6.979	0.0978	7.8212
0.1962	7.792	7.020	0.1966	7.7912
0.2694	7.869	7.887	0.2655	7.8736
0.4300	7.816	7.605	0.4066	7.8274
0.5417	7.848	7.281	0.5394	7.8369
0.5739	7.747	7.509	0.5717	7.8551
0.7489	7.935	6.786	0.7400	7.7798
1.0350	7.795	6.800	1.0377	7.8043
1.3760	7.853	6.903	1.3738	7.8513
1.7730	7.921	7.275	1.7427	7.9379
2.0120	7.768	6.882	1.9800	7.7824
2.4960	7.809	6.830	2.8672	7.8043
2.8220	7.822	7.190	2.8566	7.8410
4.1790	7.771	6.738	4.096	7.7878
4.7290	7.784	7.371	4.774	7.7452
3.6000	4.547	4.157	3.738	4.5466

Table 4.2 Sample weights (g) converted to moles for all systems: S represents the diester derivative of $Ru(bipy)_3^{2+}$, $((bipy)_2Ru(II)(2,2'\text{-}bipy\text{-}4,4'(COOC_{18}H_{37})_2))^{2+}$ $(PF_6)_2^{2-}$

4.8 RESULTS AND DISCUSSION

If reference is made to table 4.3 (which gives the mole fractions of water for the various systems) it appears that, despite the small progressive change in $^{x}H_2O$; the two chemical shifts tend to get more divergent as the ratio of water: surfactant increases. However, the values of $^{x}H_2O$ in the +S and -S systems are not always identical. Therefore, in order to ensure that the chemical systems, with or without the surfactant derivative (S) were comparable, it proves necessary to plot the chemical shift versus mole fraction for each system (see fig. 4.7). This supports the divergence of the two shift variations; the last three points are omitted from this consideration because of doubt concerning their compositions.

From an examination of the graph shown in fig. 4.7 it is evident that many of the parameters which were fundamental to an N.M.R. application of the Benesi-Hildebrand relationship ([D] >> [A] for instance) for weak molecular interaction [101] remain pertinent to this study. In view of the fact that the complex could not be assigned a 1:1 stoicheiometry with certainty, the data were treated assuming a 1:m (m is an integer) stoicheiometry of reactants.

SYSTEMS + (S)	SYSTEMS -(S)	Chemical Shift of H_2O relative to $(CH_3)_2CO$ (Hz)	
		+S	-S
$^{x}H_2O \times 10$	$^{x}H_2O \times 10$	δ_{obs}	δ_{free}
0.12	0.12	48.00	47.33
0.25	0.25	48.17	49.00
0.33	0.33	52.17	51.00
0.52	0.49	54.99	54.33
0.65	0.64	57.50	60.00
0.67	0.68	58.00	57.33
0.86	0.87	57.67	60.33
1.17	1.17	63.33	65.00
1.49	1.49	68.67	70.67
1.83	1.80	74.00	74.67
2.06	2.03	77.67	78.33
2.42	2.69	81.00	86.67
2.65	2.67	80.67	87.33
3.43	3.45	99.83	98.33
3.78	3.81	103.17	100.00
4.37	4.51	110.67	111.33

Table 4.3 The observed chemical shifts of water measured relative to acetone for systems containing various mole fractions of water ($^{x}H_2O$) dissolved in acetone, but with or without a fixed mole fraction of $((bipy)_2Ru(II)(2,2'\text{-bipy} - 4,4'(COOC_{18}H_{37})_2))^{2+}$ $(PF_6)_2^{2-}$ - shown as (S)

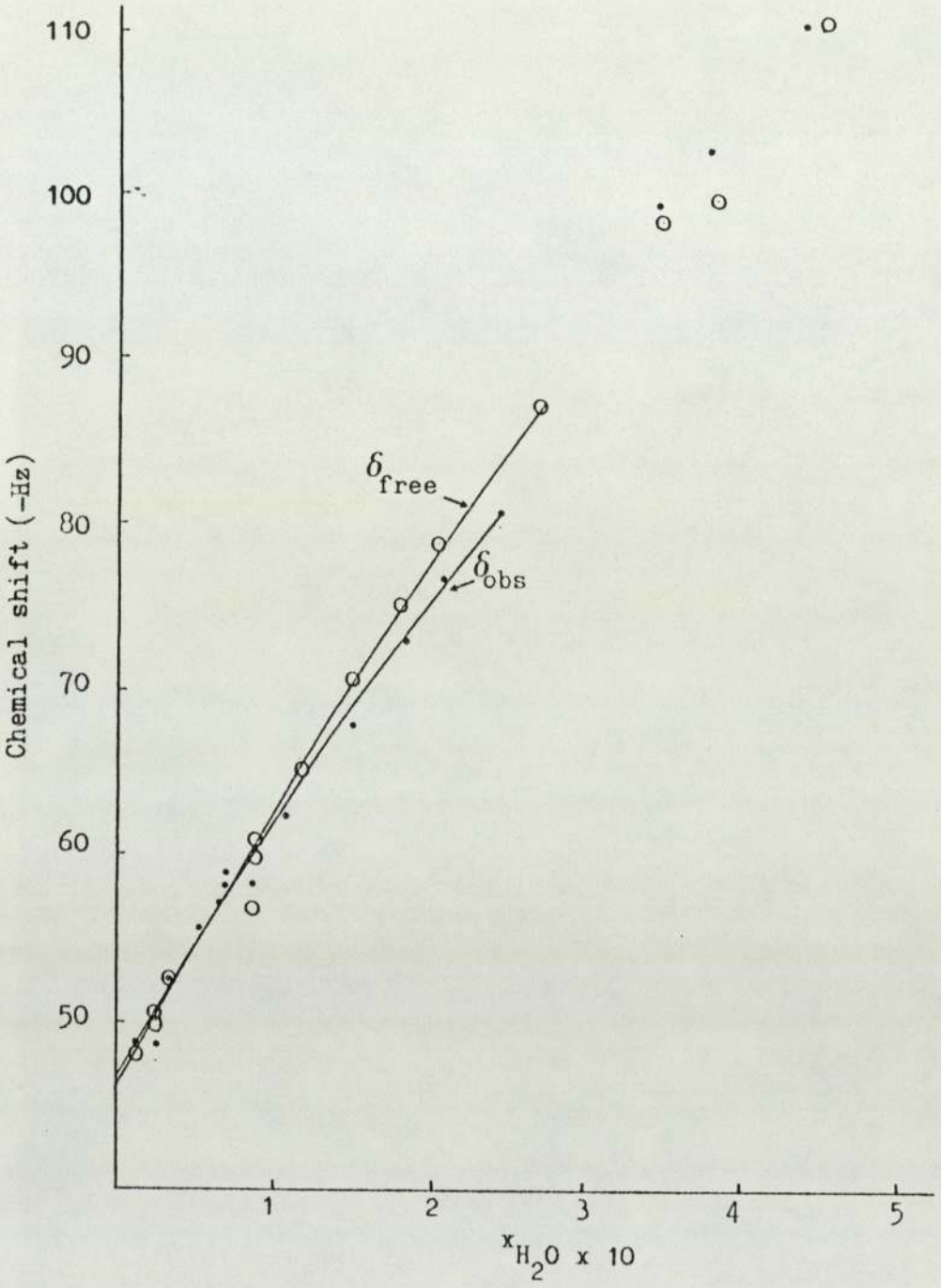

Fig. 4.7 The variation of δ_{obs} and δ_{free} (relative to acetone) of water for systems containing various mole fractions of water ($^{x}H_2O$) dissolved in acetone, but with (+S) or without (-S) a fixed mole fraction of the diester derivative of $Ru(bipy)_3^{2+}$, respectively.

It has been proposed in section 4.1 that the molecular interaction of the diester derivative of $Ru(bipy)_3^{2+}$ (A) and water (D) in acetone solvent (I) may be represented by

$$A + mD \underset{\longleftarrow}{\longrightarrow} AD_m \qquad (4.23)$$

Initial amounts in moles	n_A	n_D	
Equilibrium amounts	$n_A - n_{AD_m}$	$n_D - m.n_{AD_m}$	n_{AD_m}

Thus, the equilibrium constant in terms of mole fraction is given by

$$K_x = \frac{n_{AD_m}(n_A + n_D + n_I - n_{AD_m})^m}{(n_A - n_{AD_m})\,(n_D - m.n_{AD_m})^m} \qquad (4.24)$$

As the experimental conditions are essentially $n_A < n_D << n_I$ (see table 4.2) it is reasonable to expect that Henry's law is obeyed (which states that for dilute solutions (behaving ideally) the pressure (p) of a gas above a solution is proportional to the mole fraction (x) of the solute (gas) in solution) and activity coefficients can therefore be neglected. Provided that m is not too large and the equilibrium constant is reasonably small, it may be assumed that

$$n_D >> m.n_{AD_m}$$

such that

$$K_x = \frac{n_{AD_m}}{(n_A - n_{AD_m})x_D^m} \qquad (4.25)$$

for which x_D^m can be either equal to or a function of the mole fraction of D.

In order to account for the difference in size of water and acetone, x_D is defined by [108]

$$\frac{n_D}{(n_A + n_D + V_{I/V_D} n_I - (n_{A---D_m})} \qquad (4.26)$$

where V_I and V_D are molar volumes of acetone and water respectively.

As the chemical shift of water is being studied, it is a necessary step to define the fraction of the original amount of water that is complexed, namely,

$$\frac{m.n_{AD_m}}{n_D} \qquad (4.27)$$

From equation 4.25 it follows that:-

$$K_x\, n_A\, x_D^m - K_x\, n_{AD_m}\, x_D^m = n_{AD_m} \qquad (4.28)$$

or
$$K_x\, n_A\, x_D^m = n_{AD_m}(1 + K_x\, x_D^m) \qquad (4.29)$$

and
$$n_{AD_m} = \frac{K_x\, n_A\, x_D^m}{1 + K_x\, x_D^m} \qquad (4.30)$$

Thus,
$$\frac{m.n_{AD_m}}{n_D} = \frac{m.K_x\, n_A\, x_D^m}{n_D(1+K_x\, x_D^m)} \qquad (4.31)$$

At this point it is necessary to introduce the measured chemical shift of water into the derivation. This is given by

$$\delta_{obs} = \left(\frac{m.n_{AD_m}}{n_D}\delta_c\right) + \left(1 - \frac{m.n_{AD_m}}{n_D}\delta_{free}\right) \qquad (4.32)$$

Because $$\Delta_{obs} = \delta_{obs} - \delta_{free} \text{ (see fig. 4.8)} \qquad (4.33)$$

and $$\Delta_c = \delta_c - \delta_{free} \qquad (4.34)$$

$$\Delta_{obs} = \frac{m.n_{AD_m}\,\Delta_c}{n_D} \qquad (4.35)$$

Alternatively by using equation (4.31)

$$\Delta_{obs} = \frac{m.K_x\,x_D^m\,n_A\,\Delta_c}{(1 + K_x\,x_D^m)\,n_D} \qquad (4.36)$$

or $$\frac{1}{\Delta_{obs}} = \frac{n_D}{n_A}\frac{1}{\Delta_c} - \frac{(1 + K_x\,x_D^m)}{(m\,K_x\,x_D^m)} \qquad (4.37)$$

and from equation (4.37) it follows that

$$\frac{n_A}{n_D}\frac{1}{\Delta_{obs}} = \frac{1}{m\,K_x\,x_D^m\,\Delta_c} + \frac{1}{m\,\Delta_c} \qquad (4.38)$$

Thus, by plotting $n_A/n_D\Delta_{obs}$ against x_D^{-m} a straight line graph should be obtained for the correctly chosen value of m. That value of m corresponds to the stoicheiometric value of water in the complex formed with the diester derivative of $Ru(bipy)_3^{2+}$. Furthermore, by

knowing m and that the intercept is given by $m^{-1}\Delta_c^{-1}$ (4.39), it is possible to derive Δ_c. Correspondingly, a value for the equilibrium constant, K_x, is obtainable from the slope, which is given by $m^{-1}K_x^{-1}\Delta_c^{-1}$ (4.40)

Consequently, plots corresponding to equation 4.38 were made for the data in tables 4.4 and 4.5 using various values of m: In fact data for the plots were taken from the best lines through the experimental points of fig. 4.7 (see fig. 4.8). In order to identify the most linear plot with a particular value of m, it was found necessary to carry out 7 plots in total (see fig.4.9). It is evident that some parts of the plots approximate to linearity at relatively low mole fractions of water, that is above the inflection, indicating that linearity would be achieved for a value of m between 4 and 5, although at higher mole fractions (below the inflection) there is also some evidence of linearity (possible reasons for the inflection are dealt with later in this chapter). The choice of which graphical lines are truly representative of equation 4.38 must take into account Henry's law, while satisfying the Benesi-Hildebrand requirement that [D]>>[A]. Both conditions are open to some freedom in their interpretation in the desired application. For instance, it is questionable whether water can be free from all activity considerations over the complete range of D/A shown in fig 4.9 (covering approximately 395:1 to 128:1 (values obtainable from table 4.4) and below which Δ_{obs} cannot be measured with any certainty). It is equally questionable whether [D] can be considered very much larger than [A] in that same range and so fulfil the Benesi-Hildebrand condition. Thus, it would seem reasonable to choose as a compromise the most linear lines above the inflection which are at the lower mole

fractions of water (with an approximate D/A range of say 171:1 to 128:1) at which Henry's law is most likely to be obeyed while still observing the Benesi-Hildebrand criterion. Linearity for the graphical lines was therefore judged to be best represented by those plots for which m = 5 or 6. Accordingly, detailed evaluations of the plots where m is 6 and 5 were made using the intercept and slope as follows:-

m = 6

Slope of linear plot $= \underline{1.21 \times 10^{-8}}(Hz^{-1})$ (4.41)

Intercept $= \underline{22.5 \times 10^{-4}}(Hz^{-1})$ (4.42)

Thus, equations 4.39 and 4.40 give $K_x = \frac{2.25 \times 10^{-3}}{1.21 \times 10^{-8}} = \underline{1.86 \times 10^{5}}$,

which converted to K_c (using a relevant form of equation 4.21, viz. $K_c = K_x V_{mol}^{m}$) gives

$$K_c \approx \underline{0.029 dm^{18}}\ \underline{mol^{-6}} \quad (4.43)$$

Equation (4.39) gives Δ_c = 74.10 Hz, which expressed in p.p.m.

$= \underline{1.23\ p.p.m.}$ (4.44)

m = 5

Slope of linear plot $= \underline{1.12 \times 10^{-7}}(Hz^{-1})$ (4.45)

Intercept $= \underline{19.20 \times 10^{-4}}(Hz^{-1})$ (4.46)

Thus, equations 4.39 and 4.40 give $K_x = \frac{19.20 \times 10^{-4}}{1.12 \times 10^{-7}} = \underline{1.71 \times 10^{4}}$,

which expressed in terms of moles gives

$$K_c \approx \underline{0.036 dm^{15}}\ \underline{mol^{-5}} \quad (4.47)$$

Equation (4.39) gives Δ_c = 104.17 Hz, which expressed in p.p.m.

$= \underline{1.74\ p.p.m.}$ (4.48)

δ_{free}	δ_{obs}	Δ_{obs}	$x_{H_2O} \times 10^1$	$1/x_{H_2O}$	$n_A/n_D \times 10^3$	$\frac{1}{\Delta_{obs}}$ (Hz^{-1})	$\frac{n_A}{n_D}\frac{1}{\Delta_{obs}} \times 10^4$ (Hz^{-1})
61.85	61.45	0.40	0.95	10.53	8.692	2.500	217.290
63.50	62.81	0.69	1.05	9.52	7.777	1.449	112.694
65.10	64.15	0.95	1.15	8.70	7.023	1.053	73.955
66.70	65.55	1.15	1.25	8.00	6.389	0.876	55.587
68.30	66.95	1.35	1.35	7.41	5.846	0.741	43.319
69.90	68.35	1.55	1.45	6.90	5.380	0.645	34.699
71.50	69.75	1.75	1.55	6.45	4.975	0.571	28.410
73.00	71.10	1.90	1.65	6.06	4.619	0.526	24.294
74.45	72.38	2.07	1.75	5.71	4.563	0.483	23.999
75.85	73.65	2.20	1.85	5.41	4.019	0.455	19.411
77.30	74.95	2.35	1.95	5.13	3.767	0.426	16.047
78.70	76.25	2.45	2.05	4.88	3.538	0.408	14.434
80.12	77.42	2.78	2.15	4.65	3.332	0.360	11.994
81.50	78.60	2.90	2.25	4.44	3.143	0.345	10.842
82.90	79.80	3.10	2.35	4.26	2.970	0.323	9.594
84.20	80.99	3.21	2.45	4.08	2.812	0.312	8.772
85.45	82.10	3.35	2.55	3.92	2.666	0.299	7.971
86.66	83.20	3.46	2.65	3.80	2.531	0.289	7.314

Table 4.4. Data relating to the derivation of $\frac{n_A}{n_D}\frac{1}{\Delta_{obs}}$ and $1/x_{H_2O}$

$\frac{n_A}{n_D}\frac{1}{\Delta_{obs}} \times 10^4 (Hz^{-1})$	$1/x^2$	$1/x^3$	$1/x^4$	$1/x^5 \times 10^{-2}$	$1/x^6 \times 10^{-4}$	$1/x^7 \times 10^{-6}$
217.29	110.80	1116.4	12277	1292.4	136.04	14.3
112.69	90.70	863.8	8227	783.5	74.68	7.1
73.96	75.61	657.5	5718	497.2	43.23	3.8
55.59	64.00	512.00	4096	327.7	26.21	2.1
43.32	54.87	406.4	3011	223.0	16.52	1.2
34.70	47.56	328.0	2262	156.0	10.75	0.74
28.41	41.62	268.5	1732	111.8	7.21	0.47
24.29	36.73	222.6	1349	81.8	4.96	0.30
24.00	32.65	186.6	1066	60.9	3.48	0.19
19.41	29.22	157.9	854	46.0	2.49	0.13
16.05	26.30	134.9	692	35.5	1.82	0.093
14.43	23.80	116.1	566	27.6	1.35	0.065
11.99	21.63	100.6	468	21.8	1.01	0.047
10.84	19.75	87.8	390	17.3	0.77	0.034
9.59	18.18	77.1	328	14.0	0.59	0.025
8.77	16.66	68.0	278	11.3	0.46	0.019
7.97	15.38	60.3	237	9.3	0.36	0.014
7.31	14.24	53.7	203	7.7	0.29	0.011

Table 4.5. Various values of $1/x^n$ (where n represents an integer up to 7) together with respective values of $\frac{n_A}{n_D}\frac{1}{\Delta_{obs}}$

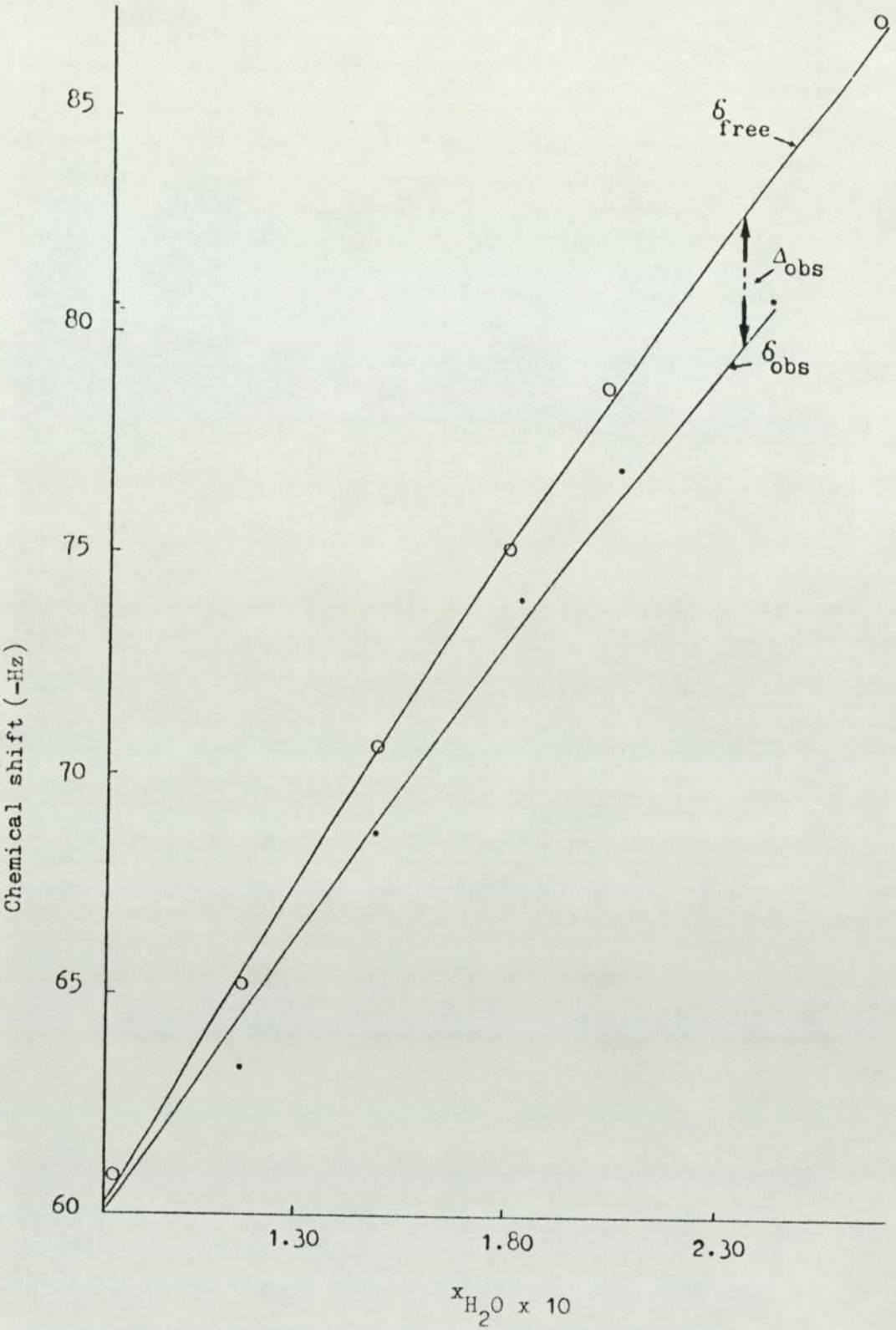

Fig. 4.8 An enlarged area of fig. 4.7 to clearly show the divergence of δ_{obs} and δ_{free} and the method of acquisition of all Δ_{obs}.

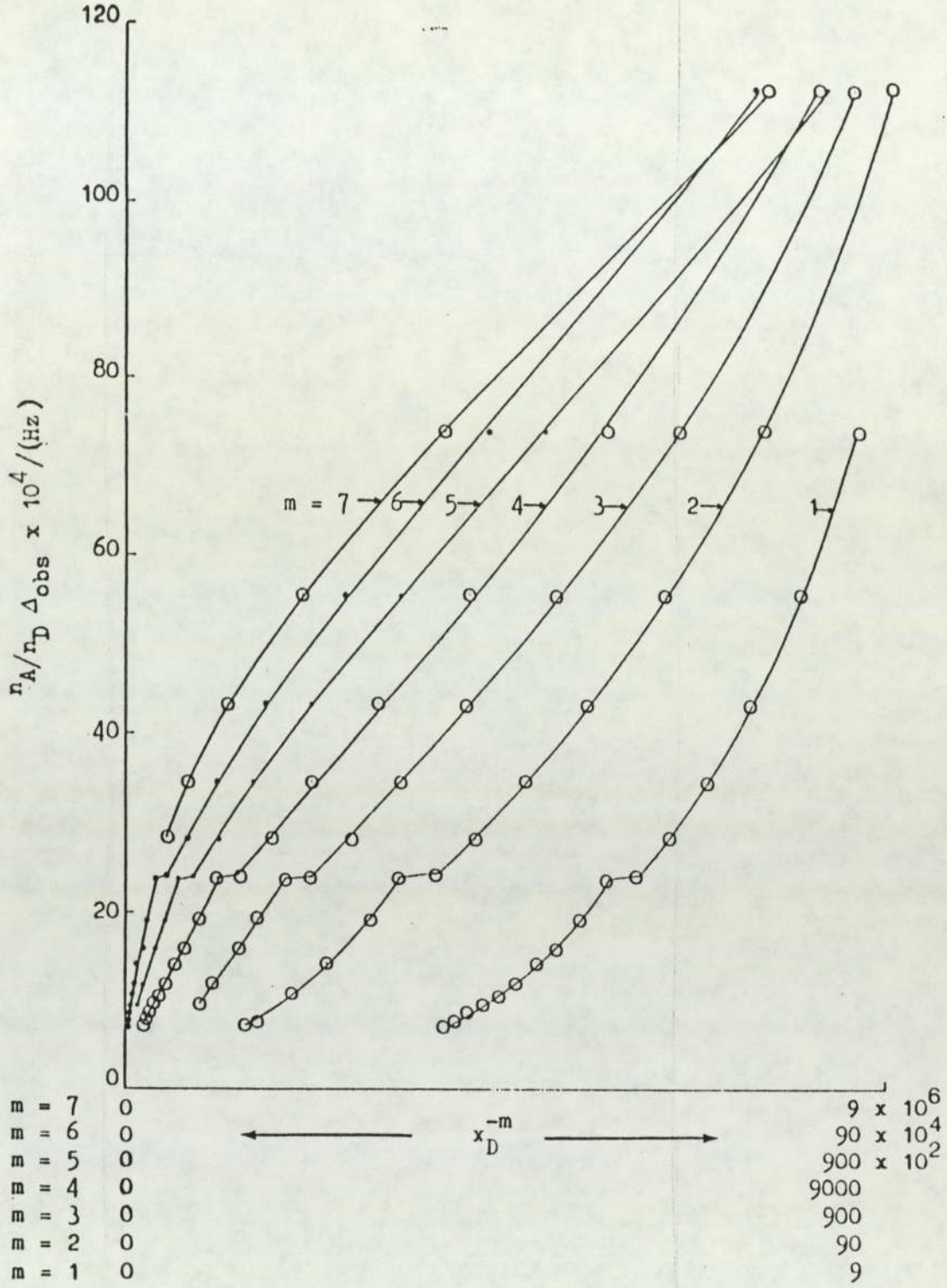

Fig. 4.9 Plots of $^{n}A/n_D\ \Delta_{obs}$ versus x_D^{-m} (where m is an integer up to 7).

4.4.9 CONCLUSION AND FURTHER DISCUSSION

A revised N.M.R. variation of the Benesi-Hildebrand method for studying 1:m complexes has been devised. Its application to the complex formed between water and the diester derivative of $Ru(bipy)_3^{2+}$ (Whitten-type surfactant) in acetone suggests that the stoicheiometry of the complex is either 6:1 or 5:1. In the absence of this knowledge, it would seem reasonable to have argued that the electronegative ester groups of the surfactant (depicted in fig. 4.10) provide ideal sites for H-bonding interactions with water, but presumably on a 1:1 basis, by bridging the gap between ester groups. However, such sites might be sterically hindered from attack by water because of the nearness of the dioctadecyl tails of the bidentate ligand.

Since the experimental evidence suggests that the stoicheiometry of the complex could be 5:1 or 6:1, alternative reaction sites need to be considered, although H-bonding interactions between water and the ester groups of the surfactant cannot be wholly discounted.

If reference is made to fig. 4.7 which represents the variation of chemical shift for complexed and non-complexed water it is apparent that these shifts are negative relative to acetone. Such an observation is explained by the deshielding effects arising from H-bonding between H_2O--H_2O and possibly H_2O--acetone; this increases with increasing water concentration. In addition, it is noticeable that at a given mole fraction of water its shift in systems with added surfactant (δ_{obs}) is upfield (positive relative shift) of the shift corresponding to systems which are without the surfactant (δ_{free}).

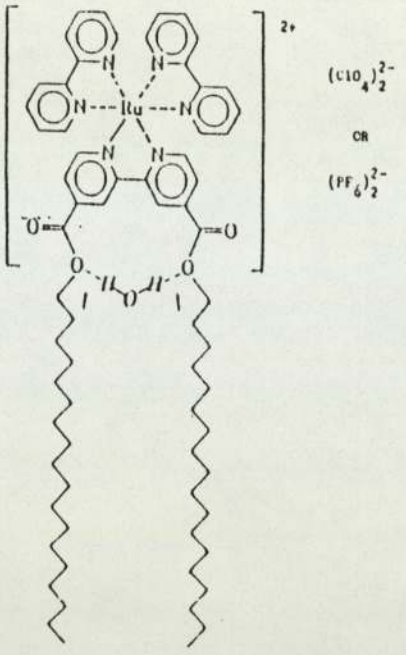

Fig. 4.10 H-bonding interaction between the ester groups of the surfactant, $(bipy)_2Ru(II)(2,2'\text{-bipy-}4,4'(COOC_{18}H_{37})_2))^{2+}$, and water (not drawn to scale).

This upfield trend for δ_{obs} is indicative of complexed water being shielded by anisotropic screening effects (see section 4.3.1.c) originating from electronic currents within the neighbouring ring system of the surfactant. As there is an overall shielding of water in the presence of the surfactant, this suggests that the most likely reaction sites are near each 'six fold' axis of each member ring of the ligands of the surfactant; these sites would be very similar in their screening effects. Indeed this overall suggestion is supported by the values of full induced screening (Δ_c) for the complex when m = 6 and 5, in that both values of Δ_c (which are in the order of 1-2 p.p.m) roughly equate to those Δ_c values given for similar complex forming interactions at the six fold axis of benzene [105].

Whilst the graphical points at higher mole fractions (shown as isolated points in fig. 4.7) must in hindsight be discounted, because

they relate to an independent batch of samples prepared at a later date, and which may have degraded, it is, from a speculative viewpoint, interesting that if these latter graphical points do have any credibility, they suggest a convergence of δ_{free} and δ_{obs}. This suggests that at lower mole fractions of water, its induced shielding due to the presence of the surfactant is dominated by the effects of H_2O--H_2O and/or H_2O--acetone H-bonding.

The values of K_x obtained when m = 6 and 5 are relatively high, but not unexpected, because if electron transfer processes occur between the surfactant and water, to enable dihydrogen production (as Whitten's [16] experiments suggest), then the equilibrium of reaction (4.23) must strongly favour the formation of the complex.

It would seem justifiable to quote the magnitude of K_x instead of that of the much smaller K_c, because it has been demonstrated by Homer et al [108], when commenting on equilibrium data handling, that for K_c to be strictly applicable in the situation given, the molar volumes of water and acetone must be the same: Using data from table 4.2 it can be shown that this condition is not fully met. Unfortunately it often appears that the accepted practice of evaluating equilibrium data in terms of K_c is still made; a practice of which Homer et al[108] are critical, because of the frequent invalidity of the assumptions regarding molar volumes.

One outstanding point that must be mentioned is the inflection in fig. 4.9 which occurs almost independently of m at a value of approximately 4.6×10^{-3} for $^{n}A/n_D$. The inflection occurs at relatively high concentrations of water to that of surfactant and it

might be reasoned that the inflection corresponds to a departure from ideal behaviour of the 'isolated' complex in solution. Indeed, such an argument could find its basis in the well known change in physical properties of surfactant solutions at increasingly higher concentrations, when over a discrete range of concentration there is an organized aggregation of monomeric units of surfactant to form a so called micelle. The range of concentration where micellization happens is narrow enough to be called critical and the term critical micellization concentration, or c.m.c., has been adopted as a conventional parameter to characterize this phenomenon. If a micelle is formed it is difficult to envisage how this influences the shift of water, particularly as the surfactant is present at a constant concentration in all the systems examined. It is possible that a micelle formed in a non-aqueous medium like acetone, is in some way intimately associated with added water, which would have a different chemical shift from when it is in normal solution. As only one ^{1}H resonance was observed for water over its whole concentration range, the above argument would imply that below the inflection (lefthand side of fig. 4.9) the water is entirely involved with the micelles and above the inflection (righthand side of fig. 4.9) it is entirely in normal solution.

Such a postulate goes part-way in justifying the derivation of K_x from the straight line section of the graphs in fig. 4.9 (where Henry's Law is assumed to be obeyed and activities are set to 1) rather than those graphical sections below the inflection when the true Benesi-Hildebrand condition $[D] >> [A]$ is more evidently approached. In consequence the data corresponding to low mole fractions of water to the right of the inflection are the only ones that can be evaluated using equation (4.38).

CHAPTER 5

SOME CONSIDERATIONS OF THE STRENGTH OF THE COMPLEX FORMED BY THE REACTION BETWEEN WATER AND A DIESTER DERIVATIVE OF $Ru(bipy)_3^{2+}$, $((bipy)_2Ru(II)(2,2'\text{-bipy-}4,4'(COOC_{18}H_{37})_2))^{2+}(PF_6)_2^{2-}$

5.1 INTRODUCTION

In Chapter 4 it has been tentatively proposed that the stoicheiometry of the complex, water: diester derivative of $Ru(bipy)_3^{2+}$, is possibly 6:1 or 5:1. Whichever stoicheiometry is correct, its value offers very little information on the strength of the bonding interaction that holds the complex together. Nevertheless, the possible stoicheiometry does serve to support previous hypotheses (originating from members of the research group who initiated this project) regarding the most energetically favoured disposition of water molecules about the bipyridyl ring system of the $Ru(bipy)_3^{2+}$ derivative viz, one water molecule per member ring of the bipyridine unit.

In order to be able to characterize the strength of the complex, it is necessary to determine the thermodynamic changes that occur as a result of complex formation. The thermodynamic parameters used to express the strength of a complex are either the standard enthalpy (ΔH^o) or Gibbs free energy (ΔG^o) of formation and, the corresponding change in entropy (ΔS^o).

For example, it is known [109, 110] that ΔH^o for the specific type of molecular interaction which is suggested to take place between

water and the derivative of $Ru(bipy)_3^{2+}$, is generally of the order of a few $kJmole^{-1}$, showing the weak nature of the complexes so formed. The possibility that ΔG^o, rather than ΔH^o should be used as a measure of the strength of the complex has also been critically examined [111]. The constancy of ΔH^o with temperature has been used to indicate the presence of a single complex [112]. Furthermore, in relation to this work, it is expected that negative entropy changes are most likely for the proposed reaction, since the probability is that the motional characteristics of the interacting species will be constrained when the complex is formed.

In section 4.8 it has been shown that if the concentrations in solution of the diester derivative of $Ru(bipy)_3^{2+}$ and water comply with Henry's law, then the activity coefficients of each species may be taken as unity. Provided these constraints on the concentration of the interacting species are kept, ΔG^o for the equilibrium reaction between them is related to the equilibrium constant K_x, (derived using mole fraction) at a temperature T, by

$$\Delta G^o = -RT\ln K_x \qquad (5.1)$$

where R is the gas constant. As K_x is expressed in mole fractions, ΔG^o represents the free energy change when one mole of each of the reacting species combine to produce one mole of complex. On the molar scale K_x is replaced by K_c which is effected by the molar volume of the solvent [113] (the importance of this statement is illustrated in section 4.8, Chapter 4, where K_x and K_c are calculated for the equilibrium reaction between water and a surfactant derivative of $Ru(bipy)_3^{2+}$).

From a knowledge of ΔG and its variation with temperature at constant pressure, Gibbs and Helmholtz have shown a relationship involving ΔH whereby

$$\frac{\partial(\Delta G/T)}{\partial(1/T)} = \Delta H \qquad (5.2)$$

Moreover, if it is stipulated that equation 5.2 is describing a process where substances are present in their standard states, the combination of equations 5.2 and 5.1 can lead to the van't Hoff expression, the appropriate form of which for reactons in solution and at constant pressure is

$$\frac{\partial \ln K_x}{\partial(1/T)} = -\frac{\Delta H^o}{R} \qquad (5.3)$$

Equation 5.3 is extremely useful, because if $\ln K_x$ is plotted against $1/T$, the slope of the line at any temperature should be equal to $-\Delta H^o/R$ and therefore ΔH^o is obtainable. With values of ΔG^o and ΔH^o, it becomes possible to obtain ΔS^o by using the relationship:

$$\Delta G^o = \Delta H^o - T\Delta S^o \qquad (5.4)$$

which refers to the reaction at a particular constant temperature (T).

Closer examination of equation 5.3 shows that K_x must increase with temperature if $\Delta H>0$, whereas if $\Delta H<0$ the increasing temperature will cause K_x to decrease. If such proposals are true and providing ΔH remains independent of T over the relevant temperature ranges,

N.M.R. can be used to detect changes in the equilibrium state of a system through measurement of relative chemical shifts of a selected nucleus at different temperatures (due to the dependence of chemical shifts on the equilibrium constant). Indeed, other workers have found that this approach is valid after comparing certain types of solvent-induced shifts measured at various temperatures [114, 115].

It has been shown previously in this work that the equilibrium constant (K) for the reaction of water and a diester derivative of $Ru(bipy)_3^{2+}$ can be obtained from N.M.R. chemical shift data. Thus, it follows that by performing N.M.R. chemical shift measurements on those same systems at different temperatures and obtaining the corresponding values of K, that ΔH^o, ΔG^o and ΔS^o for complex formation can be determined.

5.2 A GENERAL DESCRIPTION OF THE PRINCIPLES OF OPERATION OF THE F.T. N.M.R. INSTRUMENT USED FOR CHEMICAL SHIFT STUDIES AT VARIOUS TEMPERATURES

5.2.1 ORIGINS OF THE N.M.R. SIGNAL

The earlier shift measurements were made using a c.w. spectrometer and its operation was described in Chapter 4. For the measurements at various temperatures a pulsed F.T. spectrometer was used and the principles of its operation will now be outlined.

5.2.1a CONVENTIONAL N.M.R.

It has been previously stated that the basic resonance condition for the N.M.R. experiment is given by

$$\nu = \frac{\gamma B_0}{2\pi} \qquad (5.5)$$

where ν is the oscillating radio frequency (the nuclear resonant value is more commonly known as the Larmor frequency) γ the gyromagnetic constant and B_0 the applied magnetic field. For the resonance condition to be detectable, a nucleus must have angular momentum (I), which determines that there will be an associated magnetic moment (μ). When the nucleus experiences the torque due to the field acting on its magnetic moment the angular momentum and hence μ precess about B_0 at the Larmor frequency (see fig. 5.1).

In fig 5.1 an oscillating magnetic field has been resolved into two magnetic vectors of which one is depicted as B_1 and is chosen because it can be arranged to have the same angular velocity as the precessing nucleus (resonance). At resonance, the effect of B_1 causes the cone of vectors to turn into a different plane and induce a radio frequency current in a receiver coil specifically placed about the N.M.R. sample. As the Larmor frequency is found for each nuclear type, signals corresponding to resultant magnetizations transverse to B_0 are detected.

5.2.1b FOURIER TRANSFORM (F.T.) N.M.R.

The efficiency of the N.M.R. experiment can be greatly improved by exciting all possible resonances simultaneously rather than successively as in the example above. In order to achieve this improvement, the N.M.R. sample is subjected to a short burst or pulse of radio frequency (r.f.) energy. This results in all possible

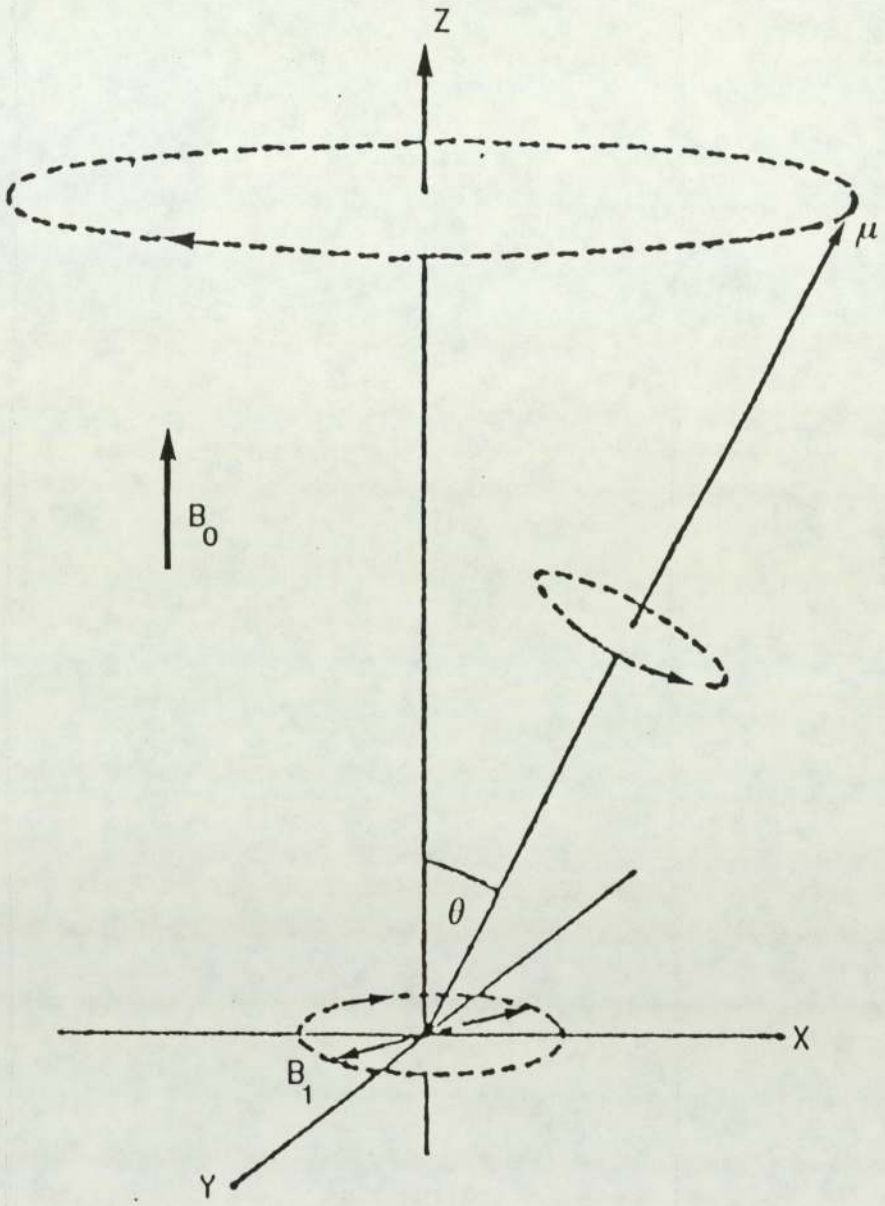

Fig. 5.1 Vector representation of the classical Larmor precession.

resonance frequencies being produced in the range of interest. In essence, a sufficiently long or powerful B_1 will turn the precession cone of each nucleus, such that the whole of the nuclear magnetization can contribute to the signal which is subsequently picked up by a receiver coil. If reference is made to fig. 5.2 the effects of a 90^o pulse are shown (only the resultant nuclear magnetization is represented).

After the cessation of each pulse the precessing nuclear magnetization decays owing to various mechanisms. It is this decaying magnetization which induces a r.f. current in the receiver coil at the characteristic Larmor frequencies of the nuclei: The whole process is known as free induction decay (F.I.D.). The induced signals are simultaneously detected by the receiver coil and after a fourier transform (F.T.) are converted to normal spectra.

5.2.2. F.T. N.M.R. SPECTROMETERS

A visible comparison of the modern-day F.T. instrument (depicted in fig. 5.3) and the earlier scanning (or continuous wave (c.w.)) N.M.R. instrument described in section 4.6 (fig. 4.2) shows that outwardly at least, there are many similar features in both instruments. Indeed, the F.T. instrument has been the culmination of a continuing development of the c.w. instrument. However, considerable technical advances are to be found in the design and functionality of electronics and the stability of magnets used in the F.T. instrument. It is these components which are now briefly discussed.

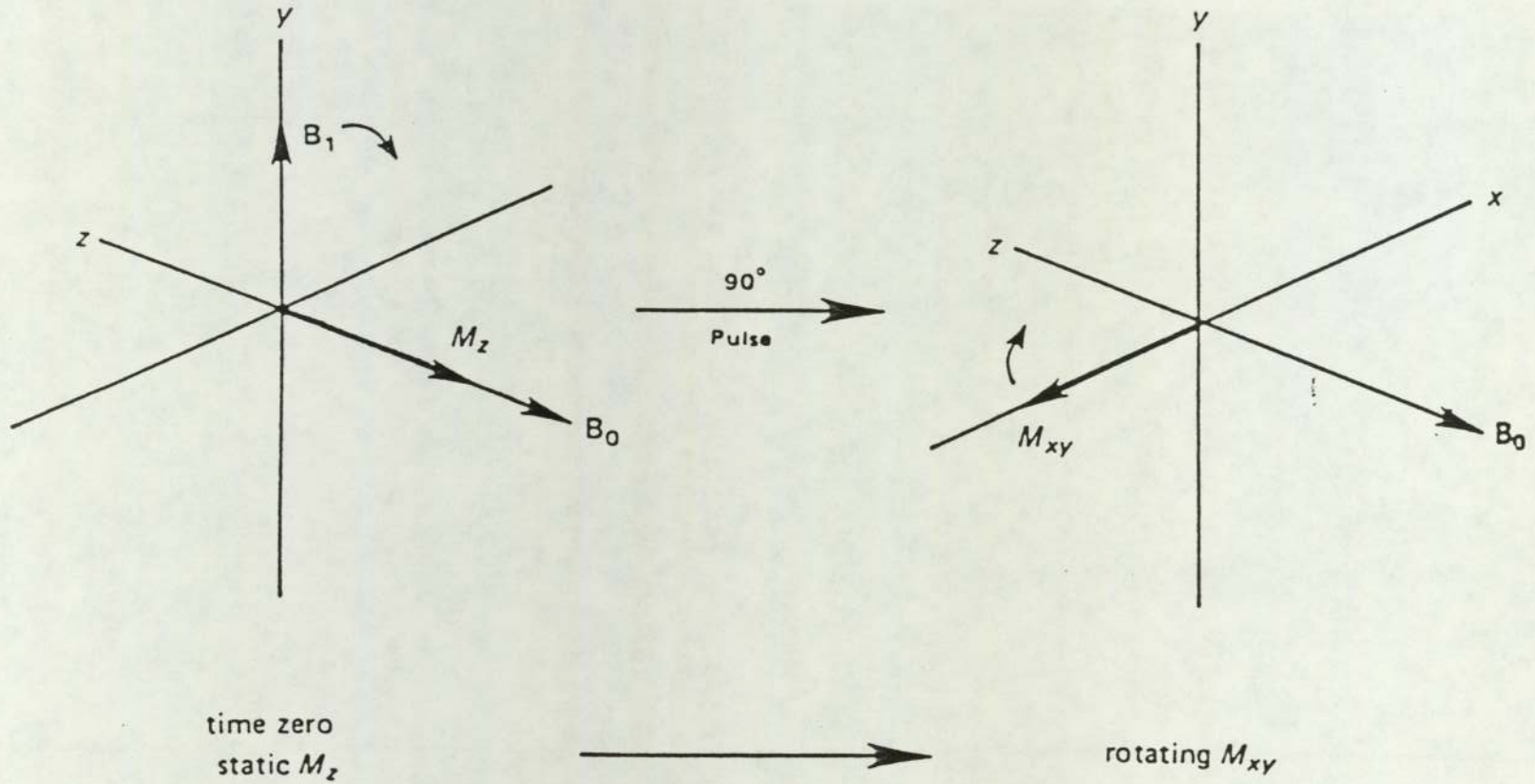

Fig. 5.2 The effects of a sufficiently long or powerful B_1 (applied in the form of a 90° pulse), in which the axis of the nuclear precession cone (only the resultant nuclear magnetization is depicted) is turned into the xy plane: The whole of the nuclear magnetization contributes to the signal detected by a receiver coil.

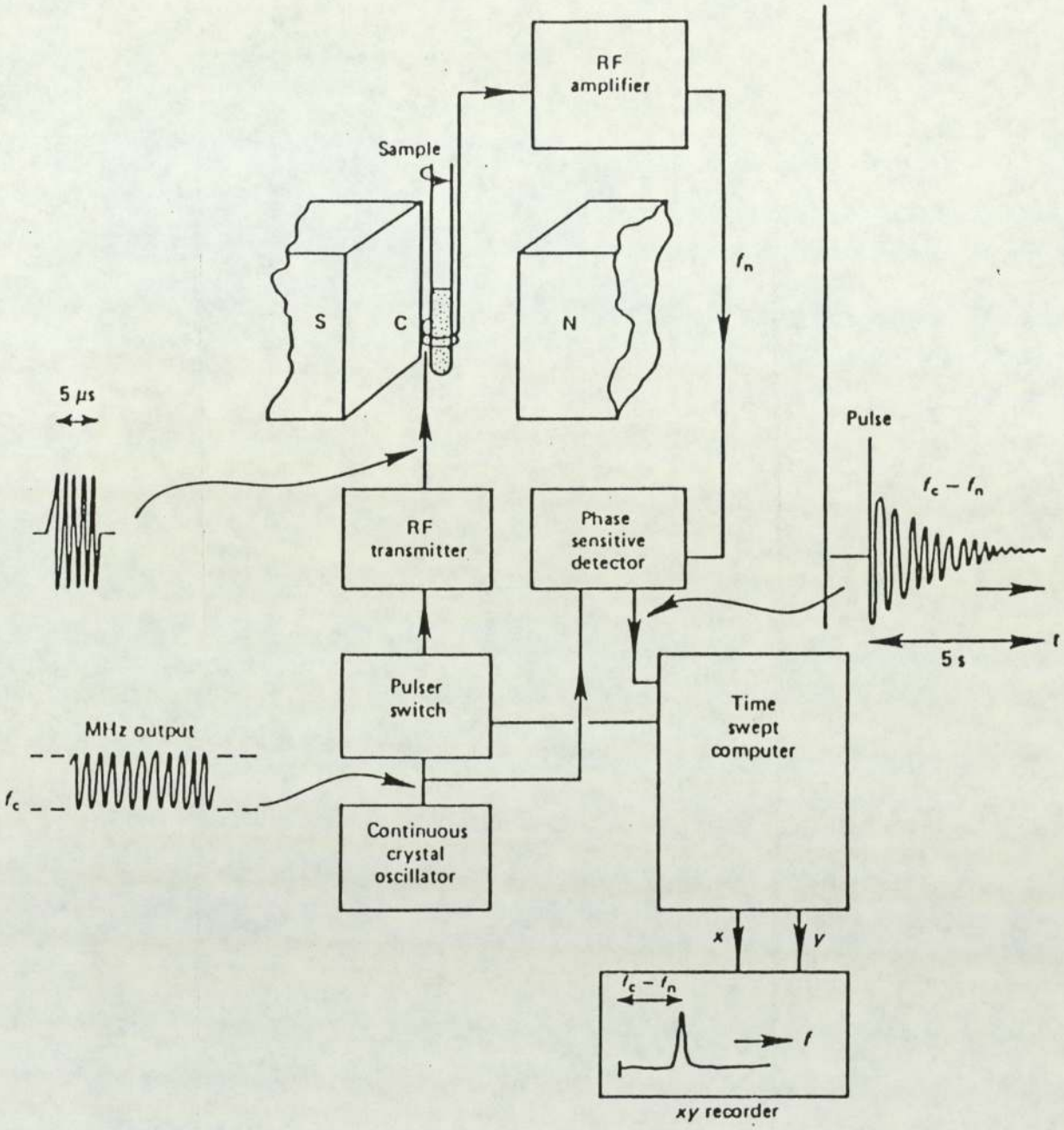

Fig. 5.3 A schematic representation of a basic Fourier transform N.M.R. spectrometer.

The greatest stride forward in the development of magnets has been the introduction of superconducting (cryo) magnets, which offer much higher field strengths and hence increased N.M.R. sensitivity. Permanent and electromagnets also feature in the relatively cheaper F.T. instruments.

The source of B_1 is a gated (switched input) power amplifier driven by a stable, crystal controlled continuous oscillator; in effect the output of a monochromatic crystal oscillator (used in the c.w. instrument) is pulsed by a switching device. Provided the Larmor frequencies of the resonant nuclei fall within the bandwidth of the pulse (bandwidth being defined as 1/t, where t is the length of the pulse) then the nuclear signals can be amplified and detected. Following their detection the nuclear signals are compared electronically with the original oscillator output (B_1 carrier) and a time dependent (analogue) signal is derived by phase sensitive detection. Frequency, phase and amplitude information are contained within the analogue signal, which after digitization is in a form which can be accepted by a computer. If the digitized output is collected over N pulses, then an averaged spectrum is obtained which has a signal to noise ratio that is improved by $N^{1/2}$ over a signal detected from a single pulse. As a final processing step, the Larmor frequencies are calculated using a fourier transform program. The N.M.R. spectrum that results is classified as being in a frequency domain rather than time domain.

5.2.3b THE F.T. N.M.R. USED IN THIS STUDY

A Jeol FX90Q F.T.N.M.R. spectrometer (see fig. 5.4) was used for the determination of accurate chemical shifts at various temperatures. The instrument has a frequency range up to about 90 MHz, a built-in field frequency lock device (the principle of operation is described in section 4.6) and an ancillary variable temperature facility.

5.3 EXPERIMENTAL

The samples which were used for the variable temperature N.M.R. studies had been previously prepared (see section 4.7.3 for precise preparative details). These samples provided different paired formulations of water (mole fractions kept as constant as possible), with or without a fixed amount of the Whitten-type surfactant, $((bipy)_2Ru(II)(2,2'\text{-}bipy\text{-}4,4'(COOC_{18}H_{37})_2))^{2+}\ (PF_6)_2^{2-}$, in acetone (solvent) which was also used as the reference.

Before commencing the chemical shifts measurements each sealed sample was placed into a larger N.M.R. tube containing D_2O, which provided an N.M.R. signal for the purposes of field/frequency locking. The relative chemical shifts given by the acetone and water resonances, were determined for each sample pair at nominal temperatures of 5^o, 10^o, 15^o, 20^o, 25^o, 30^o, 35^o, 40^o and 45^oC. At the commencement and termination of each experimental session the relative ^1H chemical shift of the two resonances of ethylene glycol was measured in order to provide a more exact measurement of temperature [116].

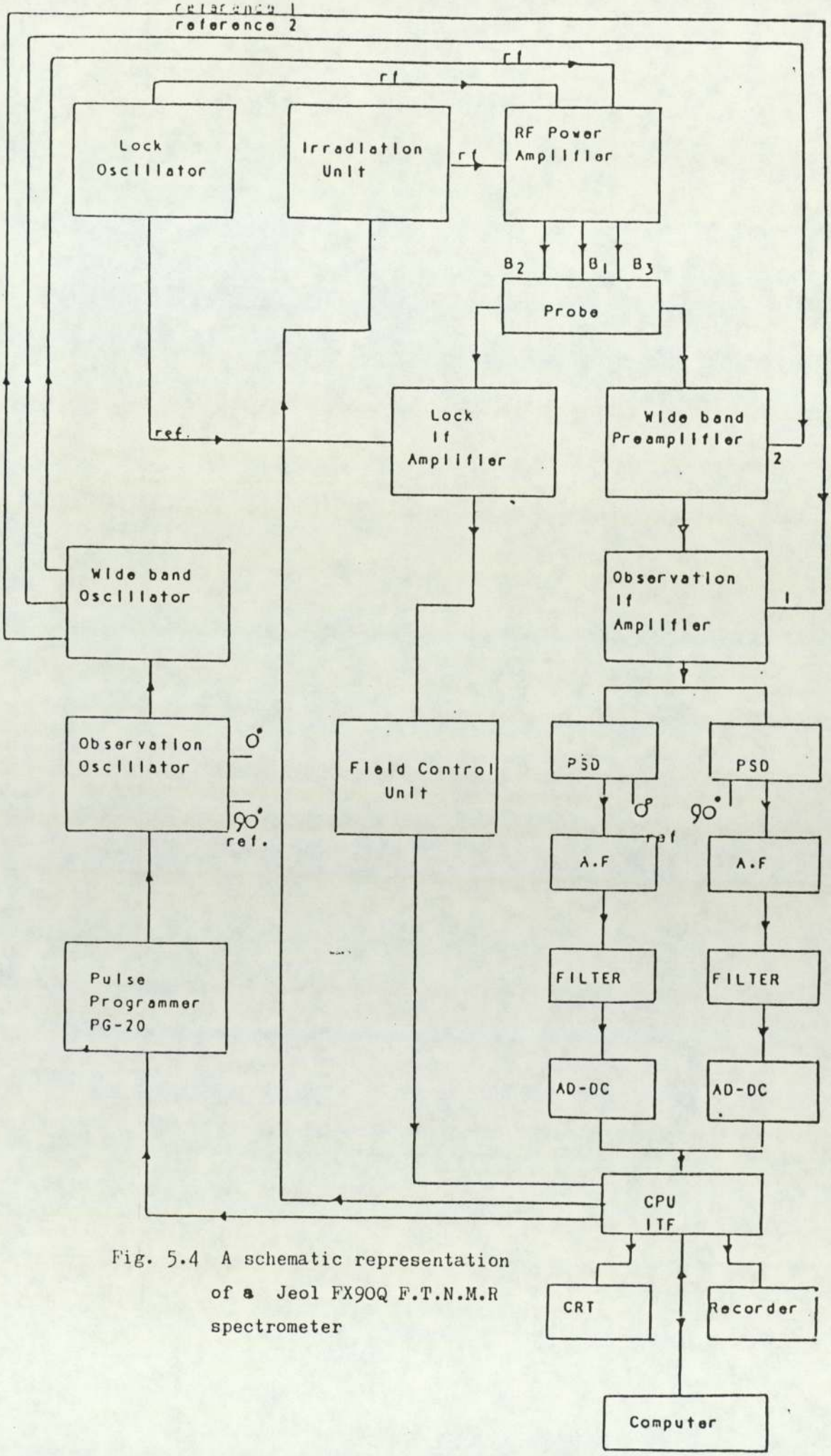

Fig. 5.4 A schematic representation of a Jeol FX90Q F.T.N.M.R spectrometer

5.4 RESULTS AND DISCUSSION

Tables 5.1 - 5.9 give the mole fractions of water with the diester derivative of $Ru(bipy)_3^{2+}$ in acetone (+S) and of water in acetone alone (-S), together with their respective relative chemical shift, for each of the stated temperatures. In keeping with the principles previously developed (section 4.8) for determining the equilibrium constants for the reaction of the diester derivative of $Ru(bipy)_3^{2+}$ with water at a fixed temperature, an initial step was to calculate Δ_{obs} for each sample pairing; Δ_{obs} being the chemical shift difference between free, δ_{free}, (the reference) and complexed water, δ_{obs}. A close inspection of the tabulated data reveals that taken as a whole, Δ_{obs} for most sample pairings is fairly constant: Based on the best line fit from graphical plots of all the data, Δ_{obs} varies by (±2Hz) (see figs. 5.5 and 5.6, which are graphical plots of data from tables 5.1 (5.5°C) and 5.9 (51.4°C) respectively). However, there are some spurious values for Δ_{obs} and this finding must be attributed to the temperature instability of the N.M.R. probe of the F.T. instrument when used at temperatures other than ambient i.e. the c.w. instrument used for the work described in Chapter 4 has a permanent magnet, which is thermally more stable than the electromagnet used in the F.T. instrument.

Previous arguments based on the application of the van't Hoff expression (equation 5.3) to the reaction between water and the surfactant (section 5.1) and an initial proposal that the stoicheiometry of the single complex so formed is 6:1 or 5:1 (Chapter 4) suggest that the constancy of Δ_{obs} at various temperatures

TABLES 5.1 - 5.9. THE OBSERVED CHEMICAL SHIFTS OF WATER MEASURED RELATIVE TO ACETONE, FOR PAIRED SYSTEMS CONTAINING ACETONE AS SOLVENT AND VIRTUALLY IDENTICAL MOLE FRACTIONS OF WATER ($^{x}H_2O$), BUT WITH OR WITHOUT A FIXED MOLE FRACTION OF $((bipy)_2 Ru (II)(2,2' - bipy - 4,4' (COOC_{18}H_{37})_2))^{2+}(PF_6)_2^{2-}$ (WHITTEN-TYPE SURFACTANT (S)) REPRESENTED BY (+S) AND (-S) RESPECTIVELY

TABLE 5.1 TEMPERATURE FIXED AT 5.5°C (NOMINALLY 5°C)

(+S)	(-S)	(+S)	(-S)	
$^{x}H_2O \times 10$	$^{x}H_2O \times 10$	Chemical shift of water (Hz), δ_{obs}	Chemical shift of water (Hz), δ_{free}	Δ_{obs} (Hz)
0.12	0.12	88.62	88.62	0.00
0.25	0.25	88.87	93.26	4.39
0.33	0.33	95.46	95.46	0.00
0.52	0.49	100.59	101.32	0.73
0.65	0.64	105.22	105.47	0.25
0.67	0.68	105.96	105.96	0.00
0.86	0.87	106.20	111.33	5.13
1.17	1.17	116.46	120.61	4.15
1.49	1.49	125.49	129.64	4.15
1.83	1.80	133.30	135.99	2.69
2.06	2.03	139.65	141.36	1.71
2.42	2.69	145.26	155.03	9.77
2.65	2.67	-	155.27	-
3.43	3.45	173.59	171.63	-1.96
3.78	3.81	179.44	174.56	-4.88
4.37	4.51	187.74	190.92	3.18

TABLE 5.2 TEMPERATURE FIXED AT 7.1°C (NOMINALLY 10°C)

(+S)	(-S)	(+S)	(-S)	
$x_{H_2O} \times 10$	$x_{H_2O} \times 10$	Chemical shift of water (Hz), δ_{obs}	Chemical shift of water (Hz), δ_{free}	Δ_{obs} (Hz)
0.12	0.12	87.89	88.38	0.49
0.25	0.25	78.13	93.51	15.38
0.33	0.33	89.36	95.21	5.85
0.52	0.49	100.59	101.07	0.48
0.65	0.64	105.22	105.22	0.00
0.67	0.68	105.96	106.20	0.24
0.86	0.87	105.47	111.33	5.86
1.17	1.17	115.97	120.61	4.64
1.49	1.49	116.21	129.15	12.94
1.83	1.80	133.06	126.95	-6.11
2.06	2.03	136.47	133.30	-3.17
2.42	2.69	146.00	146.97	0.97
2.65	2.67	135.50	155.27	19.71
3.43	3.45	172.85	171.63	-1.22
3.78	3.81	171.39	174.32	2.93
4.37	4.51	188.23	189.94	1.71

TABLE 5.3 TEMPERATURE FIXED AT 16.3°C (NOMINALLY 15°C)

(+S)	(-S)	(+S)	(-S)	
$x_{H_2O} \times 10$	$x_{H_2O} \times 10$	Chemical shift of water (Hz), δ_{obs}	Chemical shift of water (Hz), δ_{free}	Δ_{obs} (Hz)
0.12	0.12	81.54	77.39	-4.15
0.25	0.25	82.03	86.67	4.64
0.33	0.33	84.72	88.62	3.90
0.52	0.49	93.50	93.75	0.24
0.65	0.64	97.17	97.17	0.00
0.67	0.68	98.62	98.14	-0.48
0.86	0.87	96.92	103.52	6.60
1.17	1.17	107.67	111.08	3.41
1.49	1.49	116.94	120.85	3.91
1.83	1.80	124.27	126.71	2.44
2.06	2.03	130.62	133.06	2.44
2.42	2.69	135.99	145.51	9.52
2.65	2.67	-	146.24	-
3.43	3.45	164.79	156.49	-8.30
3.78	3.81	170.41	165.53	-4.88
4.37	4.51	179.93	182.13	2.20

TABLE 5.4 TEMPERATURE FIXED AT 26.2°C (NOMINALLY 20°C)

(+S)	(-S)	(+S)	(-S)	
$x_{H_2O} \times 10$	$x_{H_2O} \times 10$	Chemical shift of water (Hz), δ_{obs}	Chemical shift of water (Hz), δ_{free}	Δ_{obs} (Hz)
0.12	0.12	73.97	74.22	0.25
0.25	0.25	74.71	78.59	3.88
0.33	0.33	80.32	81.30	0.98
0.52	0.49	85.45	85.69	0.24
0.65	0.64	88.13	89.11	0.98
0.67	0.68	88.86	88.38	-0.48
0.86	0.87	93.75	94.73	0.98
1.17	1.17	98.63	102.78	4.15
1.49	1.49	107.42	111.33	3.91
1.83	1.80	114.26	118.65	4.39
2.06	2.03	121.09	123.78	2.69
2.42	2.69	130.62	135.50	4.88
2.65	2.67	126.22	136.47	10.25
3.43	3.45	154.79	153.08	-1.71
3.78	3.81	159.67	155.03	-4.64
4.37	4.51	169.68	171.63	1.95

TABLE 5.5 TEMPERATURE FIXED AT 26.2°C (NOMINALLY 25°C)

(+S)	(-S)	(+S)	(-S)	
$x_{H_2O} \times 10$	$x_{H_2O} \times 10$	Chemical shift of water (Hz), δ_{obs}	Chemical shift of water (Hz), δ_{free}	Δ_{obs} (Hz)
0.12	0.12	73.49	74.22	0.73
0.25	0.25	74.46	78.61	4.15
0.33	0.33	79.83	79.83	0.00
0.52	0.49	84.47	84.96	0.49
0.65	0.64	88.38	88.62	0.24
0.67	0.68	89.11	89.60	0.49
0.86	0.87	89.60	94.48	4.88
1.17	1.17	98.39	102.78	4.39
1.49	1.49	107.18	110.60	3.42
1.83	1.80	114.50	117.19	2.69
2.06	2.03	120.36	122.56	2.20
2.42	2.69	125.98	135.25	9.27
2.65	2.67	-	135.74	-
3.43	3.45	155.27	152.83	-2.44
3.78	3.81	159.91	154.54	-5.37
4.37	4.51	169.19	171.63	2.44

TABLE 5.6 TEMPERATURE FIXED AT 34.3°C (NOMINALLY 30°C)

(+S)	(-S)	(+S)	(-S)	
$x_{H_2O} \times 10$	$x_{H_2O} \times 10$	Chemical shift of water (Hz), δ_{obs}	Chemical shift of water (Hz), δ_{free}	Δ_{obs} (Hz)
0.12	0.12	65.43	65.19	-0.24
0.25	0.25	65.92	72.51	6.59
0.33	0.33	70.56	74.22	3.66
0.52	0.49	78.13	78.86	0.73
0.65	0.64	81.54	82.52	0.98
0.67	0.68	79.83	79.35	-0.48
0.86	0.87	79.10	87.16	8.06
1.17	1.17	87.40	95.21	7.81
1.49	1.49	96.68	104.00	7.32
1.83	1.80	102.29	105.71	3.42
2.06	2.03	112.06	111.33	-0.73
2.42	2.69	117.68	123.78	6.10
2.65	2.67	-	123.29	-
3.43	3.45	146.97	141.36	-5.61
3.78	3.81	152.59	146.97	5.62
4.37	4.51	161.62	160.89	-0.73

TABLE 5.7 TEMPERATURE FIXED AT 41.2°C (NOMINALLY 35°C)

(+S)	(-S)	(+S)	(-S)	
$x_{H_2O} \times 10$	$x_{H_2O} \times 10$	Chemical shift of water (Hz), δ_{obs}	Chemical shift of water (Hz), δ_{free}	$\triangle_{obs}$ (Hz)
0.12	0.12	62.99	63.48	0.49
0.25	0.25	64.70	69.09	4.39
0.33	0.33	69.34	69.09	-0.25
0.52	0.49	73.49	74.22	0.73
0.65	0.64	77.39	76.42	-0.97
0.67	0.68	77.39	78.61	1.22
0.86	0.87	77.15	82.28	5.13
1.17	1.17	85.69	89.84	4.15
1.49	1.49	95.46	97.41	1.95
1.83	1.80	100.34	103.27	2.93
2.06	2.03	106.69	108.89	2.20
2.42	2.69	111.08	122.56	11.48
2.65	2.67	112.79	121.09	8.30
3.43	3.45	140.14	139.89	-0.25
3.78	3.81	145.26	141.35	-3.90
4.37	4.51	155.52	157.96	2.44

TABLE 5.8 TEMPERATURE FIXED AT 51.1°C (NOMINALLY 40°C)

(+S)	(-S)	(+S)	(-S)	
$x_{H_2O} \times 10$	$x_{H_2O} \times 10$	Chemical shift of water (Hz), δ_{obs}	Chemical shift of water (Hz), δ_{free}	Δ_{obs} (Hz)
0.12	0.12	54.93	56.64	1.71
0.25	0.25	-	55.42	-
0.33	0.33	59.33	61.28	1.95
0.52	0.49	63.47	64.94	1.47
0.65	0.64	65.67	69.09	3.42
0.67	0.68	66.89	70.31	3.42
0.86	0.87	67.87	73.24	5.37
1.17	1.17	74.95	79.59	4.64
1.49	1.49	83.50	86.92	3.42
1.83	1.80	88.87	92.77	3.90
2.06	2.03	93.99	97.90	3.91
2.42	2.69	99.12	109.62	10.50
2.65	2.67	98.14	113.28	15.14
3.43	3.45	127.20	128.17	0.97
3.78	3.81	132.57	130.13	-2.44
4.37	4.51	143.07	149.42	6.35

TABLE 5.9 TEMPERATURE FIXED AT 51.4°C (NOMINALLY 45°C)

(+S)	(-S)	(+S)	(-S)	
$x_{H_2O} \times 10$	$x_{H_2O} \times 10$	Chemical shift of water (Hz), δ_{obs}	Chemical shift of water (Hz), δ_{free}	Δ_{obs} (Hz)
0.12	0.12	56.40	57.62	1.22
0.25	0.25	59.08	62.74	3.66
0.33	0.33	61.77	62.01	0.24
0.52	0.49	65.92	65.67	-0.25
0.65	0.64	69.34	70.80	1.46
0.67	0.68	69.82	69.34	-0.48
0.86	0.87	69.34	77.15	7.81
1.17	1.17	77.39	81.30	3.91
1.49	1.49	87.40	88.13	0.73
1.83	1.80	91.31	93.99	2.68
2.06	2.03	99.61	102.54	2.93
2.42	2.69	102.54	113.53	10.99
2.65	2.67	102.05	112.55	10.50
3.43	3.45	131.10	129.15	-1.95
3.78	3.81	136.23	131.59	4.64
4.37	4.51	147.22	148.44	1.22

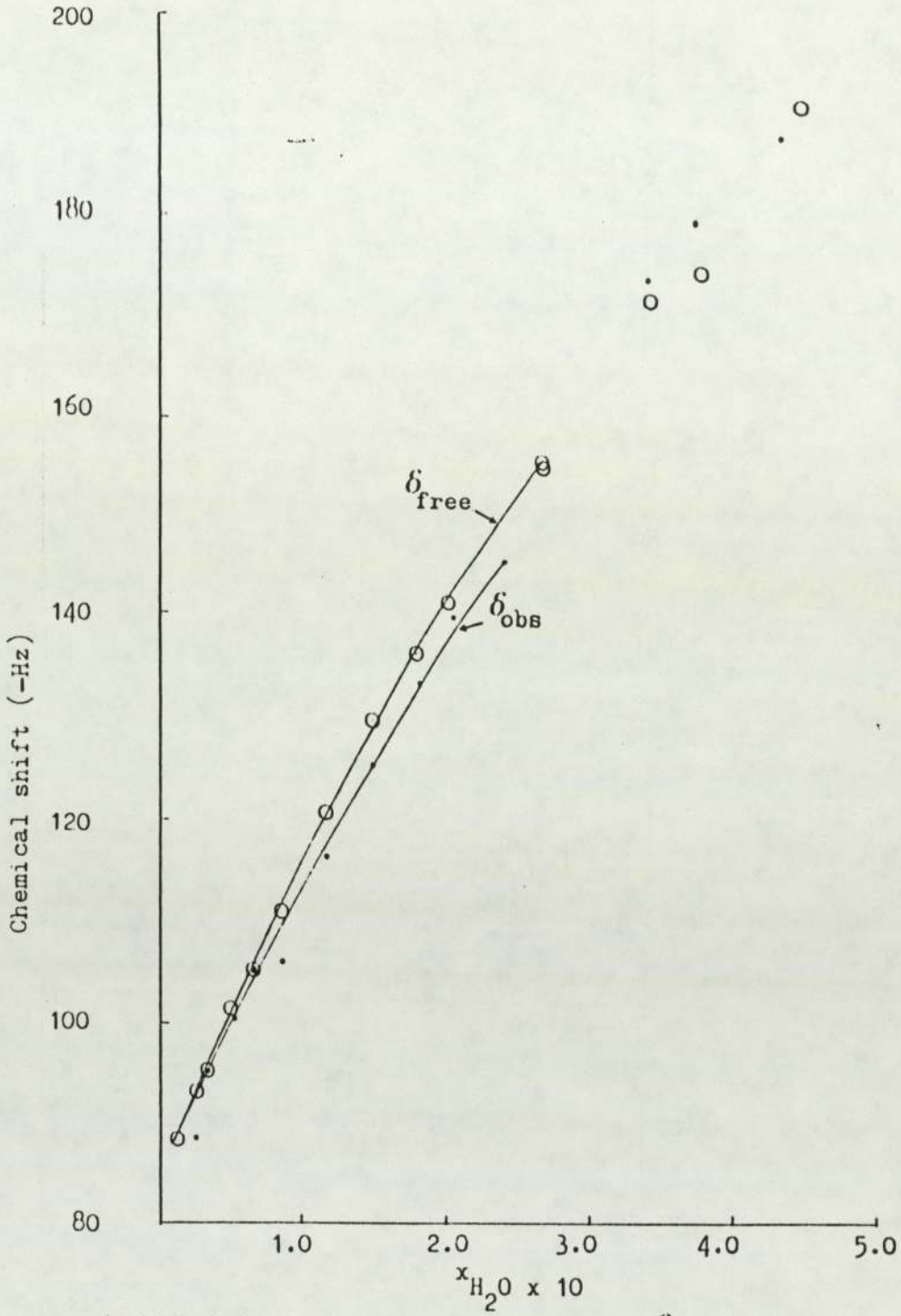

Fig. 5.5 The variation of δ_{obs} and δ_{free} (relative to acetone) of water for systems containing various mole fractions of water ($^{x}H_2O$) dissolved in acetone, but with (+S) or without (-S) a fixed mole fraction of the diester derivative of $Ru(bipy)_3^{2+}$, respectively: Temperature fixed at 5.5°C.

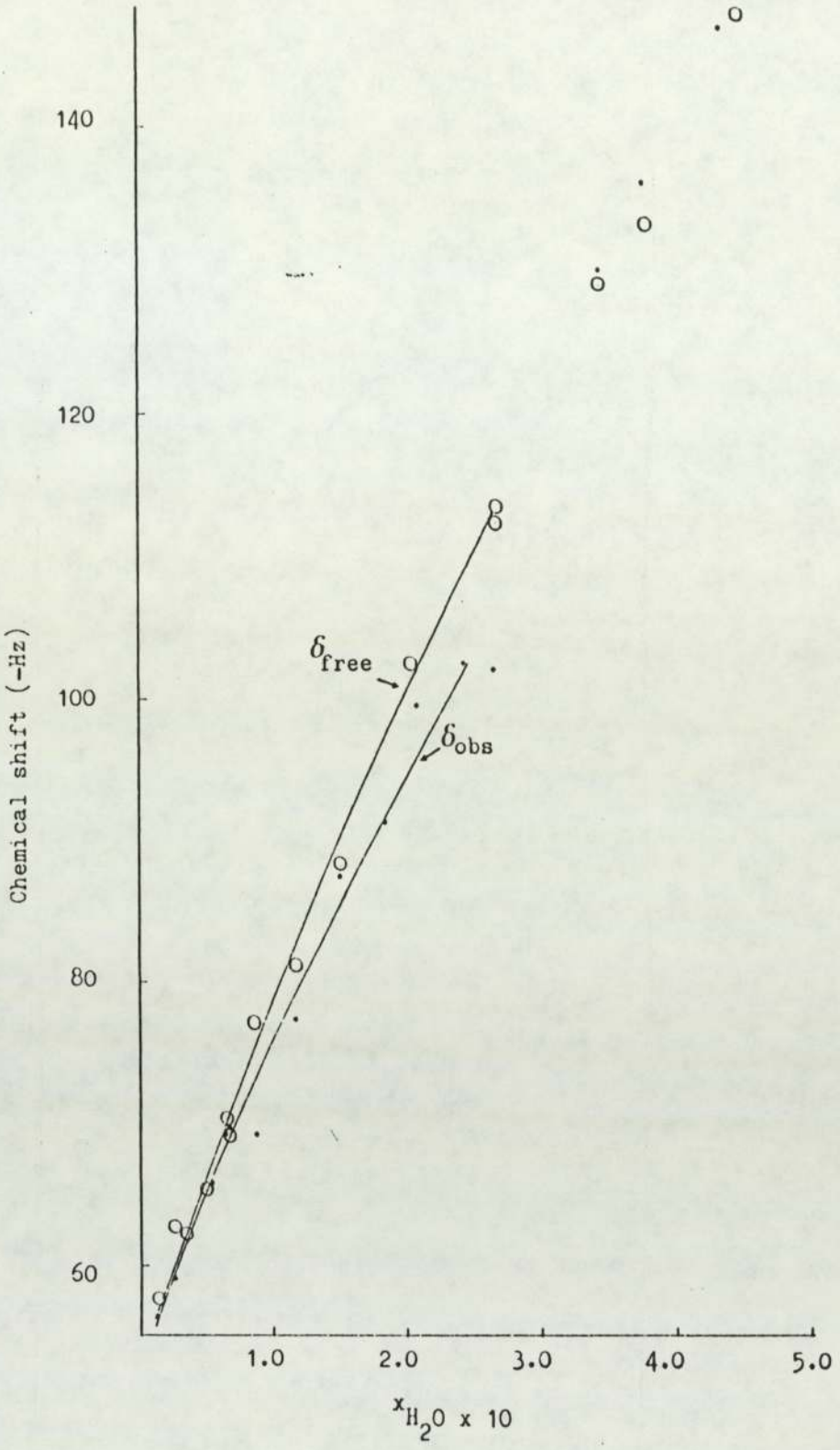

Fig. 5.6 The variation of δ_{obs} and δ_{free} (relative to acetone) of water for systems containing various mole fractions of water ($^{x}H_2O$) dissolved in acetone, but with (+S) or without (-S) a fixed mole fraction of the diester derivative of $Ru(bipy)_3^{2+}$, respectively: Temperature fixed at 51.4°C.

is unexpected. However, this experimental outcome can possibly be explained by a more searching examination of equilibria phenomena that might exist for systems containing a derivative of $Ru(bipy)_3^{2+}$ and water.

A possible explanation of the near constancy of Δ_{obs} is that the equilibrium constant, determined according to the method described in section 4.8, does in fact represent an overall equilibrium constant β_n, which is made up of stepwise equilibrium constants. It may be shown that β_n is a product of the stepwise equilibrium constants [117], and given by

$$\beta_n = K_1 \times K_2 \times K_3 \text{ ---} K_n \qquad (5.5)$$

If this hypothesis is correct then clearly K_1, could derive from the formation of a 1:1 complex from the bimolecular reaction of the surfactant and water, behaving as acceptor and donor respectively, such that

$$A + D \underset{\text{<---}}{\overset{\text{--->}}{}} A \text{ --- } D \quad \text{complex} \qquad (5.6)$$

from which $$K_1 = \frac{[AD]}{[A][D]} \qquad (5.7)$$

similarly $$AD + D \underset{\text{<---}}{\overset{\text{--->}}{}} AD_2 \qquad (5.8)$$

therefore, $$K_2 = \frac{[AD_2]}{[AD][D]} \qquad (5.9)$$

and so on. The chain of equilibria could progress further until there is a contribution to the system from a series of complexes. Δ_{obs} is given by

$$\Delta_{obs} = f_1\Delta_{c_1} + f_2\Delta_{c_2} + f_3\Delta_{c_3} \text{ ---} \qquad (5.10)$$

where f_1, f_2, f_3 --- are the fractions of water in the 1:1, 1:2 --- complexes.

As the temperature of each system is raised or lowered the values of the stepwise equilibrium constants will also change and so should f_1, f_2, f_3 --- and the chemical shift for each contributory reaction (to equation 5.10) should be correspondingly affected. If, however, the screening of the complexed water molecules is the same at each site in each type of complex formed (i.e. each complexing site provides equivalent screening of the water) then the value of Δ_{obs} for the system may not change markedly. In essence, the total number of water molecules at each reaction site may vary as the temperature is changed, but if the shifts induced at these reaction sites are equivalent, the only effect on Δ_{obs} that could occur, would be if the total amount of free species varied significantly. Because the overall value of K_x is so high it is possible that such a variation in the total amount of free species may be small over the relatively narrow range of temperature used (5.5 - 51.4^{o}C). Therefore, the effect of temperature on the various equilibrium constants may be to adjust the distribution of an essentially fixed number of bound water molecules between the various equilibria. It is however, possible that because of the changing concentration of H_2O which can contribute

to δ_{free} through the effect of H_2O - H_2O hydrogen bonding, differences in chemical shift will appear in the values δ_{free} (similarly with δ_{obs}). This is observed. One model that might be consistent with the above speculation would be if the water molecules interact with the surfactant at or near the 'six fold' axis of any ring in the bipyridyl ring system, proposed in Chapter 4: The values of Δ_c in the range of 1-2 p.p.m. is consistent with this suggestion. If this is the case, a water molecule moving to an identical site on another complex type could experience an equivalent screening effect.

It should be noted that although acetone has been found to be the best solvent so far [106] in terms of lacking N.M.R. complexity and in the mutual dissolution of water and the Whitten-type surfactant, there remains considerable doubt as to whether it is chemically inert in the situation in which it is used. For example, the polar nature of the carbonyl group of acetone would in general make it open to reaction through H-bonding, dipole-dipole interaction, dipole-induced interaction or in the extreme, classical types of addition reactions.

It must be mentioned that a final possible explanation of the constancy of Δ_{obs} with temperature, is that the chosen temperature range was too small to reveal a significant effect on the equilibrium constants and that the corresponding changes to Δ_{obs} lie within the shift limits corresponding to the overall experimental error.

5.5. CONCLUSION

Evidence is presented that more than one complex is formed from the reaction in solution of water and the surfactant derivative of $Ru(bipy)_3^{2+}$. If this is to gain any real credibility then a method has to be found that detects the existence of different types of complex and also determines their respective stoicheiometries (the next chapter deals with this point).

Furthermore, it is evident that quite extensive investigations are required to ascertain the most suitable solvent for the molecular species in question. The search for this solvent is complicated because it must remain inert, have a simple N.M.R. spectrum and be a suitable solvent for a water insoluble surfactant and also water.

The problem of measuring significant variations in Δ_{obs} (with temperature) that lies outside the detection limit of the 90 MHz N.M.R. spectrometer used in this study can in theory, be solved simply by using a higher field N.M.R. spectrometer. For example a 0.5 Hz shift for a 90 MHz spectrometer (nearing the limit of accuracy) becomes a 1.2 Hz shift when a 220 MHz instrument is used and so on. Such an instrument was unfortunately not freely available to conduct the appropriate investigations.

As a final point it must be mentioned that if K_x calculated in Chapter 4 represents an overall mole fraction based equilibrium constant, then a value of K_c calculated from K_x will only be meaningful if it is calculated using the appropriate mean molar

volumes of the mixtures. For a multi component system this is naturally difficult and serves to emphasis the advocation by Homer et al [108] for the cautious use of K_c when evaluating data from equilibrium reactions.

CHAPTER 6

THE DEVELOPMENT OF A N.M.R. METHOD TO ESTABLISH THE STOICHEIOMETRY OF THE MOLECULAR COMPLEX/ES FORMED BETWEEN A SURFACTANT DERIVATIVE OF $Ru(bipy)_3^{2+}$ AND WATER

6.1 INTRODUCTION

Evidence from the N.M.R. adaptation of the Benesi-Hildebrand method presented in Chapter 4 for determining the stoicheiometry of weak molecular complexes, suggests a 6:1 or 5:1 stoicheiometry might be assigned to the complex formed from the reaction of water and the diester derivative of $Ru(bipy)_3^{2+}$, in acetone as the solvent. Subsequent N.M.R. studies designed to produce thermodynamic parameters for the strength of complex formation, would appear to place considerable doubt on the validity of the inferred stoicheiometry of the complex (see Chapter 5). However, in concluding Chapter 4, it was appreciated that in order to substantiate the original proposal on the stoicheiometry of the complex, the same parameter would need to be determined by an independent analytical method.

From an initial examination of this problem, it would appear that the required stoicheiometry could be obtained by using freezing point depression data [118] or conducting parallel spectrophotometric studies according to the well known method of continuous variations, which is usually ascribed to Job [119, 120], (it deserves mentioning that the principles of the latter method were originally outlined by Denison [121]). However, with restricted quantities of the Whitten-type surfactant available, cryoscopic studies were ruled out and attention was drawn to the spectrophotometric form of the Job method, which in

principle offered a reasonably sensitive analytical method to determine low concentrations of the interacting species provided extinction coefficients were sufficiently high.

It is convenient at this stage, to examine a typical Job plot (see fig. 6.1) obtained for the well studied fluoranil-hexamethylbenzene systems [122]. Referring to fig. 6.1, the stoicheiometry for the complex formed between the two substances is read from the abscissa scale of the graph at the point where the system absorbs a maximum of monochromated light. Clearly, at this point the ratio of the fractional concentration terms is 1:1, which corresponds to the stoicheiometry of the complex. Other complexes may in principle be studied similarly.

There has been much controversy over the limitations of the Job method and Woldbye [123] in particular has taken to task (in the form of a critical review) the implications and validity of assumptions made in the theory of the method and showed many to be erroneous. Prior to Woldbye's publication, Vosburgh and Cooper [124] had added significantly to the versatility of the Job method by demonstrating that it was in certain circumstances applicable to cases where more than one complex was formed. These same authors [124] also show that when only a single complex is formed the results obtained are independent of the wavelength of light. However, in the context of this work they also remark that when more than one complex is formed, the results obtained depend on the wavelength of the light, and for useful conclusions the wavelengths used must be carefully selected. In essence, this means that when there is an overlap of the absorption spectra of complexes

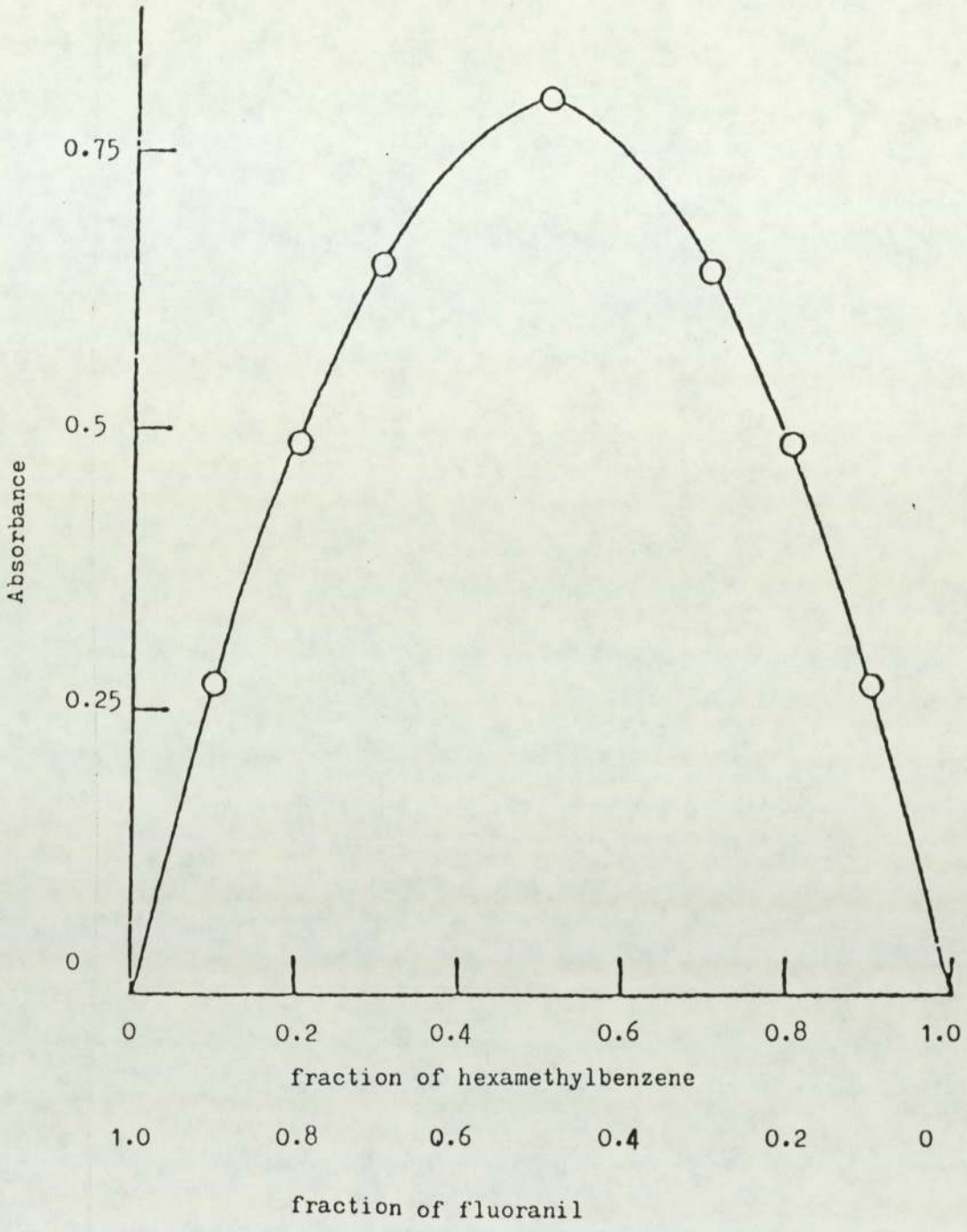

Fig. 6.1 Job plot of the system fluoranil-hexamethylbenzene in carbon tetrachloride at 486 nm, 33.5°C

in the same solution, it becomes extremely difficult or impossible to choose an appropriate wavelength at which to measure absorbances appropriate to all of the complexes present. The problem is further complicated if the complexes in solution have low molar extinction coefficients, are there in low concentration or their electronic spectra consist of a number of charge-transfer bands.

Quite clearly systems containing the complexes formed from the reaction of water and a surfactant derivative of $Ru(bipy)_3^{2+}$ may have some of the features just mentioned. It was reasoned therefore, that this would prevent an unambiguous direct application of the classical Job method to such systems. The intention in this chapter is to demonstrate how the Job method can be adapted for N.M.R. purposes and provide a novel method that offers a possible route to elucidating the stoicheiometry of complexes formed in Whitten-type $Ru(bipy)_3^{2+}$ derivatives - water systems.

6.2 THEORETICAL

If the stability of molecular complexes formed in solution is sufficiently high that N.M.R. resonances due to each of the species present can be observed, it is possible to study the complexes by intensity measurements for each of the absorptions. If, however, there is exchange of resonant species between various chemical sites, the chemical shifts of the relevant species will be time-averaged. Because this situation applies to complexes formed between water and the diester derivative of $Ru(bipy)_3^{2+}$ the following proposals are concerned with the use of time-averaged chemical shifts rather than

intensities for continuous variation studies [119, 120].

It has been previously shown that the reaction of many species to form complexes amenable to study by N.M.R. can be represented by equation 6.1.

$$A + nD = AD_n \qquad (6.1)$$

where A and D often represent the acceptor and donor components of charge transfer complexes.

Consistent with Job's assumption, it is necessary to prepare solutions of A and D separately in the same solvent and at the same molarity M. A series of mixtures of the same total volume, V, must then be prepared from the two stock solutions, such that a fraction, x, of V is attributable to the solution of D. If c_A, c_D and c_{AD_n} are the equilibrium concentrations of A, D and AD_n, the expressions for these are given by equations (6.2) - (6.4).

$$c_A = M(1 - x) - c_{AD_n} \qquad (6.2)$$

$$c_D = Mx - nc_{AD_n} \qquad (6.3)$$

$$c_{AD_n} = c_A c_D^n K \qquad (6.4)$$

where equation 6.4 derives from the ideal equation (6.5), but

$$K = (c_{AD_n}/c_A c_D^n)(\gamma_{AD_n}/\gamma_A \gamma_D^n) \qquad (6.5)$$

if the solutions are prepared with M-->0 it can be assumed that the activity coefficient ratio in equation (6.5) equates to unity. By appropriate manipulation of equations (6.2) - (6.4) it can be confirmed that [119,120,124] when

$$dc_{AD_n}/dx = 0 \qquad (6.6)$$

$$n = x/(1 - x) \qquad (6.7)$$

The problem is to ascertain how this condition can be determined from N.M.R. studies.

Woldbye [123] has suggested that the conditions appropriate to equation (6.7) can only be determined experimentally from measurements of the value, P, of a particular physical property of solutions if, and only if P is of the form

$$P = s_1(A) + s_2(D) + f(AD_n) \qquad (6.8)$$

where s_1 and s_2 are constants. The normal procedure is to evaluate the difference, Y, between the measured value of P and the value of P calculated under the assumption of no complex formation. Because dY/dx is directly proportional to dc_{AD_n}/dx, a plot of Y against x shows a maximum or minimum when equation (6.7) is valid.

In those circumstances when it is only possible to measure a time-averaged chemical shift this, according to the Gutowsky-Saika theory of fast exchange [125], is given by

$$\delta_{obs} = f\delta_c + (1-f)\,\delta_{free} \qquad (6.9)$$

where δ_{obs}, δ_{free} and δ_c are respectively the chemical shifts of the chosen species as observed in a particular mixture, of the uncomplexed species in that mixture and of the species in the complex, the amount of which contains a fraction, f, of the total amount of the species present initially. It is convenient to rearrange equation (6.9) in terms of induced shifts as

$$\Delta_{obs} = f\Delta_c \qquad (6.10)$$

where $f = c_{AD_n}/M(1-x)$. If a chemical shift for A is measured it can be shown, by differentiating equation (6.10) with respect to x that

$$d\Delta_{obs}/dx = (dc_{AD_n}/dx)(\Delta_c/M(1-x)) + \Delta_{obs}/(1-x) \qquad (6.11)$$

On the other hand, if a shift of D is measured equation (6.12) applies

$$d\Delta_{obs}/dx = ((dc_{AD_n}/dx)(n\Delta_c/Mx)) - \Delta_{obs}/x \qquad (6.12)$$

It can be seen from equations (6.11) and (6.12) that a plot of neither the induced shift for A nor D against x can lead to either a maximum or minimum. However, it is possible to determine the value of

x at which condition (6.7) holds. Inspection of equation (6.11) reveals that when $^{dc}\Delta D_n/dx = 0$ the slope of a plot of Δ_{obs} versus x will, at the appropriate value of x, be given by

$$d\Delta_{obs}/dx = \Delta_{obs}/(1-x) \qquad (6.13)$$

It should be possible, therefore, to determine the value of x appropriate to equation (6.7) and determine n. A similar treatment of equation (6.12) reveals that the value of x appropriate to equation (6.7) can be deduced from the condition

$$d\Delta_{obs}/dx = - \Delta_{obs}/x \qquad (6.14)$$

Before implementing the approach described above it is prudent to assess the conditions under which experimental shifts realistically approximate to those required for the above equations.

6.2.1 EXPERIMENTAL CONDITIONS

It has been shown previously that the screening, σ, of a nucleus (see section 4.3.2) in the liquid phase is given by [85]

$$\sigma_{sol} = \sigma_g+\sigma_b+\sigma_w+\sigma_a+\sigma_E+\sigma_c \qquad (6.15)$$

Where the respective terms on the right hand side of the equation refer to the screening due to the isolated molecule in the

gas phase, the volume magnetic susceptibility of the liquid, van der Waals forces between molecules, other magnetically anisotropic molecules, intermolecular electric fields and specific molecular interactions.

The shifts required for the approach outlined above can be measured relative to some reference compound. In this case the chemical shifts are due to the difference between two values given by equation (6.15), one for A or D and the other for the reference. Alternatively, by using a spectrometer that is field/frequency locked to the resonance of a separate sample it is possible to measure the resonance conditions appropriate to equation (6.15) directly.

The advantage of using an internal reference compound is that it eliminates the effects of volume magnetic susceptibility and minimizes the effects of van der Waals, anisotropic and electric field origin [88]. A possible disadvantage may be that the addition of a fourth component, the reference, to the mixtures may be chemically undesirable. If the alternative method of measuring absolute resonance conditions is employed it is possible that all terms on the right hand side of equation (6.15) may vary with x. However, if the molarity of the solution, M, is very low, the common solvent used for A and D will dominate the solvent screening effects, with the non-bonded effects of A on D and vice versa being of little significance. For example, by choosing a suitably low value of M, and bearing in mind the fact that volume magnetic susceptibilities are additive on a volume fraction basis [126], it is possible to keep variations in σ_b to a magnitude that is of the order of the error in the shift values; typically, therefore, M for organic systems might be

around 0.1 molar. Evidently it will also prove beneficial to choose an isotropic solvent to achieve these conditions, under which it can be deduced that σ_W and σ_E will also be approximately constant [99, 127]. Under these conditions similar arguments may be applied to the measurement of δ_{free}. Moreover, whether the shifts of A or D are studied, it may prove essential to prepare a separate reference solution for each value of x studied in which the concentration, of whichever of A or D is measured, is precisely the same as that in the interacting mixture. The measured shifts for these solutions correspond to δ_{free} and when these are subtracted from the corresponding δ_{obs} to yield Δ_{obs}, not only will the gas phase screening be eliminated but variations in the other non-specific screening terms will be further minimized.

6.2.2 FORMATION OF 1:n and 1:n+q COMPLEXES

The foregoing proposals assume that only one complex is formed in solution. This assumption is often not valid and its failure is the base of one of the several criticisms [123, 124] of the continuous variation method. Whilst the extensive evaluation of analogous criticisms that may become apparent in the context of the present proposals is beyond the scope of this work, it is prudent to examine the implications of two different complexes being formed according to

$$A + nD = AD_n + qD = AD_{n+q} \qquad (6.16)$$

In this event, modifications must be made to the equations for the equilibrium concentrations of the various species present and these

will cause changes to equations (6.11) and (6.12). In order to illustrate this point it is convenient to consider the shift of A, the relevant equation for which is

$$\Delta_{obs} = c_{AD_n} \Delta_{AD_n}/(1-x)M + c_{AD_{n+q}} \Delta_{AD_{n+q}}/(1-x)M \qquad (6.17)$$

from which it can be shown that

$$d\Delta_{obs}/dx = \Delta_{obs}/(1-x) + dc_{AD_n}/dx[\Delta_{AD_n}/(1-x)M]$$

$$+ dc_{AD_{n+q}}/dx[\Delta_{AD_{n+q}}/(1-x)M] \qquad (6.18)$$

From equation (6.18) it can be seen that condition (6.13) can only be found when the last two terms of equation (6.18) are equal and of opposite sign. Some indication of the conditions at which this equality may be achieved may be obtained by considering the definitions of equilibrium concentrations appropriate to equation (6.18). These reveal that

when $dc_{AD_n}/dx = 0$

$$dc_{AD_{n+q}}/dx = (c_A nM - c_D M)/(c_D + c_A n(n+q)), \text{ and}$$

$$n = x/(1-x)+((n+q)qc_{AD_{n+q}})/((1-x)M) \qquad (6.19)$$

and when $dc_{AD_{n+q}}/dx = 0$,

$$dc_{AD_n}/dx = - Mqc_{AD_n}/(c_D - nqc_{AD_n}), \text{ and}$$

$$n = x/(1-x)-q - nqc_{AD_n}/M(1-x) \qquad (6.20)$$

If these two conditions relate to maxima in the concentrations of the two complex species it is necessary, for the range of x between them or outside them, that the change in concentration of both complexes with x must be of opposite sign. Consequently, if $^{\Delta}AD_n$ and $^{\Delta}AD_{n+q}$ are of the same sign the limits between which criterion (6.13) applies may be deduced. If $^{\Delta}AD_n >> {}^{\Delta}AD_{n+q}$, $^{dc}AD_n/dx$ can approach zero for the required condition to hold. Alternatively, if $^{\Delta}AD_{n+q} >> {}^{\Delta}AD_n$, $^{dc}AD_{n+q}/dx$ can approach zero for condition (6.13) to apply. It follows from equations (6.19) and (6.20) that condition (6.13) should be found at a value of x between limits somewhat below the value that would be found for the 1:n complex if formed alone and above that for the 1:n+q complex if it were formed alone. It is possible, for a system in which more than one complex is formed, that condition (6.13) may be found fortuitously at a value of x corresponding to the formation of a single complex only. In order to resolve this possible ambiguity the proposed method must be implemented for more than one value of M.

6.2.3 THE EFFECT OF M ON THE SIGNIFICANCE OF INDUCED SHIFTS

If A and D have suitable characteristics that facilitate, for example, the formation of a 1:2 complex, it is appropriate to enquire whether or not the choice of M influences the significance of the experimental shifts. It is interesting, therefore, to consider, at least qualitatively, the implications of the collisional mechanism for forming a 1:2 complex. If a 1:2 complex is formed this can arise in two ways. First, a 1:1 intermediate can be formed, but this must have a sufficiently long life-time that will enable it to undergo a

subsequent collision with another molecule of D to form AD_2. At low concentrations of species forming relatively unstable complexes the probability of this occurring is low. Second, AD_2 may be formed by an appropriate termolecular collision, but again the probability of this happening at low concentrations is low. It is likely, therefore, that, unless the equilibrium constant for the formation of a 1:n complex is large, only 1:1 complexes will be formed at low values of M. Consequently, under these conditions it is probable that the induced shifts will, when analysed by the procedure outlined above (and by the classical spectrophotometric method) indicate the presence of only a lower complex, possibly that of 1:1 stoicheiometry. It is essential, therefore, that continuous variation studies are carried out with at least two separated values of M.

6.2.4 SHAPES OF THE PLOTS OF Δ_{obs} vs x

In anticipation of the possibility that 1:1 complex formation will be encountered frequently it is worth considering what shape the plot of Δ_{obs} vs x will have in this case.

If c_A, and c_D, in equation (6.5) which is taken to be devoid of activity coefficients and for 1:1 complex formation, are substituted from equation (6.2) and (6.3) it can be shown that f in equation (6.10) is given by

$$f = KMx/(1 + KM) \qquad (6.21)$$

provided that c_{AD}^2 is equated to zero. Consequently, from equation (6.10) it follows that the plot of Δ_{obs} vs x could be linear. In these circumstances the slopes (S) of linear plots at different values of M can be used to deduce the equilibrium constant from

$$1/S = 1/KM\Delta_{AD} + 1/\Delta_{AD} \qquad (6.22)$$

The attraction of this, is that K, and Δ_{AD}, could be determined over a range of M for which the stoicheiometry could be established. Consequently, it is important to note that equations (6.21) and (6.22) only apply when

$$c_{AD}^2/M^2(1-x) << x \qquad (6.23)$$

Some of the experimental data presented later suggest that the left hand side of equation (6.23) need only be less than 0.1x for linear plots to be observed. However, it is probably wise to cautiously equate the limiting value to 0.05x. Table 6.1 contains upper limits to M for selected values of K (obtained by numerical analysis) for which the plots of Δ_{obs} vs x will be linear over the complete range of x.

For complexes other than 1:1, Δ_{obs} will depend on higher powers of x than 1 and the relevant plots will be curved.

In order to evaluate the above proposals the well-studied [122,128] system of fluoranil-hexamethylbenzene (for which a classical Job plot is shown earlier [122]) and that of acetonitrile-benzene [129] were studied.

TABLE 6.1

Values of M for selected values of K for equations 6.21 and 6.22 to apply.

Upper value of K/dm^3mol^{-1}	Upper limit to $M/moldm^{-3}$
0.1	6
0.3	2
0.4	0.1
5	0.1
10	0.06
70	0.01

6.3 EXPERIMENTAL

The materials used were ANALAR grade or better. In the case of both systems, stock solutions of the compounds corresponding to A (hexamethylbenzene and acetonitrile) and D (fluoranil and benzene) were prepared gravimetrically to the same molarity. Initially, a molarity of 0.02 was chosen for fluoranil-hexamethylbenzene in carbon tetrachloride and for acetonitrile-benzene in carbon tetrachloride. Because the induced shifts for this initial study of acetonitrile-benzene were found to be less than 1Hz the system was subsequently studied at 0.1M and at higher concentrations in carbon tetrachloride. For each system, mixtures corresponding to a range of values of x were made to a fixed volume of $6.5 \times 10^{-3} dm^3$. At each value of x two samples were prepared, one to yield $_{obs}$ and the other $_{free}$. The solutions were transferred using hypodermic syringes and injected via suba seals into the mixing vessels. The mixtures were sealed into 5mm O.D. N.M.R. sample tubes. The ^{19}F chemical shifts of fluoranil were measured at 84.34MHz and the ^{1}H chemical shifts of acetonitrile were measured at 89.56MHz using a field/frequency locked JEOL FX90Q pulsed FT N.M.R. spectrometer operating at $25^{o}C$ (described in section 5.2). Before investigation the samples were stored in a thermostatted bath, at the N.M.R. probe temperature, for at least one hour.

6.4 RESULTS AND DISCUSSION

Tables 6.2 - 6.11 give all the data relating to the derivation of parameters suitable for evaluation by the N.M.R. analogue of the Job Method.

Tables 6.2 - 6.11 Data relating to derivation of parameters suitable for evaluation by the N.M.R analogue of the Job method. The chemical shifts correspond to those of ^{19}F of fluoranil and ^{1}H of acetonitrile measured at 84.34 MHz and 89.56MHz respectively.

Table 6.2 Data for fluoranil (F)/hexamethyl-benzene in CCl_4 at 0.02M (- 25°C)

	Chemical shifts (Hz)		
x^F	δ_{obs}	δ_{free}	Δ_{obs}
0.85	189.45	172.85	16.60
0.77	196.29	173.83	22.46
0.69	202.15	171.88	30.27
0.62	212.89	174.80	38.09
0.50	219.73	172.85	46.88
0.46	227.54	169.92	57.62
0.38	234.38	172.85	61.53
0.31	240.23	170.90	69.33
0.23	250.00	173.83	76.17
0.15	254.88	169.92	84.96

Table 6.3 Data for acetonitrile (A)/benzene (B) in CCl_4 (C) at 0.1M (~ 25°C)

x^B	Chemical shifts (Hz) δ_{obs}	δ_{free}	Δ_{obs}
0.85	336.91	334.47	2.44
0.77	336.79	334.47	2.32
0.69	336.47	334.47	2.00
0.62	336.42	334.47	1.95
0.54	336.06	334.47	1.59
0.50	335.87	334.47	1.40
0.31	335.45	334.47	0.98
0.23	334.96	334.47	0.49
0.15	334.84	334.47	0.37
0.08	334.47	334.20	0.27

Table 6.4 Data for acetonitrile (A) /benzene (B) in CCl_4 (C) at 0.4M(-25°C)

x^B	Chemical shifts (Hz)					Volume fractions		
	δ_{obs}	δ_{obs}^{corr}	δ_{free}	δ_{free}^{corr}	Δ_{obs}^{corr}	V_A	V_B	V_C
0.85	52.86	181.09	43.9453	172.53	8.56	0.0032	0.0303	0.9670
0.77	51.15	179.31	43.3349	171.87	7.44	0.0048	0.0275	0.9677
0.69	50.17	178.32	43.3349	171.82	6.50	0.0064	0.0248	0.9688
0.62	49.44	177.58	43.3349	171.79	5.79	0.0080	0.0220	0.9700
0.54	48.83	176.96	43.4570	171.85	5.11	0.0097	0.0193	0.9710
0.46	48.71	176.83	44.1894	172.54	4.29	0.0112	0.0165	0.9723
0.38	47.24	175.36	43.4570	171.76	3.60	0.0128	0.0138	0.9736
0.31	46.51	174.60	43.5791	171.82	2.78	0.0148	0.0110	0.9742
0.23	46.02	174.11	43.5791	171.78	2.33	0.0164	0.0083	0.9754
0.15	45.77	173.85	44.1894	172.34	1.51	0.0180	0.0055	0.9757

$$\delta_{obs}^{corr} = \delta_{obs} + (2\pi/3((V_A \times 0.531) + (V_B \times 0.613) + (V_C \times 0.686))) \times \text{Obs. Freq. (MHz)}$$

$$\delta_{free}^{corr} = \delta_{free} + (2\pi/3 ((V_A \times 0.531) + (1-V_A) \times 0.686)) \times \text{Obs. Freq. (MHz)}$$

Table 6.5 Data for acetonitrile (A) /benzene (B) in CCl_4(C) at 1M (~ 25°C)

x^B	Chemical shifts (Hz)					Volume fractions		
	δ_{obs}	δ_{obs}^{corr}	δ_{free}	δ_{free}^{corr}	Δ_{obs}^{corr}	V_A	V_B	V_C
0.85	65.30	192.72	44.07	172.51	20.21	0.008	0.075	0.917
0.77	62.86	190.23	44.07	172.27	17.96	0.012	0.070	0.918
0.69	60.55	187.94	43.95	172.16	15.96	0.016	0.060	0.924
0.62	58.22	185.57	43.82	171.98	13.59	0.020	0.055	0.925
0.46	54.20	181.49	43.95	171.81	9.68	0.028	0.042	0.930
0.38	52.62	179.89	43.95	171.69	8.20	0.032	0.035	0.933
0.31	50.54	177.76	43.96	171.55	6.21	0.037	0.028	0.935
0.23	48.83	176.03	43.95	171.43	4.60	0.041	0.021	0.938
0.15	47.36	174.53	44.31	171.68	2.85	0.045	0.015	0.940
0.08	45.66	172.64	44.31	171.39	1.25	0.055	0.007	0.938

$$\delta_{obs}^{corr} = \delta_{obs} + (2\pi/3((V_A \times 0.531) + (V_B \times 0.613) + (V_C \times 0.686))) \times \text{Obs. Freq. (MHz)}$$

$$\delta_{free}^{corr} = \delta_{free} + (2\pi/3 ((V_A \times 0.531) + (1-V_A) \times 0.686)) \times \text{Obs. Freq. (MHz)}$$

Table 6.6 Data for acetonitrile (A) /benzene (B) in CCl_4 (C) at 1.6M (~ 25°C)

x^B	Chemical shifts (Hz)					Volume fractions		
	δ_{obs}	δ_{obs}^{corr}	δ_{free}	δ_{free}^{corr}	Δ_{obs}^{corr}	V_A	V_B	V_C
0.85	74.82	201.48	44.07	172.37	29.11	0.013	0.120	0.867
0.77	70.80	197.38	43.82	171.94	25.44	0.019	0.112	0.864
0.69	67.01	193.63	43.82	171.55	21.88	0.026	0.096	0.878
0.63	63.96	190.51	43.70	171.45	19.06	0.032	0.088	0.880
0.54	61.15	182.64	43.95	171.49	16.32	0.032	0.077	0.884
0.46	58.40	184.87	43.95	171.32	13.55	0.045	0.066	0.889
0.38	55.85	182.28	44.19	171.38	10.90	0.051	0.055	0.894
0.31	53.28	179.64	43.99	170.90	8.74	0.059	0.044	0.897
0.23	51.21	177.53	44.62	171.44	6.09	0.066	0.033	0.902
0.15	49.32	175.58	44.80	171.23	4.23	0.072	0.023	0.905

$$\delta_{obs}^{corr} = \delta_{obs} + (2\pi/3((V_A \times 0.531) + (V_B \times 0.613) + (V_C \times 0.686))) \times \text{Obs. Freq. (MHz)}$$

$$\delta_{free}^{corr} = \delta_{free} + (2\pi/3((V_A \times 0.531) + (1-V_A) \times 0.686)) \times \text{Obs. Freq. (MHz)}$$

Table 6.7 Data for acetonitrile (A) /benzene (B) in CCl_4 (C) at 2M (- 25°C)

x^B	Chemical shifts (Hz)					Volume fractions		
	δ_{obs}	δ_{obs}^{corr}	δ_{free}	δ_{free}^{corr}	Δ_{obs}^{corr}	V_A	V_B	V_C
0.85	79.68	205.87	44.07	172.28	33.59	0.016	0.150	0.834
0.77	74.56	200.64	43.82	171.83	28.81	0.024	0.140	0.838
0.69	71.29	197.39	44.07	171.86	25.53	0.032	0.120	0.848
0.62	67.38	193.39	44.07	171.64	21.75	0.040	0.110	0.850
0.46	62.46	188.29	44.37	171.50	16.79	0.056	0.083	0.861
0.38	59.03	184.83	44.43	171.34	13.49	0.064	0.069	0.867
0.31	55.05	180.85	44.80	171.86	9.49	0.073	0.550	0.613
0.23	52.26	178.01	45.04	171.37	6.64	0.081	0.041	0.878
0.15	50.30	176.00	45.41	171.52	4.48	0.089	0.028	0.883
0.08	48.09	173.52	45.65	171.32	2.20	0.105	0.014	0.881

$$\delta_{obs}^{corr} = \delta_{obs} + (2\pi/3((V_A \times 0.531) + (V_B \times 0.613) + (V_C \times 0.686))) \times \text{Obs. Freq. (MHz)}$$

$$\delta_{free}^{corr} = \delta_{free} + (2\pi/3 ((V_A \times 0.531) + (1-V_A) \times 0.686)) \times \text{Obs. Freq. (MHz)}$$

Table 6.8 Data for acetonitrile (A) /benzene (B) in CCl_4 (C) at 1M (25°C)

x^B	δ_{obs}	δ^{corr}_{obs}	δ_{free}	δ^{corr}_{free}	Δ^{corr}_{obs}	Volume fractions V_A	V_B	V_C
0.85	65.30	192.72	44.07	172.51	20.21	0.008	0.075	0.917
0.77	62.86	190.23	44.07	172.27	17.96	0.012	0.070	0.918
0.69	60.55	187.94	43.95	172.16	15.96	0.016	0.060	0.924
0.62	58.22	185.57	43.82	171.98	13.59	0.020	0.055	0.925
0.46	54.20	181.49	43.95	171.81	9.68	0.028	0.042	0.930
0.38	52.62	179.89	43.95	171.69	8.20	0.032	0.035	0.933
0.31	50.54	177.76	43.96	171.55	6.21	0.037	0.028	0.935
0.23	48.83	176.03	43.95	171.43	4.60	0.041	0.021	0.938
0.15	47.36	174.53	44.31	171.68	2.85	0.045	0.015	0.940
0.08	45.66	172.64	44.31	171.39	1.25	0.055	0.007	0.938

$$\delta^{corr}_{obs} = \delta_{obs} + (2\pi/3((V_A \times 0.531) + (V_B \times 0.613) + (V_C \times 0.686))) \times \text{Obs. Freq. (MHz)}$$

$$\delta^{corr}_{free} = \delta_{free} + (2\pi/3((V_A \times 0.531) + (1-V_A) \times 0.686)) \times \text{Obs. Freq. (MHz)}$$

Table 6.9 Data for acetonitrile (A) /benzene (B) in CCl_4 (C) at 11M (- 25°C)

x^B	Chemical shifts (Hz)					Volume fractions		
	δ_{obs}	δ^{corr}_{obs}	δ_{free}	δ^{corr}_{free}	Δ^{corr}_{obs}	V_A	V_B	V_C
0.85	180.54	295.24	45.90	171.99	123.25	0.089	0.832	0.079
0.77	162.72	277.19	47.36	172.20	104.99	0.132	0.757	0.111
0.69	148.08	262.31	48.71	172.26	90.05	0.176	0.681	0.143
0.62	134.28	248.27	50.29	172.57	75.70	0.220	0.605	0.175
0.54	123.29	236.92	51.51	172.40	64.52	0.268	0.530	0.202
0.46	112.42	225.93	53.22	172.94	52.99	0.308	0.454	0.238
0.38	103.02	216.29	54.44	172.89	43.40	0.352	0.378	0.270
0.31	94.00	206.69	55.91	172.75	33.94	0.407	0.303	0.290
0.23	84.72	197.17	57.37	172.94	24.23	0.451	0.227	0.322
0.15	76.66	188.88	58.96	173.24	15.64	0.495	0.151	0.354

$$\delta^{corr}_{obs} = \delta_{obs} + (2\pi/3((V_A \times 0.531) + (V_B \times 0.613) + (V_C \times 0.686))) \times \text{Obs. Freq. (MHz)}$$

$$\delta^{corr}_{free} = \delta_{free} + (2\pi/3 ((V_A \times 0.531) + (1-V_A) \times 0.686)) \times \text{Obs. Freq. (MHz)}$$

Table 6.10 Data for acetonitrile (A) /benzene (B) in CCl_4(C) at 11M (3°C)

x^B	δ_{obs}	δ^{corr}_{obs}	δ_{free}	δ^{corr}_{free}	Δ^{corr}_{obs}	Volume fractions V_A	V_B	V_C
0.85	199.95	318.63	58.59	188.63	130.00	0.086	0.808	0.106
0.77	181.03	299.44	59.69	188.42	111.02	0.130	0.734	0.136
0.69	165.16	283.33	61.16	188.62	94.71	0.173	0.660	0.167
0.62	150.64	168.55	62.62	188.79	79.76	0.216	0.587	0.197
0.54	139.72	256.82	63.96	188.89	67.93	0.259	0.514	0.227
0.46	127.80	245.18	65.55	189.09	56.09	0.303	0.441	0.256
0.38	118.52	235.66	68.12	190.40	45.26	0.346	0.367	0.287
0.31	108.64	255.52	68.60	189.63	35.89	0.389	0.294	0.317
0.23	98.52	215.15	70.07	189.84	25.31	0.432	0.220	0.348
0.15	90.21	206.56	71.65	190.02	16.54	0.476	0.147	0.377

$$\delta^{corr}_{obs} = \delta_{obs} + (2\pi/3((V_A \times 0.548) + (V_B \times 0.632) + (V_C \times 0.707))) \times \text{Obs. Freq. (MHz)}$$

$$\delta^{corr}_{free} = \delta_{free} + (2\pi/3 ((V_A \times 0.548) + (1-V_A) \times 0.707)) \times \text{Obs. Freq. (MHz)}$$

Table 6.11 The densities (ρ) [130] and volume magnetic susceptibilities [131] (χ_v) of acetonitrile, benzene and carbon tetrachloride at temperatures (T) relating to the use of the N.M.R. analogues of the Job method.

Substance	T(°C)	$10^{-3}\rho/kgm^{-3}$	$-10^{6}\chi_v$
Acetonitrile	23.4	0.77840	0.531
Benzene	23.4	0.87366	0.613
Carbon Tetrachloride	25.0	1.58430	0.686
Acetonitrile	0.0	0.80350	0.548
Benzene	0.0	0.89996	0.632
Carbon Tetrachloride	0.0	1.63274	0.707

6.4.1 FLUORANIL-HEXAMETHYLBENZENE

Fig. 6.2 presents the plot of the fluoranil ^{19}F shifts, Δ_{obs}, versus x. The individual shifts were not internally referenced and derive from directly measured resonance frequencies that were not corrected for volume magnetic susceptibility because of the low value of M. The most striking feature of the plot is that the best fit line appears to be linear. As indicated earlier this in itself suggests that only a 1:1 complex is formed. The slope, S, of the line corresponds to equation (6.14), and using this together with the appropriate intercept, I, enables the value of x corresponding to equation (6.7) to be deduced from

$$x = I/2S \qquad (6.24)$$

This yields x = 0.5 which corresponds precisely with the value of n = 1 obtained by the spectrophotometric application of Job's method [122] (see Fig. 6.1). It should be noted that if the shifts of A are studied x should be obtained from

$$x = (S - I)/2S \qquad (6.25)$$

6.4.2 ACETONITRILE-BENZENE

Initially, this system was studied at 0.02M in carbon-tetrachloride but no significant variation in the induced ^{1}H shifts of acetonitrile could be detected. The system was then investigated at 0.02M in perdeuterocyclohexane. The deuterated

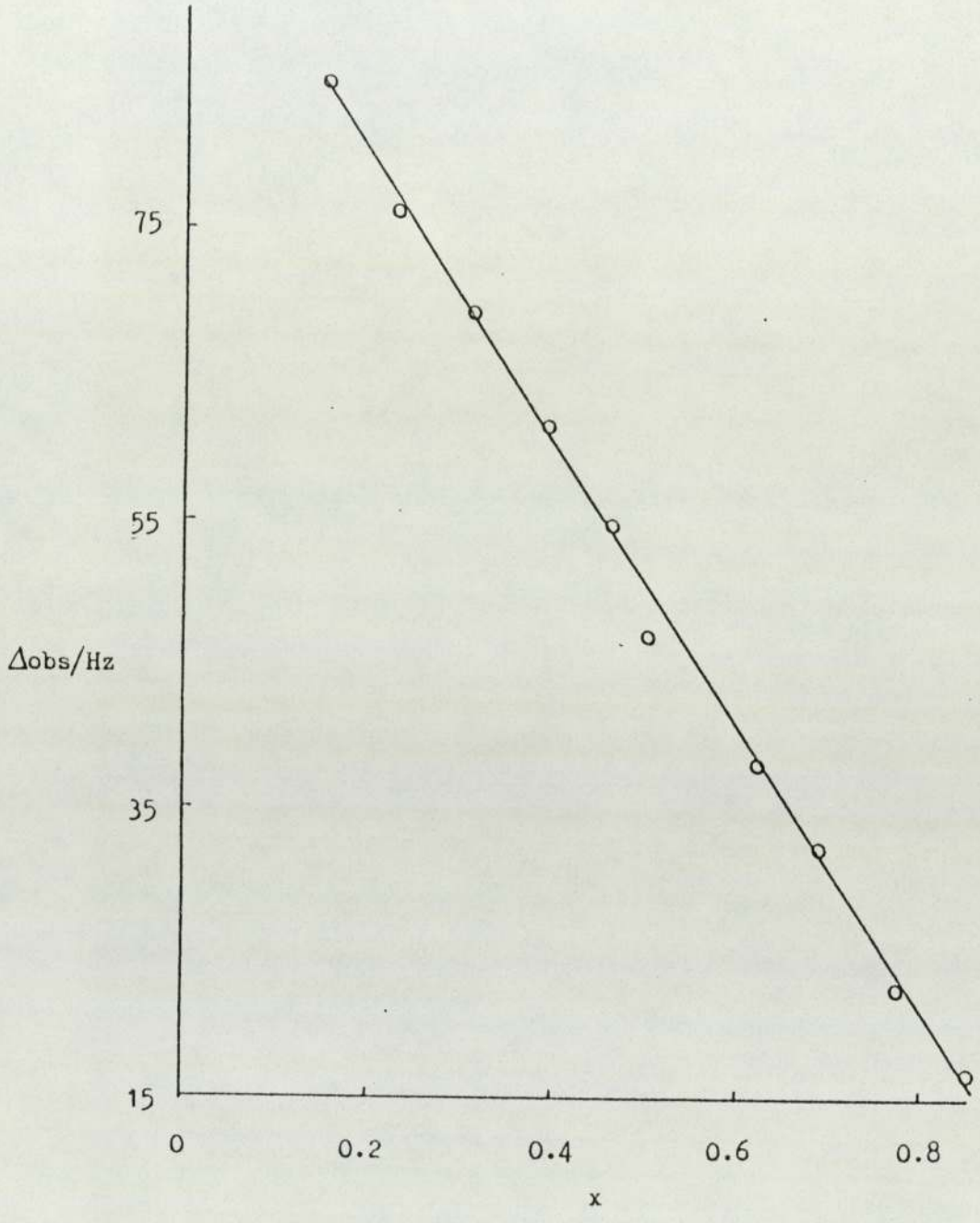

Fig. 6.2 N.M.R. Job plot for fluoranil/hexamethyl benzene in CCl_4 at .02M (~25°C)

(The line of best fit obtained by least squares computer analysis is given by $\Delta_{obs} = 99.6160 + (-99.2439x)$)

compound was used in order to avoid potential problems arising from the overlap of proton resonances of the protonated analogue with that of acetonitrile. In this case small, but significant, induced shifts were observed and their variation with x appeared to be linear and this indicates that a complex of 1:1 stoicheiometry is formed. However, because, as mentioned earlier, the induced shifts are so small the above conclusion could be open to question. Consequently, the system was re-investigated at 0.1M in carbon-tetrachloride (the directly measured resonance frequencies were not corrected for volume magnetic susceptibility because of the low value of M). The relevant plot is shown in fig. 6.3 which again indicates the formation of a 1:1 complex. This is particularly surprising because Polanun [129] has shown by very careful cryoscopic experiments that a 1:2 complex is formed. This leads to speculation on the suggestions made earlier that the choice of M may influence the origin of the induced shifts and that at low values of M only a 1:1 complex may be detected. Bearing these points in mind the acetonitrile-benzene system was reinvestigated at values of M up to 11 in carbon-tetrachloride: The shifts in each case were measured absolutely and corrected for volume magnetic susceptibility on a volume fraction basis. The values of χ_v were deduced from the density and specific susceptibilities given in references 130 and 131 respectively (see table 6.11). The data are presented graphically in fig. 6.4. The plots in each case are non-linear and this suggests that a 1:1 complex is not present alone.

It can be seen from fig. 6.4 that the curvature of the plots increases with M. Each set of data was fitted to the polynomial of the lowest degree that yielded the most satisfactory intercept on the

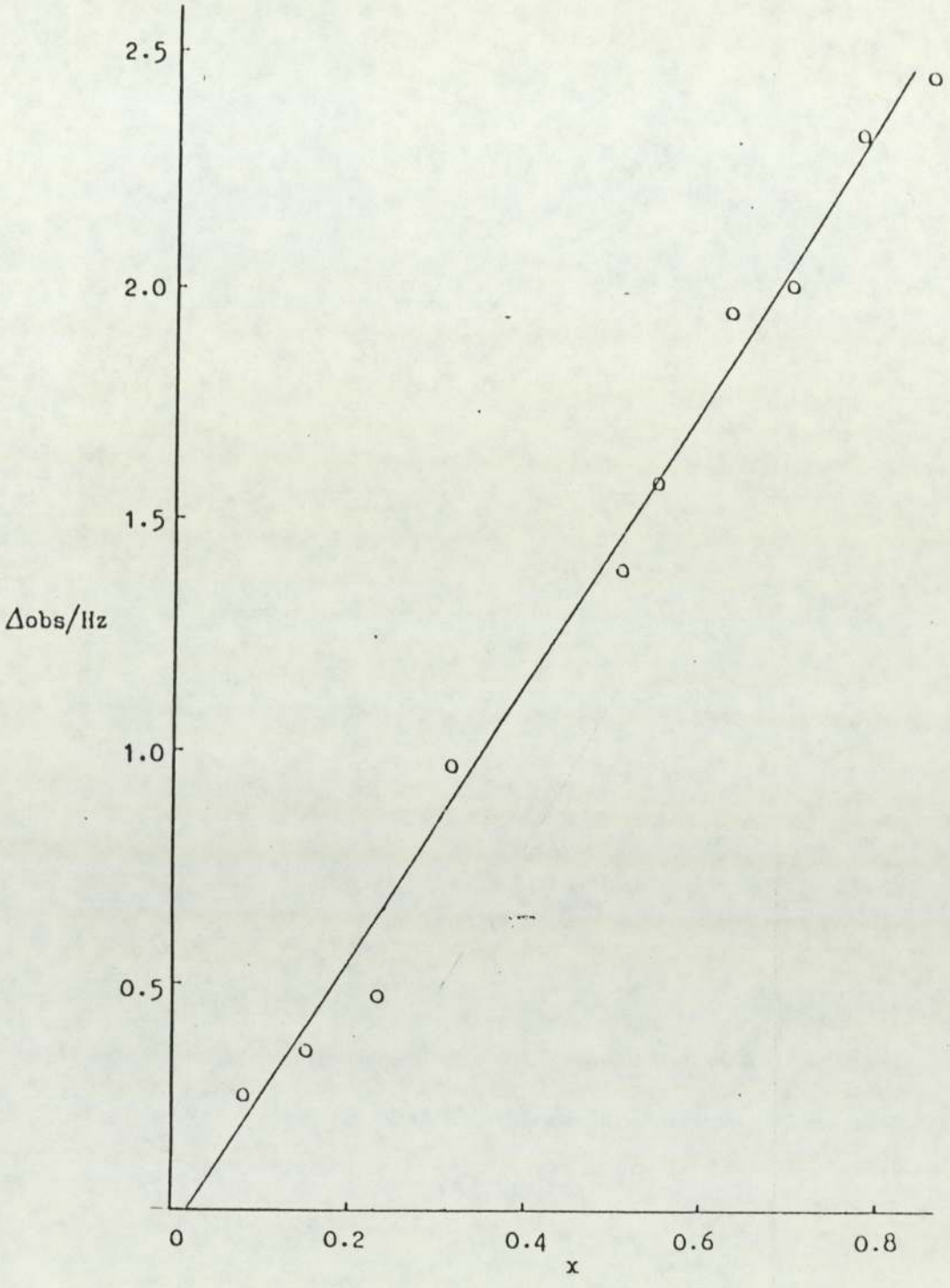

Fig.6.3 N.M.R. Job plot for acetonitrile/benzene in CCl_4 at 0.1M (- 25°C)

(The line of best fit obtained by least squares computer analysis is given by $\Delta_{obs} = -0.0461 + 3.0150x$)

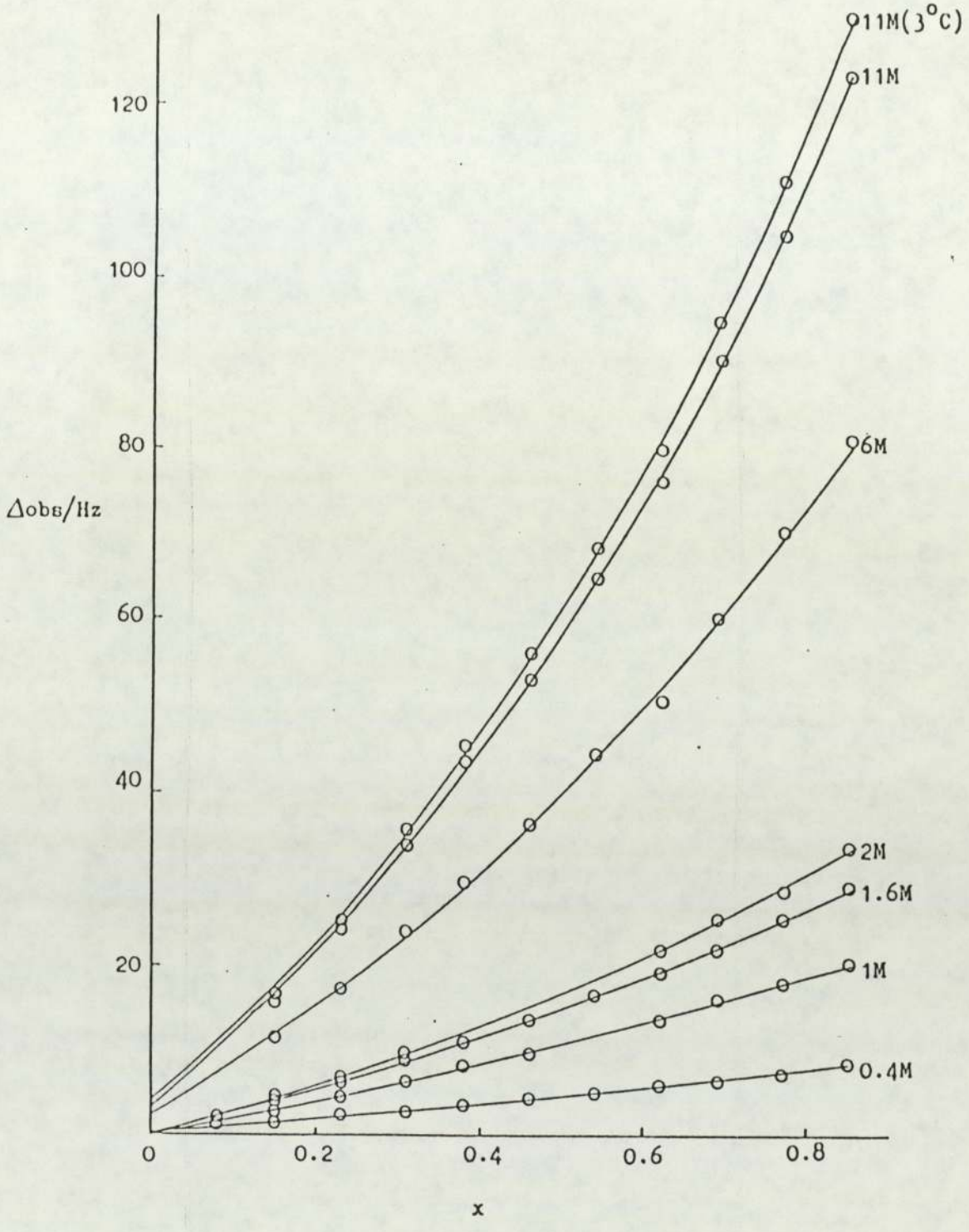

Fig. 6.4 N.M.R. Job-plots for acetonitrile/benzene in CCl_4 for different initial molarities (- 25°C)

Δ_{obs} axis. In all cases polynomials of degree 2 and higher superficially gave satisfactory numerical least squares fits to the data. However, for polynomials of degree 3 and above, a visual inspection of the iterated least squares best fit line to the data, showed that this had been achieved while not following the regular variation in the data and gave a negative intercept. In the case of a polynomial of degree 2 the iterated best fit line followed the regular variation in the data and gave an undistorted intercept on the Δ_{obs} axis (see table 6.12 for the equations that describe each of the graphical lines).

It has been mentioned above that the intercept was not always zero. This could be due either to residual solvent effects or to the fact that two or more complexes co-exist. The polynomial equations were subject to further computer analyses to establish the values of x at which condition (6.13) applies. The values of x so found lie in the range 0.51 to 0.59. From the earlier discussion of the effect of the presence of two complexes on the value of x deduced from condition (6.13) it would appear that both 1:1 and 1:2 complexes co-exist in the acetonitrile-benzene systems studied here. This conclusion was confirmed in the following manner:-

At very small values of x the probability of 1:2 complexes contributing to the measured values of Δ_{obs} must be small. Consequently, the initial slopes of the Δ_{obs} vs x plots may be taken to reflect the contribution to Δ_{obs} of the dominant 1:1 complex in the presence of the smaller amount of 1:2 complex. The linear equations corresponding to the initial slopes can be used to correct the experimental values of Δ_{obs} and produce plots of Δ_{obs}, now labelled Y, vs x that reflect the effect of the second complex alone over the

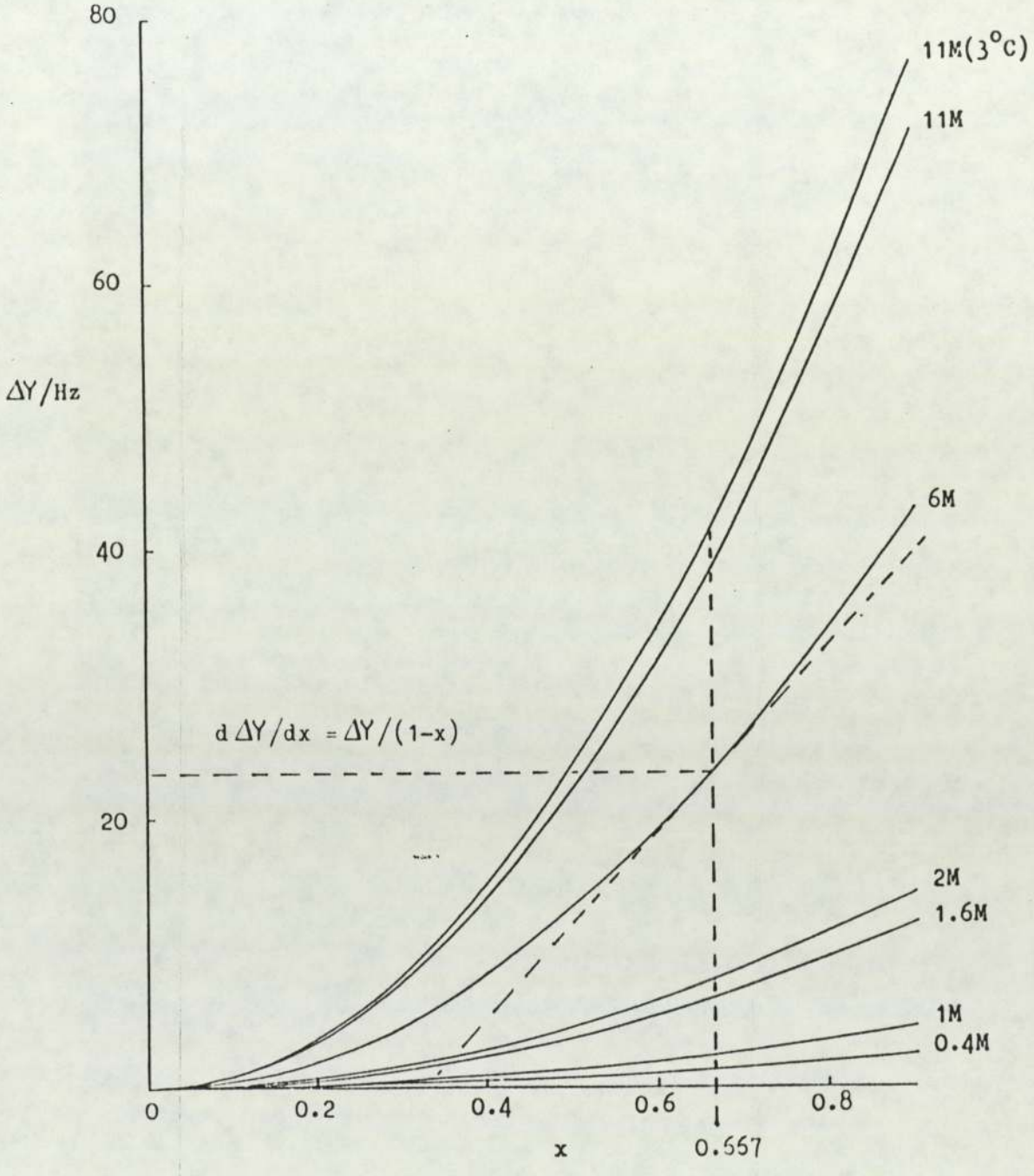

Fig. 6.5 N.M.R. Job plots for acetonitrile/benzene systems: ΔY represents the difference between the experimental induced shifts (Hz) and the shifts corresponding to 1:1 complex formation only ($-25^{\circ}C$)

complete range of x. The relevant data are shown in fig.6.5. Iterative computer analyses of each plot to establish when $dY/dx = Y/(1 - x)$ revealed that in each case this occurred at $x = 0.667$. Because ${}^{C}AD_{n}$ in equation (6.20) has been effectively set equal to zero it follows that $n+q = 2$ and a 1:2 complex was detected. This is consistent with the finding of Polanun [129] who presumably only identified a complex of this stoicheiometry because his cryoscopic studies were on binary mixtures of the interacting species at effectively high concentration and low temperature when the 1:2 complex would dominate the 1:1. In order to investigate qualitatively the effect of temperature on the relative amounts of 1:1 and 1:2 complexes the 11M system was studied at $3^{o}C$. The results are shown in fig. 6.4 and 6.5. From the former the higher value of x at which condition (6.13) is found and from the latter the increased curvature both indicate that a reduction in temperature favours the formation of the 1:2 over the 1:1 complex.

The overall consistency of the immediately foregoing treatment of the experimental data appear to justify the underlying assumptions. It follows that the initial slopes of the plots in fig. 6.4 should be amenable to evaluation using equation (6.22) - (see table 6.13). Figure 6.6 shows the appropriate plot from which a value of $K_{1:1} = 0.245\ dm^{3}mol^{-1}$ may be obtained. Although there is no reference value for comparison it is worth noting that concurrent investigations [132] on quite different systems show that equation (6.22) and a conventional Benesi-Hildebrand [102] study yield almost identical values for $K_{1:1}$.

Table 6.12 Coefficients (a, b and c) of best fit quadratic equations ($\Delta_{obs} = a + bx + cx^2$) that give the relationship between Δ_{obs} and x at a temperature of ~25°C (unless indicated otherwise) for acetonitrile/benzene systems in CCl_4 for different initial molarities, M.

Molarity (M)	a*	b	c
0.4	0.5152	6.6912	3.1060
1.0	0.2292	19.3435	5.5292
1.6	0.7542	20.8373	14.5549
2.0	0.3137	23.8267	17.7676
6.0	4.3457	44.6742	52.7953
11.0	5.3544	62.1465	88.2915
11.0(~3°C)	5.7371 (~3°C)	64.4960 (~3°C)	94.3770 (~3°C)

* a ----Hz

Table 6.13 Various values of $^{1}/_{M}$ and $^{1}/_{slope}$ to evaluate K(~25°C) according to equation (6.22).

M(moldm^{-3})	slope	$^{1}/_{M}$ (dm^{3}mol^{-1})	$^{1}/_{slope}$
0.4	6.6912	2.500	0.1495
1.0	19.3535	1.000	0.0517
1.6	20.2953	0.625	0.0493
2.0	23.8267	0.500	0.0420
6.0	44.6742	0.167	0.0224
11.0	62.1465	0.091	0.0161

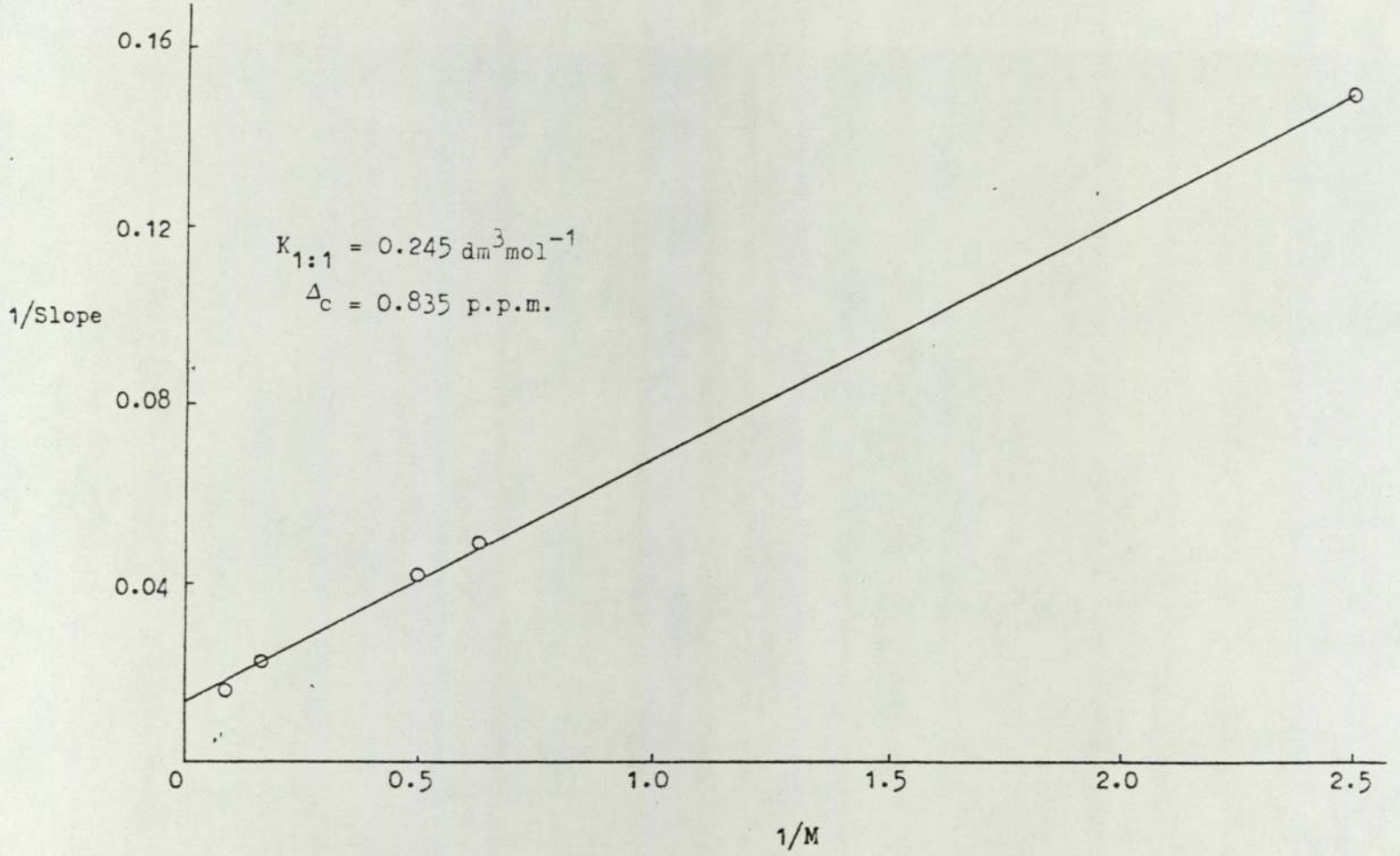

Fig. 6.6 Inverse dependence of initial (x=0) slope of Job plot with molarity for the acetonitrile/benzene system in CCl_4 (-25°C)

6.5 CONCLUSION

Although the limitations of the proposals presented here need to be evaluated fully, it does appear from preliminary investigations that the N.M.R. analogue of the Job or continuous variation method affords a sensitive method of determining the stoicheiometries of complexes formed in solution. Of particular interest is the fact that it is possible to comment on whether one or more complexes are present and in the specific case of the co-existence of 1:1 and 1:2 complexes it is possible to identify both. When 1:1 complexes can be identified it is possible to determine the equilibrium constants for their formation from the same experiments that confirm their existence. The method has a significant advantage over its spectrophotometric analogue in that it does not require the complexes formed to show a charge-transfer band or in a wider sense be "coloured". In the context of experimentation with systems containing complexes formed between water and a Whitten-type surfactant, the problems presented by having a wide ultra-violet/visible absorption spectrum (see fig 2.17) for the surfactant would seem in principle to be overcome by using the N.M.R. approach.

Whilst the intention was to apply the new method to systems containing a Whitten-type surfactant derivative of $Ru(bipy)_3^{2+}$ and water, a shortage of time precluded this. Nevertheless, such a study would undoubtedly throw valuable light on the earlier N.M.R. deductions made concerning this system.

GENERAL CONCLUSION

At the beginning of this study Whitten et al [16] had reported the photochemical cleavage of water to form dihydrogen and dioxygen using the dioctadecyl ester of (4,4'-dicarboxy-2,2'-bipyridine)bis (2,2'bipyridine)ruthenium(II)$^{2+}$ as a catalyst in monolayer assemblies. Attempts by Whitten [17] to repeat those initial findings proved unsuccessful. Whitten's failure [17] prompted a surge of research interest to either investigate or repeat Whitten's initial findings, mainly because of the commercial prospects of producing an alternative fuel to the dwindling resources of the widely used fossilised fuels. As a consequence, much concentrated research into the cleavage experiments was carried out in which the Whitten-type surfactant was investigated in various physical states. This project has been directed to studying factors affecting the behaviour of Whitten-type surfactants in those states:-

Film thickness measurements of Whitten-type surfactants indicate that the irreproducible behaviour of monolayers of such surfactants in the photosensitized cleavage of water, might be explained by unusual heterogeneous monomolecular layering. It would seem that this affect is largely due to the inconsistent chemical behaviour of the subphase supporting the monolayer prior to deposition on a slide. For example, quite often it has been found that the first use of the subphase results in the formation of a multi-layer, whereas second use of the same subphase results in the formation of a monolayer. i.e. in each case the film: slide deposition ratios are approximately 1:1.

Particle size distribution studies of the type of dispersions designed by Cooke [36] and used with partial success by him to mimic the monolayer (by using a solid hydrocarbon to support the Whitten-type surfactant) suggest that whilst particles are usually distributed about the 2μ size it is possible under certain conditions to produce irregular shaped particles. The possibility of forming irregular shaped particles could enable some favoured orientation of the surfactant on the solid support to be achieved. Such a hypothesis might explain the irreproducibility of Cookes photolysis experiments using dispersions.

N.M.R. solution studies have revealed the formation of transient collision complexes between a surfactant derivative of $Ru(bipy)_3^{2+}$ and water; the formation of the complexes being energetically favoured with the corresponding overall equilibrium constant being very high ($\Sigma K_x = 1.71 \times 10^4$). The initial proposal was that the stoicheiometry of the complex so formed was either 6:1 or 5:1 for water: surfactant and from data obtained on the fully induced chemical shift of the complex it was likely that the water molecules were sited at or near the 'six fold' axis of each ring of the bipyridine unit. However, subsequent N.M.R. temperature studies of the complex system have indicated that the measured equilibrium constant is in fact an overall equilibrium constant made up of stepwise equilibrium constants corresponding to the formation of different types of transiently formed collision complex.

An N.M.R. analogue of the Job method for measuring complex stoicheiometries has been developed and would appear to offer a solution to determining the stoicheiometries of different complexes formed between water and the surfactant derivative of $Ru(bipy)_3^{2+}$ in the same solution.

Although, the findings in this thesis are important to the development of further photochemical systems containing water and the surfactant derivative of $Ru(bipy)_3^{2+}$ as monolayer, dispersion or in solution, it appears that the techniques developed could be used beneficially at every stage of photolysis experiments in order to monitor the nature of the participating species.

For instance, monolayer thicknesses should be measured before and after photolysis, and in this way the most favoured orientation of the monolayer that enables cleavage of water could be found. Similarly, particle size distribution studies of the Cooke-type dispersions should be carried out before and after photolysis; although this should be coupled with some sort of microscopy experiment as particle shape is a likely factor in the success of Cooke-type dispersions to cleave water.

Quite clearly the N.M.R. analogue of the Job method for determining complex stoicheiometry has wider applications than its restricted use for systems containing complexes formed between water and the surfactant derivative of $Ru(bipy)_3^{2+}$. However, the applications of the Job analogue to such systems are wide and numerous, as for example different derivatives could be studied at different concentrations and temperatures.

LITERATURE CITED

1. G. Porter, "Light Chemical Change and Life": A Source Book in Photochemistry, The Open University Press, 1982, P3.

2. V. Balzani, L. Moggi, M. F. Manfrin, F. Bolletta and M. Gleria, Science, 1975, 189, 852.

3. J. N. Demas and A. W. Adamson, J. Amer. Chem. Soc., 1971, 93, 1800.

4. H. Gafney and A. W. Adamson, J. Amer. Chem. Soc., 1972, 94, 8238.

5. J. N. Demas and A. W. Adamson, J. Amer. Chem. Soc., 1973, 95, 5159.

6. P. Natarajan and J. F. Endicott, J. Phys. Chem., 1973, 77, 1823.

7. C. R. Bock, T. J. Meyer and D. G. Whitten, J. Amer. Chem. Soc., 1974, 96, 4710.

8. G. Navon and N. Sutin, Inorg. Chem., 1974, 13, 2159.

9. G. S. Lawrence and V. Balzani, Inorg. Chem., 1974, 13, 2976.

10. C. Creutz and N. Sutin, Proc. Natl. Acad. Sci. U.S.A., 1975, 72, 2858.

11. C. T. Lin, W. Bottcher, M. Chou, C. Creutz and N. Sutin, J. Amer. Chem. Soc., 1976, 98, 6536.

12. N. Sutin and C. Creutz, Adv. Chem. Ser., 1978, 168, 1.

13. C. Creutz and N. Sutin, Inorg. Chem., 1976, 15, 496.

14. T. Saji and S. Aoyagui, J. Electroanal. Chem., 1975, 58, 401

15. C. R. Bock, T. J. Meyer and D. G. Whitten, J. Am. Chem. Soc., 1975, 97, 2909.

16. G. Sprintschnik, H. W. Sprintschnik, P. P. Kirsch and D. G. Whitten, J. Amer. Chem. Soc., 1976, 98, 2337.

17. G. Sprintschnik, H. W. Sprintschnik, P. P. Kirsch and D. G. Whitten, J. Amer. Soc., 1977, 99, 4947.

18. G. D. Gaines Jr. and S. J. Valenty, J. Amer. Chem. Soc., 1977, 99, 1285.

19. L. T. Yellowlees, R. G. Dickinson, C.S. Halliday, J. S. Bonham and L.E. Lyons, Aus. J. Chem., 1977, 99, 4947.

20. K. P. Seefeld, D. Mobius and H. Kuhn, Helv. Chim. Acta., 1977, 60, 2608.

21. A. Harrison, J. Chem. Soc., Chem. Comm., 1977, 777.

22. G. L. Gaines, Jr., P. E. Behnken and S. J. Valenty, J. Amer. Chem. Soc., 1978, 100, 6549.

23. M.S. Henry and M.Z. Hoffman, J. Amer. Soc. Comm., 1977, 99, 5201.

24. R. D. Gillard and C. T. Hughes, J. Chem. Soc. Comm., 1977, 27, 776.

25. S. J. Valenty, Analytical Chemistry, 1978, 50, 669.

26. P. J. Delaive, J. T. Lee, H. W. Sprintschnik, H. Abruna, T. J. Meyer, D. G. Whitten, J. Amer. Chem. Soc., 1977, 99, 7094., Adv. Chem. Ser., 1978, 168, 28.

27. P. J. Delaive, G. Giannotti, D.G. Whitten, J. Amer Chem. Soc., 1978, 100, 7413.

28. J. M.Lehn and J. P. Sauvage, Nouv. J. Chim., 1977, 1, 449.

29. M. Kirch, J. M. Lehn and J. P. Sauvage, Helv. Chim. Acta., 1979, 62, 1345.

30. B. V. Koryakin, T.S. Dzhabiev and A. E. Shilov, Doke. Akad. Nauk. S.S.S.R., 1977, 233, 620.

31. J. R. Darwent, "Photogeneration of Hydrogen", Academic Press, 1982, P.23.

32. D. Rehm and A. Weller, Isr. J. Chem., 1970, 8, 259.

33. D. Mobius, J. Amer. Chem. Soc., 1981, 14, 63.

34. D. G. Whitten, Angew. Chem. Ind. Ed. Engl., 1979, 18, 440.

35. M. C. Cooke, J. Homer, A. W. P. Jarvie and J. D. Miller, J. Chem. Soc., Faraday Trans. 1, 1984, 80, 1855.

36. ibid ; 1984, 80, 2715..

37. D. J. Shaw, "Introduction to Colloid and Surface Chemistry", Butterworths, 1975, 2nd edition, P.4.

38. P. A. D.deMaine, J. Chem. Physic, 1957, 26, 1199.

39. R. Foster, "Molecular Complexes", Academic Press, 1969, 2, P.113.

40. H. Kuhn and D. Mobius, Angew. Chem. Int. Ed. Engl., 1971, 10, 620.

41. F. H. Quina and D. G. Whitten, J. Amer. Chem. Soc., 1977, 99, 877.

42. I. Langmuir, J. Amer. Chem. Soc., 1917, 39, 1848.

43. N. K. Adam and G. Jessop, Proc. Roy. Soc. (London), 1926, A110, 423.

44. I. Langmuir, Trans. Faraday Soc., 1920, 15, 62.

45. K. B. Blodgett, J. Amer. Chem. Soc., 1935, 57, 1007.

46. D. G. Shaw, "Introduction to Colloid and Surface Chemistry", Butterworths, 1975, 2nd edition, P.80.

47. C. W. Pitt and L.M. Walpitta, Electrocomponent Science and Technology, 1977, 3, 191.

48. S. Tolanski, "Multiple Beam Interferometry", Oxford Uniy Press, 1948.

49. G. Scott, J. Appl. Phys., 1950, 21, 843.

50. A. Rothen, Rev. Sci. Inst., 1957, 28, 283.

51. K. R. Oshea, Ph.D. Thesis, University of Aston in Birmingham, (1973).

52. A. Rothen, Rev. Sci. Inst., 1945, 16, 26.

53. F. L. McCrackin, E. Passaglia, R. R. Stromberg and H. L. Steinberg, J. Res, Natl. Bur. Stand., 1963, 67A, 363.

54. D. Clarke and J. F. Grainger, "Polarized Light and Optical Measurement", Pergamon Press, 1971, Appendix 1.

55. J. R. Beattie and G. K. T. Conn, Philos. Mag., 1955, 46, 222.

56. G. K. T. Conn and G. K. Eaton, J.Opt. Soc. Am., 1954, 44, 546.

57. P. Drude, Ann. Phys. (Leipzig), 1890, 39, 481.

58. A.D. Cauchy, Compt. Rend., 1848, 26, 88.

59. R. W. Ditchburn, J. Opt. Soc. Am., 1955, 45, 743.

60. W. C. J. Neal, Surface Technology, 1977, 6, 81.

61. M. C. Cooke, Private Communication.

62. G. D. Gaines, Jr., "Insoluble Monolayers at Liquid-Gas Interfaces", Willey Interscience: New York, 1966, P.327.

63. Bikerman, Proc. Roy. Soc. (London), 1939, A170, 130.

64. See, e.g. L. E. Scriven and C. V. Steinling, Nature, 1960, 187, 186.

65. J. H. Schulman, R. B. Waterhouse and J. A. Spink, Kolloid - Z, 1956, 146, 77.

66. R. J. Myers and W. D. Harkins, Nature, 1937, 139, 367.

67. G. L. Gaines, Jr., Insoluble Monolayers at Liquid-Gas Interfaces, Wiley Interscience: New York, 1966, P.34.

68. N. K. Adam, Physics and Chemistry of Surfaces, pp 46ff.

69. J. T. Davies and E. K. Rideal, Can. J. Chem., 1955, 33, 947.

70. M. C. Cooke, Private Communication.

71. E. D. Goddard, O. Kao and H.C. Kung, J. Colloid Interface Sci., 1968, 27, 616.

72. B. D. H. Analar water (pH 5.5 to 7.5).

73. G. Martin, C. E. Blythe and H. Tongue, Trans. Ceram. Soc. (Eng); 1924, 23, 61.

74. L. R. Feret, Assoc. Int. pour l'Essai des Mat.2, group D. Zurich, 1931.

75. H. S. Patterson and W. Cawood, Trans. Faraday. Soc., 1936, 32, 1084.

76. A. D. Randolph and N. A. Larson, "Theory of Particulate Processes", Academic Press, 1971, P.14.

77. J. Homer, J. Magn. Reson., 1983, 54, 1.

78. M. C. Cooke, Private Communication.

79. J. W. Emsley, J. Feeney and L. H. Sutcliffe, "High Resolution N.M.R. Spectroscopy", Pergamon, 1965.

80. A. Saika and C. P. Slichter, J. Chem. Phys., 1954, 22, 26.

81. T. P. Das and R. Bersohn, Phys. Rev., 1956, 104, 476.

82. C. P. Slichter, "Principles of Magnetic Resonance", Harper and Row, N.Y.

83. J. A. Pople, Proc. Roy. Soc., 1957, A239, 541.

84. H. M. McConnell, J. Chem. Phys., 1957, 27, 226.

85. A. D. Buckingham, T. Schaeffer and W. G. Schneider, J. Chem. Phys., 1960, 32, 1227.

86. W. C. Dickinson, Phys. Rev., 1951, 81, 717.

87. D. J. Frost and G. E. Hall, Mol. Phys., 1964, 10, 191.

88. J. Homer, Solvent effects on nuclear magnetic resonance chemical shift, Appl. Spectroscopy Rev., 1975, 9, 1, and references therein.

89. J. Homer, J. Magn. Reson., 1979, 34, 31.

90. A. A. Bothner-By and R. E. Glick, J. Chem. Phys., 1957, 26, 1651.

91. R. J. Abraham, Mol. Phys., 1961, 4, 369.

92. J. K. Becconsall, Mol. Phys., 1970, 18, 337.

93. F. H. A. Rummens, J. Amer. Chem. Soc., 1970, 92, 3214

94. J. K. Becconsall, Mol. Phy., 1968, 15, 129.

95. J. Homer and D. L. Redhead, J. Chem. Soc., Faraday II, 1972, 68, 1049.

96. A. A. Bothner-By, J. Mol. Spect., 1960, 5, 52.

97. B. B. Howard, B. Linder and M. T. Emerson, J. Chem. Phys., 1962, 36, 485.

98. L. Onsager, J. Amer. Soc., 1936, 58, 1486.

99. A. D. Buckingham, Can. J. Chem., 1960, 38, 300.

100. P. Diehl and R. Freeman, Mol. Phys., 1961, 4, 39.

101. C. G. Cresswell and A.L. Allred. J. Phys. Chem; 1962, 66, 1469

102. H. A. Benesi and J. H. Hildebrand, J. Am. Soc., 1949, 71, 2703.

103. J. Tyrell, Canad. J. Chem., 1965, 43, 783.

104. R. Foster and D. R. Twiselton, Rec. Trav. Chim., 1970, 89, 325.

105. C. E. Johnson and R. A. Bovey, J. Chem. Phys., 1958, 29, 1012.

106. G. Luton, B.Sc. Project Report, University of Aston in Birmingham, 1977.

107. A. I. Vogel, "A Textbook of Practical Organic Chemistry", Longmans, Green and Co., 1956, P.171.

108. J. Homer, M. H. Everdell, C. J. Jackson and P. M. Whitney, J. Chem. Soc., Faraday II, 1972, 68, 874.

109. P. Laszlo and D. H. Williams, J. Am. Chem., 1966, 88, 2799.

110. J. H. Bowie, J. Ronayne and D. H. Williams, J. Chem. Soc., (B), 1966, 785.

111. C. J. Jackson. Ph.D. Thesis, University of Aston in Birmingham, (1970).

112. L. E. Orgel and R.S. Mulliken, J. Am. Chem. Soc., 1957, 79. 4839.

113. P. M. Whitney, Ph.D. Thesis, University of Aston, Birmingham, (1973).

114. M. C. Cooke, Ph.D. Thesis, University of Aston in Birmingham (1970).

115. R. R. Yadava " " " "

116. "Practical N.M.R. Spectroscopy", M. L. Martin. J.J. Delpuech, G. L. Martin, Heyden and Son Ltd., 1980 e.g. therein.

117. See e.g. F. R. Hartley, C. Burgess and R. Alcock, "Solution Equilibria", Ellison Horwood Publishers, P21-22.

118. L. W. Reeves and W. G. Schneider, Canad. J. Chem., 1957, 35, 251.

119. P. Job, Compt. Rend., 1925, 180, 928.

120. P. Job, Ann. Chim., 1928, 9, 113.

121. R. B. Denison, Trans. Faraday Soc., 1912, 8, 20, 35.

122. B. Dodson and R. Foster and in part A.A.S. Bright, M. I. Forman and J. Gorton, J. Chem. Soc., (B), 1971, 1283.

123. F. Woldbye, Acta Chem. Scand., 1955, 9, 299.

124. W. C. Vosburgh and G. R. Cooper, J. Amer. Chem. Soc., 1941, 63, 437.

125. H. S. Gutowsky and A. Saika, J. Chem. Phys., 1953, 21, 1688.

126. See e.g. J. A. Pople, W. G. Schneider and H. J. Berstein, "High Resoultion Nuclear Magnetic Resonance", McGraw-Hill, London, 1959.

127. J. Homer and C. C. Percival, J. Chem. Soc., Faraday II, 1984, 80, 1.

128. R. Foster and D. R. Twiselton, Rec. Trav. Chim., 1970, 89, 1211.

129. P. Polamun, Ph.D Thesis, The University of Aston in Birmingham (1973).

130. J. Timmermans "Physico-Chemical Constants of Rare Organic Compounds", Elsevier, Amsterdam, 1965.

131. Handbook of Chemistry and Physics, Ed. Weast, Chemical Rubber Co., 57th Edition, 1976-77.

132. J. Homer, M. M. Ayad and R. M. Issa, unpublished results.